AFRL-PR-WP-TR-2001-2061

PRESSURE SCALING OF NON-EQUILIBRIUM PHENOMENA IN PLASMAS

PETER HAALAND
CHARLES JIAO

MOBIUM ENTERPRISES, INC.
5100 SRINGFIELD PIKE, SUITE 420
DAYTON, OH 45431-1231

DECEMBER 2000

FINAL REPORT FOR PERIOD 21 MAY 1996 – 31 DECEMBER 2000

Approved for public release; distribution unlimited

This material may be reproduced only by or for the U.S. Government pursuant the copyright license in the contract.
© 2000 Elsevier Science B.V.
© 1999 IOP Publishing Ltd

PROPULSION DIRECTORATE
AIR FORCE RESEARCH LABORATORY
AIR FORCE MATERIEL COMMAND
WRIGHT-PATTERSON AIR FORCE BASE, OH 45433-7251

REPORT DOCUMENTATION PAGE

Form Approved OMB No. 0704-0188

Public reporting burder for this collection of information is estibated to average 1 hour per response, including the time for reviewing instructions, searching existing data sources, gathering and maintaining the data needed, and completing and reviewing this collection of information. Send comments regarding this burden estimate or any other aspect of this collection of information, including suggestions for reducing this burder to Department of Defense, Washington Headquarters Services, Directorate for Information Operations and Reports (0704-0188), 1215 Jefferson Davis Highway, Suite 1204, Arlington, VA 22202-4302. Respondents should be aware that notwithstanding any other provision of law, no person shall be subject to any penalty for failing to comply with a collection of information if it does not display a currently valid OMB control number. PLEASE DO NOT RETURN YOUR FORM TO THE ABOVE ADDRESS.

1. REPORT DATE (DD-MM-YYYY)	2. REPORT TYPE	3. DATES COVERED (FROM - TO)
01-12-2000	Final	21-05-1996 to 31-12-2000

4. TITLE AND SUBTITLE Pressure Scaling of Non-Equilibrium PHenomena in Plasmas Unclassified	5a. CONTRACT NUMBER F33615-96-C-2613 5b. GRANT NUMBER 5c. PROGRAM ELEMENT NUMBER
6. AUTHOR(S) Haaland, Peter ; Jiao, Charles ;	5d. PROJECT NUMBER 5e. TASK NUMBER 5f. WORK UNIT NUMBER
7. PERFORMING ORGANIZATION NAME AND ADDRESS Mobium Enterprises, Inc. 5100 Springfield Pike, Suite 420 Dayton, OH45431-1231	8. PERFORMING ORGANIZATION REPORT NUMBER
9. SPONSORING/MONITORING AGENCY NAME AND ADDRESS Propulsion Directorate Air Force Research Laboratory Air Force Materiel Command Wright-Patterson AFB, OH45433-7251	10. SPONSOR/MONITOR'S ACRONYM(S) 11. SPONSOR/MONITOR'S REPORT NUMBER(S)

12. DISTRIBUTION/AVAILABILITY STATEMENT
APUBLIC RELEASE
,

13. SUPPLEMENTARY NOTES

14. ABSTRACT
The ionization of molecules by electrons and the reactions of the resulting ions with neutral reagents are essential elements of gaseous electronics. The partitioning among simple and dissociative ionization by electron impact and the kinetics of charge transfer reactions have been evaluated using pulsed ion cyclotron resonance mass spectrometry.

15. SUBJECT TERMS
electron impact; ionization; fourier transform mass spectrometry; ion-molecule reactions

16. SECURITY CLASSIFICATION OF:			17. LIMITATION OF ABSTRACT	18. NUMBER OF PAGES	19. NAME OF RESPONSIBLE PERSON
			Same as Report (SAR)	135	Fenster, Lynn lfenster@dtic.mil
a. REPORT Unclassified	b. ABSTRACT Unclassified	c. THIS PAGE Unclassified			19b. TELEPHONE NUMBER International Area Code Area Code Telephone Number 703767-9007 DSN 427-9007

Standard Form 298 (Rev. 8-98)
Prescribed by ANSI Std Z39.18

NOTICE

USING GOVERNMENT DRAWINGS, SPECIFICATIONS, OR OTHER DATA INCLUDED IN THIS DOCUMENT FOR ANY PURPOSE OTHER THAN GOVERNMENT PROCUREMENT DOES NOT IN ANY WAY OBLIGATE THE US GOVERNMENT. THE FACT THAT THE GOVERNMENT FORMULATED OR SUPPLIED THE DRAWINGS, SPECIFICATIONS, OR OTHER DATA DOES NOT LICENSE THE HOLDER OR ANY OTHER PERSON OR CORPORATION; OR CONVEY ANY RIGHTS OR PERMISSION TO MANUFACTURE, USE, OR SELL ANY PATENTED INVENTION THAT MAY RELATE TO THEM.

THIS REPORT IS RELEASABLE TO THE NATIONAL TECHNICAL INFORMATION SERVICE (NTIS). AT NTIS, IT WILL BE AVAILABLE TO THE GENERAL PUBLIC, INCLUDING FOREIGN NATIONS.

THIS TECHNICAL REPORT HAS BEEN REVIEWED AND IS APPROVED FOR PUBLICATION.

CHARLES A. DeJOSEPH, JR.
Project Engineer
Electrical Technology and Plasma Physics Branch
Power Division

JOSEPH A. WEIMER
Chief
Electrical Technology and Plasma Physics Branch
Power Division

JOANN L. ERNO, Lt Colonel, USAF
Deputy Chief
Power Division

Do not return copies of this report unless contractual obligations or notice on a specific document requires its return.

REPORT DOCUMENTATION PAGE

Form Approved
OMB No. 0704-0188

Public reporting burden for this collection of information is estimated to average 1 hour per response, including the time for reviewing instructions, searching existing data sources, gathering and maintaining the data needed, and completing and reviewing the collection of information. Send comments regarding this burden estimate or any other aspect of this collection of information, including suggestions for reducing this burden, to Washington Headquarters Services, Directorate for Information Operations and Reports, 1215 Jefferson Davis Highway, Suite 1204, Arlington, VA 22202-4302, and to the Office of Management and Budget, Paperwork Reduction Project (0704-0188), Washington, DC 20503.

1. AGENCY USE ONLY *(Leave blank)*

2. REPORT DATE
Dec 2000

3. REPORT TYPE AND DATES COVERED
FINAL REPORT FOR 05/21/96-12/31/00

4. TITLE AND SUBTITLE
PRESSURE SCALING OF NON-EQUILIBRIUM PHENOMENA IN PLASMAS

5. FUNDING NUMBERS
C: F33615-96-C-2613
PE: 61102F
PR: 2301
TA: P1
WU: 03

6. AUTHOR(S)
PETER HAALAND AND CHARLES JIAO

7. PERFORMING ORGANIZATION NAME(S) AND ADDRESS(ES)
MOBIUM ENTERPRISES, INC.
5100 SPRINGFIELD PIKE, SUITE 420
DAYTON, OHIO 45431-1231

8. PERFORMING ORGANIZATION REPORT NUMBER

9. SPONSORING/MONITORING AGENCY NAME(S) AND ADDRESS(ES)
PROPULSION DIRECTORATE
AIR FORCE RESEARCH LABORATORY
AIR FORCE MATERIEL COMMAND
WRIGHT-PATTERSON AFB, OH 45433-7251
POC: C. A. DeJOSEPH, JR., AFRL/PRPE, 937-255-2923

10. SPONSORING/MONITORING AGENCY REPORT NUMBER
AFRL-PR-WP-TR-2001-2061

11. SUPPLEMENTARY NOTES
This report contains copyright material.

12a. DISTRIBUTION AVAILABILITY STATEMENT
APPROVED FOR PUBLIC RELEASE, DISTRIBUTION UNLIMITED.

12b. DISTRIBUTION CODE

13. ABSTRACT *(Maximum 200 words)*

The ionization of molecules by electrons and the reactions of the resulting ions with neutral reagents are essential elements of gaseous electronics. The partitioning among simple and dissociative ionization by electron impact and the kinetics of charge transfer reactions have been evaluated using pulsed ion cyclotron resonance mass spectrometry. These crucial gaseous electronic data for perfluorinated microelectronic plasma etch precursors including C2F4, c-C5F8, C3F6, C4F6, C2F6, C3F8, c-C4F8, and NF3 are reported. The ionization cross sections and ion-molecule reactions of hydrofluorocarbon etchants C2HF5 and C2HF4 are also presented. Ion formation and reactions in organometallic species whose plasma chemistry leads to film deposition such as HSi(CH3)3, Ge(C2H5)4, Al(CH3)-3, and Ga(CH3)3 are presented, as are the properties of the fire suppressants CF3Br and CF3I. Electron impact ionization in a simple hydrocarbon fuel, and the subsequent reactions of dissociatively ionized fragments with n-octane, are reported as well. The data presented in this report can provide the basis for critical evaluation of quantum theoretical analyses of dissociative ionization as well as practical information on ion chemical constraints on the performance of plasma devices such as etching reactors, coating and film deposition systems, and electrical ignition systems.

14. SUBJECT TERMS
ELECTRON IMPACT IONIZATION; FOURIER TRANSFORM MASS SPECTROMETRY;ION-MOLECULE REACTIONS

15. NUMBER OF PAGES
140

16. PRICE CODE

17. SECURITY CLASSIFICATION OF REPORT	18. SECURITY CLASSIFICATION OF THIS PAGE	19. SECURITY CLASSIFICATION OF ABSTRACT	20. LIMITATION OF ABSTRACT
UNCLASSIFIED	UNCLASSIFIED	UNCLASSIFIED	SAR

Standard Form 298 (Rev. 2-89) (EG)
Prescribed by ANSI Std. 239.18
Designed using Perform Pro, WHS/DIOR, Oct 94

TABLE OF CONTENTS

List of Figures ..... *iv*

List of Tables ..... *v*

Introduction *1*

Ion Chemistry in tetrafluoroethylene, C_2F_4 ..... *1*

Dissociative Ionization of C_2F_4 ..... **1**

Charge Transfer Reactions in C_2F_4 ..... **5**

Composition of plasmas that contain C_2F_4 ..... **7**

Ion chemistry of perfluorocyclopentene, c-C_5F_8 ..... *8*

Dissociative ionization of c-C_5F_8 ..... **8**

Charge transfer reactions of c-C_5F_8 ..... **11**

Ion Chemistry of perfluoropropene, C_3F_6 ..... *13*

Dissociative ionization of C_3F_6 ..... **13**

Charge transfer reactions of C_3F_6 ..... **16**

Ion Chemistry of perfluorobutadiene, C_4F_6 ..... *19*

Electron Impact Ionization **19**

Ion Chemistry of perfluorobutadiene, C_4F_6 ..... *22*

Dissociative Ionization of C_4F_6 ..... **22**

Charge Transfer Reactions of C_4F_6 ..... **26**

Ion chemistry in pentafluoroethane, C_2HF_5 ..... *26*

Dissociative ionization of pentafluoroethane **26**

Charge transfer chemistry in C_2HF_5 ..... **28**

Ion chemistry of 1,1,1,2 tetrafluoroethane, $C_2H_2F_4$ *31*

Dissociative ionization of $C_2H_2F_4$ **31**

Charge transfer reactions of $C_2H_2F_4$ **32**

Binary Encounter Bethe estimates of fragmentation in C_2F_6 ..... *34*

Appendix A: Ion Chemistry in trifluoromethyl bromide and iodode: *38*

Appendix B Mass Spectrometry of n-Octane *48*

Appendix C Gas-Phase Ion Chemistries of Trimethylaluminum and Trimethylgallium *64*

Appendix D Ion Chemistry in boron trichloride, BCl_3 ..... *72*

Appendix E Ion Chemistry in hexafluoroethane, C_2F_6 ..... *78*

Appendix F Ionization of perfluoropropane, C_3F_8 ..... *84*

Appendix G Ionization of perfluorocyclobutane, c-C_4F_8 ..... *94*

Appendix H Ionization of nitrogen trifluoride, NF_3 ..... *101*

Appendix I Ionization of tetraethyl germane, $Ge(C_2H_5)_4$ *114*

Appendix J Ion Chemistry of trimethylsilane, $SiH(CH_3)_3$ *123*

List of Figures

Figure 1. Partial ionization cross sections of C_2F_4 2
Figure 2. Comparison of total ionization cross sections measured by FTMS and computed using the Binary Encounter Bethe method of Kim et al. 4
Figure 3. Threshold behavior of the five most prominent ions in C_2F_4 ionization processes. The measured cross section for Xe^+ divided by 10 is displayed to anchor the energy scale 5
Figure 4. Evolution of charged species following 25 eV electron impact in a 1:1 C_2F_4:Ar mixture 6
Figure 5. Relaxation of ions formed by 50 eV electron impact in a 1:1 C_2F_4:Ar mixture 7
Figure 6. High resolution mass spectrum distinguishes F^+ that is formed from dissociative ionization of C_5F_8 from traces of protonated water that are produced from background moisture through the reaction $H_2O^+ + H_2O \rightarrow H_3O^+ + OH$ 8
Figure 7. Total ionization section for c-C_5F_8 with the cross section for Argon ionization shown as a scale reference 9
Figure 8. Partial ionization sections of perfluorocyclopentene (c-C_5F_8) 10
Figure 9. Evolution of ion ensemble following irradiation of an Ar:C_5F_8 mixture with 50 eV electrons..... 12
Figure 10. Threshold behavior of dissociative ionization cross sections for $Ar^+$and $C_3F_3^+$ 13
Figure 11. Dissociative ionization cross sections for perfluoropropene, C_3F_6..... 14
Figure 12. Total ionization cross section of perfluoropropene 16
Figure 13. Evolution of ion composition in an Ar:C_3F_6 mixture following irradiation by50 eV electrons. Reactant ions whose concentration decays are indicated by diamonds; product species with increasing concentrations are shown by circles 18
Figure 14. Partial ionization cross sections of perfluorobutadiene, C_4F_6 19
Figure 15. Total ionization cross section for perfluorobutadiene 20
Figure 16. Ion composition following irradiation of a 1:1 mixture of Ar and C_4F_6 with 50 eV electrons... 22
Figure 17. Partial ionization cross sections of perfluorobutadiene, C_4F_6 23
Figure 18. Total ionization cross section for perfluorobutadiene 24
Figure 19. Ion composition following irradiation of a 1:1 mixture of Ar and C_4F_6 with 50 eV electrons... 26
Figure 20. Partial ionization cross-sections of C_2HF_5 27
Figure 21. BEB estimate of total ioniztion cross section for pentafluoroethane..... 28
Figure 22. Relaxation of ion composition in a mixture of pentafluoroethane and argon. The background pressure of water vapor is approximately 6 x 10^{-8} Torr 29
Figure 23. Outline of chemical mechanism for production of $C_2HF_2O^+$ 29
Figure 24. Outline of mechanism for production of other oxygen bearing hydrofluorocarbons from $C_3F_7^+$ produced by perfluoropropane. 30
Figure 25. Ionization of 1,1,1,2 tetrafluoroethane by electron impact..... 31
Figure 26. Total ionization cross section of 1,1,1,2 tetrafluoroethane by the BEB model (solid line) and from FTMS measurements (diamonds) 32
Figure 27. Evolution of ion composition following radiolysis of a mixture of argon and 1,1,1,2 tetrafluoroethane..... 33
Figure 28. BEB cross-sections for C_2F_6 ionization summed by orbital symmetry 34
Figure 29. Cross-sections using Kim orbital energies. Legend is identical to that of figure 28 36
Figure 30. Contributions to BEB ionization cross section of silicon tetrafluoride from orbitals of each symmetry 36
Figure 31. Contributions from each orbital symmetry to the BEB ionization cross section of difluoromethane. Circles are experimental values for each of the six fragment channels 37

List of Tables

Table 1. Partial Ionization Cross sections for C_2F_4 in units of $10^{-16}cm^2$ 3
Table 2. Partial and total ionization sections of perfluorocyclopentene ($10^{-16}cm^2$) 11
Table 3. Partial and total ionization cross sections of perfluoropropene ($10^{-16}cm^2$) 15
Table 4. Decay rates and approximate bimolecular rate coefficients for charge transfer to perfluoropropene 17
Table 5. Partial ionization cross sections of perfluorobutadiene; columns correspond to successive ion mass/charge ratios, units are 10^{-16} cm^2 21
Table 6. Partial ionization cross sections of perfluorobutadiene; columns correspond to successive ion mass/charge ratios, units are 10^{-16} cm^2 25
Table 7. Summary of orbital potential (U) and kinetic (T) energies (eV) for perfluoroethane from Kim (http://physlab.nist.gov/cgi-bin/Ionization) and Carl Winstead 35

Introduction

The ionization of molecules by electrons and the reactions of the resulting ions with neutral reagents are essential elements of gaseous electronics. The partitioning among simple and dissociative ionization by electron impact and the kinetics of charge transfer reactions have been evaluated using pulsed ion cyclotron resonance mass spectrometry. These crucial gaseous electronic data for perfluorinated microelectronic plasma etch precursors including C_2F_4, c-C_5F_8, C_3F_6, C_4F_6, C_2F_6, C_3F_8, c-C_4F_8, and NF_3 are reported. The ionization cross sections and ion-molecule reactions of hydrofluorocarbon etchants C_2HF_5 and C_2HF_4 are also presented. Ion formation and reactions in organometallic species whose plasma chemistry leads to film deposition such as $HSi(CH_3)_3$, $Ge(C_2H_5)_4$, $Al(CH_3)_3$, and $Ga(CH_3)_3$ are presented, as are the properties of the fire suppressants CF_3Br and CF_3I. Electron impact ionization in a simple hydrocarbon fuel, and the subsequent reactions of dissociatively ionized fragments with n-octane, are reported as well. The data presented in this report can provide the basis for critical evaluation of quantum theoretical analyses of dissociative ionization as well as practical information on ion chemical constraints on the performance of plasma devices such as etching reactors, coating and film deposition systems, and electrical ignition systems.

Ion Chemistry in tetrafluoroethylene, C_2F_4

Dissociative Ionization of C_2F_4

Dissociative ionization of perfluoroethylene has been examined by Fourier transform mass spectrometry. A sample of C_2F_4 graciously provided by Air Products was used without further purification. Mixtures of C_2F_4 with calibrated quantities of Ar and Xe were used to ascertain both the magnitude and threshold for partial ionization of this material.

Ten ions are observed upon electron impact:

$$C^+, F^+, C_2^+, CF^+, CF_2^+, CF_3^+ C_2F^+, C_2F_2^+, C_2F_3^+, \text{and } C_2F_4^+.$$

If any other ions, such as F_2^+ or CF_4^+, are formed, their cross sections must be less than $10^{-19}cm^2$.

Analysis of the C_2F_4 provided by Air Products revealed CO_2 impurity at a concentration of 4.5%. This contamination was inferred from the measured CO_2^+ yield and values for the CO_2 ionization cross section between 80 and 130 eV published by Rapp and Englander-Golden (*J. Chem. Phys.*, **43**, 1464 (1965)).

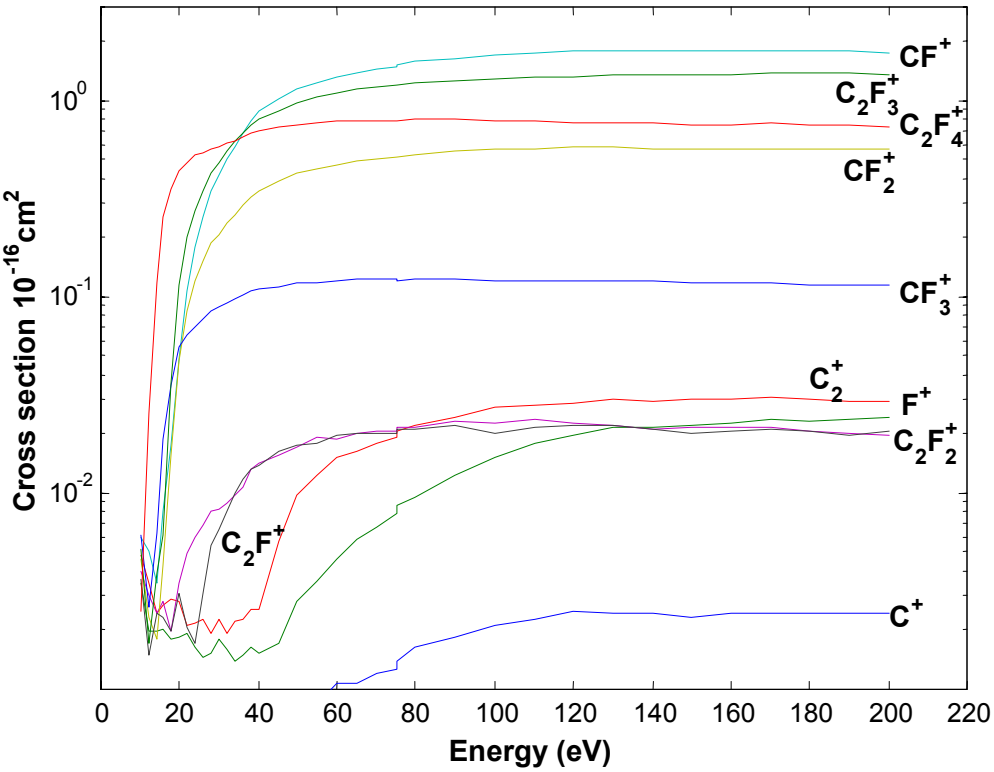

Figure 1. Partial ionization cross sections of C_2F_4

Table 1. Partial Ionization Cross sections for C_2F_4 in units of $10^{-16}cm^2$

Energy	C^+	F^+	C_2^+	CF^+	C_2F^+	CF_2^+	$C_2F_2^+$	CF_3^+	$C_2F_3^+$	$C_2F_4^+$
10	0.001	0.004	0.005	0.006	0.004	0.005	0.004	0.006	0.005	0.003
12	0.000	0.002	0.004	0.005	0.003	0.002	0.002	0.003	0.002	0.025
14	0.000	0.002	0.002	0.004	0.002	0.002	0.002	0.006	0.004	0.116
16	0.000	0.002	0.003	0.008	0.003	0.004	0.002	0.019	0.006	0.257
18	0.000	0.002	0.003	0.018	0.002	0.016	0.002	0.036	0.036	0.357
20	0.000	0.002	0.003	0.048	0.003	0.047	0.003	0.056	0.116	0.434
22	0.000	0.002	0.002	0.107	0.005	0.084	0.002	0.064	0.204	0.477
24	0.000	0.002	0.002	0.178	0.006	0.119	0.002	0.071	0.276	0.523
26	0.000	0.002	0.002	0.258	0.007	0.152	0.003	0.077	0.345	0.536
28	0.000	0.002	0.002	0.343	0.008	0.187	0.005	0.084	0.424	0.571
30	0.000	0.002	0.002	0.415	0.008	0.208	0.007	0.088	0.484	0.579
32	0.000	0.002	0.002	0.499	0.009	0.236	0.008	0.093	0.555	0.614
34	0.000	0.001	0.002	0.586	0.010	0.262	0.010	0.098	0.618	0.629
36	0.000	0.002	0.002	0.688	0.011	0.294	0.012	0.103	0.691	0.657
38	0.001	0.002	0.003	0.792	0.013	0.325	0.013	0.106	0.757	0.682
40	0.001	0.002	0.003	0.876	0.014	0.349	0.014	0.110	0.809	0.701
45	0.001	0.002	0.006	1.020	0.016	0.386	0.017	0.112	0.894	0.725
50	0.001	0.003	0.010	1.152	0.017	0.424	0.018	0.117	0.982	0.753
55	0.001	0.004	0.013	1.235	0.019	0.446	0.018	0.118	1.035	0.766
60	0.001	0.005	0.015	1.322	0.019	0.469	0.020	0.121	1.092	0.782
65	0.001	0.006	0.017	1.397	0.020	0.490	0.020	0.122	1.138	0.784
70	0.001	0.007	0.018	1.439	0.021	0.500	0.020	0.123	1.163	0.790
75	0.001	0.008	0.019	1.485	0.021	0.512	0.020	0.123	1.193	0.790
75	0.001	0.009	0.021	1.530	0.022	0.520	0.021	0.121	1.192	0.790
80	0.002	0.010	0.022	1.588	0.022	0.532	0.021	0.122	1.221	0.799
90	0.002	0.013	0.025	1.647	0.023	0.547	0.022	0.125	1.260	0.800
100	0.002	0.015	0.028	1.720	0.023	0.566	0.020	0.121	1.297	0.790
110	0.002	0.018	0.028	1.743	0.024	0.569	0.022	0.119	1.305	0.779
120	0.003	0.020	0.029	1.776	0.023	0.578	0.022	0.119	1.333	0.776
130	0.003	0.022	0.030	1.786	0.022	0.579	0.022	0.120	1.353	0.777
140	0.002	0.022	0.030	1.773	0.021	0.570	0.021	0.119	1.346	0.762
150	0.002	0.022	0.030	1.774	0.022	0.567	0.020	0.116	1.351	0.757
160	0.002	0.023	0.030	1.784	0.022	0.571	0.021	0.116	1.364	0.758
170	0.002	0.024	0.031	1.789	0.022	0.572	0.021	0.117	1.370	0.760
180	0.002	0.024	0.030	1.780	0.021	0.570	0.021	0.116	1.369	0.753
190	0.002	0.024	0.030	1.775	0.020	0.568	0.020	0.114	1.372	0.748
200	0.003	0.025	0.030	1.762	0.020	0.564	0.021	0.114	1.364	0.737

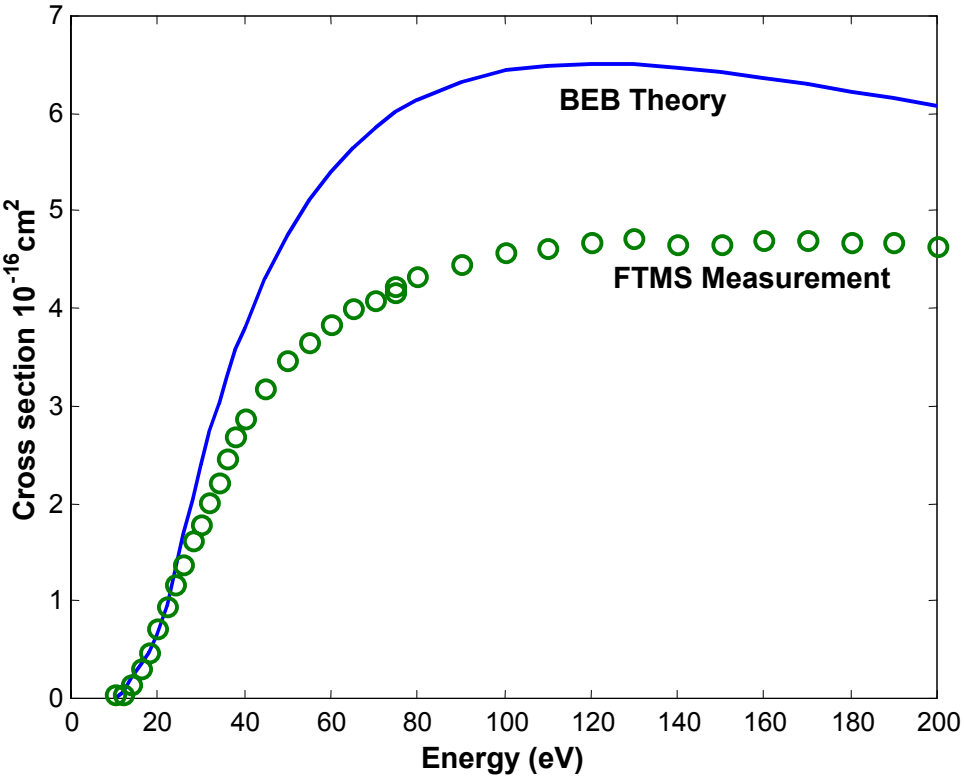

Figure 2. Comparison of total ionization cross sections measured by FTMS and computed using the Binary Encounter Bethe method of Kim et al.

The total ionization cross section for C_2F_4 may be estimated using the Binary Encounter Bethe model of Kim (Kim and Rudd, *Phys. Rev.* A50, 3594 (1994)) and orbital potential and kinetic energies from *ab initio* electronic structure theory. Figure 2 displays a comparison of total ionization cross sections measured by FTMS and computed from orbital energies provided by Winstead and McKoy (Personal communication, May 2000). The theoretical and experimental cross sections are in remarkable agreement between threshold and 25 eV, after which the BEB model overestimates the total ionization cross section by about 20%.

The threshold for generation of the $C_2F_4^+$ ion is approximately 1 eV below the 12.13 eV threshold for generation of Xe^+ from Xe, as illustrated in figure 3. This threshold is in good agreement with the Koopman's theorem ionization potential inferred from the $2b_{2u}$ orbital binding energy of 11.17 eV.

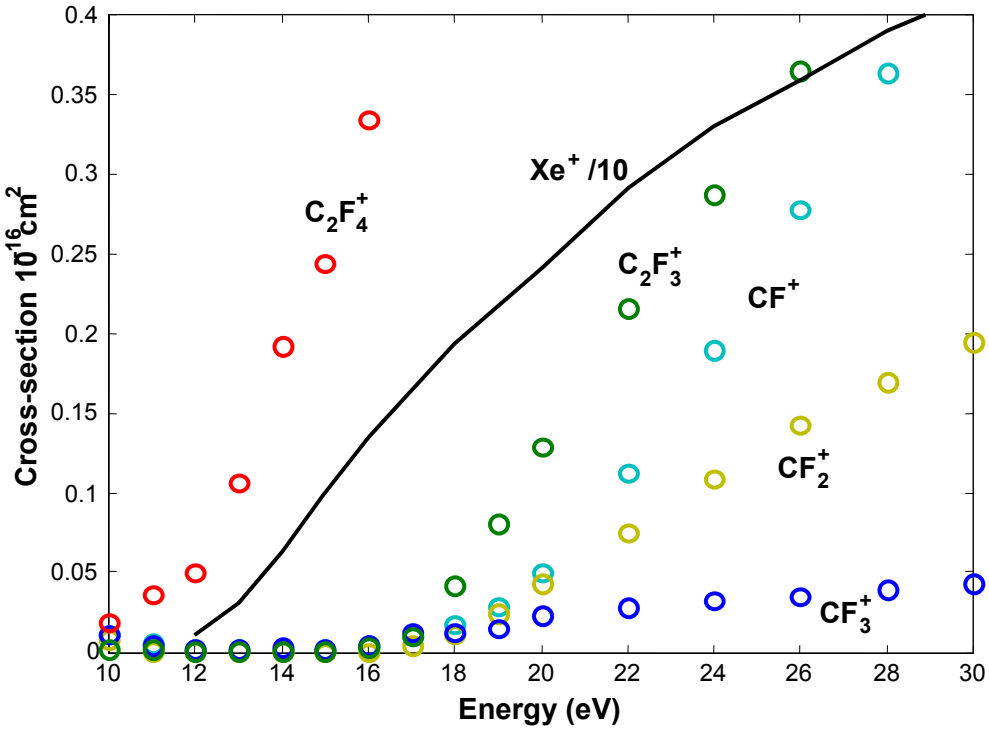

Figure 3. Threshold behavior of the five most prominent ions in C_2F_4 ionization processes. The measured cross section for Xe^+ divided by 10 is displayed to anchor the energy scale

The fragmentation of tetrafluoroethylene is unusual compared with that of other fluorocarbons and hydrofluorocarbons we have examined. Below 18 eV, only $C_2F_4^+$ is produced. Between 18 and 60 eV, there is competition among nine dissociative channels involving bond cleavage and rearrangement. The partitioning among these dissociative ionization channels stops varying with energy above 60 eV. The 7 eV difference between the threshold for generation of $C_2F_4^+$ and that for fragment ions implies higher production rates of this ion in plasmas whose electron energy distribution functions are monotonically decreasing with energy.

Charge Transfer Reactions in C_2F_4

Evolution of the ion composition following electron impact was studied by introducing a delay between electron beam irradiation of the gas mixture and acquisition of the mass spectrum. Figure 4 displays the fate of ions formed by 25 eV electron impact in a 1:1 Ar:C_2F_4 mixture. Figure 5 shows analogous results at 50 eV. The primary reaction is that of Ar^+ with C_2F_4 to produce $C_2F_4^+$. This result might be anticipated on thermodynamic grounds, because the ionization potential of Ar, 15.6 eV, is between the thresholds for

production of $C_2F_4^+$ and those for production of the other $C_xF_y^+$ ions. However, CF_3^+ is also produced by charge transfer from Ar^+ at one half the rate for C_2F_4.

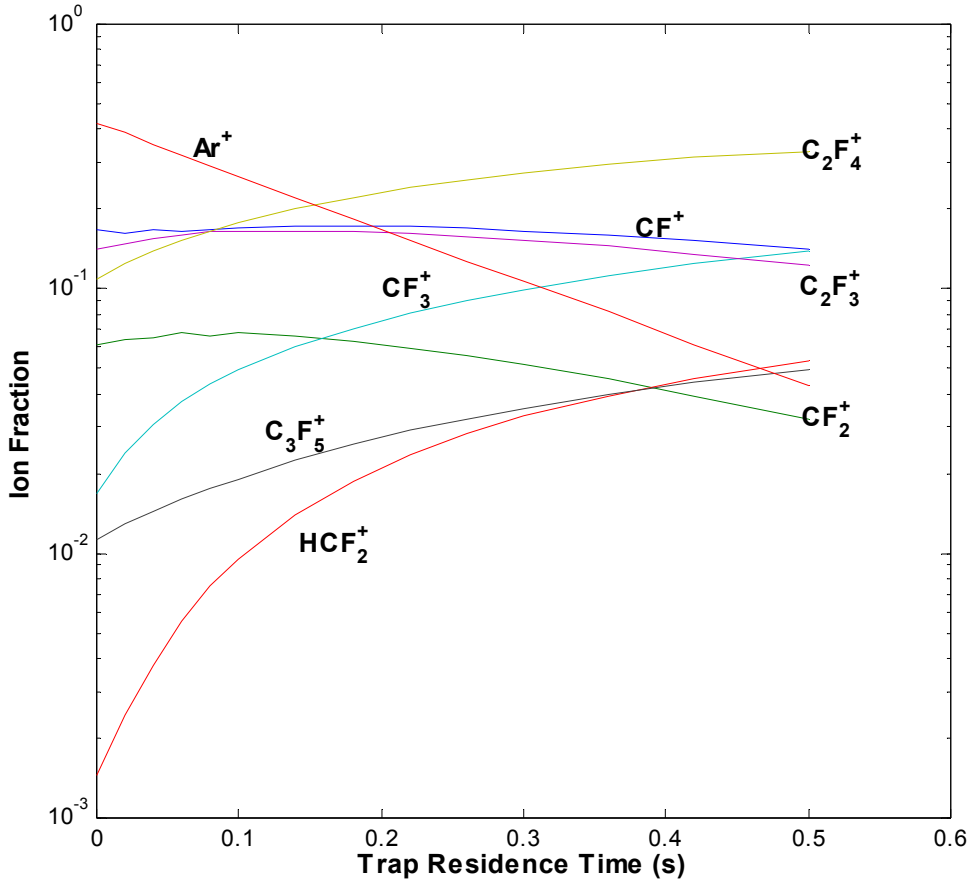

Figure 4. Evolution of charged species following 25 eV electron impact in a 1:1 C_2F_4:Ar mixture

CF^+ does not react with the parent gas at appreciable rates; however, $C_2F_3^+$ reacts with tetrafluoroethylene to form a new carbon-carbon bond:

$$C_2F_3^+ \quad + \quad C_2F_4 \rightarrow \quad C_3F_5^+ \quad + \quad \{CF_2\}.$$

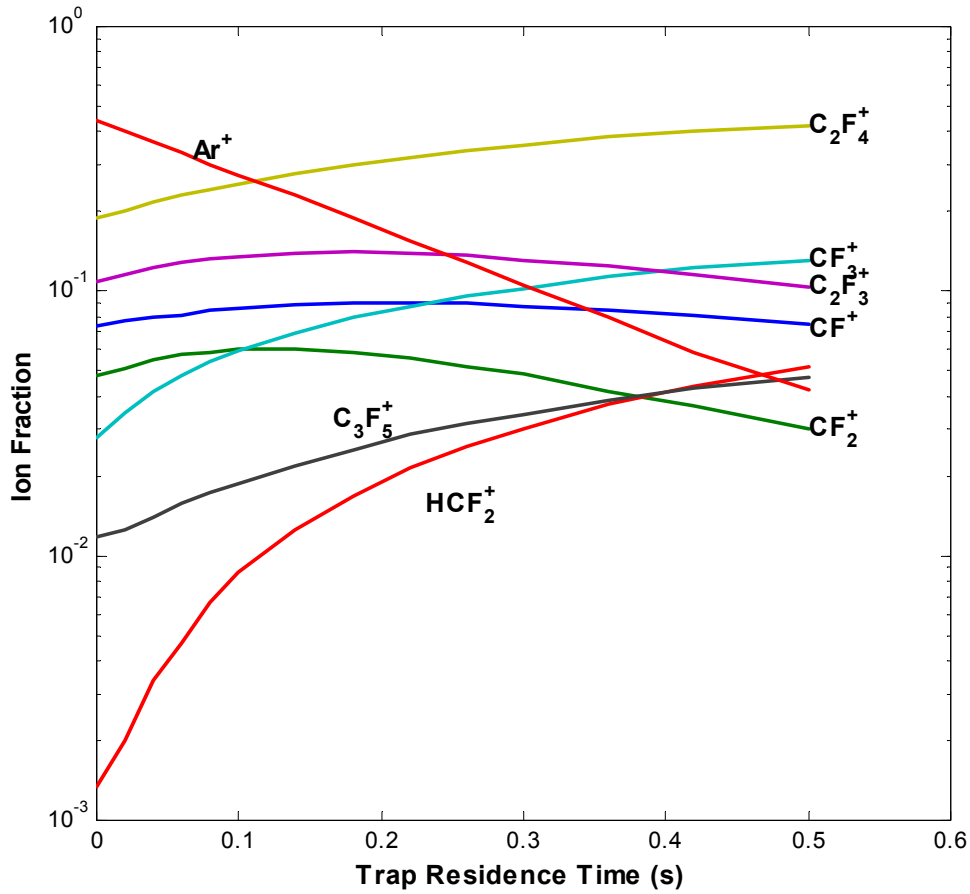

Figure 5. Relaxation of ions formed by 50 eV electron impact in a 1:1 C_2F_4:Ar mixture

The final reaction of interest is the production of HCF_2^+ from traces of water vapor in the vacuum chamber:

$$H_2O \quad + \quad CF_2^+ \quad \rightarrow \quad HCF_2^+ \quad + \quad HO$$

The same kinetics are observed in figure 5 following irradiation of the mixture by 50 eV electrons. These data supports the idea that internally excited $C_xF_y^+$ ions that might be produced by more energetic electron impact are no more reactive than those formed at 25 eV.

Composition of plasmas that contain C_2F_4

The ionization of C_2F_4 by plasma electrons will yield primarily the parent $C_2F_4^+$ ion, which is also the primary product of Ar^+ charge transfer to C_2F_4. $C_2F_4^+$ is unreactive with neutral C_2F_4. We therefore anticipate that it will dominate the ion distribution for many plasma configurations. Only electrons with kinetic energies above 18 eV can produce fragment ions. Among the fragments, CF^+ has the highest yield above 30 eV, followed

closely by $C_2F_3^+$. The latter reacts with C_2F_4 to form $C_3F_5^+$ but at a rate quite slow compared to that of the $Ar^+ + C_2F_4$ reaction.

Ion chemistry of perfluorocyclopentene, c-C_5F_8

Dissociative ionization of c-C_5F_8

The collisional ionization of perfluorocyclopentene, C_5F_8, by electrons has been examined using pulsed ion cyclotron resonance mass spectrometry. The parent molecular ion is found to have the lowest appearance potential and a qualtitatively distinctive cross section shape as seen in figure 8. Thirteen dissociative ionization channels are also found with sections that exceed 10^{-18} cm^2. Above 20 eV the most abundant ion species results from the loss of two fluorine and one carbon atoms (or CF_2) , but the dominant channel switches to that yielding $C_3F_3^+$ above 35 eV. $C_5F_7^+$ and $C_4F_5^+$, which result from loss of a fluorine atom and CF_3 or its fragments round out the contributions with thresholds below 20 eV.

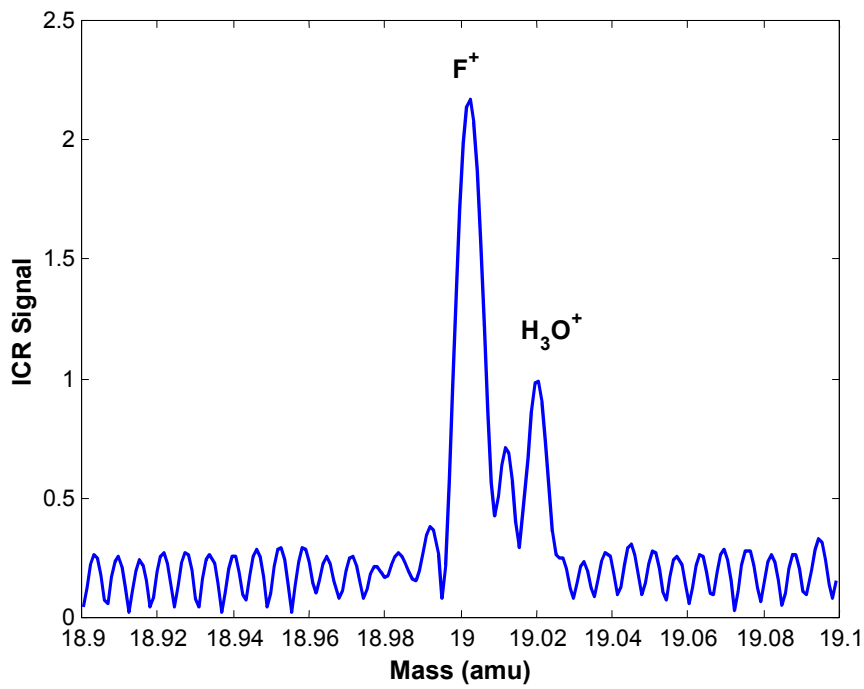

Figure 6. High resolution mass spectrum distinguishes F^+ that is formed from dissociative ionization of C_5F_8 from traces of protonated water that are produced from background moisture through the reaction $H_2O^+ + H_2O \rightarrow H_3O^+ + OH$

A second group of processes have appearance potentials between 20 and 30 eV and give rise to CF^+ , CF_3^+, $C_3F_2^+$, $C_3F_4^+$, $C_4F_4^+$, $C_2F_4^+$, $C_3F_5^+$, and $C_2F_3^+$. There is a small yield of F^+ as well, which can be cleanly distinguished from traces of H_3O^+ using the high resolution ICR data as seen in figure 6 above. The F^+formation process has a threshold at

about 60 eV and the smallest measured cross section for the detected dissociatively ionized fragments.

The total ionzation section rises to a maximum value of 1.2 x 10^{-15} cm^2, or about four times that for argon ionization, as can be seen by inspection of figure 7. The threshold for production of ions from perfluorocyclopentene is 13 +/- 0.5 eV, well below that for single ionization of argon.

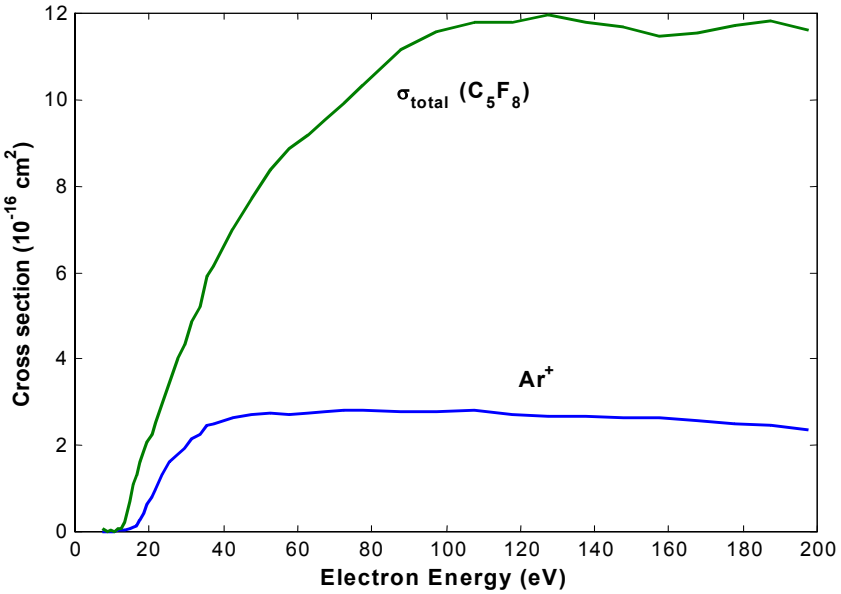

Figure 7. Total ionization section for c-C_5F_8 with the cross section for Argon ionization shown as a scale reference

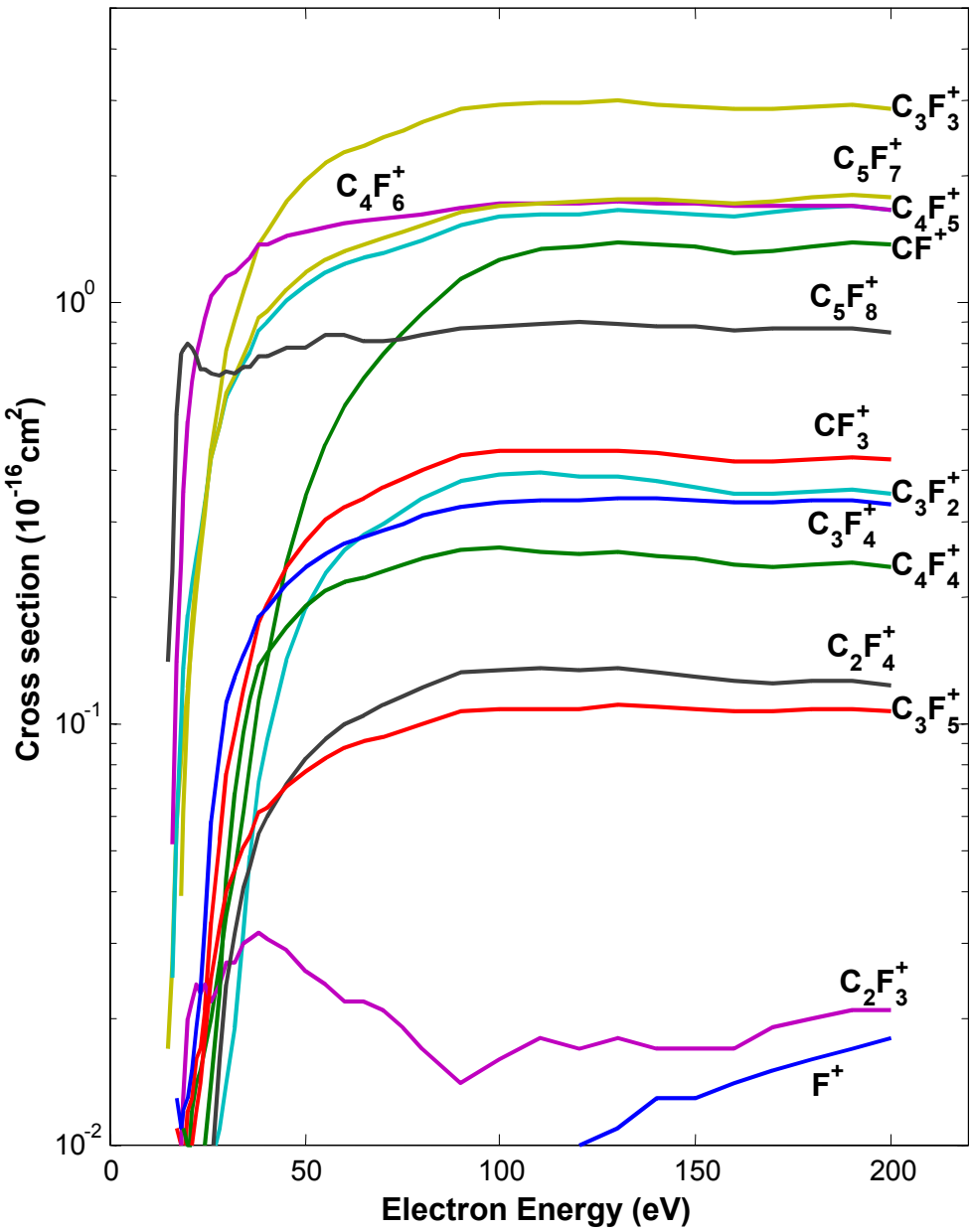

Figure 8. Partial ionization sections of perfluorocyclopentene (c-C_5F_8)

Table 2. Partial and total ionization sections of perfluorocyclopentene ($10^{-16}cm^2$)

eV	F+	CF+	CF3+	C3F2+	C2F3+	C3F3+	C2F4+	C3F4+	C4F4+	C3F5+	C4F5+	C4F6+	C5F7+	C5F8+	total
15						0.017								0.141	0.158
16						0.027					0.025	0.052		0.230	0.335
17			0.011			0.058		0.013			0.057	0.141		0.543	0.824
18			0.010		0.010	0.083		0.011			0.100	0.243	0.039	0.751	1.246
19		0.007	0.009		0.013	0.096		0.012	0.011	0.008	0.135	0.355	0.062	0.772	1.478
20		0.008	0.012		0.020	0.122		0.013	0.010	0.008	0.181	0.523	0.113	0.796	1.805
21		0.012	0.013	0.007	0.022	0.159		0.015	0.010	0.010	0.214	0.648	0.171	0.785	2.065
22		0.014	0.016	0.007	0.024	0.208		0.019	0.008	0.012	0.250	0.751	0.226	0.744	2.278
23		0.015	0.017	0.008	0.023	0.255		0.023	0.008	0.014	0.284	0.827	0.273	0.692	2.438
24		0.017	0.021	0.008	0.024	0.315	0.006	0.033	0.010	0.018	0.334	0.924	0.332	0.691	2.734
26		0.020	0.034	0.009	0.022	0.448	0.009	0.059	0.014	0.025	0.430	1.038	0.428	0.677	3.212
28		0.027	0.053	0.011	0.024	0.601	0.016	0.086	0.023	0.033	0.512	1.096	0.510	0.670	3.662
30		0.035	0.076	0.014	0.027	0.774	0.024	0.112	0.043	0.040	0.599	1.158	0.609	0.687	4.198
32		0.045	0.095	0.019	0.027	0.906	0.032	0.129	0.069	0.045	0.652	1.173	0.672	0.679	4.544
34		0.062	0.120	0.032	0.030	1.055	0.041	0.146	0.095	0.051	0.718	1.242	0.749	0.701	5.042
36		0.081	0.141	0.049	0.031	1.179	0.046	0.159	0.115	0.054	0.767	1.278	0.811	0.706	5.417
38		0.114	0.173	0.073	0.032	1.380	0.055	0.180	0.138	0.062	0.863	1.372	0.918	0.744	6.104
40		0.143	0.192	0.092	0.031	1.472	0.060	0.189	0.147	0.063	0.897	1.374	0.957	0.743	6.360
45		0.240	0.237	0.143	0.029	1.731	0.072	0.215	0.170	0.071	1.007	1.434	1.075	0.783	7.207
50		0.349	0.272	0.189	0.026	1.946	0.083	0.235	0.190	0.077	1.097	1.478	1.173	0.781	7.899
55		0.463	0.305	0.228	0.024	2.136	0.092	0.254	0.207	0.083	1.182	1.516	1.263	0.838	8.592
60		0.567	0.328	0.259	0.022	2.270	0.100	0.267	0.217	0.088	1.240	1.544	1.330	0.839	9.070
65		0.661	0.345	0.280	0.022	2.364	0.105	0.277	0.223	0.091	1.276	1.565	1.373	0.814	9.393
70		0.751	0.362	0.299	0.021	2.462	0.111	0.288	0.231	0.093	1.316	1.587	1.420	0.810	9.751
75	0.006	0.844	0.381	0.320	0.019	2.568	0.117	0.299	0.239	0.097	1.363	1.600	1.467	0.817	10.138
80	0.006	0.944	0.401	0.342	0.017	2.677	0.122	0.311	0.248	0.100	1.413	1.622	1.521	0.835	10.561
90	0.007	1.133	0.434	0.376	0.014	2.874	0.132	0.329	0.260	0.107	1.532	1.678	1.634	0.865	11.375
100	0.007	1.258	0.445	0.390	0.016	2.960	0.134	0.336	0.261	0.109	1.603	1.709	1.700	0.875	11.801
110	0.008	1.346	0.447	0.393	0.018	2.991	0.135	0.339	0.257	0.109	1.619	1.721	1.720	0.888	11.992
120	0.010	1.360	0.443	0.386	0.017	2.968	0.134	0.339	0.253	0.109	1.623	1.720	1.732	0.900	11.995
130	0.011	1.393	0.447	0.388	0.018	3.002	0.135	0.345	0.255	0.111	1.652	1.742	1.767	0.892	12.157
140	0.013	1.375	0.438	0.376	0.017	2.962	0.132	0.342	0.250	0.110	1.636	1.725	1.752	0.876	12.004
150	0.013	1.356	0.430	0.366	0.017	2.927	0.130	0.338	0.246	0.109	1.619	1.707	1.741	0.879	11.878
160	0.014	1.310	0.418	0.352	0.017	2.868	0.127	0.334	0.239	0.107	1.606	1.695	1.720	0.862	11.668
170	0.015	1.324	0.418	0.350	0.019	2.872	0.125	0.334	0.237	0.107	1.634	1.703	1.741	0.869	11.748
180	0.016	1.360	0.426	0.356	0.020	2.916	0.126	0.338	0.239	0.109	1.668	1.706	1.783	0.867	11.932
190	0.017	1.383	0.431	0.360	0.021	2.943	0.127	0.340	0.242	0.109	1.687	1.705	1.809	0.870	12.043
200	0.018	1.367	0.423	0.352	0.021	2.892	0.124	0.333	0.235	0.107	1.662	1.666	1.784	0.847	11.831

Charge transfer reactions of c-C_5F_8

The ion chemistry of the dissociatively ionized fragments was probed by introducing a delay between ion formation at 50 eV and the recording of the mass spectrum. No evidence for high molecular weight clusters, that is ions with more than five carbon atoms, was observed under the single collision conditions of the FTMS experiment. The primary reaction was reduction of Ar^+ to three products:

$$Ar^+ + C_5F_8 \Longrightarrow C_5F_7+ + \{Ar,F\}, \quad k=1.0 \text{ (relative)}$$
$$Ar^+ + C_5F_8 \Longrightarrow C_5F_8+ + Ar, \quad k=0.5$$
$$Ar^+ + C_5F_8 \Longrightarrow C_4F_6+ + \{Ar,C,2F\}, \quad k=0.3$$

with a 10:5:3 branching ratio.

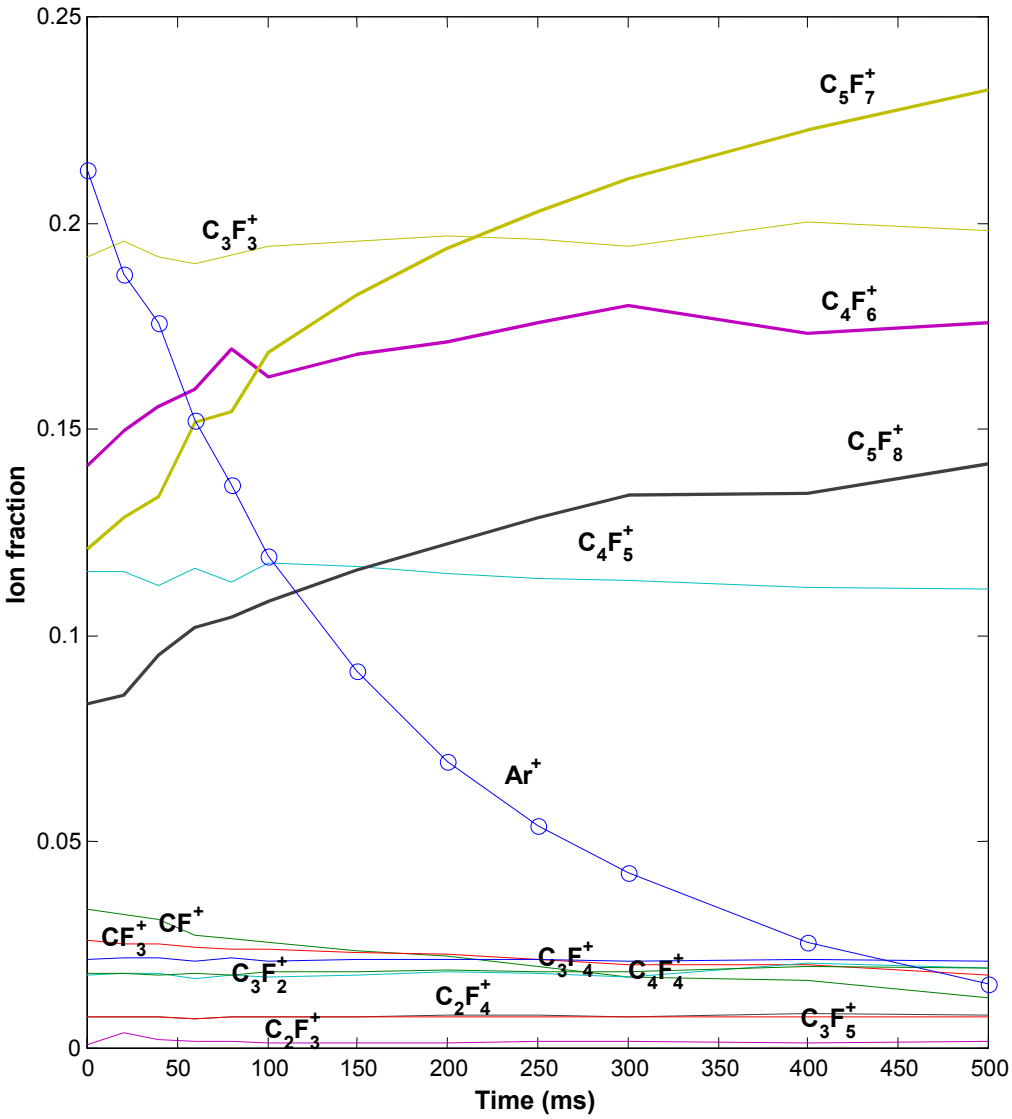

Figure 9. Evolution of ion ensemble following irradiation of an Ar:C_5F_8 mixture with 50 eV electrons

Although the reagent pressure in the ion relaxation experiment is not precisely known, the approximate perfluorocyclopentene pressure of 10^{-6} Torr implies rate coefficients of 8.3, 4.1, and 2.5 10^{-11} cm^3s^{-1} for these three charge transfer reactions. In other words, the total charge transfer rate of 1.5 x 10^{-10} cm^3s^{-1} is of the order one expects from classical Langevin collision theory for ion-molecule reactions. The three observed products have appearance potentials below that of argon, however the branching ratios differ from the cross section ratios observed following 16 eV electron impact. The $C_3F_3^+$ ion, which is not produced by charge transfer from Ar^+, has an appearance potential very close to that

of Ar, as seen below in figure 10. The remaining ion fragments are neither produced by charge transfer nor, with the possible exception of CF^+, consumed by reaction with C_5F_8.

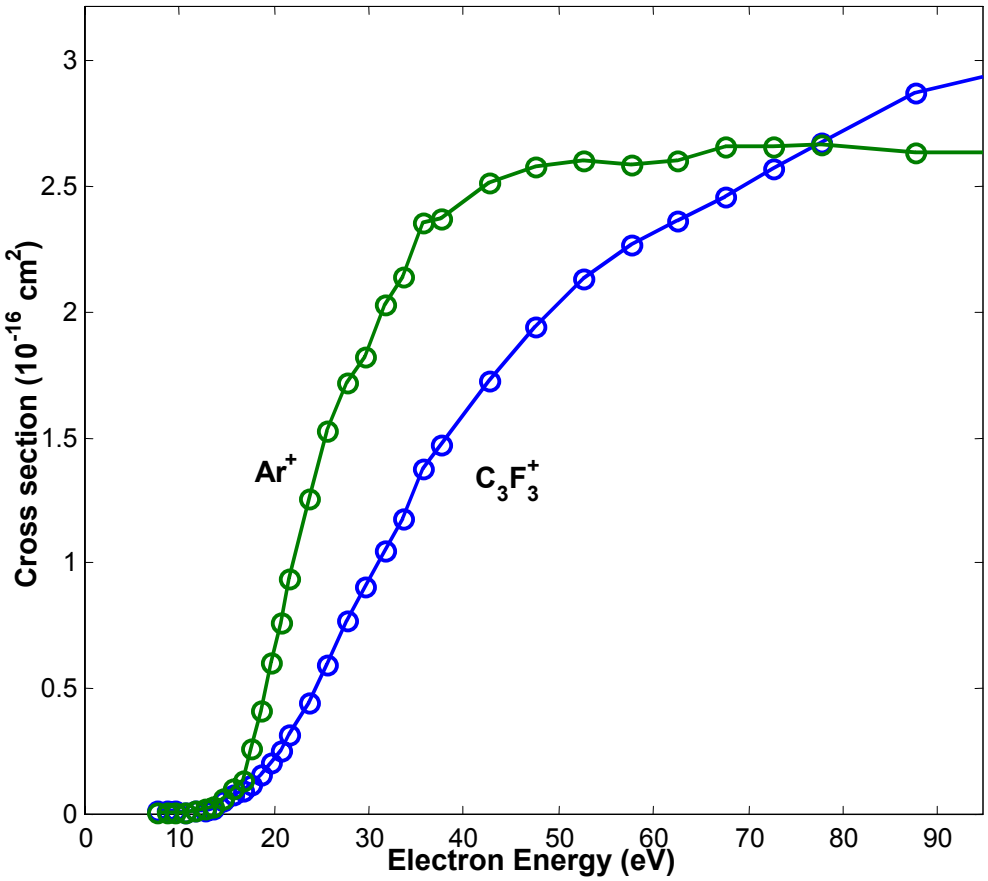

Figure 10. Threshold behavior of dissociative ionization cross sections for $Ar^+$and $C_3F_3^+$

In a weakly ionized plasma that contains perfluorocyclopentene one expects the $C_3F_3^+$ ion to be dominant at low pressures with a transition to enhancement of the $C_5F_7^+$ concentration as the partial pressure of perfluorocyclopentene increases.

Ion Chemistry of perfluoropropene, C_3F_6

Dissociative ionization of C_3F_6

Perfluoropropene produces a cornucopia of ion fragments by electron impact. Virtually every plausible fragment that might be formed is observed to have a cross section greater than 10^{-18}cm^2 (figure 11).

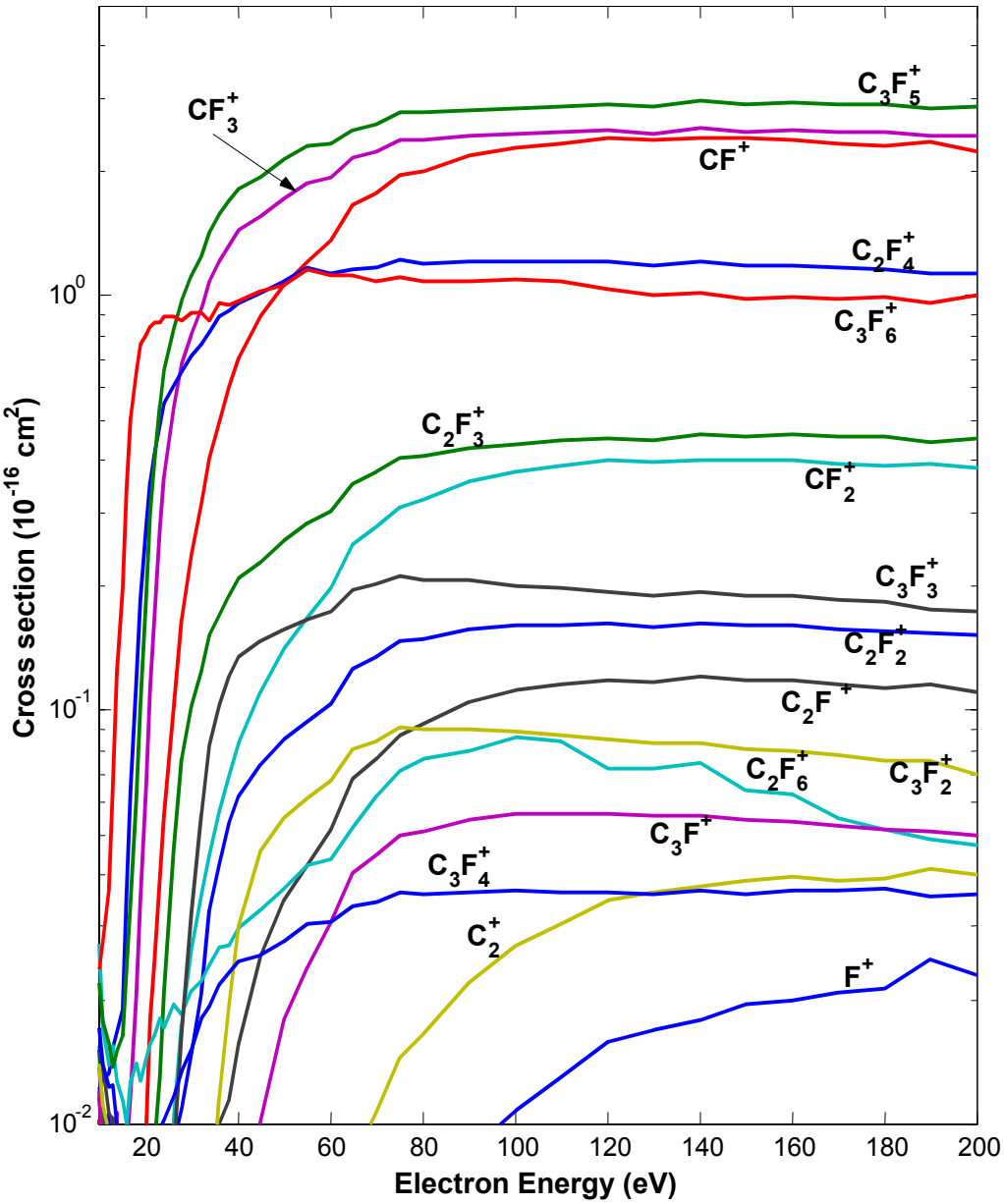

Figure 11. Dissociative ionization cross sections for perfluoropropene, C_3F_6

As was observed with perfluorocyclopentene, the parent molecular ion has the lowest appearance potential and a distinctive cross section shape. This cross section rises rapidly but the yield for the unfragmented $C_3F_6^+$ ion is overtaken by production of $C_3F_5^+$ (+ F), then CF_3^+, $C_2F_4^+$ and finally CF^+ as the electron energy increases.

Table 3. Partial and total ionization cross sections of perfluoropropene ($10^{-16}cm^2$)

eV	F+	CF+	CF2+	CF3+	C2+	C2F+	C2F2+	C2F3+	C2F4+	C2F6+	C3F+	C3F2+	C3F3+	C3F4+	C3F5+	C3F6+	total
11																0.028	0.028
12																0.037	0.037
13									0.015						0.014	0.064	0.093
14									0.017						0.015	0.122	0.154
15									0.019						0.016	0.196	0.232
16									0.036						0.024	0.341	0.401
17				0.012					0.065						0.035	0.510	0.622
18				0.020					0.117						0.061	0.658	0.856
19		0.006		0.035					0.184						0.102	0.761	1.088
20		0.010		0.067					0.279				0.007		0.191	0.811	1.364
21		0.018		0.113					0.356				0.007		0.298	0.839	1.631
22		0.024		0.164				0.009	0.415				0.007		0.392	0.857	1.869
23		0.039		0.272				0.013	0.486				0.007		0.546	0.860	2.223
24		0.055		0.366				0.021	0.548				0.007		0.664	0.894	2.556
26		0.101	0.010	0.538			0.009	0.046	0.610				0.009	0.012	0.831	0.887	3.053
28		0.165	0.017	0.685			0.011	0.076	0.655				0.017	0.013	0.972	0.869	3.480
30		0.237	0.026	0.811			0.015	0.102	0.712				0.032	0.015	1.115	0.906	3.973
32		0.314	0.036	0.927			0.021	0.125	0.762			0.005	0.056	0.018	1.247	0.910	4.420
34		0.405	0.044	1.079			0.033	0.151	0.814			0.007	0.083	0.019	1.421	0.872	4.929
36		0.494	0.057	1.203			0.042	0.169	0.889			0.011	0.102	0.022	1.574	0.956	5.521
38		0.599	0.069	1.324			0.053	0.190	0.922			0.019	0.120	0.023	1.699	0.949	5.967
40		0.710	0.083	1.438		0.016	0.062	0.208	0.963			0.030	0.135	0.025	1.820	0.970	6.459
45		0.886	0.111	1.556		0.025	0.074	0.227	1.018		0.010	0.046	0.146	0.026	1.943	1.030	7.098
50		1.057	0.141	1.722		0.035	0.085	0.256	1.081		0.018	0.055	0.157	0.028	2.123	1.058	7.815
55		1.207	0.168	1.871	0.003	0.042	0.094	0.282	1.167		0.024	0.061	0.166	0.030	2.307	1.154	8.576
60	0.002	1.363	0.198	1.940	0.005	0.052	0.104	0.303	1.129		0.031	0.067	0.172	0.031	2.329	1.118	8.844
65	0.003	1.658	0.250	2.148	0.008	0.068	0.126	0.353	1.160		0.041	0.081	0.196	0.034	2.526	1.120	9.771
70	0.004	1.779	0.276	2.229	0.011	0.076	0.135	0.374	1.167		0.045	0.085	0.201	0.034	2.608	1.088	10.110
75	0.005	1.951	0.309	2.373	0.014	0.087	0.146	0.405	1.216		0.050	0.090	0.211	0.036	2.766	1.103	10.764
80	0.006	2.008	0.323	2.376	0.017	0.092	0.149	0.410	1.201	0.076	0.051	0.090	0.207	0.036	2.761	1.080	10.883
90	0.009	2.190	0.356	2.439	0.022	0.105	0.156	0.429	1.207	0.080	0.055	0.090	0.205	0.036	2.810	1.085	11.273
100	0.011	2.281	0.376	2.466	0.027	0.112	0.160	0.438	1.213	0.086	0.056	0.089	0.200	0.037	2.841	1.099	11.492
110	0.013	2.325	0.387	2.477	0.031	0.115	0.161	0.446	1.212	0.084	0.056	0.087	0.196	0.036	2.866	1.085	11.578
120	0.016	2.408	0.401	2.500	0.035	0.119	0.162	0.453	1.204	0.072	0.056	0.085	0.194	0.036	2.895	1.040	11.677
130	0.017	2.378	0.396	2.464	0.036	0.117	0.159	0.447	1.181	0.072	0.055	0.083	0.189	0.036	2.861	1.006	11.497
140	0.018	2.410	0.401	2.536	0.037	0.120	0.162	0.462	1.210	0.075	0.055	0.083	0.194	0.037	2.960	1.013	11.774
150	0.019	2.399	0.400	2.494	0.039	0.119	0.161	0.458	1.178	0.064	0.054	0.081	0.188	0.036	2.911	0.981	11.581
160	0.020	2.386	0.401	2.517	0.040	0.118	0.160	0.463	1.181	0.062	0.054	0.079	0.189	0.037	2.941	0.988	11.635
170	0.021	2.329	0.394	2.489	0.039	0.115	0.156	0.458	1.165	0.055	0.052	0.078	0.185	0.037	2.905	0.986	11.465
180	0.021	2.306	0.389	2.474	0.039	0.113	0.155	0.455	1.155	0.051	0.051	0.075	0.182	0.037	2.890	0.988	11.384
190	0.025	2.365	0.391	2.427	0.042	0.116	0.154	0.445	1.135	0.049	0.051	0.075	0.176	0.036	2.836	0.958	11.279
200	0.023	2.218	0.383	2.434	0.040	0.110	0.151	0.451	1.133	0.047	0.050	0.070	0.173	0.036	2.850	1.002	11.170

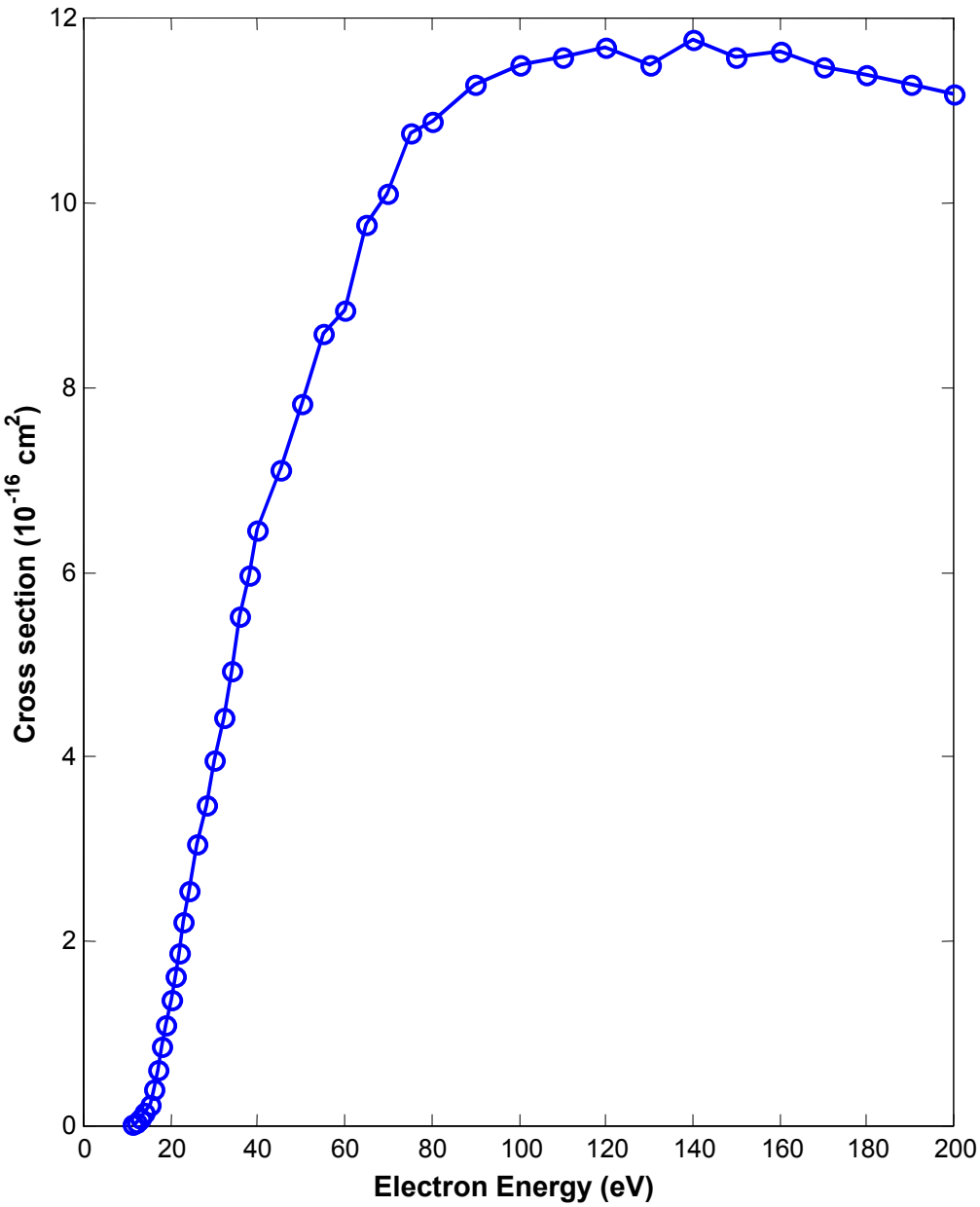

Figure 12. Total ionization cross section of perfluoropropene

Charge transfer reactions of C_3F_6

The varied dissociative ionization channels for perfluoropropene provide a rich and diverse source of reactive ion fragments. In addition to reactions with the Ar^+ ion, we see evidence of charge transfer from CF_3^+, CF^+ $C_2F_3^+$, CF_2^+, and $C_2F_2^+$ to perfluropropene. The most prominent reaction is

$$Ar^+ + C_3F_6 \rightarrow C_3F_5^+ + \{Ar, F\} \qquad k \sim 1.7 \times 10^{-10}\ cm^3s^{-1}.$$

At least some of the remaining reactive ions also yield $C_3F_5^+$ by charge transfer, but the precise relationship between minor reactant and product channels must await double resonance experiments. The rate constants shown below for reaction of each fragment produced by 50 eV electron impact are approximate and presume a chamber pressure of 10^{-6-} Torr. The *relative* rates are more precise, as can be inferrred from the data shown in figure 13.

Table 4. Decay rates and approximate bimolecular rate coefficients for charge transfer to perfluoropropene

Ion Species	Decay rate from figure 13 (s^{-1})	Approximate k ($10^{-10}cm^3s^{-1}$)
Ar^+	6.12	1.7
CF_3^+	1.13	0.32
CF^+	2.3	0.66
$C_2F_3^+$	2.02	0.57
CF_2^+	4.37	1.2
$C_2F_2^+$	3.00	0.85

Although the $C_3F_5^+$ ion accounts for 86% of the product, smaller yields of $C_3F_6^+$(7%), $C_2F_4^+$ (6%), $C_2F_6^+$ (1%), $C_3F_3^+$ and $C_3F_4^+$ (<0.5%) are also observed. In contrast to perflurocyclopentene, the species with the largest dissociative ionization cross section, $C_3F_5^+$, is also the most prominent product when the product of gas pressure and interaction time is of the order of 10^{-6} Torr-seconds. The combination of millitorr pressures and millisecond ambipolar diffusion times typical of etching reactors are in this range, leading to the inference that higher molecular weight fluorocarbon species, if observed in etching reactors, are the result of other chemistry.

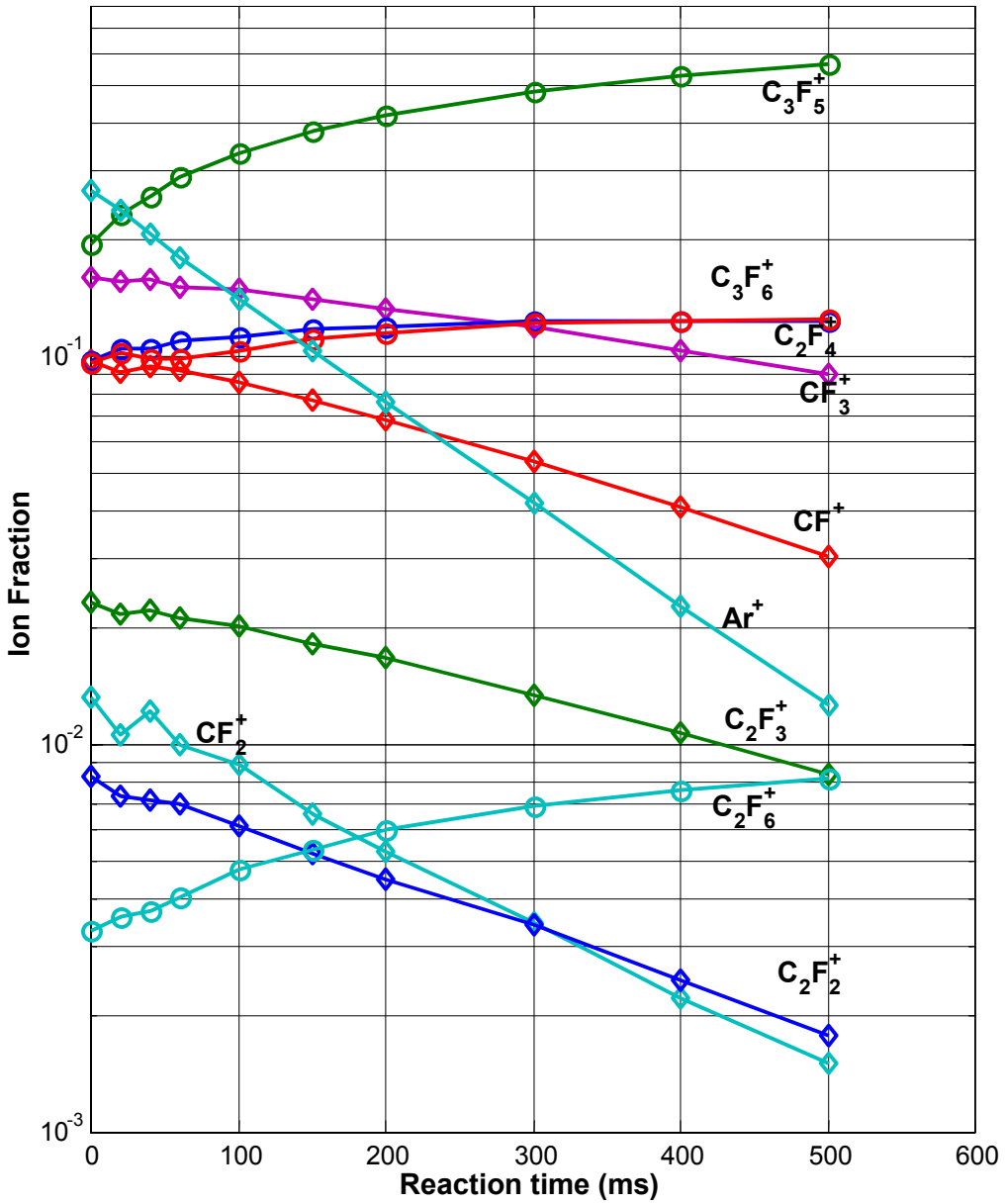

Figure 13. Evolution of ion composition in an Ar:C_3F_6 mixture following irradiation by50 eV electrons. Reactant ions whose concentration decays are indicated by diamonds; product species with increasing concentrations are shown by circles

Ion Chemistry of perfluorobutadiene, C_4F_6

Electron Impact Ionization

The most abundant product of electron impact ionization of perfluorobutadiene is the trifluoropropyl ion $C_3F_3^+$, while the product with the lowest appearance potential is the parent $C_4F_6^+$ molecular ion. A rich melange of dissociated ions are also produced by electron collisions with C_4F_6. A total of 16 dissociative ionization channels have been identified and can be seen in figure 14 and table 5, below. The higher thresholds, smaller $d\sigma/dE$ values, and lower cross-section magnitudes for dissociative ionization imply that the undissociated $C_4F_6^+$ will be the dominant species produced by plasma eThe most abundant product of electron impact ionization of perfluorobutadiene is the trifluoropropyl ion $C_3F_3^+$, while the product with the lowest appearance potential is the parent $C_4F_6^+$ molecular ion. A rich melange of dissociated ions are also produced by electron collisions with C_4F_6. A total of 16 dissociative ionization channels have been identified and can be seen in figure 14 and table 5, below. The higher thresholds, smaller $d\sigma/dE$ values, and lower cross-section magnitudes for dissociative ionization imply that the undissociated $C_4F_6^+$ will be the dominant species produced by plasma electrons.

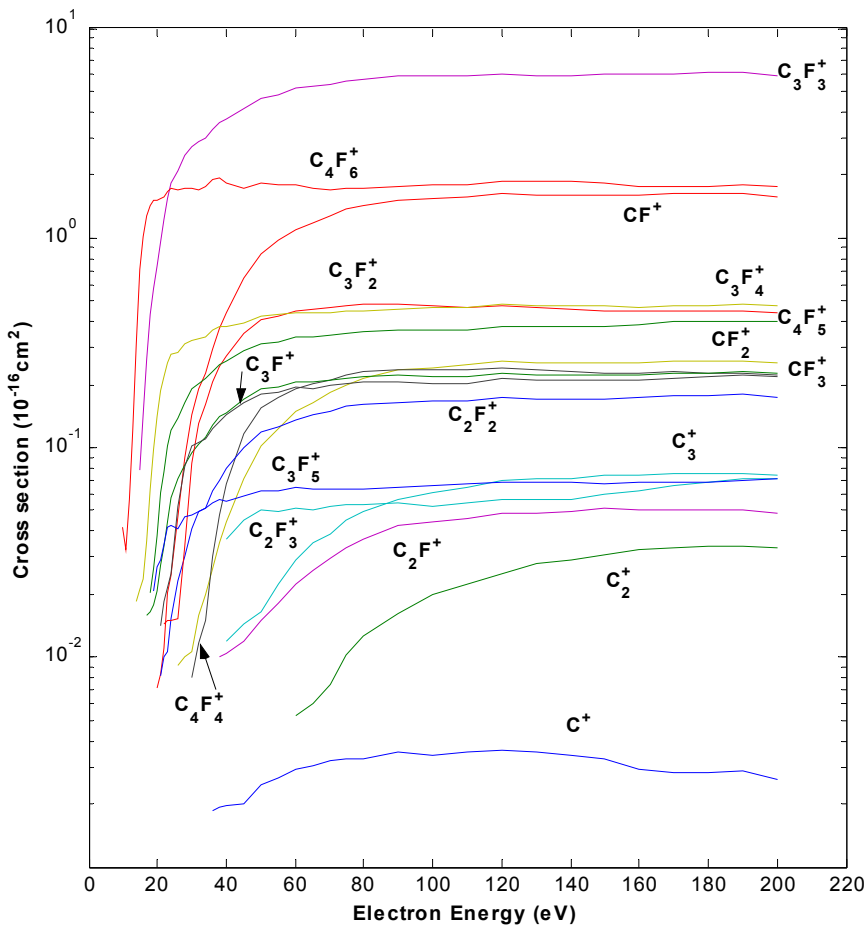

Figure 14. Partial ionization cross sections of perfluorobutadiene, C_4F_6

As can be seen in Figure 15, the total ionization cross section rises to a maximum value of 1.2 x 10^{-15}cm^2, almost five times that of Argon at 200 eV.

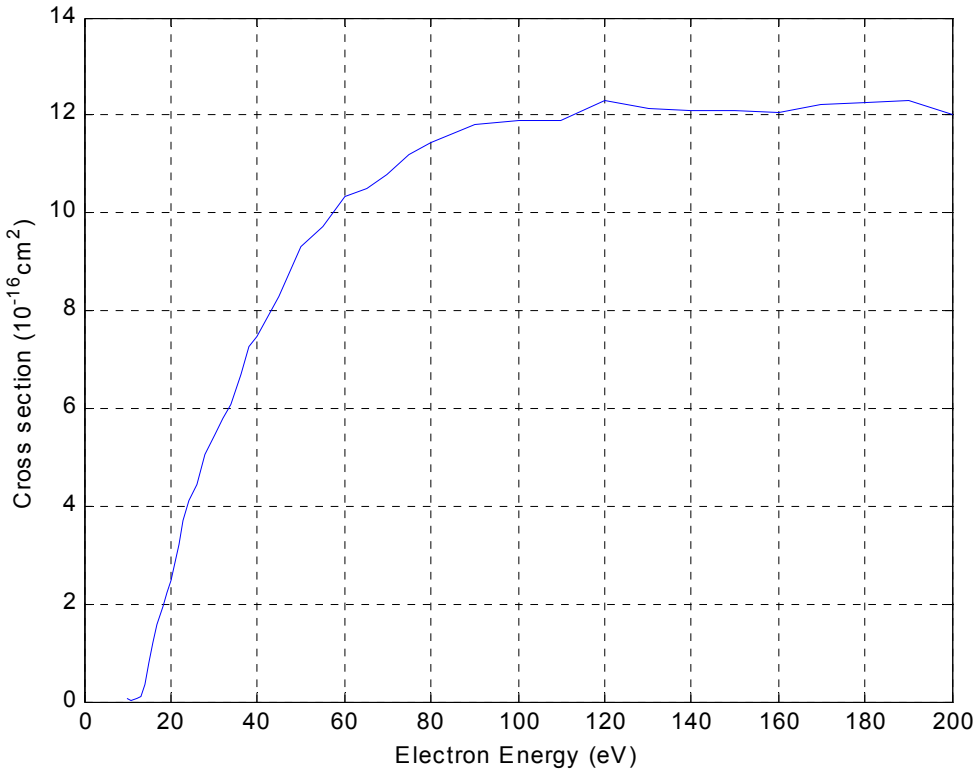

Figure 15. Total ionization cross section for perfluorobutadiene

Table 5. Partial ionization cross sections of perfluorobutadiene; columns correspond to successive ion mass/charge ratios, units are 10^{-16} cm^2

m/e	12 amu	24	31	36	43	50	55	62	69	74	81	93	112	124	131	143	162
10	0.000	0.000	0.000	0.000	0.000	0.000	0.000	0.000	0.000	0.000	0.000	0.000	0.000	0.000	0.000	0.000	0.042
11	0.000	0.000	0.000	0.000	0.000	0.000	0.000	0.000	0.000	0.000	0.000	0.000	0.000	0.000	0.000	0.000	0.033
12	0.000	0.000	0.000	0.000	0.000	0.000	0.000	0.000	0.000	0.000	0.000	0.000	0.000	0.000	0.000	0.000	0.056
13	0.000	0.000	0.000	0.000	0.000	0.000	0.000	0.000	0.000	0.000	0.000	0.000	0.000	0.000	0.000	0.000	0.122
14	0.000	0.000	0.000	0.000	0.000	0.000	0.000	0.000	0.000	0.000	0.000	0.000	0.018	0.000	0.000	0.000	0.310
15	0.000	0.000	0.000	0.000	0.000	0.000	0.000	0.000	0.000	0.000 sd	0.000	0.078	0.021	0.000	0.000	0.000	0.708
16	0.000	0.000	0.000	0.000	0.000	0.000	0.000	0.000	0.000	0.000	0.000	0.145	0.023	0.000	0.000	0.000	1.021
17	0.000	0.000	0.000	0.000	0.000	0.000	0.000	0.000	0.016	0.000	0.000	0.263	0.036	0.000	0.000	0.000	1.269
18	0.000	0.000	0.000	0.000	0.000	0.000	0.000	0.000	0.017	0.000	0.000	0.428	0.064	0.000	0.000	0.020	1.430
19	0.000	0.000	0.000	0.000	0.000	0.000	0.000	0.000	0.018	0.000	0.000	0.575	0.098	0.000	0.021	0.027	1.502
20	0.000	0.000	0.007	0.000	0.000	0.000	0.000	0.000	0.021	0.000	0.000	0.735	0.141	0.000	0.027	0.038	1.504
21	0.000	0.000	0.008	0.000	0.000	0.000	0.000	0.008	0.027	0.000	0.000	0.962	0.186	0.014	0.029	0.060	1.537
22	0.000	0.000	0.011	0.000	0.000	0.000	0.000	0.010	0.034	0.014	0.000	1.222	0.218	0.018	0.034	0.077	1.580
23	0.000	0.000	0.020	0.000	0.000	0.000	0.000	0.011	0.044	0.015	0.000	1.527	0.253	0.022	0.042	0.102	1.652
24	0.000	0.000	0.025	0.000	0.000	0.000	0.000	0.015	0.058	0.015	0.000	1.815	0.278	0.025	0.043	0.121	1.711
26	0.000	0.000	0.047	0.000	0.000	0.009	0.000	0.023	0.070	0.015	0.000	2.083	0.284	0.053	0.041	0.138	1.681
28	0.000	0.000	0.089	0.000	0.000	0.010	0.000	0.030	0.083	0.034	0.000	2.454	0.312	0.082	0.047	0.163	1.740
30	0.000	0.000	0.142	0.000	0.000	0.011	0.008	0.041	0.095	0.084	0.000	2.720	0.322	0.102	0.047	0.189	1.720
32	0.000	0.000	0.190	0.000	0.000	0.016	0.012	0.049	0.104	0.131	0.000	2.883	0.330	0.106	0.050	0.202	1.699
34	0.000	0.000	0.225	0.000	0.000	0.020	0.015	0.052	0.112	0.160	0.000	3.013	0.338	0.111	0.051	0.213	1.755
36	0.002	0.000	0.297	0.000	0.000	0.026	0.030	0.063	0.127	0.204	0.000	3.302	0.362	0.122	0.055	0.231	1.880
38	0.002	0.000	0.369	0.000	0.010	0.035	0.047	0.070	0.141	0.242	0.000	3.575	0.378	0.133	0.056	0.248	1.947
40	0.002	0.000	0.443	0.012	0.010	0.044	0.067	0.079	0.146	0.273	0.036	3.694	0.378	0.143	0.055	0.259	1.825
45	0.002	0.000	0.640	0.014	0.012	0.072	0.115	0.100	0.170	0.349	0.045	4.122	0.395	0.163	0.059	0.288	1.731
50	0.002	0.000	0.843	0.016	0.015	0.102	0.154	0.118	0.190	0.405	0.050	4.635	0.427	0.180	0.062	0.315	1.812
55	0.003	0.000	0.969	0.022	0.018	0.124	0.172	0.125	0.195	0.423	0.049	4.849	0.429	0.184	0.063	0.319	1.793
60	0.003	0.005	1.097	0.029	0.022	0.148	0.190	0.136	0.206	0.448	0.052	5.168	0.444	0.194	0.064	0.335	1.791
65	0.003	0.006	1.185	0.035	0.026	0.165	0.200	0.142	0.208	0.455	0.051	5.279	0.437	0.192	0.063	0.336	1.722
70	0.003	0.007	1.270	0.039	0.030	0.182	0.211	0.148	0.211	0.465	0.052	5.427	0.441	0.197	0.064	0.343	1.701
75	0.003	0.010	1.364	0.045	0.033	0.199	0.223	0.156	0.215	0.478	0.053	5.623	0.448	0.202	0.063	0.350	1.713
80	0.003	0.013	1.435	0.049	0.036	0.215	0.229	0.160	0.218	0.482	0.054	5.745	0.452	0.204	0.063	0.356	1.729
90	0.004	0.016	1.519	0.056	0.042	0.233	0.237	0.164	0.220	0.485	0.054	5.904	0.459	0.205	0.065	0.365	1.763
100	0.003	0.020	1.546	0.061	0.044	0.239	0.236	0.166	0.219	0.472	0.053	5.944	0.462	0.201	0.066	0.365	1.795
110	0.004	0.022	1.568	0.065	0.046	0.247	0.235	0.167	0.219	0.467	0.054	5.912	0.462	0.204	0.067	0.367	1.803
120	0.004	0.025	1.631	0.070	0.049	0.257	0.239	0.173	0.226	0.475	0.056	6.094	0.481	0.212	0.069	0.380	1.875
130	0.004	0.028	1.603	0.070	0.049	0.254	0.234	0.170	0.222	0.462	0.056	5.987	0.477	0.208	0.068	0.375	1.868
140	0.003	0.029	1.602	0.072	0.049	0.253	0.229	0.170	0.223	0.457	0.057	5.977	0.475	0.209	0.068	0.377	1.856
150	0.003	0.031	1.605	0.073	0.051	0.254	0.228	0.172	0.221	0.451	0.060	6.002	0.471	0.210	0.068	0.381	1.817
160	0.003	0.033	1.609	0.073	0.050	0.256	0.227	0.173	0.223	0.448	0.062	6.005	0.469	0.211	0.069	0.386	1.762
170	0.003	0.033	1.632	0.075	0.050	0.260	0.228	0.176	0.227	0.451	0.066	6.101	0.477	0.215	0.068	0.396	1.766
180	0.003	0.034	1.627	0.075	0.050	0.260	0.228	0.178	0.228	0.452	0.068	6.110	0.478	0.219	0.069	0.400	1.770
190	0.003	0.034	1.623	0.075	0.050	0.261	0.227	0.179	0.231	0.450	0.071	6.123	0.484	0.222	0.069	0.403	1.784
200	0.003	0.033	1.578	0.073	0.049	0.253	0.221	0.175	0.227	0.439	0.071	5.983	0.476	0.218	0.070	0.398	1.758

The evolution of an ion ensemble produced by 50 eV electron impact on a 1:1 Ar:C_4F_6 mixture is shown in figure 16. The fastest reactions are the ion-molecule reaction of Ar^+:

$$Ar^+ + C_4F_6 \rightarrow Ar + C_4F_5^+ + \{Ar, F\}$$
$$\rightarrow Ar + C_4F_3^+ + \{Ar, CF_3\}$$

with a branching ratio of approximately 3:2. Although these preliminary measurements suggest that lighter ions such as CF^+ produces $C_4F_6^+$, double resonance experiments would be required to isolate these reactive channels. We also observed traces of the $C_6F_6^+$ and $C_6F_7^+$ ions at the longest delays. It is intriguing to speculate on whether these ions are cyclic or aromatic, however their yield is too low (less than 3% after 500 ms at 10^{-6} Torr) to infer much about their bonding. This is one of the few perfluorocarbon cases that we have studied where products with masses greater than that of the parent neutral have been observed.

s

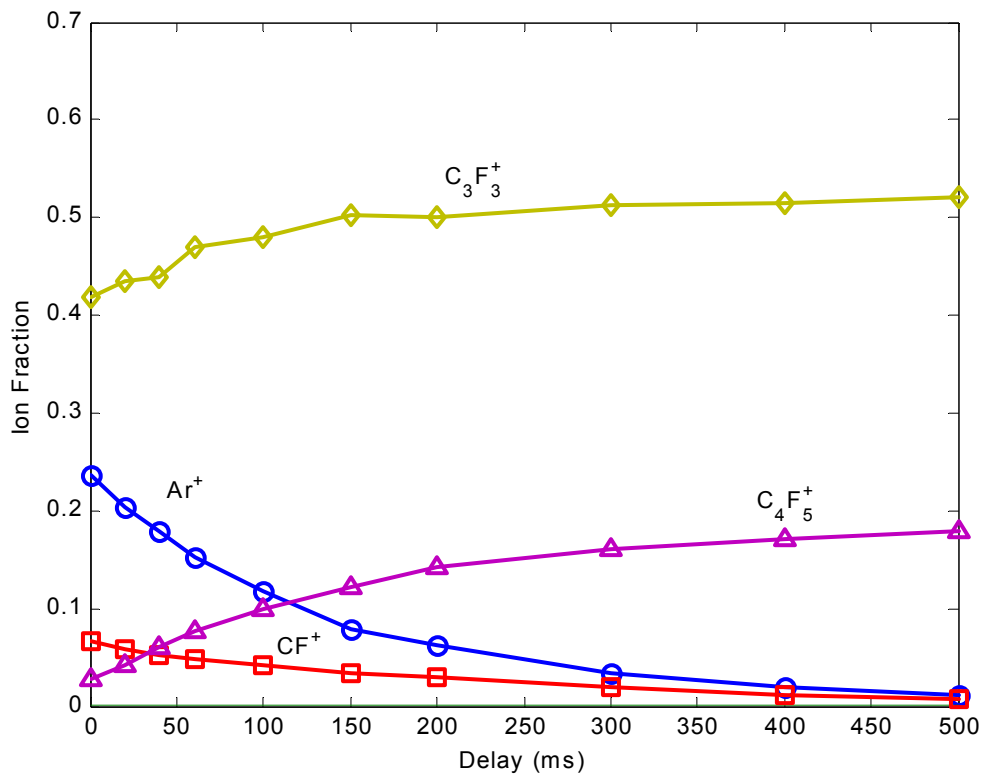

Figure 16. Ion composition following irradiation of a 1:1 mixture of Ar and C_4F_6 with 50 eV electrons

Ion Chemistry of perfluorobutadiene, C_4F_6

Dissociative Ionization of C_4F_6

The most abundant product of electron impact ionization of perfluorobutadiene is the trifluoropropyl ion $C_3F_3^+$, while the product with the lowest appearance potential is the

parent $C_4F_6^+$ molecular ion. A rich melange of dissociated ions are also produced by electron collisions with C_4F_6. A total of 16 dissociative ionization channels have been identified and can be seen in figure 17 and table 6, below. The higher thresholds, smaller dσ/dE values, and lower cross-section magnitudes for dissociative ionization imply that the undissociated $C_4F_6^+$ will be the dominant species produced by plasma electrons.

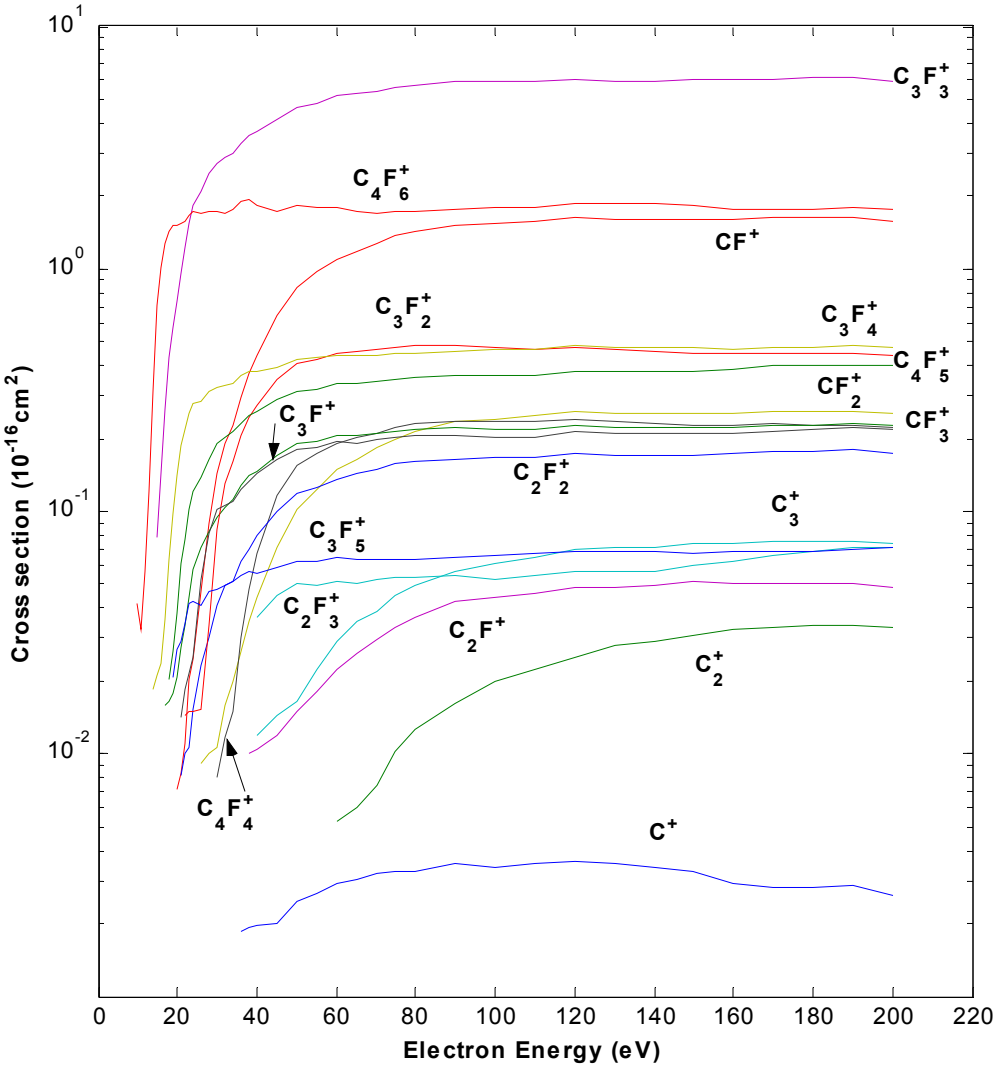

Figure 17. Partial ionization cross sections of perfluorobutadiene, C_4F_6

As can be seen in Figure 18, the total ionization cross section rises to a maximum value of 1.2 x 10^{-15}cm^2, almost five times that of Argon at 200 eV.

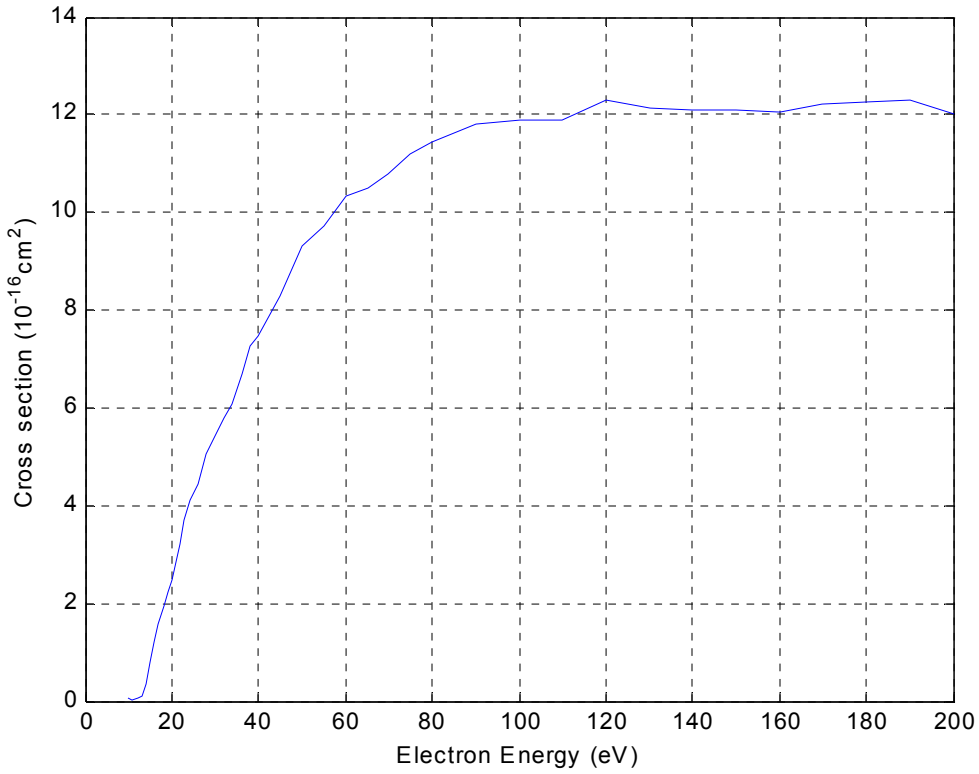

Figure 18. Total ionization cross section for perfluorobutadiene

Table 6. **Partial ionization cross sections of perfluorobutadiene; columns correspond to successive ion mass/charge ratios, units are 10^{-16} cm^2**

m/e	12 amu	24	31	36	43	50	55	62	69	74	81	93	112	124	131	143	162
10	0.000	0.000	0.000	0.000	0.000	0.000	0.000	0.000	0.000	0.000	0.000	0.000	0.000	0.000	0.000	0.000	0.042
11	0.000	0.000	0.000	0.000	0.000	0.000	0.000	0.000	0.000	0.000	0.000	0.000	0.000	0.000	0.000	0.000	0.033
12	0.000	0.000	0.000	0.000	0.000	0.000	0.000	0.000	0.000	0.000	0.000	0.000	0.000	0.000	0.000	0.000	0.056
13	0.000	0.000	0.000	0.000	0.000	0.000	0.000	0.000	0.000	0.000	0.000	0.000	0.000	0.000	0.000	0.000	0.122
14	0.000	0.000	0.000	0.000	0.000	0.000	0.000	0.000	0.000	0.000	0.000	0.000	0.018	0.000	0.000	0.000	0.310
15	0.000	0.000	0.000	0.000	0.000	0.000	0.000	0.000	0.000	0.000 sd	0.000	0.078	0.021	0.000	0.000	0.000	0.708
16	0.000	0.000	0.000	0.000	0.000	0.000	0.000	0.000	0.000	0.000	0.000	0.145	0.023	0.000	0.000	0.000	1.021
17	0.000	0.000	0.000	0.000	0.000	0.000	0.000	0.000	0.016	0.000	0.000	0.263	0.036	0.000	0.000	0.000	1.269
18	0.000	0.000	0.000	0.000	0.000	0.000	0.000	0.000	0.017	0.000	0.000	0.428	0.064	0.000	0.000	0.020	1.430
19	0.000	0.000	0.000	0.000	0.000	0.000	0.000	0.000	0.018	0.000	0.000	0.575	0.098	0.000	0.021	0.027	1.502
20	0.000	0.000	0.007	0.000	0.000	0.000	0.000	0.000	0.021	0.000	0.000	0.735	0.141	0.000	0.027	0.038	1.504
21	0.000	0.000	0.008	0.000	0.000	0.000	0.000	0.008	0.027	0.000	0.000	0.962	0.186	0.014	0.029	0.060	1.537
22	0.000	0.000	0.011	0.000	0.000	0.000	0.000	0.010	0.034	0.014	0.000	1.222	0.218	0.018	0.034	0.077	1.580
23	0.000	0.000	0.020	0.000	0.000	0.000	0.000	0.011	0.044	0.015	0.000	1.527	0.253	0.022	0.042	0.102	1.652
24	0.000	0.000	0.025	0.000	0.000	0.000	0.000	0.015	0.058	0.015	0.000	1.815	0.278	0.025	0.043	0.121	1.711
26	0.000	0.000	0.047	0.000	0.000	0.009	0.000	0.023	0.070	0.015	0.000	2.083	0.284	0.053	0.041	0.138	1.681
28	0.000	0.000	0.089	0.000	0.000	0.010	0.000	0.030	0.083	0.034	0.000	2.454	0.312	0.082	0.047	0.163	1.740
30	0.000	0.000	0.142	0.000	0.000	0.011	0.008	0.041	0.095	0.084	0.000	2.720	0.322	0.102	0.047	0.189	1.720
32	0.000	0.000	0.190	0.000	0.000	0.016	0.012	0.049	0.104	0.131	0.000	2.883	0.330	0.106	0.050	0.202	1.699
34	0.000	0.000	0.225	0.000	0.000	0.020	0.015	0.052	0.112	0.160	0.000	3.013	0.338	0.111	0.051	0.213	1.755
36	0.002	0.000	0.297	0.000	0.000	0.026	0.030	0.063	0.127	0.204	0.000	3.302	0.362	0.122	0.055	0.231	1.880
38	0.002	0.000	0.369	0.000	0.010	0.035	0.047	0.070	0.141	0.242	0.000	3.575	0.378	0.133	0.056	0.248	1.947
40	0.002	0.000	0.443	0.012	0.010	0.044	0.067	0.079	0.146	0.273	0.036	3.694	0.378	0.143	0.055	0.259	1.825
45	0.002	0.000	0.640	0.014	0.012	0.072	0.115	0.100	0.170	0.349	0.045	4.122	0.395	0.163	0.059	0.288	1.731
50	0.002	0.000	0.843	0.016	0.015	0.102	0.154	0.118	0.190	0.405	0.050	4.635	0.427	0.180	0.062	0.315	1.812
55	0.003	0.000	0.969	0.022	0.018	0.124	0.172	0.125	0.195	0.423	0.049	4.849	0.429	0.184	0.063	0.319	1.793
60	0.003	0.005	1.097	0.029	0.022	0.148	0.190	0.136	0.206	0.448	0.052	5.168	0.444	0.194	0.064	0.335	1.791
65	0.003	0.006	1.185	0.035	0.026	0.165	0.200	0.142	0.208	0.455	0.051	5.279	0.437	0.192	0.063	0.336	1.722
70	0.003	0.007	1.270	0.039	0.030	0.182	0.211	0.148	0.211	0.465	0.052	5.427	0.441	0.197	0.064	0.343	1.701
75	0.003	0.010	1.364	0.045	0.033	0.199	0.223	0.156	0.215	0.478	0.053	5.623	0.448	0.202	0.063	0.350	1.713
80	0.003	0.013	1.435	0.049	0.036	0.215	0.229	0.160	0.218	0.482	0.054	5.745	0.452	0.204	0.063	0.356	1.729
90	0.004	0.016	1.519	0.056	0.042	0.233	0.237	0.164	0.220	0.485	0.054	5.904	0.459	0.205	0.065	0.365	1.763
100	0.003	0.020	1.546	0.061	0.044	0.239	0.236	0.166	0.219	0.472	0.053	5.944	0.462	0.201	0.066	0.365	1.795
110	0.004	0.022	1.568	0.065	0.046	0.247	0.235	0.167	0.219	0.467	0.054	5.912	0.462	0.204	0.067	0.367	1.803
120	0.004	0.025	1.631	0.070	0.049	0.257	0.239	0.173	0.226	0.475	0.056	6.094	0.481	0.212	0.069	0.380	1.875
130	0.004	0.028	1.603	0.070	0.049	0.254	0.234	0.170	0.222	0.462	0.056	5.987	0.477	0.208	0.068	0.375	1.868
140	0.003	0.029	1.602	0.072	0.049	0.253	0.229	0.170	0.223	0.457	0.057	5.977	0.475	0.209	0.068	0.377	1.856
150	0.003	0.031	1.605	0.073	0.051	0.254	0.228	0.172	0.221	0.451	0.060	6.002	0.471	0.210	0.068	0.381	1.817
160	0.003	0.033	1.609	0.073	0.050	0.256	0.227	0.173	0.223	0.448	0.062	6.005	0.469	0.211	0.069	0.386	1.762
170	0.003	0.033	1.632	0.075	0.050	0.260	0.228	0.176	0.227	0.451	0.066	6.101	0.477	0.215	0.068	0.396	1.766
180	0.003	0.034	1.627	0.075	0.050	0.260	0.228	0.178	0.228	0.452	0.068	6.110	0.478	0.219	0.069	0.400	1.770
190	0.003	0.034	1.623	0.075	0.050	0.261	0.227	0.179	0.231	0.450	0.071	6.123	0.484	0.222	0.069	0.403	1.784
200	0.003	0.033	1.578	0.073	0.049	0.253	0.221	0.175	0.227	0.439	0.071	5.983	0.476	0.218	0.070	0.398	1.758

Charge Transfer Reactions of C_4F_6

The evolution of an ion ensemble produced by 50 eV electron impact on a 1:1 Ar:C_4F_6 mixture is shown in figure 19. The fastest reactions are the ion-molecule reaction of Ar^+:

$$Ar^+ + C_4F_6 \rightarrow Ar + C_4F_5^+ + \{Ar, F\}$$
$$\rightarrow Ar + C_4F_3^+ + \{Ar, CF_3\}$$

with a branching ratio of approximately 3:2. Although these preliminary measurements suggest that lighter ions such as CF^+ produces $C_4F_6^+$, double resonance experiments would be required to isolate these reactive channels. We also observed traces of the $C_6F_6^+$ and $C_6F_7^+$ ions at the longest delays. It is intriguing to speculate on whether these ions are cyclic or aromatic, however their yield is too low (less than 3% after 500 ms at 10^{-6} Torr) to infer much about their bonding. This is one of the few perfluorocarbon cases that we have studied where products with masses greater than that of the parent neutral have been observed.

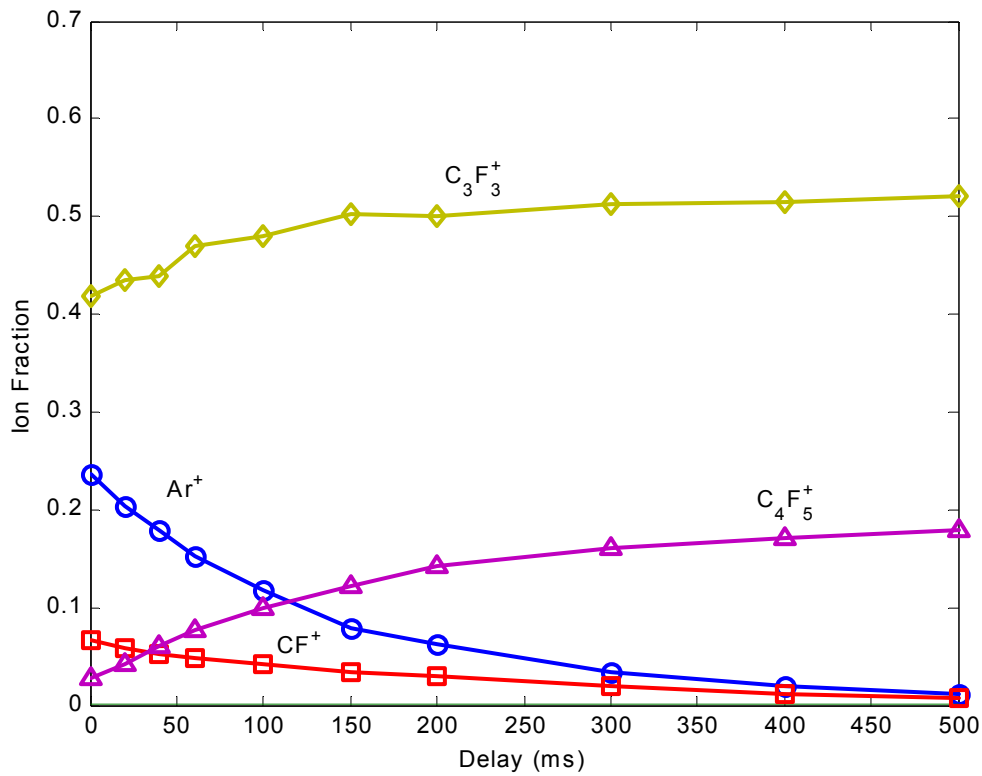

Figure 19. Ion composition following irradiation of a 1:1 mixture of Ar and C_4F_6 with 50 eV electrons

Ion chemistry in pentafluoroethane, C_2HF_5

Dissociative ionization of pentafluoroethane

The ionization of difluoromethane has been examined by FTMS. The total ionization cross section peaks at 5.2 x 10^{-16} cm^2 at 85 eV. As seen in figure 20 below, the CHF_2^+ ion

is the principal species, accounting for about 40% of the ion yield above 30 eV. The remaining ions include products of C-C, C-H, and C-F bond cleavage, but no parent molecular ion is observed. Traces of F^+ are observed, but the cross section for this channel is less than 10^{-18} cm^2 at energies below 200 eV.

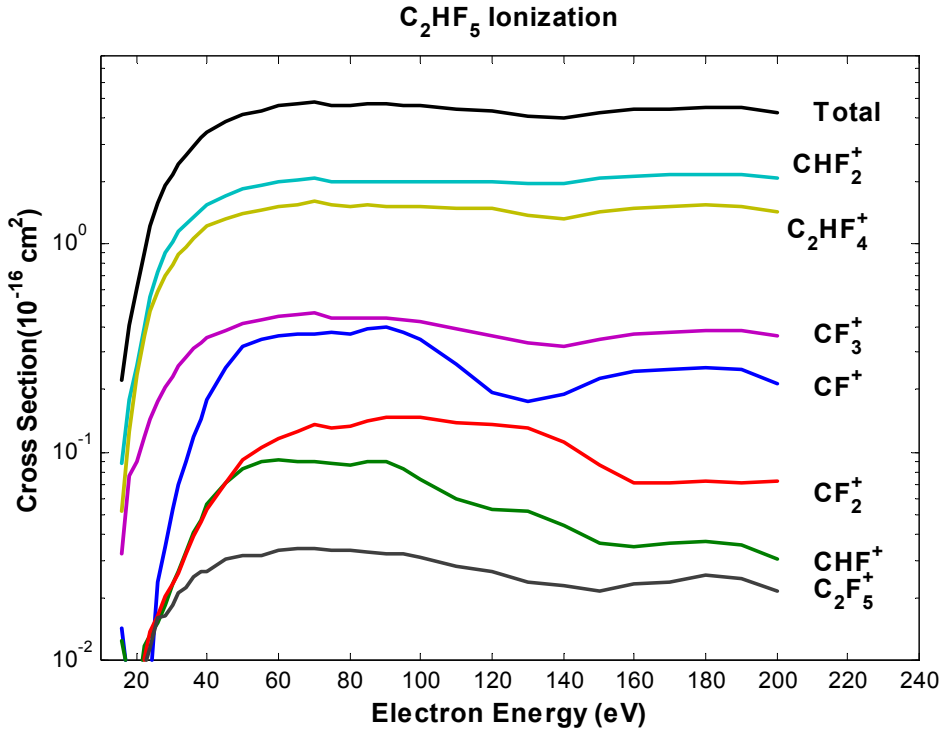

Figure 20. Partial ionization cross-sections of C_2HF_5

The BEB estimate for ionization of pentafluoroethane represents the slope of the cross section near threshold with good agreement, but the peak value of 7.5 x $10^{-16}cm^2$ is substantially higher than the experimental cross section of 4.2 x $10^{-16}cm^2$.

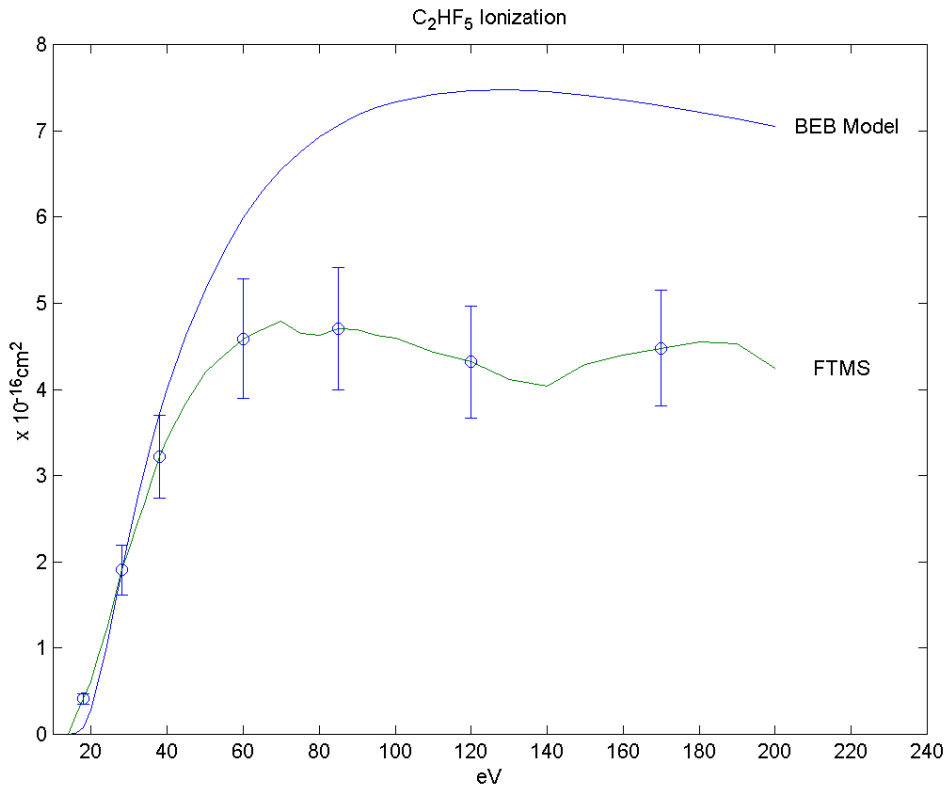

Figure 21. BEB estimate of total ioniztion cross section for pentafluoroethane

Charge transfer chemistry in C_2HF_5

The principal fate of an ion ensemble that contains Ar and C_2HF_5 is net abstraction of F^- by Ar^+ to produce $C_2HF_4^+$. At longer times, however, traces of water vapor provide a rich mixture of oxygen bearing ionic products. As can be seen in 19 below, 15% of the ion composition contains oxygen after half a second at 10^{-6} Torr total pressure. The overall reaction that is most likely to be responsible for CO bond formation is shown in figure 23:

$$C_2HF_4^+ \ + \ H_2O \ \rightarrow C_2HF_2O^+ \ + \ 2HF$$

The thermodynamic driving force for reactions of this type is HF bond formation, and the mechanism seems general for several of the hydrofluorocarbon cations, as outlined in for the fate of heptafluoropropyl cations (produced from perfluoropropane) in figure 24.

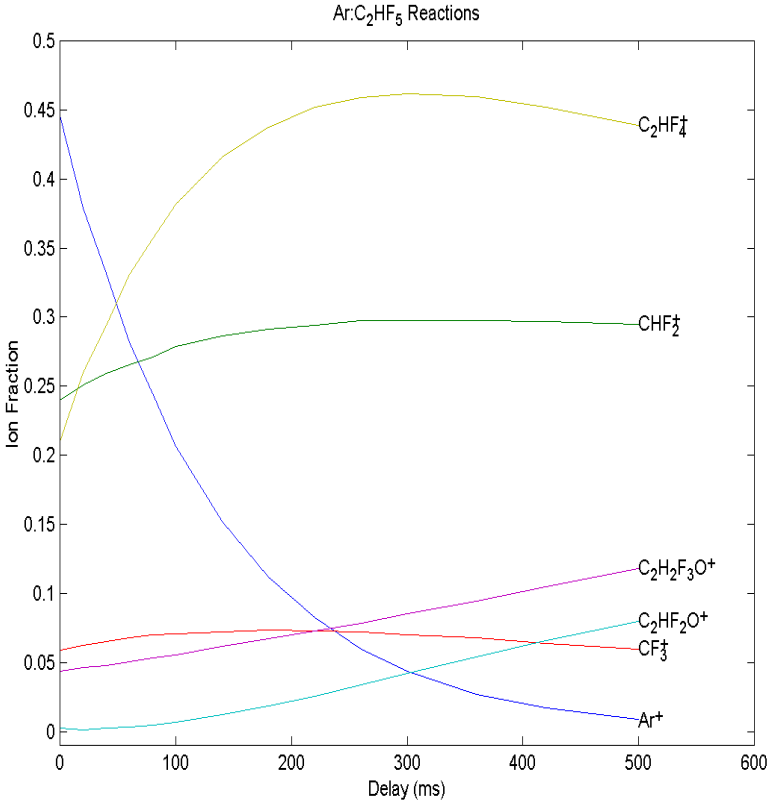

Figure 22. Relaxation of ion composition in a mixture of pentafluoroethane and argon. The background pressure of water vapor is approximately 6 x 10^{-8} Torr

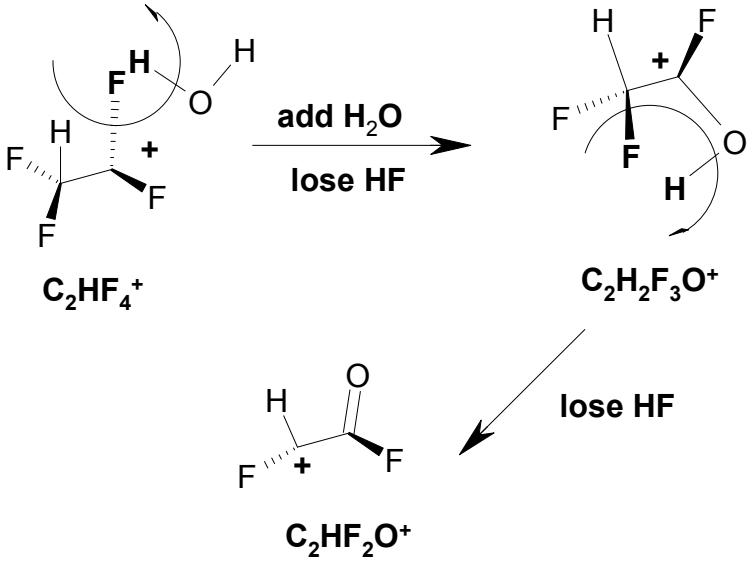

Figure 23. Outline of chemical mechanism for production of $C_2HF_2O^+$

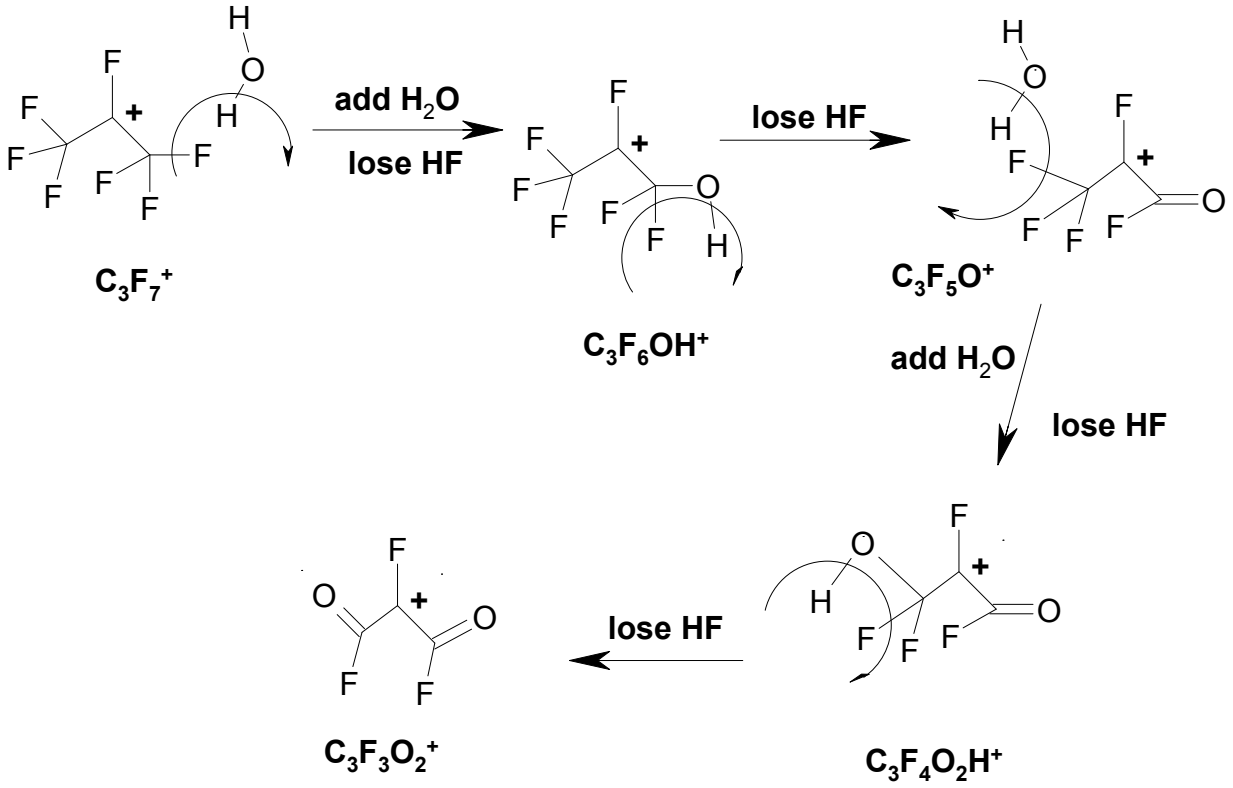

Figure 24. Outline of mechanism for production of other oxygen bearing hydrofluorocarbons from $C_3F_7^+$ produced by perfluoropropane. The overall reaction is

$$C_3F_7^+ + 2\ H_2O \text{ è } C_3F_3O_2^+ + 4\ HF$$

Ion chemistry of 1,1,1,2 tetrafluoroethane, $C_2H_2F_4$

Dissociative ionization of $C_2H_2F_4$

Ten ion species, including the parent $C_2H_2F_4^+$ and F^+ ions, are produced by electron impact on 1,1,1,2 tetrafluoroethane.

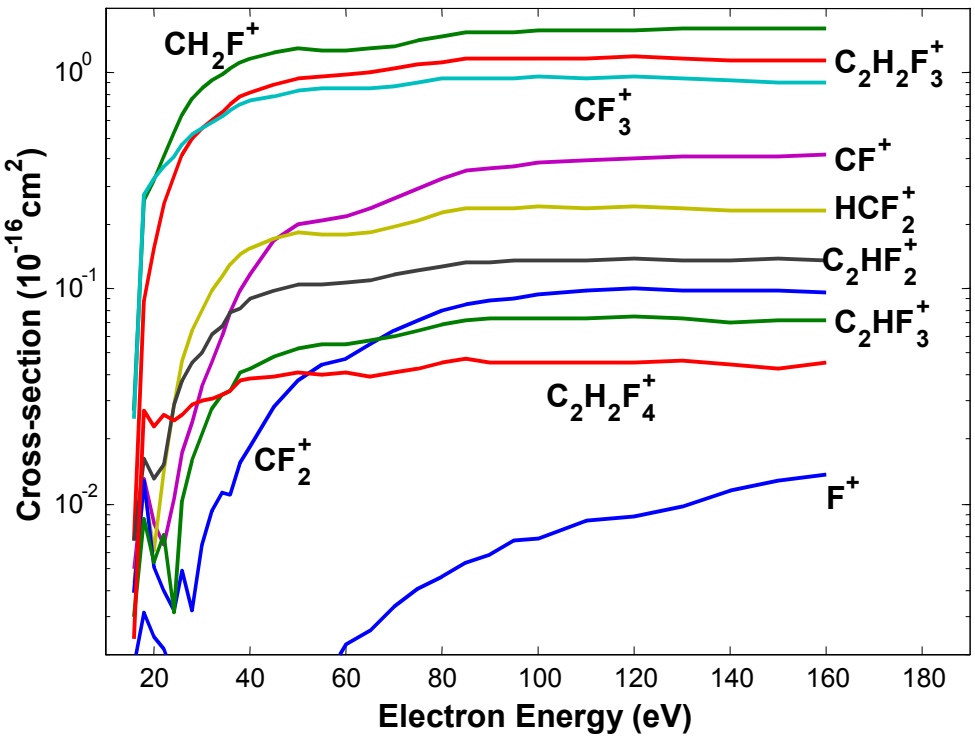

Figure 25. Ionization of 1,1,1,2 tetrafluoroethane by electron impact

The BEB model overestimates the total ionization cross section but has a plausible energy dependence near threshold, as may be sen in figure 26.

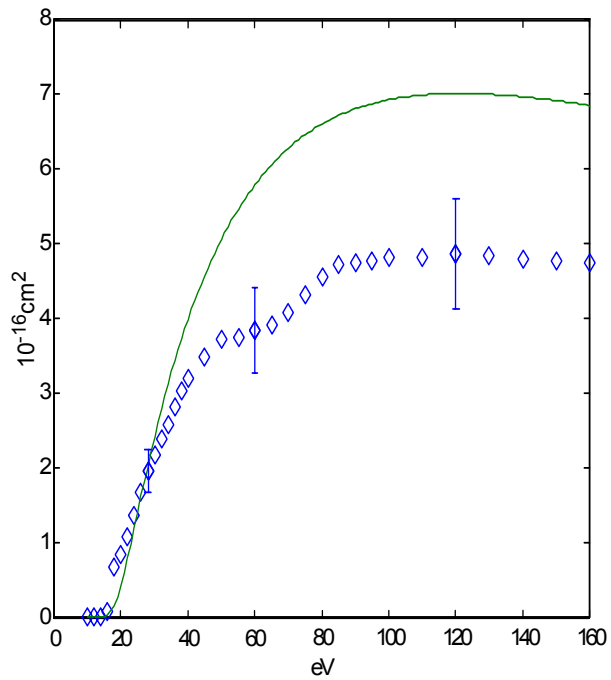

Figure 26. Total ionization cross section of 1,1,1,2 tetrafluoroethane by the BEB model (solid line) and from FTMS measurements (diamonds)

Charge transfer reactions of $C_2H_2F_4$

The principal reaction following irradiation of an argon:tetrafluoroethane mixture is net abstraction of an F^- to produce $C_2H_2F_3^+$:

$$Ar^+ + C_2H_2F_4 \rightarrow C_2H_2F_3^+ + \{Ar,F\}.$$

Net abstraction of H^- also occurs, but at a rate that is 100 times slower:

$$Ar^+ + C_2H_2F_4 \rightarrow C_2HF_4^+ + \{Ar,H\}.$$

Although no clusters with more than two carbons were observed to form, reaction with background water vapor ($P<10^{-8}$ Torr) appears to protonate the latter according to the reactions:

$$C_2H_2F_3^+ + H_2O \rightarrow H_3O^+ + \{C_2F_3\} \text{ and}$$
$$CH_2F^+. + H_2O \rightarrow H_3O^+ + \{CHF\}$$

A less prominent reaction of water that was found in pentafluoroethane ion chemistry is observed in figure 27:

$$H_2O + C_2HF_4^+ \rightarrow C_2HF_2O^+ + 2HF,$$

as is a similar hydration reaction with CF_3^+

$$H_2O + CF_3^+ \rightarrow CHF_2O^+ + HF.$$

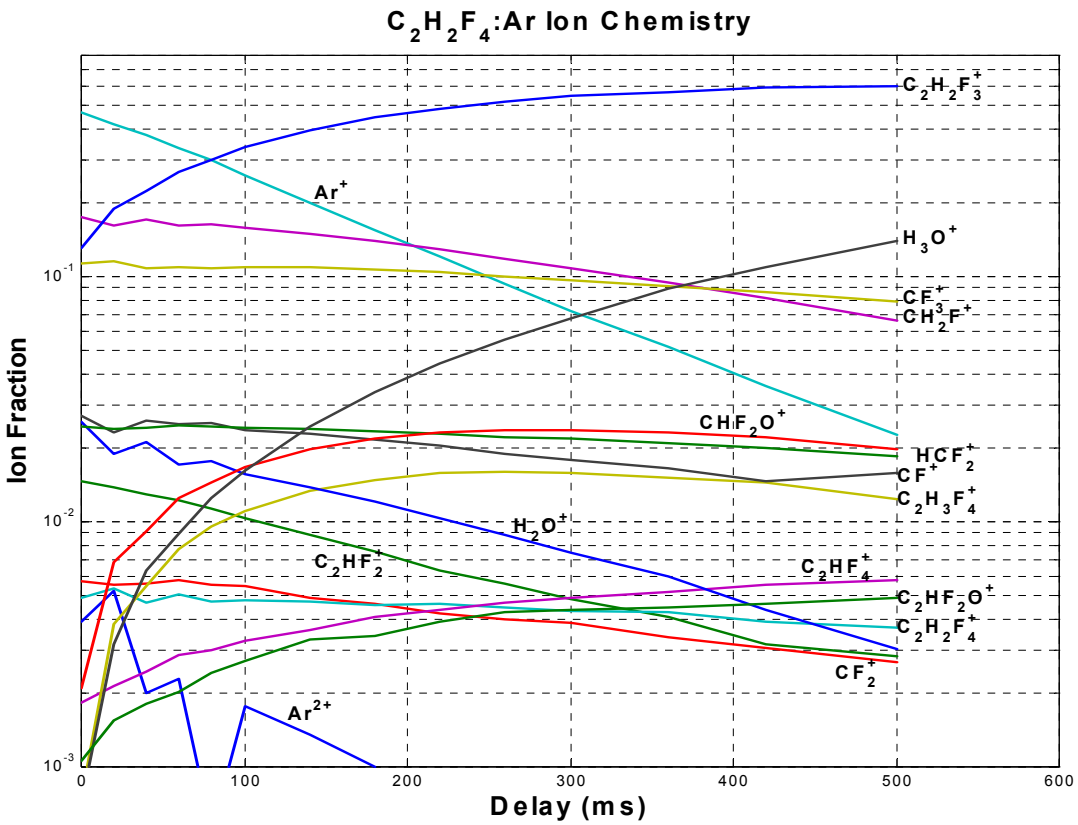

Figure 27. Evolution of ion composition following radiolysis of a mixture of argon and 1,1,1,2 tetrafluoroethane

Binary Encounter Bethe estimates of fragmentation in C_2F_6

There are, on statistical grounds, 21 possible ion species that might be formed by dissociative ionization of perfluoroethane. Of these, several are unlikely (F_6^+ for example). On chemical grounds I think that the following 14 possible stoichiometries remain plausible:

$$F, F_2, C, CF, CF_2, CF_3, CF_4, C_2, C_2F, C_2F_2, C_2F_3, C_2F_4, C_2F_5, C_2F_6.$$

Of these possible fragments only four are observed to form by electron impact: CF_2^+, CF^+, $C_2F_5^+$, and CF_3^+.

Why? There are, it turns out, molecular orbitals with four distinct symmetries in the electronic structure of perfluoroethane: e_g, e_u, a_g, and a_u. When I sum the contributions to the BEB cross-section for each symmetry I get the results shown in the figure 28 below:

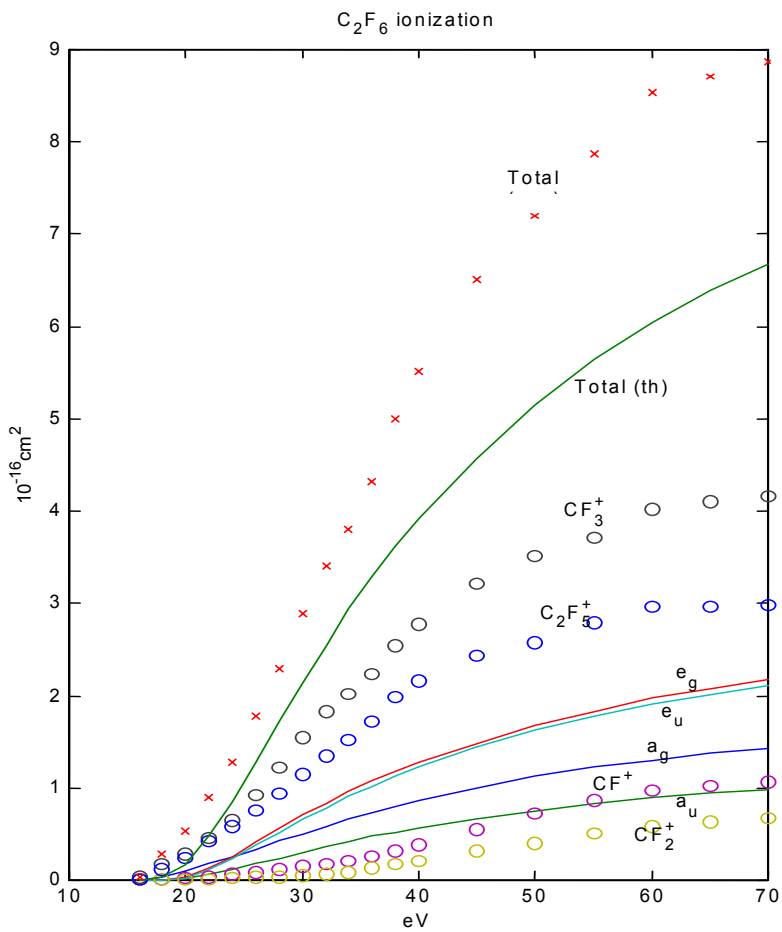

Figure 28. BEB cross-sections for C_2F_6 ionization summed by orbital symmetry

Theoretical values are shown as solid lines. Note that the doubly degenerate contributions have about the same magnitude, arguably the CF_3 and C_2F_5 fragments are produced in roughly equal yield. The singly degenerate orbitals make smaller contributions in rough proportion to the observed cross-sections for CF^+ (a_g) and CF_2^+ (a_u).

The results at left were computed using Carl's RHF 6-311+g* GAMESS results. I tried the same thing using the HF potential and kinetic energies posted by Kim on the nist web site. The energies are compared in the table 7 below.

Similar results are obtained for the partial ionization cross-sections using the Kim orbital energies (figure 29).The extent to which these orbital energies are 'tweaked' is not discussed in the web page, so the apparent qualitative agreement between Carl's and Kim's numbers is quite good, with the same ordering and relative importance computed for contributions from each orbital symmetry.

Table 7. Summary of orbital potential (U) and kinetic (T) energies (eV) for perfluoroethane from Kim (http://physlab.nist.gov/cgi-bin/Ionization) and Carl Winstead

Symmetry	U (Kim)	T (Kim)	# of electrons	U(Carl)	T(Carl)
1EG	717.05	1013.49	4	717.93	1013.44
1EU	717.05	1013.50	4	717.93	1013.44
1A2U	717.05	1013.51	2	717.93	1013.44
1A1G	717.05	1013.53	2	717.93	1013.44
2A1G	314.56	436.28	2	314.75	436.57
2A2U	314.55	436.53	2	314.73	436.57
3A1G	48.90	88.82	2	48.92	88.10
3A2U	48.16	94.16	2	48.22	93.65
2EU	46.05	103.39	4	46.01	103.58
2EG	45.60	107.04	4	45.72	106.25
4A1G	29.74	69.84	2	30.04	69.42
4A2U	26.56	83.75	2	26.73	83.50
5A1G	24.98	65.27	2	24.99	66.40
3EU	24.12	74.26	4	24.21	74.92
3EG	23.17	78.30	4	23.37	77.47
5A2U	20.68	84.03	2	21.03	83.76
4EG	20.86	82.12	4	20.49	85.43
4EU	19.82	87.85	4	20.43	86.26
5EU	18.40	88.57	4	19.49	8<9.53
5EG	16.36	94.04	4	18.98	94.15
6A1G	17.56	95.50	2	18.68	95.98
6A2U	17.39	93.54	2	18.68	95.98
7A1G	14.48	79.89	2	16.43	81.75

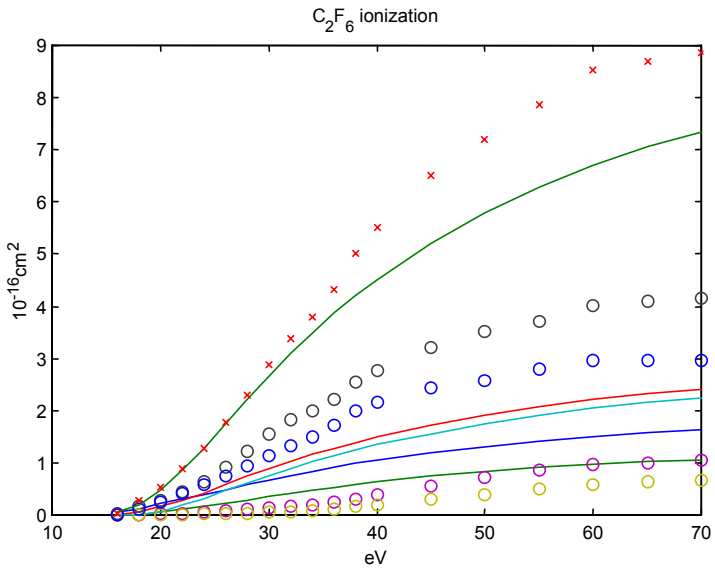

Figure 29. Cross-sections using Kim orbital energies. Legend is identical to that of figure 28

Summing orbital contributions to the BEB cross section of SiF_4:gives four contributions as shown below in figure 30:

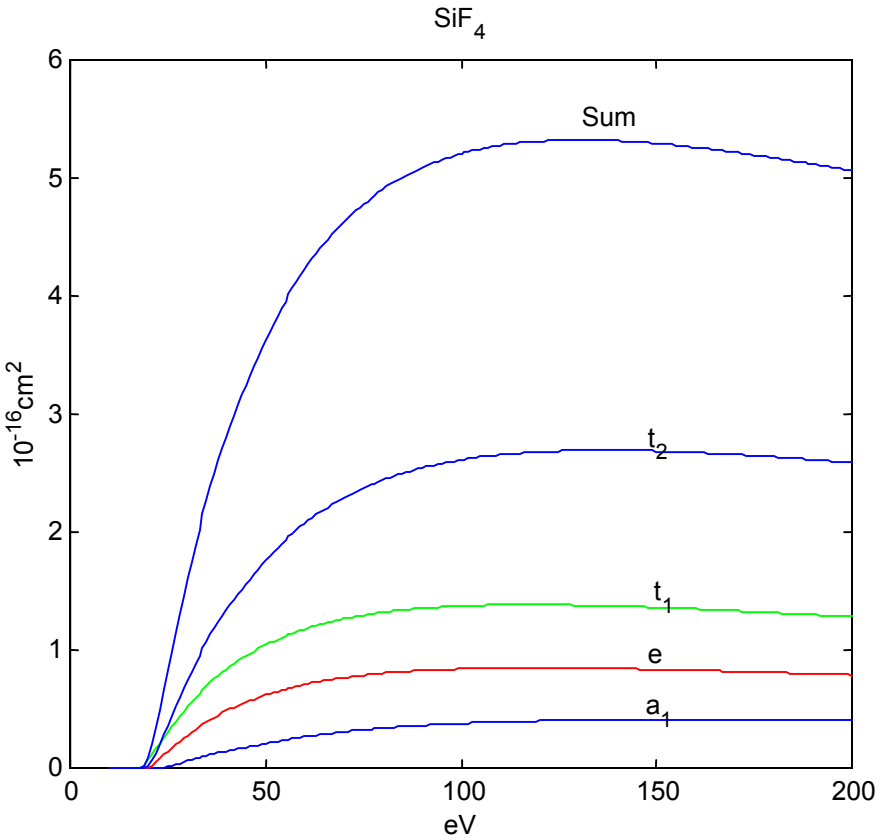

Figure 30. Contributions to BEB ionization cross section of silicon tetrafluoride from orbitals of each symmetry

Below 200 eV the numbers of electrons in each symmetry are (A_1 6), (E 4), (T_1 6), and (T_2 24).. There does not appear to be a correlation between the occupancy in each symmetry and the relative cross-sections. At first glance the quantitative disparity between the largest and next largest partial ionization cross-section is greater (experimentally) than that inferred from the t2-t1 disparity shown above.

Symmetry summed contributions to the BEB cross section for CH_2F_2:are shown below. The electron count below 80 eV by symmetry is (a1, 8), (a2, 2), (b1,6), and (b2,4). Again, there is no obvious correlation between the electron count and the peak cross-sections. The difference between Carl Winstead's latest HF wavefunctions and the earlier values is insignificant.

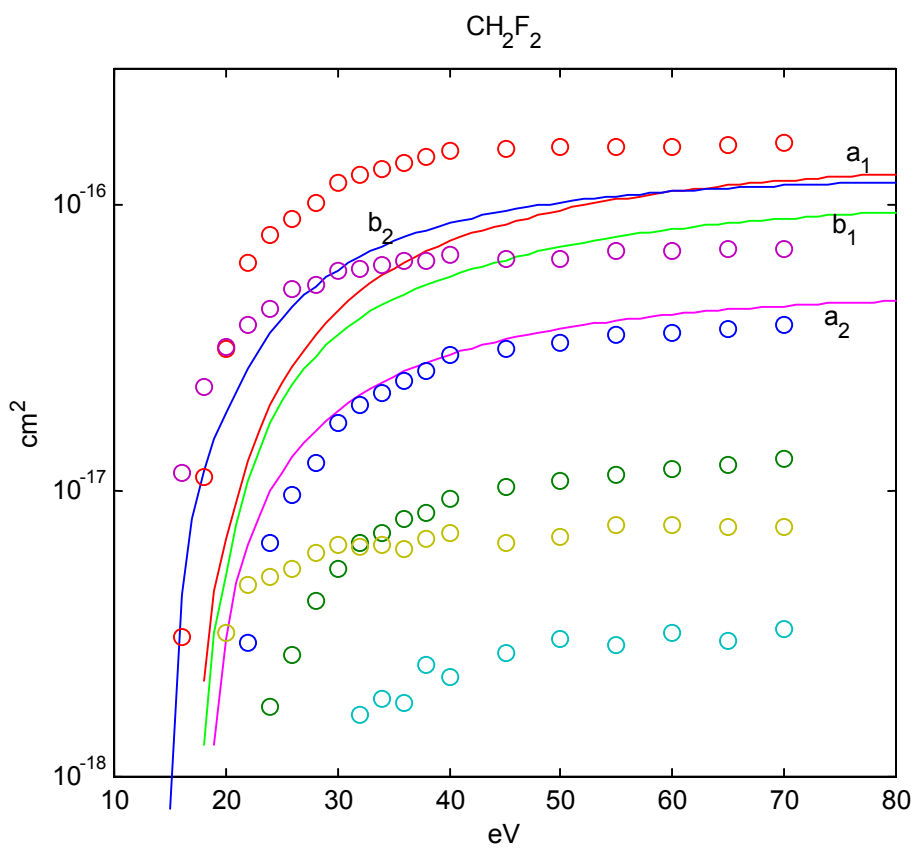

Figure 31. Contributions from each orbital symmetry to the BEB ionization cross section of difluoromethane. Circles are experimental values for each of the six fragment channels

Circles show the experimental cross-sections. Note that six fragments are observed, though only four distinct symmetries are possible for the MO's. Also, the cross-sections' cross-overs ~20 eV is not reproduced by the symmetry-summed contributions.

Appendix A: Ion Chemistry in trifluoromethyl bromide and iodode:

A Comparison of Ion Chemistries of CF_3Br and CF_3I

C.Q. Jiao[a], B. Ganguly[b], C.A. DeJoseph Jr.[b], A. Garscadden[b,*]
[a] Mobium Enterprises, Inc., 5100 Springfield Pike, Dayton, OH 45431-1231, USA
[b] Air Force Research Laboratory, Wright-Patterson AFB, OH 45433-7251, USA
(December 15, 2000)

Abstract
A comparison of the electron impact ionization and ion-molecule reactions of CF_3Br vs. CF_3I is made by studying the two compounds using Fourier-transform mass spectrometry. The ionization of the two compounds over the energy range from threshold to 70 eV produces primarily the molecular ion and 6 fragment ions, with the dominant ion from CF_3Br being CF_3^+ and, from CF_3I, CF_3I^+. The total cross-sections at 70 eV are 8.3 ± 0.8 and 9.0 ± 0.9 $x10^{-16}$ cm^2 for CF_3Br and CF_3I, respectively. The ion-molecule reactions in the two compounds are similar, with CF^+ and X^+ (X = Br or I) being the most reactive ions ($k \sim 8 - 13$ $x10^{-10}$ cm^3s^{-1}). Ar^+ reactions with the two compounds are also studied. Results of our study on the ion kinetics are compared with those from previous studies by other groups.

I. Introduction

CF_3Br had been widely used as a fire suppressant in the past fifty years and as an etching gas in many plasma applications. Now its uses are greatly restricted by law because of its significant contribution to stratospheric ozone depletion due to its long lifetime in the troposphere and its ready photodissociation by short wavelength ultraviolet light in the stratosphere. In the search for halon alternatives during the past years, CF_3I has become a leading replacement agent, in either the fire suppression or plasma assisted fabrication applications.[1-6] A comparison of the chemistries of these two compounds, in terms of ionic as well as neutral processes, and in terms of gas-phase collisions as well as surface interactions, is therefore of interest and importance. There is a limited amount of information about the basic physical/chemical mechanisms of the two compounds' applications. In the fire suppression by CF_3Br the chemical effectiveness is considered to be mainly due to Br radicals.[7] In the etching of SiO_2 using CF_3I, it is reported that while CF_2 radicals are the main gas precursors for deposition of the fluoropolymer that is useful to protect any adjacent Si, ions including CF_3^+ are important in the reactive ion etching of SiO_2.[5]

This paper presents cross-sections of the electron impact ionization of CF_3Br and CF_3I, and the kinetics of gas-phase reactions between the ions derived from the two compounds and the parent molecules. Although the ionization cross-sections of the two compounds are reported for the first time, the gas-phase ion-molecule reactions, of CF_3I in particular, have been an object of several studies by different groups in the past decades.[8-11] However, there are numerous differences among the results reported from different groups. Some of these differences have been explained by the different experimental methods in which ions are formed and reacted under varied conditions resulting in various internal-state distributions of ions and reaction mechanisms.[9,11] In our study the experimental technique differs from the others in either (1) the gas pressure is low (10^{-7} Torr) so only bimolecular processes are important, or (2) the reactant ions to be studied are isolated from each other so the reactant-product relationship and the product branching ratios can be determined less ambiguously. On the other hand, our rates are for the ions as formed by electron impact or from charge transfer. The ions are nascent and have energy distributions that are relevant to plasma processing models.

II. Experimental

All experiments are performed on a modified Extrel Fourier-transform mass spectrometer (FTMS) equipped with a cubic ion cyclotron resonance trapping cell (5 cm on a side) and a 2 T superconducting magnet.[12] The theory and methodology of FTMS have been well documented in the literature.[13-15] Typically, CF_3Br (99%, GL Service) or CF_3I (99%, Aldrich) is mixed with argon (99.999%, Matheson Research Grade) with a ratio about 1:1 to a total pressure of ~800 Torr, as determined by capacitance manometry. The mixture is admitted through a precision leak valve into the FTMS system. Ions are formed by electron impact in the trapping cell at pressures in the 10^{-7} Torr range. An electron gun (Kimball Physics ELG2, Wilton, NH) irradiates the cell with a few hundred picocoulombs of low-energy electrons. The motion of the ions is constrained radially by the superconducting magnetic field and axially by an electrostatic potential (1 V) applied to the trap faces that are perpendicular to the magnetic field. Ions of all mass-to-charge ratios are simultaneously and coherently excited into cyclotron orbits using Stored Waveform Inverse Fourier Transform (SWIFT)[16-18] applied to two opposing trap faces

which are parallel to the magnetic field. Following cyclotron excitation, the image currents induced on the two remaining faces of the trap are amplified, digitized and Fourier analyzed to yield a mass spectrum. In some experiments ions are selected using SWIFT[18] for further kinetic studies.

The integrated peak intensities, which are proportional to the number of ions in the trapping cell,[15] are used to establish the cross sections, as described previously.[12,19] The intensity ratios of the ions from CF_3Br (or CF_3I) to Ar^+ give cross sections relative to those for argon ionization[20] since the pressure ratio of CF_3Br (or CF_3I) to Ar is known. As a cross check, and for ion molecule kinetic analyses, the gas pressure is calibrated using accumulated gas pulses from a pulsed valve and a spinning rotor friction gauge (MKS Instruments model SRG2, Burlington, MA) with the vacuum chamber sealed off from the pumps. The electron current is collected on a Faraday cup and recorded with a digital oscilloscope after passage of the electron beam through the ion trap. The quantitative relationship between the image current and the number of ions is based on an analysis of the image currents induced on the detection plates of the cubic ICR cell. This analysis, is similar to those described in the literature.[15]

III. Results and Discussion

IIIa. Electron impact ionization

Electron impact ionization on CF_3Br at energies from threshold to 70 eV produces molecular ions and 6 fragment ions, with a total ionization cross-section reaching $8.3\pm0.8 \times 10^{-16}$ cm^2 at 70 eV. Cross-sections for each partial ionization channel are shown in Figure 1. Trace amounts of $CFBr^+$ and F^+ (not shown in the figure) have been observed but the cross-sections are less than 10^{-18} cm^2. CF_3^+ is the most abundant ion in the energy range studied. The appearance potentials of CF_3^+ (from CF_3Br) and CF_3Br^+ are rather close, being 12.2 and 12.3 eV,[21] respectively, and the Jahn-Teller distortion effect results in an increased probability of the molecular ion dissociating to form CF_3^+, which makes CF_3Br^+ less abundant than CF_3^+ even at energies near threshold. At energies above 15 eV, a second dissociation channel forming CF_2Br^+ becomes available. In brief, the neutral radicals produced by the electron impact ionization at energies from the threshold to 20 eV are expected to be primarily Br and, secondly, F atoms, as they are the counter partners of the ionic product CF_3^+ and CF_2Br^+, respectively.

Electron impact ionization on CF_3I produces a similar set of ions corresponding to those from CF_3Br, but the relative order of the ion abundances is different. Figure 2 presents the partial ionization cross-sections of CF_3I, showing that the molecular ion CF_3I^+ dominates over the whole energy range. Compared to CF_3Br, the ionization threshold is lower and the total ionization cross-section is slightly greater, reaching $9.0\pm0.9 \times 10^{-16}$ cm^2 at 70 eV. The most abundant fragment ion at energies below 20 eV is still CF_3^+, followed by I^+ and CF_2I^+, and therefore the corresponding neutral radical products are I, CF_3 and F, in the order of decreasing importance. CF_3^+ and I^+ appear to be the products of two competing dissociation channels via the cleavage of CF_3-I bond in the molecular ion. At energies near threshold, CF_3^+ prevails because it has a lower ionization potential than I^+,[22] complying with Stevenson's rule that states that the positive charge will remain on the fragment of lower ionization potential.[23] Data in Figure 2 show that in the higher energy range, I^+ has greater intensities than CF_3^+, which may be due to the formation of I^+ by more extensive fragmentation of the molecule rather than a simple

CF_3-I bond cleavage, and therefore it is implied that as the collisional energy increases, the neutral partner of the I^+ product may not be simply CF_3.

IIIb. Gas-phase ion-molecule reactions

Table 1 presents the kinetics of the reactions of ions derived from CF_3Br or CF_3I with their parent molecules (CBr^+ and CI^+ are not included because they have too small intensities to be studied), which are compared with the results from other studies. Also included in the table are Ar^+ reactions with the two compounds. The reactant ions are generated by 50 eV electron impact ionization on a mixture of CF_3Br or CF_3I with Ar. Each of the reactant ions is separated from the others by rf excitation to eject all of the unwanted ions out of the trapping cell, followed by a varying reaction time to study the reaction kinetics of the selected ion. The rate coefficients listed in the table are accurate to within $\pm$20%, based on the uncertainty in the pressure measurements. The relative rate coefficients are more accurate, however, with the uncertainties estimated to be $\pm$10%. The ion chemistries in both of the compounds are similar: CF_2^+ and X^+ (X = Br or I) are the most reactive ions, CF^+ and CF_3^+ are relatively less reactive, and CF_2X^+ and CF_3X^+ are basically unreactive. We noted that a small portion of CF_3Br^+ undergoes collision-induced dissociation yielding CF_3^+, due to the internally energetic ions that have sufficient energy to permit bond-breaking. After CF_3Br^+ is trapped for 0.3 s under the gas pressure of ~10^{-7} Torr, no more reaction producing CF_3^+ is observed, because the CF_3Br^+* excited ion population has been reduced to a negligible amount by a combination of reactive collisions and collisional/radiative quenching. In table 1, the reactions of CF_3^+ have the lowest reaction rates. It was found that semilogarithmic plots of the CF_3^+ reactions show a linear CF_3^+ decay up to 0.5 s reaction time when about 30% of CF_3^+ has been consumed. At longer reaction time CF_3^+ is found to continue reacting but the data at that time were not used to define the reaction rate because, at these long times, the ion signal has been reduced to a value too small to be quantitatively meaningful. There is a slow loss of ions due to collisional diffusion across the magnetic field.[19] The CF_3^+ reactions, however, are believed to be caused by the excited state(s) of the ion, as suggested by the endothermicities of the following reaction equation that are calculated using the heats of formation of the ground state ions:

$$CF_3^+ + CF_3X \rightarrow CF_2X^+ + CF_4 .$$

The reaction heats are 26.2 and 16.1 kJ/mol for X = Br and I, respectively, based on the thermochemical data from reference 24. If the heat of formation for CF_3^+ is taken to be the recently published values, 360.8 kJ/mol[25] or 407.5 kJ/mol[26], the endothermicities are even greater. Other equations for the CF_3^+ reaction (i.e., in which different neutral products are formed) are possible but they are more endothermic than the above equation. We have experimental evidence, as mentioned below, suggesting that at least ground state CF_3^+ is unreactive. The CF_3^+ reactivities given above suggest that long-lived excited state(s) of CF_3^+ having a rather low collisional quenching rate are formed by the electron impact ionization of CF_3Br or CF_3I.

The difference among the results from different studies shown in Table 1, in terms of the reaction rates and product branching ratios, are believed to be mainly due to different experimental conditions that result in different ion internal energies and/or ion-molecule reaction mechanisms. At the pressure of ~10^{-7} Torr the reactant ions generated from the electron impact ionization do not experience enough collisions to be thermalized

before being reacted with their parent molecules. A comparison of our results with Morris *et al.*'s SIFDT (Selected Ion Flow Drift Tube) experiments in Table 1 appears to demonstrate that the reactant ions in our experiments have some population of excited states. CF^+ and CF_3^+ are shown in Morris *et al.*'s study to have significant negative temperature-dependences of reaction rates,[10] which may be the explanation of lower reaction rates we observed because of the more energetic ions. In our experiments, we also observed that as a function of the reaction time the product percentage of CF_3^+ decreases and the percentage of CF_2X^+ increases. Although the changes of the percentages may be partly due to the secondary reaction of CF_3^+ as discussed later, it may be that the branching ratios of the reactions forming CF_3^+ and CF_2X^+ change as functions of the reaction time because of the reactant ions are being thermalized. The thermalized reactant ions may have the reaction branching ratios more or less in line with Morris *et al.*'s data. Secondary reactions have been observed for some ions. For example, I^+ reacts with CF_3I to yield CF_3^+ among other products, which, when isolated from other ions and allowed to collide with CF_3I, is found to react producing CF_2I^+. However, CF_3^+ derived from the Ar^+ reactions with CF_3X is not found to undergo secondary reactions with CF_3X, which may be an indicator that at least ground state CF_3^+ is unreactive with CF_3X.

The most significant differences between the SIFDT results and our FTMS results are the reactions of CF_2^+ with CF_3Br. While we observed a significant fraction of the molecular ion CF_3Br^+, none was reported in Morris *et al.*'s study. The explanation may be that under their experimental conditions either this ions is not formed or the ion is very weakly bound and is collisionally dissociated. The situation in the reaction of CF_2^+ with CF_3I appears similar but with the evidence that the molecular ion is formed and being detected in both experiments. The branching ratio of CF_3I^+ reported in the FTMS experiments equals to the sum of the branching ratios of CF_3I^+ and CF_3^+ reported in the SIFDT experiments, again raising the possibility of collision dissociation of the molecular ion.

The behaviors of the unreactive ions CF_2X^+ and CF_3X^+ when they are kinetically excited have been studied. CF_2X^{+*} ions are still not very reactive at a kinetic excitation energy range of 5-25 eV (laboratory-frame), producing only an insignificant amount of CF_3^+. At 50 eV kinetic excitation energy,

$CF_2Br^{+*} + CF_3Br \rightarrow CF^+(8\%), CF_2^+(26\%), CF_3^+(44\%), Br^+(5\%), CF_3Br^+(17\%)$;

$CF_2I^{+*} + CF_3I \rightarrow CF^+(3\%), CF_3^+(354\%), I^+(18\%), CF_3I^+(44\%)$.

In the above equations only the ionic products are listed, with the branching ratios shown in the parentheses. In the reaction of CF_2Br^+, the channel of producing Br^+ is identified to be a collision-induced dissociation while the channel of producing CF_3Br^+ is via a charge-transfer mechanism, as determined by the isotopic pattern of the product ions. Kinetically excited CF_3X^{+*} (made in our experiment by rf exciting the ion after its selection) undergoes reactions more readily, producing exclusively CF_3^+ in the energy range of 5-50 eV.

IV. Summary

Absolute ionization cross-sections have been measured for CF_3Br and CF_3I Electron impact ionization on CF_3Br or CF_3I produces primarily the molecular ion and 6 fragment ions with a total ionization cross-section at 70 eV of 8.3 ± 0.8 or $9.0\pm0.9 \times 10^{-16}$ cm^2, respectively. In CF_3Br, CF_3^+ is the principal ion over the energy range from threshold to 70 eV, while in CF_3I, the molecular ion CF_3I^+ is the most abundant. At low

electron energies (from threshold to 20 eV), which are most relevant to processing plasmas, the most important dissociative ionization channel is the production of CF_3^+ and X radical (X=Br or I) for both compounds. Other less important dissociative ionization processes at these low energies include the formation of CF_2X^+ and F radical. Among the ions derived from the ionization of the two compounds, CF_2^+ and X^+ are found to be the most reactive ions, while CF^+ and CF_3^+ are relatively less reactive, and CF_3X^+ and CF_2X^+ are basically unreactive. CF_3^+ reactions are believed to be caused by the hard-to-quench long-lived excited state(s) of CF_3^+. Some of the product ions from the primary ion-molecule reactions undergo further reactions with the neutral molecules, forming mainly CF_2X^+. In summary, the electron impact ionization on these two compounds produces the same set of ions, with slightly lower threshold and higher cross-section for the total ionization of CF_3I compared to CF_3Br. The ion-molecule reactions in these two compounds are similar, the differences including the additional minor products in CF_3I reactions.

Acknowledgements

The authors thank the reviewers for their valuable comments and the Air Force Office of Scientific Research for support.

References

* Corresponding author. Fax: 937-656-4657; E-mail: alan.garscadden@wpafb.af.mil

1. S. Solomon, J.B. Burkholder, A.R. Ravishankara, R. R. Garcia, Journal of Geophysical Research, 99 (1994) 20929.
2. W.L. Grosshandler, R. G. Gann, W. M. Pitts, Eds., "Evaluation of Alternative In-Flight Fire Suppressants for Full-Scale Testing in Simulated Aircraft Engine Nacelles and Dry Bays," NIST SP 861, 1994.
3. R. G. Gann, Ed., "Fire Suppression System Performance of Alternative Agents in Aireraft Engine and Dry Bay Laboratory Simulations," NIST SP 890, 1995.
4. K.C. Smyth, D.A. Everest, *Twenty-Sixth Symposium (International) on Combustion*, The Combustion Institute, Pittsburgh, 1996, p. 1385.
5. S. Samukawa, K. Tsuda, Jpn. J. Appl. Phys., 37 (1998) L1095.
6. F. Fracassi, R. d'Agostino, J. Vac. Sci. Technol. B 16 (1998) 1867.
7. R.R. Casias, J. T. Mchinnon, *Twenty-Seventh Symposium (International) on Combustion*, The Combustion Institute, Pittsburgh, 1998, p. 2731.
8. T. Hsieh, J.R. Eyler, R. J. Hanrahan, Int. J. Mass Spectrom. Ion Phys., 28 (1978) 113.
9. D.W. Berman, J.L. Beauchamp, Int. J. Mass Spectrom. Ion Phys., 39 (1981) 47.
10. R.A. Morris, A.A. Viggiano, J.M. Van Doren, J.F. Paulson, J. Phys. Chem. 96 (1992) 2597.
11. R.A. Morris, J.M. Van Doren, A.A. Viggiano, J.F. Paulson, J. Chem. Phys. 97 (1992) 173.
12. P. D. Haaland, Chem. Phys. Lett. 170 (1990) 146.
13. M. B. Comisarow, A. G. Marshall, Chem. Phys. Lett., 25 (1974), 282.

14. A. G. Marshall, P. B. Grosshans, Anal. Chem. 63 (1991), 215A.
15. Z. Liang, A. G. Marshall, Anal. Chem. 62 (1990), 70.
16. A. G. Marshall, T. L. Wang, T. L. Ricca, J. Am. Chem. Soc. 107 (1985) 7893.
17. S. Guan, J. Chem. Phys. 91 (1989) 775.
18. L. Chen, A. G. Marshall, Int. J. Mass Spectrom. Ion Processes, 79 (1987) 115.
19. P. Haaland, J. Chem. Phys. 93 (1990), 4066.
20. R. C. Wetzel, F. A. Baioochi, T. R. Hayes, R. S. Freund, Phys. Rev. 35 (1987) 559.
21. V.H. Dibeler, R.M. Reese, F.L. Mohler, J. Research NBS 57 (1956) 113.
22. There are different ionization potentials for CF_3 reported from different sources, ranging from 8.7±0.2 eV (reference 27) to 9.17±0.08 eV (reference 24), but they are all smaller than the ionization potential of iodine, 10.45 eV (reference 27 or 24).
23. D.H. Williams, I. Howe, "Principles of Organic Mass Spectrometry", McGraw-Hill, London, 1972.
24. H.M. Rosenstock, K. Draxl, B.W. Steiner, J.T. Herron, *Energetics of Gaseous Ions*, Journal of Physical and Chemical Reference Data, 1977, Vol. 6.
25. E.R. Fisher, P.B. Armentrout, Int. J. Mass Spectrom. Ion Processes 101 (1990) R1.
26. R.L. Asher, B. Ruscic, J. Chem. Phys. 106 (1997) 210.
27. *CRC Handbook of Chemistry and Physics*, 66th ed.; R.C Weast., Ed.; CRC Press; Boca Raton, FL, 1985.

Table 1. Rate coefficients (k, in 10^{-10} cm^3/s) and ionic products (branching ratios shown in the parentheses) of the gas-phase reaction between the ions derived from CF_3Br and CF_3I with their parent molecules. The reactions of Ar^+ with these compounds are also included. In this work the reactant ions have not been thermalized prior to their reactions.

Reactant ions	Hsieh *et al.*[8]	Berman and Beauchamp[9]	Morris *et al.*[10,11]	This work
With CF_3Br				
CF^+			$k = 12$ CF_2Br^+ (100)	$k = 3.2$ CF_3^+ (30) CF_2Br^+ (70)
CF_2^+			$k = 12$ CF_3^+ (22) CF_2Br^+ (78)	$k = 9.9$ CF_3^+ (35) CF_2Br^+ (20) CF_3Br^+ (45)
CF_3^+			$k = 4.3$ CF_2Br^+ (100)	$k = 0.81$ CF_2Br^+ (100)
Br^+				$k = 9.8$ CF_3^+ (50) CF_3Br^+ (50)
Ar^+			$k = 13$ CF_3^+ (25) CF_2Br^+ (75)	$k = 11$ CF_3^+ (20) CF_2Br^+ (80)
With CF_3I				
CF^+			$k = 16$ CF_2I^+ (100)	$k = 5.8$ CF_3^+ (35) CF_2I^+ (65)
CF_2^+			$k = 14$ CF_2I^+ (24) CF_3I^+ (76)	$k = 13$ CF_3^+ (30) CF_3I^+ (70)
CF_3^+	$k = 4.8$ CF_2I^+ (100)	$k = 2.5$ CF_2I^+ (68) CF_3I^+ (32)	$k = 8.7$ CF_2I^+ (100)	$k = 1.9$ CF_2I^+ (100)
I^+	$k = 7.4$ CF_3^+ (47) CF_3I^+ (53)	$k = 2.9$ CF_3I^+ (72) I_2^+ (28)	$k = 8.7$ CF_3^+ (63) CF_2I^+ (5) CF_3I^+ (26) I_2^+ (6)	$k = 8.2$ CF_3^+ (20) CF_2I^+ (5) CF_3I^+ (70) I_2^+ (5)
Ar^+			$k = 16$ CF_3^+ (11) CF_2I^+ (68) I^+ (20)	$k = 14$ CF_3^+ (7) CF_2I^+ (90) I^+ (3)

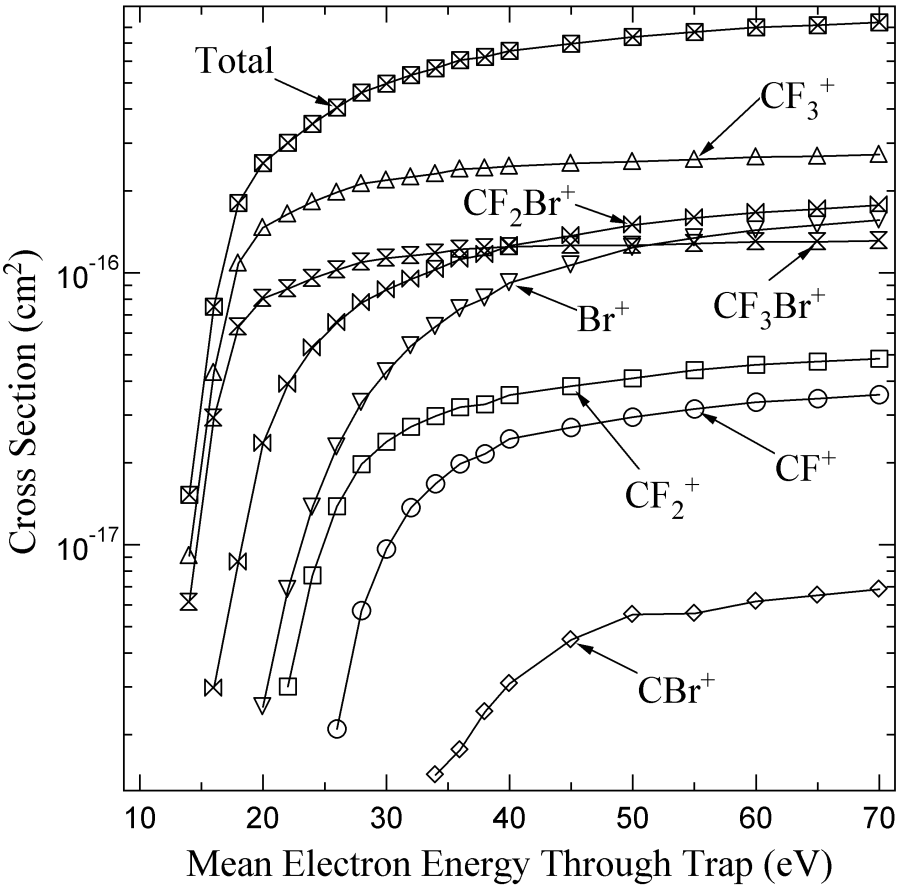

Figure 1. Cross-sections for electron impact ionization of CF_3Br.

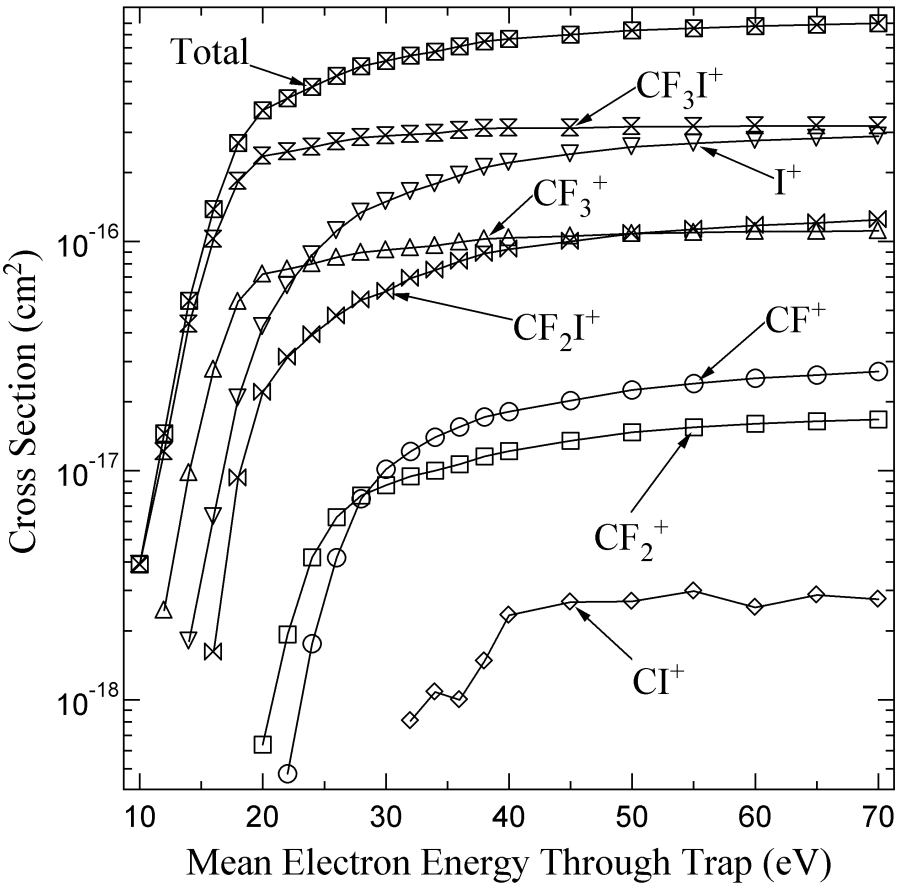

Figure 2. Cross-sections for electron impact ionization of CF_3I.

Appendix B Mass Spectrometry of n-Octane

A Mass Spectrometry Study of n-Octane:
Electron Impact Ionization and Ion-Molecule Reactions

C.Q. Jiao[a], C.A. DeJoseph Jr.[b], A. Garscadden[b,*]
[a] Mobium Enterprises, Inc., 5100 Springfield Pike, Dayton, OH 45431-1231, USA
[b] Air Force Research Laboratory, Wright-Patterson AFB, OH 45433-7251, USA

(September 24, 2000)

Abstract

Electron impact ionization of n-octane over an energy range of 10-70 eV and the subsequent ion-molecule reactions with the parent molecule have been studied using Fourier-transform mass spectrometry. Molecular ion and fragment ions C_1^+-C_6^+ are produced from the electron impact with a total ionization cross section of $1.4\pm0.2 \times 10^{-15}$ cm^2 between 60-70 eV. $C_3H_7^+$ is the most abundant ion at most of the ionizing energies with the exception for $E \leq 16$ eV where $C_6H_{13}^+$ and $C_6H_{12}^+$ are the most abundant. Among the fragment ions only $C_4H_7^+$ and smaller ions react readily with the parent molecule, producing primarily $C_5H_{11}^+$ and $C_4H_9^+$, with rate coefficients of $0.32 - 2.4 \times 10^{-9}$ cm^3s^{-1}. Essentially all of the ions, including the molecular ion and the large fragment ions, undergo decomposition upon collision with neutral molecules after they are kinetically excited to an energy range of 1-5 eV, forming a variety of small hydrocarbon ions. Many of the decomposition product ions in turn are capable of further reacting with n-octane. Isotope reagents have been utilized in experiments to probe the type of the ion-molecule reactions studied.

1. Introduction

The role played by the charged particle collisions in combustion and ignition has been reevaluated recently.[1] Because ion-molecule reactions are typically 100 times faster than the neutral particle reactions, they are considered to be capable of enhancing the rate of combustion or ignition by breaking chemical bonds, creating radicals, and speeding up the first and slowest step in the combustion reaction. The reactions of selected ions including N_2^+, O_2^+, N^+, O^+, NO^+, and H_3O^+ with n-octane and iso-octane have been recently studied by Arnold *et al*.[2,3] While N_2^+, O_2^+, N^+, and O^+ react at collision rates via charge transfer, NO^+ and H_3O^+ react primarily via hydride-abstraction and proton transfer, respectively, with relatively slow rates. The products of these ion-molecule reactions are found to be the types of radicals that would result from a conventional combustion initiation step involving thermal decomposition of alkanes at higher temperature.

In this paper we report on our study using Fourier-transform mass spectrometry on the electron impact ionization and ion chemistries of n-octane. The ion chemistries under study are the reactions of the ions from n-octane with the parent molecule at pressures of 10^{-7} Torr so that the two-body collision kinetics only are measured. To further estimate the contribution of the ion chemistries to the ignition process, we are probing the possibility of ion recycling in which the reactant ions are regenerated enabling the ionic chain reaction to be continued. Our study finds that only the small fragment ions react at thermal energy with n-octane to form larger ions that mostly are unreactive with n-octane. Therefore, one possible way to regenerate the reactive ions is to kinetically excite the larger ions and have them undergo collisions with neutral target molecules yielding small fragment ions. Our preliminary results of this aspect will be discussed. To probe the mechanism of ion-molecule reactions, isotope reagents, n-C_8H_{18} and n-C_8D_{18}, are used in experiments in which the isotope product distribution and the kinetic isotope effects are measured.

The data presented here provide some basic data for the modeling of spark ignition. The simulation of spark ignition is often separated into two parts: breakdown phase and glow phase. For the breakdown phase, the majority of simulations use a fluid model that is computationally easy but without consideration of the details of the electron and ion kinetics.[4-7] With the advent of more powerful computers, breakdown simulations using kinetic models that make use of knowledge of the ionization cross sections are becoming more popular,[8-11]. For the glow phase, most of the simulation work involves only the neutral particle reaction scheme.[12-18] This is probably not adequate because at the early stages of expansion of the ionized kernel in spark ignition, the concentration of ions relative to the neutral radicals is significant. In recent years, at least two simulation works that use mechanisms involving the ion-molecule reactions have been reported.[19,20]

2. Experimental

All experiments are performed on a modified Extrel Fourier-transform mass spectrometer (FTMS) equipped with a cubic ion cyclotron resonance trapping cell (5 cm on a side) and a 2 T superconducting magnet.[21] Typically, octane (99+%, Aldrich) is mixed with argon (99.999%, Matheson Research Grade) with a ratio about 1:1 to a total pressure of ~2 Torr, as determined by capacitance manometry. For the isotope reagent experiments, octane-d_{18} (98+% atom % D, Aldrich) is mixed with octane and argon with

a ratio of ~1:1:2. The mixture is admitted through a precision leak valve into the FTMS system. Ions are formed by electron impact in the trapping cell at pressures in the 10^{-7} Torr range. An electron gun (Kimball Physics ELG2, Wilton, NH) irradiates the cell with a few hundred picocoulombs of low-energy electrons. The motion of the ions is constrained radially by the superconducting magnetic field and axially by an electrostatic potential (1 V) applied to the trap faces that are perpendicular to the magnetic field. Ions of all mass-to-charge ratios are simultaneously and coherently excited into cyclotron orbits using a stored waveform[22,23] applied to two opposing trap faces which are parallel to the magnetic field. Following cyclotron excitation, the image currents induced on the two remaining faces of the trap are amplified, digitized and Fourier analyzed to yield a mass spectrum.

The calculation of cross sections from the mass spectrum intensities requires knowledge of the gas densities, the electron beam current and the number of ions produced. These calibration issues have been described previously.[21,24] The intensity ratios of the ions from octane to Ar^+ give cross sections relative to those for argon ionization[25] since the pressure ratio of Ar to octane is known. As a cross check, and for ion molecule kinetic analyses, the gas pressure is calibrated using a pulsed valve and a spinning rotor friction gauge (MKS Instruments model SRG2, Burlington, MA) with the vacuum chamber sealed off from the pumps. After passage of the electron beam through the ion trap, electron current is collected on a Faraday cup and recorded with a digital oscilloscope. The quantitative relationship between the image current and the number of ions is based on a lengthy, but elementary, solution of Maxwell's equations for the cubic ICR cell. This is required to quantify both excitation of the ions and detection of the resulting image current.[21]

The technique of collision-induced dissociation (CID) in FTMS has been described previously.[26] The ion to be studied is first isolated using a stored waveform and then excited by another waveform to a larger orbit, increasing its kinetic energy. By varying the radius of the orbit (typically 0.1 – 1.0 cm radius), the kinetic energy can be varied from a fraction of an eV to a few hundred eV. This excitation to higher energy typically takes place in a time short compared to the collision time with the neutral background gas. In a subsequent collision with a neutral gas molecule, part of the kinetic energy may be converted to internal energy (which may lead to dissociation) or the ion may simply be cooled by elastic scattering. Because the ion may undergo several collisions before it dissociates, the kinetic energy the ion possesses when dissociation occurs is not well defined. Only the maximum kinetic energy can be specified for CID experiments with the FTMS.

3. Results and Discussion

Electron impact ionization cross sections of n-octane over an energy range of 10-70 eV are shown in Figure 1-4. As the electron impact energy is increased, the total ionization cross section rises dramatically near threshold (12-20 eV) and levels off at ~60 eV with a value of $1.4 \pm 0.2 \times 10^{-15}$ cm^2. A significant amount of the molecular ion is observed, and fragment ions range from C_1^+ to C_6^+ with the complete absence of C_7^+. As demonstrated in a previous study by MacColl,[27] when the linear hydrocarbon molecules become larger, the amounts of fragment ions M-1 and M-15 become vanishingly smaller, which is a characteristic cracking pattern for the normal alkanes.[28] Table 1 lists the

absolute and relative cross sections of these ions at 20, 50 and 70 eV. At these energies $C_3H_7^+$ is the most abundant ion, and in each group of C_n^+ ions $C_nH_{2n+1}^+$ is always the major ion. These features generally hold true at all energies except for E ≤ 16 eV where $C_3H_7^+$ is less than $C_6H_{13}^+$ and, for $C_{4\text{-}6}^+$ near their thresholds, $C_nH_{2n}^+$ are slightly more intense than $C_nH_{2n+1}^+$. All of the fragment ions are formed by the fragmentation of the molecular ion via (1) primary decomposition (i.e., decomposition directly from the molecular ion), or (2) successive decomposition (i.e., subsequent decomposition from the daughter ions). The fragmentation can be (1) a simple C-C bond cleavage, or (2) accompanied by atom rearrangement. The fact that the C_7^+ ion is absent suggests that the formation of $C_6H_{13}^+$ or $C_6H_{12}^+$ from n-octane is a primary process,

$$C_8H_{18}^+ \rightarrow C_6H_{13}^+ + C_2H_5 \qquad \textbf{1}$$
$$C_6H_{12}^+ + C_2H_6\,. \qquad \textbf{2}$$

While reaction **1** is a simple C-C bond split process, reaction **2** is via a H-atom rearrangement before or during the C-C bond cleavage. It should be pointed out that it is possible for the H-atom rearrangement to occur after the C-C bond cleavage in both reactions **1** and **2**, yielding a more stable ion isomer(s). It has been generally observed that, compared to the simple single-bond cleavage, the bond cleavage with rearrangement has a relatively small activation energy and frequency factor.[29] The data for $C_6H_{12}^+$ and $C_6H_{13}^+$ in figure 4 exhibit this characteristic: the $C_6H_{12}^+$ cross section has a lower onset energy but rises relatively slowly, while the $C_6H_{13}^+$ cross section has a higher onset energy but rises faster. The formation of $C_5H_{11}^+$ vs. $C_5H_{10}^+$ and $C_4H_9^+$ vs. $C_4H_8^+$ near their thresholds exhibit similar trends and the following fragmentation processes at low ionizing energies are implied:

$$C_8H_{18}^+ \rightarrow C_5H_{11}^+ + C_3H_7 \qquad \textbf{3}$$
$$C_5H_{10}^+ + C_3H_8 \qquad \textbf{4}$$
$$C_4H_9^+ + C_4H_9 \qquad \textbf{5}$$
$$C_4H_8^+ + C_4H_{10}\,. \qquad \textbf{6}$$

In the literature, two studies using labeled compounds suggested that $C_6H_{13}^+$, $C_5H_{11}^+$ and $C_4H_9^+$ are formed from octane chiefly by primary processes[30] and that these primary processes are via a simple C-C bond split.[31] In summary, we believe that the major neutral fragments produced from the electron impact ionization at low energies (i.e., ≤ 16 eV) are C_2H_5 and C_2H_6; in addition, relatively small amounts of C_3H_7, C_3H_8, C_4H_9, and C_4H_{11} are present. As electron energy increases, successive decomposition increases resulting in complex fragmentation paths, which makes deducing the neutral fragments more difficult.

Among the ions generated from the electron impact ionization of n-octane, only $C_4H_7^+$ and smaller ions undergo gas-phase reactions with n-octane molecule under the condition of 10^{-7} Torr gas pressures. The reaction kinetics for some selected reactive ions that have ionization cross sections greater than 10^{-17} cm^2 at 50 eV are studied and the results are shown in table 2. The reactant ions are not thermalized prior to the reactions and therefore may have higher internal energies, which have effect on the reaction kinetics as discussed later. As n in C_n^+ gets smaller, the reaction rate increases and a greater variety of product ions is generated. The major product ions are $C_5H_{11}^+$ and $C_4H_9^+$. Relatively small amounts of $C_3H_7^+$ and $C_3H_5^+$ are also produced from small C_n^+, and these two product ions can undergo secondary reactions with n-octane to finally form $C_5H_{11}^+$ and $C_4H_9^+$ that are unreactive with n-octane. The reactions in table 2 proceed through one or more of the following mechanisms that have been proposed in the

literature for ion-molecule reactions involving paraffin molecules: oxidative-insertion-complex formation, charge-transfer, $H^{+,0,-}$-abstraction, or alkide(R^-)-abstraction. To probe the reaction mechanisms, different ions from n-octane are isolated and allowed to react individually with n-C_8H_{18} and, in another separate experiment, with a mixture of n-C_8H_{18} and n-C_8D_{18} (1:1 ratio). No isotope exchange between the reactant ion and n-octane has been observed for all of the reactions in table 2. For example, when $C_3H_7^+$ reacts with [C_8H_{18}, C_8D_{18}], only $C_5H_{11}^+$, $C_5D_{11}^+$, $C_4H_9^+$ and $C_4D_9^+$ are detected. No mixed-isotope ions, such as $C_5HD_{10}^+$ or $C_4HD_8^+$, are present. This finding appears to exclude the possibility of an oxidative-insertion-complex formation mechanism and a $H^{+,0}$-abstraction mechanism; with these mechanisms the isotope in the reactant ions should have been more or less retained in the product ions. A charge-transfer mechanism is also unlikely based on the fact that many reactant ions have lower ionization potentials than the appearance potentials of the product ions by a few eV, which means that the reactions in table 2 would have been rather endothermic if they were via the charge-transfer mechanism. For example, $C_2H_5^+$ reacting with n-octane via charge-transfer to produce $C_5H_{11}^+$ and $C_4H_9^+$ would be endothermic by 3.0 and 2.8 eV, respectively.[32] Therefore, only the hydride- and alkide- abstractions are left as candidates for the possible reaction mechanisms. Some decades ago two studies of the chemical ionization on C_6 and C_{10} paraffins using CH_4, respectively, found the M-1 ion (M represents molecular mass) to be the most abundant ion from the ion-molecule reactions.[33,34] It was suggested that $C_2H_5^+$ generated from CH_4 acted as H^- abstractor to produce the M-1 ion from C_6 or C_{10} molecules, and the M-1 ion underwent further decomposition to form smaller fragment ions. In another study in the 1970s' Lias *et al* [35] demonstrated that $C_2H_5^+$ and $C_3H_7^+$ react with n-alkanes, including n-octane, exclusively via hydride transfer to produce M-1 ions. The reaction rate of $C_3H_7^+$ reported in that study, roughly equal to the collision rate, is about twice as large as what we observed. The differences between the experimental results from the studies mentioned above and ours in table 2 may be due to different energy content in the reactant ions. One may argue that because in our experiments $C_3H_7^+$ is hot, it may react with n-C_8H_{18} via hydride-transfer followed by dissociation to produce partially $C_3H_7^+$ itself, making the apparent reaction rate smaller. In the isotope reagent experiments mentioned earlier, we do not find $C_3D_7^+$ to be produced from the reaction of $C_3H_7^+$ with n-C_8D_{18}, which excludes the above argument to be the explanation of our reaction rate of $C_3H_7^+$ differing from Lias *et al*'s. In our experiments, no M-1 ion from any of the ion-molecule reactions studied has been found. Also, we observed no significant kinetic isotope effect in the isotope reagent experiments. For example, $C_3H_7^+$ reacting with [C_8H_{18}, C_8D_{18}] produces equal amounts of $C_5H_{11}^+$ vs. $C_5D_{11}^+$, and equal amounts of $C_4H_9^+$ vs. $C_4D_9^+$; also, when $C_3D_7^+$ is used as the reactant ion, the reaction rate and the product distribution remain the same as those for $C_3H_7^+$. We propose that the alkide-transfer is likely to be involved in the majority of the reactions listed in table 2. However, an alternate mechanism by hydride-transfer followed by dissociation is also possible, although our experiments do not show a kinetic isotope effect which would support hydride-transfer mechanism.

The chemistries of ions with increased kinetic energy have also been studied. Each of the different ions is isolated and then kinetically excited to a certain energy level before there is time to react with n-octane. While a thorough examination on collision-induced dissociation (CID) of the n-octane ions in the kinetic energy range up to 500 eV is underway, we report here only the CID results at relatively low energies, ~ 1-5 eV

laboratory frame, as these energies are on the order of the upper limit of the kinetic energies of ions in the spark ignition process. Considering that the reactant ions are not initially thermalized as discussed earlier, we expect the energy level of the ions after excitation should be higher than calculated based on the excitation waveform, but not likely to be more than a few eV. The CID results from FTMS experiments are usually presented qualitatively or semi-quantitatively, because with today's FTMS techniques reliable CID reaction rates at well-defined energies are difficult to acquire even for reactant ions that are initially thermalized. Here we report only the products from the kinetically excited ion reactions. At these elevated energies ions can potentially undergo all of the possible reactions including charge-transfer and H^- or R^- abstraction, as well as CID. We find that essentially only the CID processes are involved. For example, when $C_5H_{11}^+$ is kinetically excited (here designated as $C_5H_{11}^{+*}$) we find,

$$C_5H_{11}^{+*} + M \rightarrow C_3H_7^+ + C_2H_4 + M ,$$

where M represents the neutral collision target. The neutral fragment, C_2H_4, in the above equation only represents the authors' estimate, considering that the ion has only a few eV energy, and that increased fragmentation requires more energy. The CID process is distinguished from the other endothermic reactions by the product isotope pattern. When $C_5H_{11}^+$ reacts with a 1:1 mixture of C_8H_{18} and C_8D_{18}, only $C_3H_7^+$ is observed:

$$C_5H_{11}^{+*} + M \rightarrow C_3H_7^+ + C_2H_4 + M ,$$

where M = [C_8H_{18},C_8D_{18}]. The amount of product $C_3D_7^+$ is insignificant. To determine if this product selectivity is not due to the kinetic isotope effect, $C_5D_{11}^+$ is used as the reactant ion. Then, essentially only $C_3D_7^+$ is observed:

$$C_5D_{11}^{+*} + M \rightarrow C_3D_7^+ + C_2D_4 + M .$$

Clearly, these experimental results indicate that the reaction of $C_5D_{11}^{+*}$ is a CID process. Similar experiments show that CID is also the major endothermic reaction observed for other kinetically excited ions, with the results shown in table 3. For the molecular ion $C_8H_{18}^{+*}$, the reaction with [C_8H_{18},C_8D_{18}] produces $C_5H_{11}^+$, $C_4H_9^+$, $C_3H_7^+$, and relatively small amounts of the corresponding d-isotope ions, which suggests that the CID of $C_8H_{18}^{+*}$ is mixed with other reaction(s). This other reaction is unlikely to be a H^- or R^- abstraction reaction because all of the C atoms in this $C_8H_{18}^+$ are fully ligated. The charge transfer reaction is most likely the one involved. In table 3, the kinetic isotope effects are also listed. We provide the ratios of the reaction rates of the h-isotope and d-isotope reactant ions (k_H/k_D). While the isotope effects for most of the reactions in table 3 are not remarkable, the inverse isotope effect for reaction $C_3H_6^{+*} \rightarrow C_3H_5^+ + H$ is significant and is not consistent with its seemingly simple C-H bond cleavage process. Thus, whether this reaction is in fact purely a collision-induced dissociation is not clear at this point.

The CID product ions, if smaller than $C_4H_7^+$, are observed to undergo the same reactions listed in table 2 for the corresponding ions from the electron impact ionization, although whether the CID product ions have the same structures as the corresponding ions from the electron impact ionization is in question. A study in the 1970's on CID of isomeric octane ions demonstrated that structurally isomeric ions isomerise to a common structure prior to decomposition.[36] On the other hand, another study showed that the alkyl ions from the electron impact ionization on hydrocarbons might be a mixture of structural isomers.[37] We do not see different reaction rates for the isomers, when there are any, for all of the reactions in table 2, i.e., no biexponential decay of the reactant ion has been observed.

From the results presented above we conclude that, if the ion temperature is high enough to drive its "thermal decomposition", there are many reaction cycles in the n-octane plasma: the reactant ion is reacted away with n-octane, while the product ion decomposes to regenerate the reactant ion, and the reaction goes on. Some important cycles are shown in scheme 1. In the scheme, the dash lines denote the endothermic reaction paths (CIDs, the neutral collision target not shown), and the neutral products are shown in parentheses only for the purpose to make the mass balance. Such a reaction cycle each time converts n-octane to other smaller species, such as C_2H_4, CH_4 or H_2.

4. Summary

Electron impact ionization on n-octane produces molecular ions and fragment ions that range from C_1^+ to C_6^+, with a total ionization cross section of $1.4\pm0.2 \times 10^{-15}$ cm^2 between 60-70 eV. At low energies (≤16 eV) $C_6H_{13}^+$ and $C_6H_{12}^+$ are the most abundant ions and C_2H_5 and C_2H_6 are believed to be the major neutral fragments. As the electron energy increases, $C_3H_7^+$ becomes the most abundant ion and the neutral fragments become more difficult to deduce. Among the ions generated from electron impact ionization on n-octane, only $C_4H_7^+$ and smaller ions can react with the parent molecule, producing mainly $C_5H_{11}^+$ and $C_4H_9^+$, probably via an alkide-abstraction mechanism. The reaction rates vary from 0.32 to 2.4×10^{-9} cm^3s^{-1}, with a general trend of increasing reactivity with the decreasing number of carbon atoms in the reactant ion. Upon being kinetically excited to ~1-5 eV, most of the ions studied undergo decomposition forming smaller ions which can react again with n-octane, and the reaction cycle continues.

Usually one may expect that after the electron impact ionization, the relaxation of the ion composition by ion-molecule reactions leads to a stable ion composition; the ion-molecule reactions convert the reactive ions to more stable product ions and at the end all of the ions are unreactive. The present study demonstrates that at slightly elevated energies the *reactive* ions can be recycled, and reaction chains can be accomplished that repeatedly convert large paraffins into smaller hydrocarbon molecules. In certain aspects this process resembles the neutral radical chain reaction in combustion or ignition. Ion reactions are in general much faster than the neutral particle reactions and, therefore, they should play more important roles at the early ignition stages until the high concentration of neutral radicals builds up and the thermal cracking dominates the combustion mechanisms. High-energy ions are realistic at the very early stage of spark ignition; the temperature in the spark kernel can be well above 10,000 K,[18,38] although the discharge volume at this stage is small and the gas rapidly relaxes to temperatures of a few thousand K within microseconds. Furthermore, it might be possible to design an ignition device that can increase the kinetic energy of the ions and thus enhance the overall efficiency of the ignition.

Acknowledgements

The authors thank the Air Force Office of Scientific Research for support.

References

* Corresponding author. Fax: 937-656-4657; E-mail: alan.garscadden@wpafb.af.mil

1. S. Williams, A.J. Midey, S.T. Arnold, P.M. Bench, A.A. Viggiano, R.A. Morris, L.Q. Maurice, C.D. Carter, "Progress on the Investigation of the Effects of Ionization on Hydrocarbon/Air Combustion Chemistry", AIAA 99-4907.

2. S.T. Arnold, A.A. Viggiano, R.A. Morris, J. Phys. Chem. A 1997, 101, 9351.
3. S.T. Arnold, A.A. Viggiano, R.A. Morris, J. Phys. Chem. A 1998, 102, 8881.
4. R. Morrow, Phys. Rev. A 32 (1985) 1799.
5. S. Dhali, P.F. Williams, Phys. Rev. A 31 (1985) 1219.
6. P. Bayle, B. Cornebois, Phys. Rev. A 31 (1985) 1046.
7. C. Wu, E.E. Kunhardt, Phys. Rev. A 37 (1988) 4396.
8. L.E. Kline, J.G. Stambis, Phys. Rev. A 5 (1972) 794.
9. J.M. Geary, G.W. Penney, Phys. Rev. A 17 (1978) 1483.
10. A.E. Rodriguez, W.L. Morgan, K.J. Touryan, W.M. Money, T.H. Martin, J. Appl. Phys. 70 (1991) 2015.
11. E.E. Kunhardt, Y. Tzeng, in Proceedings of the IV International Symposium on Gaseous Dielectrics, edited by L. G. Christophorou (Plenum, New York, 1984), p. 146.
12. D. Bradley, F. K-K. Lung, Combust. Flame, 69 (1987) 71.
13. G.T. Kalghargi, Combust. Flame, 77 (1989) 321.
14. Y. Ko, V.S. Arpaci, R.W. Anderson, Combust. Flame, 83 (1991) 74.
15. Y. Ko, R.W. Anderson, V.S. Arpaci, Combust. Flame, 83 (1991) 105.
16. K. Ishii, T. Tsukamoto, Y. Ujiie, M. Kono, Combust. Flame, 91 (1992) 153.
17. C.G. Foatche, T.G. Kreutz, C.K. Law, Joint Technical Meeting of the Central States, Western States, and Mexican National Sections of the Combustion Institute, April 23-26, 1995, San Antonio, Texas.
18. M. Schafer, R. Schmidt, J. Kohler, Twenty-Sixth Symposium (International) on Combustion/The Combustion Institute, 1996, p. 2701-2708.
19. Chul Park, J. Thermophysics, 3 (1989) 233.
20. T. Kravchik, E. Sher, Combust. Flame, 99 (1994) 635.
21. K. Riehl, Collisional Detachment of Negative Ions Using FTMS, Ph.D. thesis, Air Force Institute of Technology, Dayton, Ohio, USA, 1992.
22. A. G. Marshall, T. L. Wang, T. L. Ricca, J. Am. Chem. Soc. 107 (1985) 7893.
23. S. Guan, J. Chem. Phys. 91 (1989) 775.
24. P. D. Haaland, Chem. Phys. Lett. 170 (1990) 146.
25. R. C. Wetzel, F. A. Baioochi, T. R. Hayes, R. S. Freund, Phys. Rev. 35 (1987) 559.
26. B.S. Freiser, "Techniques for the Study of Ion Molecule Reactions", J.M. Farrar, W.H. Saunder, Jr., Eds.; Wiley, New York, 1988, vol. 20, Chapter 2.
27. Allan MacColl, Org. Mass Spectrom. 17 (1982) 1.
28. R.I. Reed, "Ion Production by Electron Impact", Academic Press, London, New York, 1962.
29. D. H. Williams and I. Howe, "Principles of Organic Mass Spectrometry", McGraw-Hill, London, 1972.
30. S. Meyerson, J. Chem. Phys., 42 (1965) 2181.
31. K. Levsen, H. Heimbach, G.J. Shaw, G.W.A. Milne, Org. Mass Spectrom. 12 (1977) 663.
32. H.M. Rosenstock, K. Draxl, B.W. Steiner, J.T. Herron, "Energetics of Gaseous Ions", Journal of Physical and Chemical Reference Data, 1977, vol. 6.
33. R.P. Clow, J. H. Futrell, J. Am. Chem. Soc. 94 (1972) 3748.
34. D.F. Hunt, C.N. McEwen, Org. Mass Spectrom. 7 (1973) 441.
35. S.G. Lias, J.R. Eyler, P. Ausloos, Int. J. Mass Spectrom. Ion Phys. 19 (1976) 219.
36. K. Levsen, Org. Mass Spectrom. 10 (1975) 43.
37. M.L. Gross, J. Am. Chem. Soc. 93 (1971) 253.
E. Sher, J. Ben-Ya'ish, T. Kravchik, Combust. Flame 89 (1992) 186.

Table 1. Cross sections (σ, 10^{-16} cm^2) and relative intensities of the ions from n-octane at 20, 50 and 70 eV electron impact. Ions are listed in the order of (a) increasing mass, and (b) decreasing cross section for the purpose of mass spectrometry references at 70 eV.

(a)

	20 eV		50 eV	
	σ	rel. int.	σ	rel. int.
CH_3^+	0.005	0.4	0.026	1
$C_2H_2^+$	--	--	0.023	1
$C_2H_3^+$	--	--	0.62	20
$C_2H_4^+$	--	--	0.096	3
$C_2H_5^+$	0.057	4	1.1	36
$C_3H_3^+$	--	--	0.35	11
$C_3H_4^+$	--	--	0.085	3
$C_3H_5^+$	0.20	15	1.6	51
$C_3H_6^+$	0.14	10	0.45	15
$C_3H_7^+$	1.3	100	3.1	100
$C_4H_5^+$	--	--	0.074	2
$C_4H_6^+$	--	--	0.031	1
$C_4H_7^+$	0.091	7	0.36	12
$C_4H_8^+$	0.45	33	0.69	23
$C_4H_9^+$	0.70	52	1.1	36
$C_5H_9^+$	0.061	5	0.10	3
$C_5H_{10}^+$	0.40	30	0.50	16
$C_5H_{11}^+$	0.54	40	0.73	24
$C_6H_{12}^+$	0.71	53	0.78	26
$C_6H_{13}^+$	1.1	81	1.3	43
$C_8H_{18}^+$	0.32	24	0.42	14

(b)

	70 eV	
	σ	rel. int.
$C_3H_7^+$	3.2	100
$C_3H_5^+$	1.6	51
$C_6H_{13}^+$	1.4	44
$C_4H_9^+$	1.2	37
$C_2H_5^+$	1.1	35
$C_6H_{12}^+$	0.84	26
$C_2H_3^+$	0.80	25
$C_5H_{11}^+$	0.77	24
$C_4H_8^+$	0.73	23
$C_5H_{10}^+$	0.54	17
$C_3H_3^+$	0.47	14
$C_8H_{18}^+$	0.46	14
$C_3H_6^+$	0.45	14
$C_4H_7^+$	0.35	11
$C_2H_4^+$	0.12	4
$C_5H_9^+$	0.10	3
$C_3H_4^+$	0.088	3
$C_4H_5^+$	0.082	3
$C_2H_2^+$	0.046	1
$C_4H_6^+$	0.034	1
CH_3^+	0.029	1

Table 2. Rate coefficients and branching ratios of gas-phase reactions of some selected $C_nH_m^+$ with n-octane. Reactant ions are generated from 50 eV electron impact ionization and have not been thermalized prior to the reactions.

Reactant Ion	Rate (10^{-9} cm^3s^{-1})	Product Ion	Branching Ratio %
$C_2H_3^+$	2.4	$C_5H_{11}^+$	35
		$C_4H_9^+$	44
		$C_3H_7^+$	15
		$C_3H_5^+$	6
$C_2H_5^+$	1.7	$C_5H_{11}^+$	40
		$C_4H_9^+$	44
		$C_3H_7^+$	13
		$C_3H_5^+$	3
$C_3H_3^+$	0.74	$C_5H_{11}^+$	49
		$C_4H_9^+$	46
		$C_3H_7^+$	5
$C_3H_5^+$	1.1	$C_5H_{11}^+$	46
		$C_4H_9^+$	44
		$C_3H_7^+$	10
$C_3H_6^+$	1.5	$C_5H_{11}^+$	44
		$C_4H_9^+$	42
		$C_3H_7^+$	14
$C_3H_7^+$	0.69	$C_5H_{11}^+$	59
		$C_4H_9^+$	41
$C_4H_7^+$	0.32	$C_5H_{11}^+$	54
		$C_4H_9^+$	46

Table 3. Products and the isotope effects of the collision-induced dissociation of the kinetically excited ions. The neutral fragment products represent only the authors' proposed scheme. The kinetic isotope effects presented here are the ratios of the reaction rates of the h-isotope and d-isotope reactant ions (k_H/k_D).

Reactant ions	Products	Kinetic isotope effect
$C_8H_{18}^{+*}$	$C_6H_{13}^{+} + C_2H_5$	0.7
	$C_6H_{12}^{+} + C_2H_6$	0.8
	$C_5H_{11}^{+} + C_3H_7$	--
	$C_4H_9^{+} + C_4H_9$	--
	$C_3H_7^{+} + C_5H_{11}$	--
$C_6H_{13}^{+*}$	$C_4H_9^{+} + C_2H_4$	1.0
	$C_3H_7^{+} + C_3H_6$	1.3
$C_6H_{12}^{+*}$	$C_5H_9^{+} + CH_3$	1.0
	$C_4H_8^{+} + C_2H_4$	0.6
	$C_4H_7^{+} + C_2H_5$	0.6
	$C_3H_6^{+} + C_3H_6$	0.7
	$C_3H_5^{+} + C_3H_7$	0.6
$C_5H_{11}^{+*}$	$C_3H_7^{+} + C_2H_4$	1.0
$C_5H_{10}^{+*}$	$C_4H_7^{+} + CH_4$	0.8
	$C_3H_6^{+} + C_2H_4$	1.0
$C_4H_9^{+*}$	$C_3H_5^{+} + CH_4$	0.8
	$C_2H_5^{+} + C_2H_4$	0.9
$C_4H_8^{+*}$	$C_3H_5^{+} + CH_4$	0.8
$C_3H_7^{+*}$	$C_3H_5^{+} + H_2$	0.6
$C_3H_6^{+*}$	$C_3H_5^{+} + H$	0.2

Scheme 1.

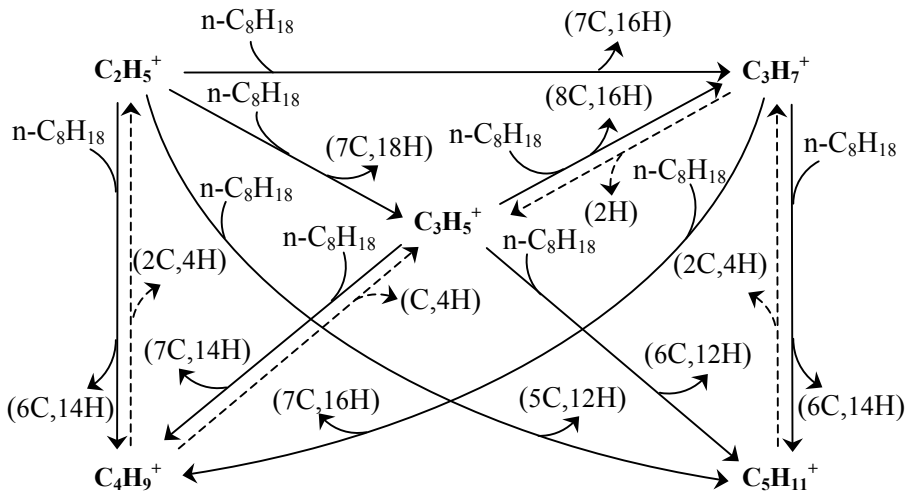
n-C8H18
(7C,16H)
C2H5+
C3H7+
n-C8H18
(8C,16H)
n-C8H18
(7C,18H)
n-C8H18
n-C8H18
n-C8H18
n-C8H18
C3H5+
(2H)
n-C8H18
n-C8H18
(2C,4H)
(2C,4H)
(C,4H)
(7C,14H)
(6C,12H)
(6C,14H)
(7C,16H)
(5C,12H)
(6C,14H)
C4H9+
C5H11+

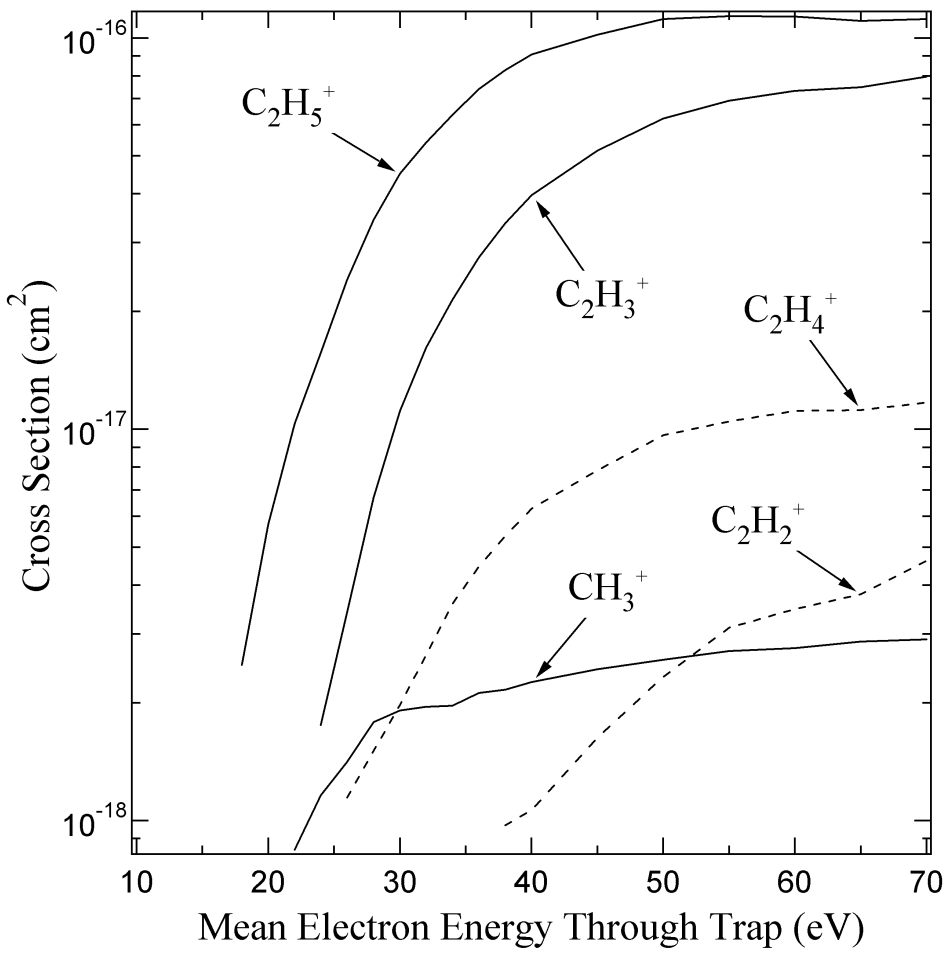

Figure 1.Cross sections for the formation of C_1^+ and C_2^+ ions from n-octane by electron impact.

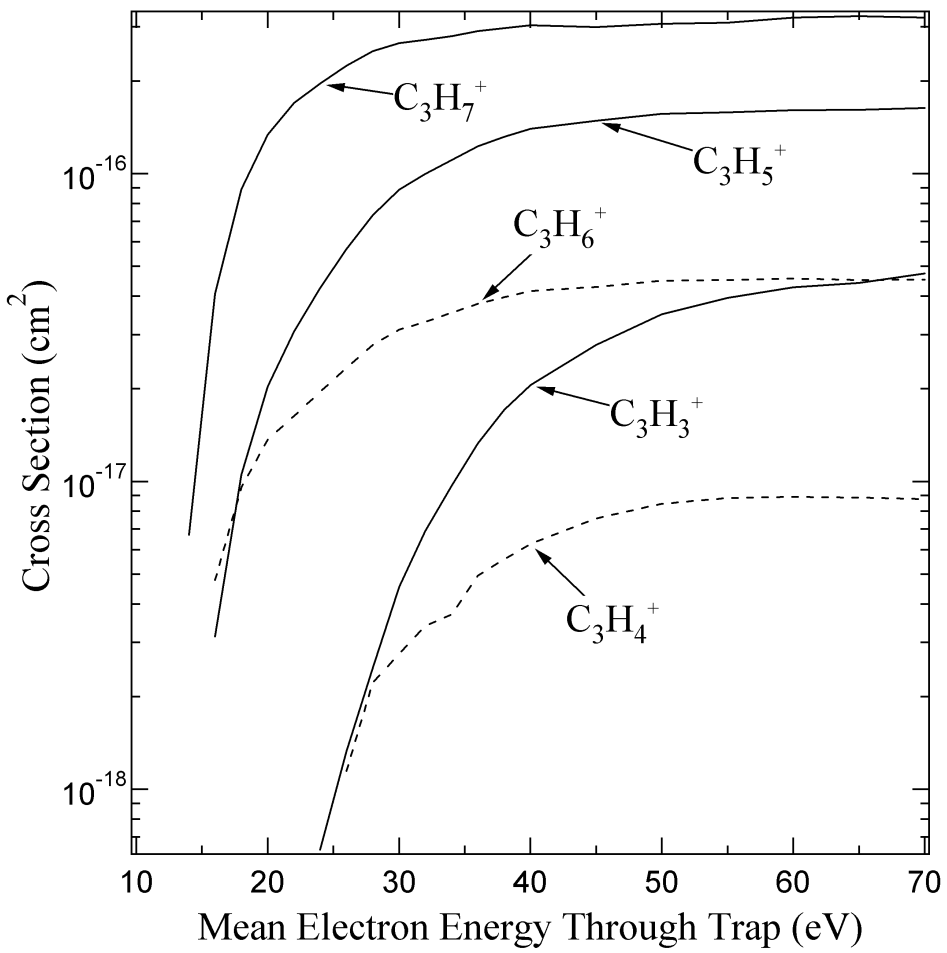

Figure 2. Cross sections for the formation of C_3^+ ions from n-octane by electron impact.

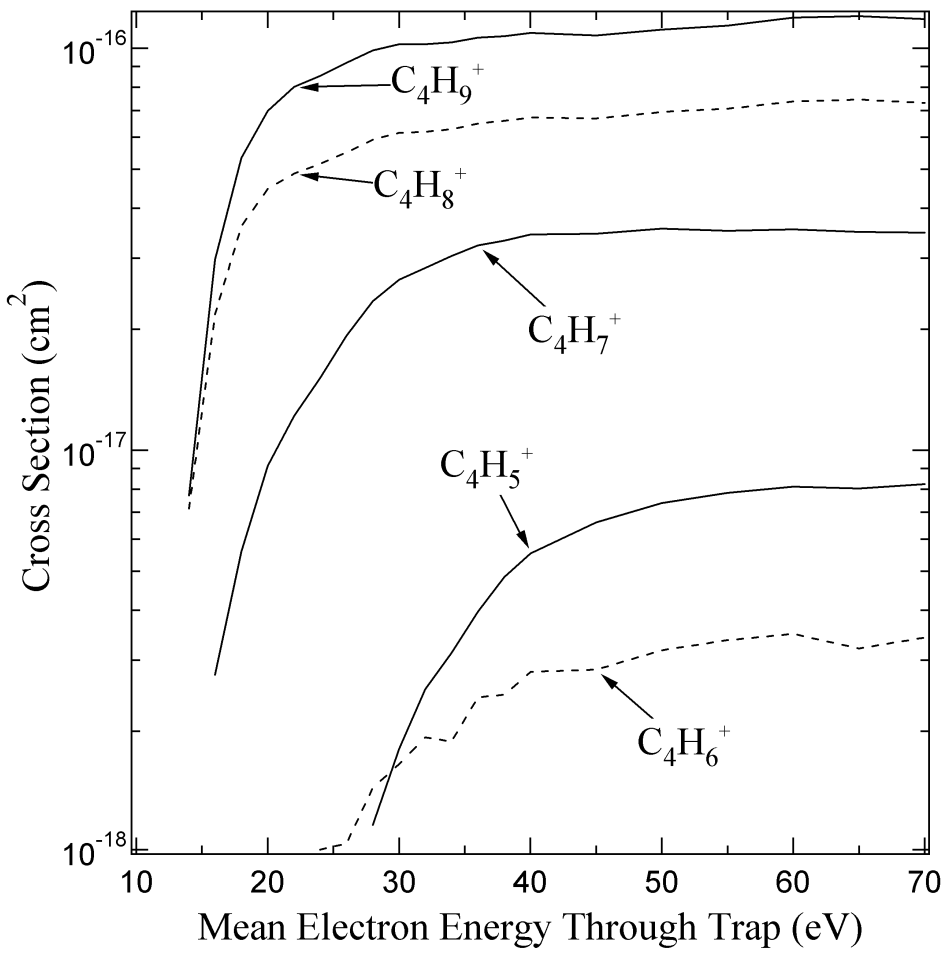

Figure 3. Cross sections for the formation of C_4^+ ions from n-octane by electron impact.

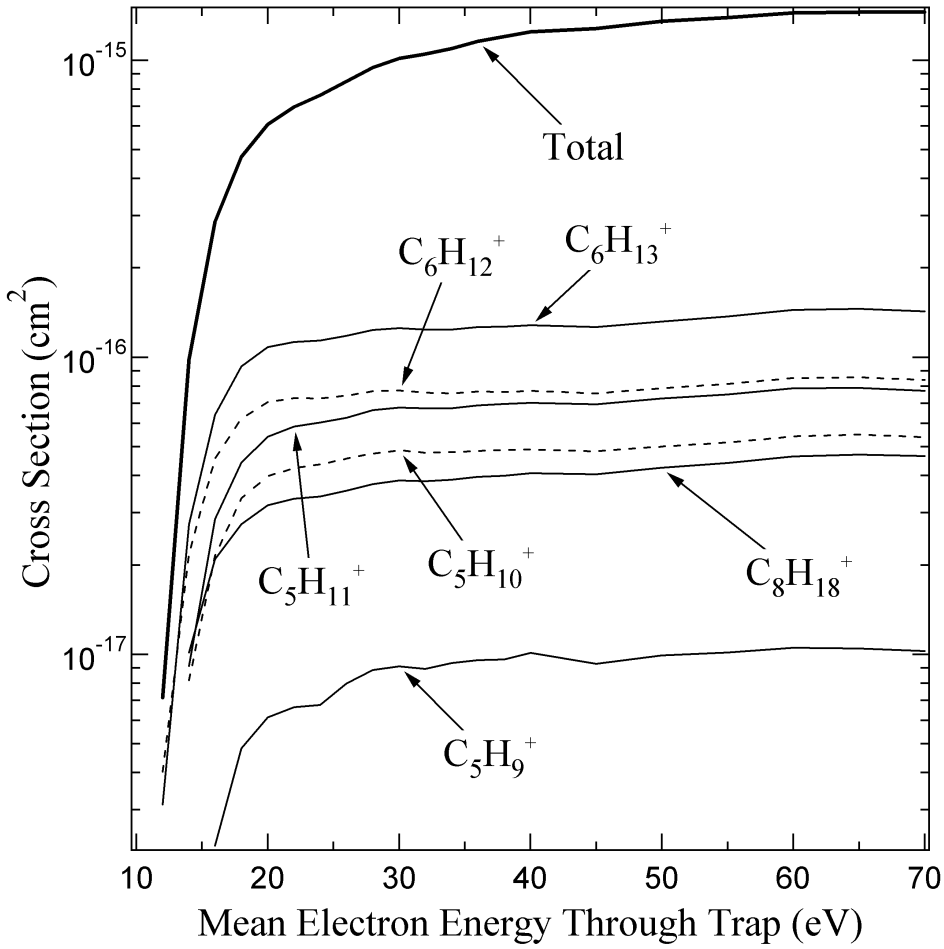

Figure 4. Cross sections for the formation of C_5^+, C_6^+ and C_8^+ ions from n-octane by electron impact. Also shown are the total ionization cross sections.

Appendix C Gas-Phase Ion Chemistries of Trimethylaluminum and Trimethylgallium

C.Q. Jiao[a], C.A. DeJoseph Jr.[b,*], P. Haaland[a], A. Garscadden[b]

[a] Mobium Enterprises, Inc., 5100 Springfield Pike, Dayton, OH 45431-1231, USA

[b] Air Force Research Laboratory, Wright-Patterson AFB, OH 45433-7251, USA

(Appeared in *Int. J. Mass. Spec.*, **202**, 345 (2000))

(July 23, 2001)

Abstract

Ionization of trimethylaluminum and trimethylgallium by electron impact from threshold to 70 eV and the reactions of the resulting ions are studied using Fourier-transform mass spectrometry. The total ionization cross sections rise from thresholds near 10 eV to $1.3 \pm 0.1 \times 10^{-15}$ and $1.2 \pm 0.1 \times 10^{-15}$ cm^2, respectively at 70 eV. The most abundant products of dissociative ionization are $MC_2H_6^+$ (M = Al or Ga) and singly charged metal ions M^+. Although these ions are unreactive with the parent molecules, other products generated by the electron impact ionization react readily with their parent molecules, yielding $MC_2H_6^+$ and M^+ as the principal products. Ions with two or three carbons have only six or nine hydrogen atoms, respectively, suggesting retention of the C-H bonding in methyl groups for $M(CH_3)_x^+$ (x=2,3). The only dications observed had stoichiometries $MC_2H_6^{2+}$. Clusters with two metal atoms were observed to form with elimation of CH_3 with rate coefficients in the $10^{-11} cm^3 s^{-1}$ range.

1. Introduction

Aluminum and Gallium are important Group III constituents of semiconductor devices including lasers and microelectronic circuits. Blue (399 nm) lasing at room temperature was recently reported in vertical cavity surface emitting structures that used AlGaN and GaN reflectors and a GaN gain medium. [1a] The high electron mobility of GaAs and the fabrication of tunable quantum well structures make AlGaAs devices attractive for high speed electroptical devices. Although group III materials can be made by molecular beam epitaxy or metal-organic chemical vapor deposition, the temperatures and deposition rates of these approaches complicate fabrication of complex structures. Synthesis of group III materials by plasma enhanced chemical vapor deposition is considered promising because rapid deposition at low temperatures has been reported. In particular, the volatile organometallic trimethyl compounds of Aluminum (TMA)[1-4] and gallium (TMG) [5,6] have been used a precursors for plasma enhanced film formation. Plasma electrons will excite, dissociate, and ionize these precursors. This paper describes the electron impact ionization of TMA and TMG as well as the subsequent reaction of the dissociatively ionized products with the neutral organometallic gas.

2. Experimental

All experiments were performed on a modified Extrel Fourier-transform mass spectrometry (FTMS) equipped with a cubic ion cyclotron resonance trapping cell (5 cm on a side) and a 2 T superconducting magnet.[7] TMA (98%, Strem Chemicals, Inc.) or TMG (99+%, Strem Chemicals, Inc.) were diluted 1:2 with argon (99.999%, Matheson Research Grade) to total pressures of 10 and 200 Torr, respectively, as determined by capacitance manometry. The gase mixtures were admitted through a precision leak valve into the FTMS system. Ions were formed by electron impact in the trapping cell at pressures in the 10^{-7} Torr range. An electron gun (Kimball Physics ELG2, Wilton, NH) irradiated the cell with a few hundred picocoulombs of low-energy electrons. The motion of the ions was constrained radially by the superconducting magnetic field and axially by an electrostatic potential (1 V) applied to the trap faces that are perpendicular to the magnetic field. Ions of all mass-to-charge ratios are simultaneously and coherently excited into cyclotron orbits using a stored voltage waveform[8,9] applied to two opposing trap faces which are parallel to the magnetic field. Following cyclotron excitation, the image currents induced on the two remaining faces of the trap are amplified, digitized and Fourier analyzed to yield a mass spectrum.

The calculation of cross sections from the mass spectrum intensities requires knowledge of the gas pressures, the electron beam current, and the number of ions produced. These calibration issues have been described previously.[7,10] The intensity ratios of the ions from TMA or TMG to Ar^+ give cross sections relative to those for argon ionization[11] since the pressure ratio of Ar to TMA or TMG is known. As a cross check, and for ion molecule kinetic analyses, the gas pressure is calibrated using a pulsed valve and a spinning rotor friction gauge (MKS Instruments model SRG2, Burlington, MA) with the vacuum chamber sealed off from the pumps. Electron current is collected on a Faraday cup and recorded with a digital oscilloscope after passage of the electron beam through the ion trap. The quantitative relationship between the image current and the number of ions is based on a lengthy, but elementary, solution of Maxwell's equations for

the cubic ICR cell. This is required to quantify both excitation of the ions and detection of the resulting image current.[7]

3. Results and discussion

Figure 1 shows the electron impact ionization cross sections of TMG from 10 to 70 eV. The total cross section rises from threshold of 10 eV to $1.2 \pm 0.1 \times 10^{-15}$ cm^2 at 70 eV. Of the 80 statistically possible singly charged ions 52 structures that satisfy normal valence are plausible:

$MC_3H_x^+$ (x=0-9); $C_3H_x^+$ (x=0-9); $MC_2H_x^+$ (x=0-7); $C_2H_x^+$ (x=0-6); MCH_x^+ (x=0-5), CH_x^+ (x=0-4); H_2^+ and H^+.

Of these 52 only eight are observed to form with cross-sections greater than 0.1% of the total cross-section. (Proton and molecular hydrogen ions may form but have cyclotron resonance frequencies too high to be detected in these experiments.) The most abundant ion at all energies is $GaC_2H_6^+$, followed by the atomic gallium ion Ga^+. It is tempting to assign the primary dissociative pathway to scission of Ga-C bonds to yield diemthyl, methyl, and bare gallium ions as the three most abundant fragments. However, the mass spectral data do not rule out more exotic bonding arrangements with the same stoichiometry..

A parent molecular ion $GaC_3H_9^+$ is observed to form in roughly 1% yield, and extensively dissociated fragments $GaCH_4^+$, $GaCH_2^+$, $GaCH^+$, and GaC^+ are formed with thresholds at 18, 24, 29, and 48 eV, respectivel. The dication $GaC_2H_6^{2+}$ ion is the only doubly charged species observed, with a peak cross-section of approximately 2.5×10^{-19} cm^2.

The ionization cross sections of TMA displayed in Figure 2 are qualitatively similar to those of TMG. The three major ion fragments are $Al(CH_3)_x^+$ where x=0-3. $AlCH_y^+$ with y={0,1,2,4} are also observed in less than 1% yield, and the total ionization cross section rises from threshold near 10 eV to $1.3 \pm 0.1 \times 10^{-15}$ cm^2 at 70 eV. The dimethyl dication $AlC_2H_6^+$ is also the only doubly charged aluminum species observed formed with a cross-section greater than $10^{-19}cm^2$.

Trimethylaluminum differs from its gallium counterpart in forming the hydrides AlH^+ and AlH_2^+. The molecular ion is $MC_3H_9^+$ is formed in higher yield (5%) when M is aluminum than when it is gallium (0.7%). We also note that ions with two or three carbons contain three or six hydrogen atoms, respectively. By contrast, ions with only one carbon are formed with 0 to 4 hydrogens. This difference suggests that the carbon hydrogen bonds remain intact in $MC_2H_6^+$ and $MC_3H_9^+$ but not in MCH_y^+ when y={0,1,2,4}. The fragments that require CH bond breaking are observed to form at higher thresholds than $M(CH_3)_x^+$.(x=0-3) and may be associated with higher lying electronic states of the $M(CH_3)_3^+$ ion.

The gas-phase reactions between the ions formed with ionization cross sections > $\sim 10^{-17}$ cm^2 at 70 eV and their neutral parent molecules are summarized in Table 1. The reactant ions were generated by electron impact at both 25 and 50 eV, but no differences in the reaction raetes or products were observed within the experimental uncertainty. Three classes of product were observed: M^+, $MC_2H_6^+$, and $M_2C_xH_y^+$. Ga^+ and $GaC_2H_6^+$ do not react with $GaMe_3$ to form new ion species, though symmetrical charge transfer cannot be excluded. (isotope ejection?) $GaCH_3^+$ produces both Ga^+ and

$GaC_2H_6^+$ as well as 2% $Ga_2C_3H_9^+$ where energy conservation is assured by the departure of a methyl group:

$$GaCH_3^+ + Ga(CH_3)_3 \rightarrow [CH_3GaGa(CH_3)_3]^+ \rightarrow Ga_2(CH_3)_3^+ + CH_3.$$

The aluminum ions are more reactive than their gallium counterparts. $AlCH_3^+$ produces $Al(CH_3)_2^+$ and Al^+, but in altered proportions as outlined in Table 1. Although Al^+ does not react with the neutral methyl compounds $AlC_3H_9^+$, $AlC_2H_6^+$, and $AlCH_3^+$ form clusters:

$$Al(CH_3)_3^+ + Al(CH_3)_3 \rightarrow [(CH_3)_3AlAl(CH_3)_3]^+ \rightarrow Al_2(CH_3)_5^+ + CH_3$$
$$\rightarrow Al(CH_3)_2^+ + \{Al(CH_3)_3 + CH_3\}$$
$$Al(CH_3)_2^+ + Al(CH_3)_3 \rightarrow [(CH_3)_2AlAl(CH_3)_3]^+ \rightarrow Al_2(CH_3)_4H^+ + CH_2$$
$$Al(CH_3)^+ + Al(CH_3)_3 \rightarrow [(CH_3)AlAl(CH_3)_3]^+ \rightarrow Al_2(CH_3)_3^+ + CH_3$$

The reactions of AlH_2^+ and $AlCH_4^+$ are very selective, producing only $AlC_2H_6^+$. $AlCH_2^+$ produces a mixture of Al^+, $AlC_2H_6^+$, and a cluster with loss of CH_3:

$$AlCH_2^+ + Al(CH_3)_3 \rightarrow [(CH_2)AlAl(CH_3)_3]^+ \rightarrow Al_2(CH_3)_2(CH_2)^+ + CH_3.$$

Since argon is commonly used as the diluent in PECVD, the argon ion reactions with TMA and TMG were also studied. Ar^+ reacts with $Al(CH_3)_3$ to yield Al^+ (19%), AlH_2^+ (8%),$AlCH_2^+$ (4%), $AlCH_3^+$ (25%), $AlCH_4^+$ (7%) and $AlC_2H_6^+$ (37%) at a rate constant of $5.9 \pm 0.5 \times 10^{-10}$ $cm^3 s^{-1}$, and with $Ga(CH_3)_3$, to yield Ga^+ (42%), $GaCH_3^+$ (13%), $GaCH_2^+$ (1%) and $GaC_2H_6^+$ (44%) at a rate constant of $4.7 \pm 0.5 \times 10^{-10}$ $cm^3 s^{-1}$. The product ions from these reactions undergo secondary reactions with their parent gases as described in Table 1, resulting in the dimethyl metal ion $MC_2H_6^+$ and the bare metal ion M^+ as the predominant product ions.

4. Conclusion

Ionization of trimethyl aluminum and trimethyl gallium by electron impact increases from thresholds near 10 eV to $1.3 \pm 0.1 \times 10^{-15}$ and $1.2 \pm 0.1 \times 10^{-15}$ cm^2 at 70 eV, respectively. The primary ion species is $MC_2H_6^+$, with the metal atomic ion being next most abundant for both aluminum and gallium. Ions with two or three carbons have six and nine hydrogen atoms, respectively suggesting that dissociative ionization occurs primarily by loss of methyl moieties. MCH_y^+ ions where y={0,1,2,4} are also observed to form with higher thresholds and peak cross-sections of less than $10^{-17}cm^2$ for M=Ga and $5 \times 10^{-17}cm^2$ for M=Al. Both TMA and TMG also produce small yields of diemethyl dications $M(CH_3)_2^{+2}$ with cross-sections in the $10^{-19}cm^2$ range. Simple hydrides of gallium are not produced, but the AlH_y^+ (y = 1,2) are formed from dissociative ionization of TMA. $MC_2H_6^+$ and M^+ do not react rapidly with the parent compounds. The remaining ions undergo dissociative charge transfer with rate constants between 0.7 and 2.9×10^{-10} cm^3s^{-1}. The principal products are the same as the most prominent dissociative ionization fragments, $MC_2H_6^+$ and M^+. Ion molecule reactions that produce clusters with two metal atoms and loss of CH_3 are observed for $AlC_3H_9^+$, $AlC_2H_6^+$, $AlCH_2^+$, $AlCH_3^+$, and $GaCH_3^+$ with rate constants in the 10^{-11} cm^3s^{-1} range. Further clustering reactions were not observed on the time scale of the present measurements. Ar^+ reacts with TMA and TMG at rates of 5.9 and $4.7 \pm 0.5 \times 10^{-10}$ cm^3s^{-1}, respectively, generating mainly $MC_2H_6^+$. The low thresholds and large cross-sections for production of $MC_2H_6^+$ and M^+ combined with their production by charge transfer from ions formed in lower yield by electron impact

suggest that plasma ion compositions will be dominated by these two species under a wide range of pressure and excitations conditions.

Acknowledgements

The authors wish to thank the Air force Office of Scientific Research for financial support.

References

* Present address: AFRL/PRPS, Bldg 450, 2645 Fifth Street Ste 13, Wright-Patterson AFB, OH 45433-7919, USA.

1a. Takao Someya, Ralph Werner, Alfred Forchel, Massimo Catalano, Roberto Cingolani, and Yasuhiko Arakawa Science 1999 September 17; 285: 1905-1906
1. F. Hashgawa, T. Takahashi, I. Onodera, Y. Nannichi, Ext. Abstr. Conf. Solid State Devices Mater. 1986, 18th, 663.
2. R. K. Sadhir, H. E. Saunders and W. A. Byers, Proc. Electr./Electron Insul. Conf. 1987, 18th, 17.
3. Y. Catherine and A. Talebian, J. Electron. Mater. 17 (1968) 127.
4. Y-C Kim, J. S. Chun, W-J Lee, Thin Solid Films, 258 (1995) 67.
5. T. P. Humphreys, C. A. Sukow, R. J. Nemanich, J. B. Posthill, R. A. Rudder, S. V. Hattangady, R. J. Markunas, Mater. Res. Soc. Symp. Proc. 162 (1990) 531.
6. Jpn. Kokai Tokkyo Koho JP 06 37,355 (Cl.Ho1L33/00) 10 Feb. 1994, Appl. 92/191,985, 20 Jul 1992, 6pp.
7. K. Riehl, Collisional Detachment of Negative Ions Using FTMS, Ph.D. thesis, Air Force Institute of Technology, Dayton, Ohio, USA, 1992.
8. A. G. Marshall, T. L. Wang, T. L. Ricca, J. Am. Chem. Soc. 107 (1985) 7893.
9. S. Guan, J. Chem. Phys. 91 (1989) 775.
10. P. D. Haaland, Chem. Phys. Lett. 170 (1990) 146.
11. R. C. Wetzel, F. A. Baioochi, T. R. Hayes, R. S. Freund, Phys. Rev. 35 (1987) 559.
12. D.H. Williams and I. Howe, “Principles of Organic Mass Spectrometry”, McGraw-Hill, London, 1972.

Table 1. Ion-molecule reaction rate coefficients and branching ratios of selected ions that have ionization cross sections greater than 10^{-17} cm^2 at 70 eV.

		Product ion (M = Ga or Al)		
Reaction	Rate ($10^{-10} cm^3 s^{-1}$)	M^+	$MC_2H_6^+$	Dimer ion
$Ga^+ + Ga(CH_3)_3$	no reaction	--	--	--
$GaCH_3^+ + Ga(CH_3)_3$	4.8±0.5	66%	32%	$Ga_2C_3H_9^+$: 2%
$GaC_2H_6^+ + Ga(CH_3)_3$	no reaction	--	--	--
$Al^+ + Al(CH_3)_3$	no reaction	--	--	--
$AlH_2^+ + Al(CH_3)_3$	6.0±0.5	0	100%	0
$AlCH_2^+ + Al(CH_3)_3$	3.7±0.5	16%	71%	$Al_2C_3H_8^+$: 13%
$AlCH_3^+ + Al(CH_3)_3$	2.1±0.2	30%	67%	$Al_2C_3H_9^+$: 3%
$AlCH_4^+ + Al(CH_3)_3$	5.4±0.5	0	100%	0
$AlC_2H_6^+ + Al(CH_3)_3$	0.18±0.02	0	0	$Al_2C_4H_{13}^+$: 100%
$AlC_3H_9^+ + Al(CH_3)_3$	4.6±0.5	0	69%	$Al_2C_5H_{15}^+$: 31%

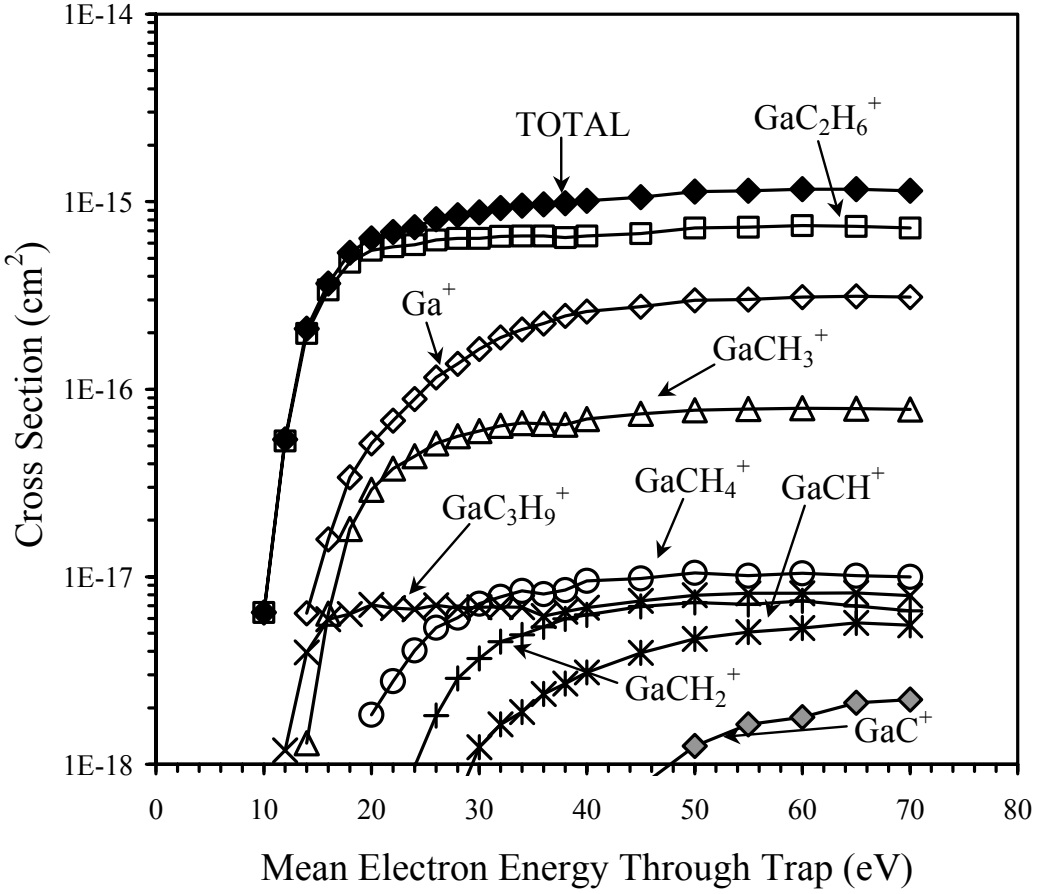

Figure 1. Cross sections for ionization of $Ga(CH_3)_3$ by electron impact.

Figure 2. Cross sections for ionization of $Al(CH_3)_3$ by electron impact.

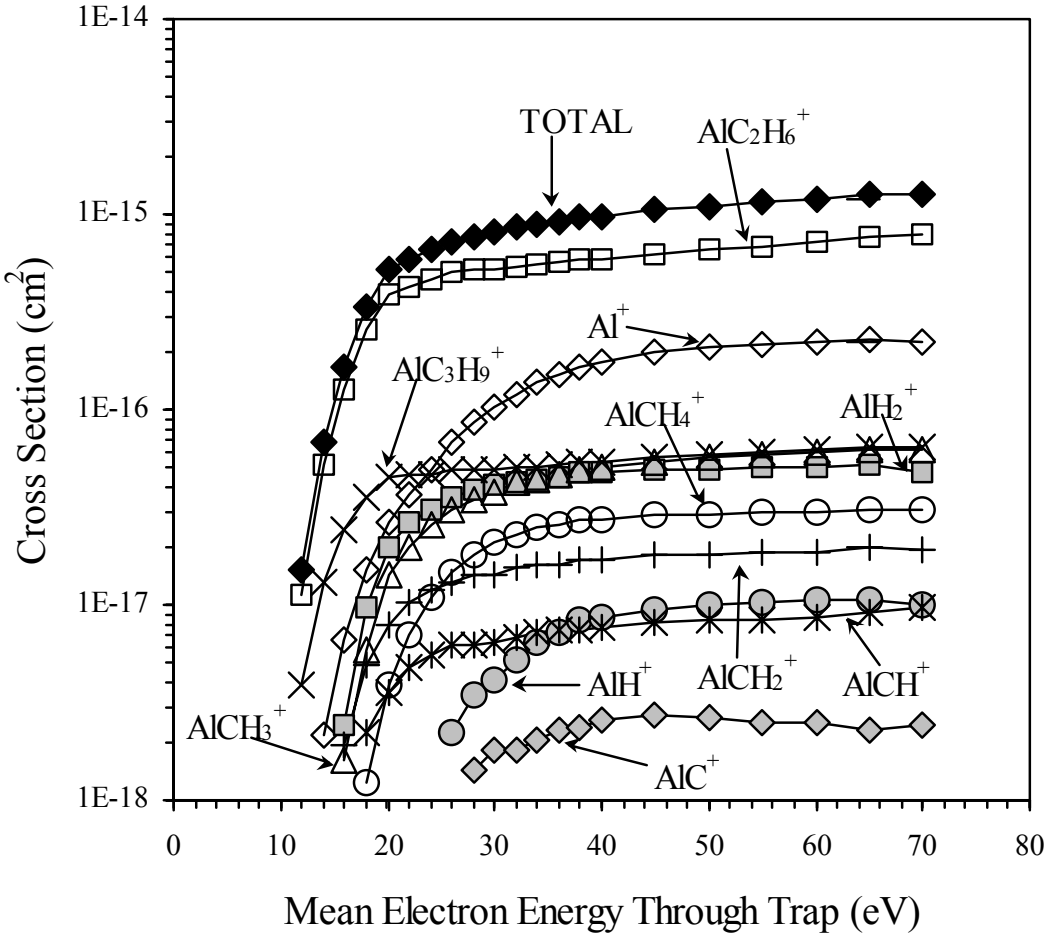

Appendix D Ion Chemistry in boron trichloride, BCl_3
Chem. Phys. Lett., ***265****, 239 (1997).*

31 January 1997

ELSEVIER

Chemical Physics Letters 265 (1997) 239-243

CHEMICAL PHYSICS LETTERS

Ion chemistry in boron trichloride BCl_3

C.Q. Jiao [1], R. Nagpal, P. Haaland

Wright Laboratory, Wright-Patterson AFB, OH 45433, USA

Received 3 June 1996; in final form 12 November 1996

Abstract

Ionization of boron trichloride by electron impact has been examined by Fourier transform mass spectrometry. The parent ion, BCl_3^+, and three fragment ions, BCl_2^+, BCl^+, and Cl+, are observed. The total ionization cross section is 1 .O ± 0.1 x 10^{-15} cm^2 between 30 and 60 eV. BCl^+ and Cl+ react with neutral BCl_3 to yield BCl_2^+ with bimolecular rates of 5.3 ± 0 5 x 10^{-10} cm^3 s^{-1} and 6.2 ± 0.5 x 10^{-10} cm^3 s^{-1}, respectively. BCl_2^+ does not react with BCl_3. Cl- and Cl; are produced by dissociative attachment of low-energy electrons to BCl_3, and Cl_2^- is found to rapidly react with BCl_3 to form BCl_4^-.

1. Introduction

Boron trichloride (BCl_3) is used in plasmas for etching of semiconductors [1–3], deposition or doping of boron [4,5], and in situ electric field measurements [25]. Literature reports on its electron impact ionization [7,8], attachment [9,10], scattering [11], dissociation kinetics [12] and spectroscopy [13–17] have appeared. Positive and negative ions formed by electron impact on BCl_3, and their appearance potentials have been reported [8,10,18]. Negative ions in BCl_3 discharges have also been probed with optogalvanic spectroscopy [19], and mass spectrometry [7,9].

Despite the technological interest in this molecule, and the many papers on its chemistry in plasmas, the cross sections for electron impact ionization of BCl_3 and the gas-phase ion-molecule reactions of its charged fragments have not been reported. We have quantified these collisional cross sections by Fourier transform mass spectrometry (FTMS) , as we have reported previously for tetramethylsilane [20], tetraethylorthosilicate [2 1], and silane [22].

2. Experimental

Boron trichloride (BCl_3, 99.9%, Aldrich) was diluted with Argon (99.999% Matheson Research Grade) in a ratio of 50:50 and admitted through a precision leak valve into a modified Fourier-transform mass spectrometry (FTMS) system that has been described in detail elsewhere[23]. In brief, ions are formed by electron impact in a cubic ion cyclotron resonance (ICR) trap cell at pressure in the 10^{-7} Torr range. An electron gun (Kimball Physics ELG2, Wilton, NH) irradiates the trap with a few hundred picoCoulombs of low-energy electrons. The ions' motions are constrained radially by a superconducting solenoidal magnetic field of ≈ 2 T and axially by a

[1] Author to whom correspondance should be addressed at Mobium Enterprises, Inc., 3055 Rodenbeck Dr., Beavercreek, OH 45432, USA.

0009-2614/97/$17.00 Copyright © 1997 Published by Elsevier Science B.V. All rights reserved.
PII S0009-2614(96)01419-4

nominal ($\approx$ 2 V) electrostatic potential applied to the trap faces that are perpendicular to the magnetic field. Ions of all mass-to-charge ratios are simultaneously and coherently excited into cyclotron orbits using a radiofrequency voltage applied to two opposing trap faces that are parallel to the magnetic field [24,25]. Following cyclotron excitation, the image currents induced on the two remaining faces of the trap are amplified, digitized, and Fourier analyzed to yield a mass spectrum.

Calculation of cross sections from the mass spectrum requires knowledge of the gas pressure, the electron beam current, and the number of ions produced. These calibration issues have been described previously [23,26]. The ratio of BCl_x^+, Cl^+ : Ar^+ signals gives cross sections relative to the well-known cross sections for argon [27,281 ionization since the BCl_3 : Ar pressure is known. As a cross-check, and for ion–molecule kinetic analyses, the gas pressure is calibrated using a pulsed valve and a spinning rotor friction gauge (MKS Instruments model SRG2, Burlington, MA) with the vacuum chamber isolated from the pumps by closed gate valves. Electron current is collected on a Faraday cup and recorded with a digital oscilloscope after passage of the electron beam through the ion trap. The quantitative relationship between the image current and the number of ions is based on a lengthy, but elementary, solution of Maxwell's equations for the cubic ICR cell. This is required to quantify both excitation of the ions and detection of the resulting image current [23].

The distribution of electron energies in the trap, based on solution of Laplace's equation for the experimental geometry, is roughly Gaussian with a full width at half maximum of 0.5 eV due to the electrostatic trapping bias [23]. The energy scale is accurate to ± 0.5 eV based on comparison of noble gas ionization thresholds with spectroscopic data. We fit the cross-section data to a heuristic but parsimonious functional form:

$$\sigma(\epsilon - T) = A \times \tanh\frac{\pi_* (\epsilon - T)}{\alpha} \times e^{-k(\epsilon - T)},$$

where σ is the cross section, ϵ is the electron energy, T is the appearance potential, A scales the amplitude, k characterizes the higher energy behavior of σ, and α quantifies $d\sigma/d\epsilon$ near threshold.

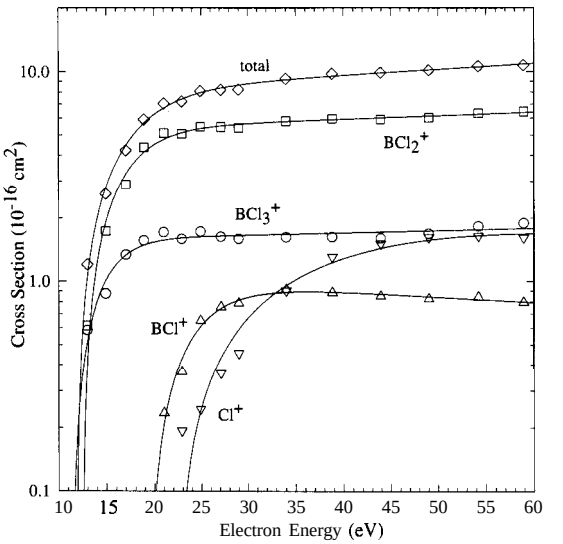

Fig. 1. Cross sections (cm^2) for ionization of BCl_3 by electron impact. Points represent experimental data. Solid lines are fits of the equation described in the text.

3. Results and discussion

Ionization cross-sections for BCl_3 are shown in Fig. 1, while parameters for functional fits to the observed cross-sections are summarized in Table 1. A striking feature of the data is the observation of the molecular ion, BCl_3^+, in substantial yield. In a recent paper on ionization in plasmas containing BCl_3 [7], no BCl_3^+ in the amplitude modulated discharge mass spectra was reported. We conclude that the BCl_3 has been substantially consumed by reactions with electrons, ions, surfaces, and neutral radicals during the long residence time of the gas in these plasmas. This conclusion is reinforced by the absence of B^+ in the FTMS spectra of BCl_3 and its presence in the amplitude modulated plasma spectra shown in reference [7]. We ascribe the observation of B^+ to dissociative ionization of species other than BCl_3 that are produced in the radiofrequency discharge [7].

The present results also update the observations in reference [8] where both B^+ and Cl_2^+ were reported in the mass spectra of BCl_3. The above work correctly attributed the formation of the latter to an artifact of pyrolysis on the ionizer filament. The present data show neither B^+ nor Cl_2^+ because pyrolysis is precluded by the 2 meter distance between the filament and ion trap. We propose that the observation of B^+ in reference [8] is likewise a consequence of filament pyrolysis.

Table I
Fitting parameters for simple and dissociative ionization cross sections. Also shown are appearance potentials estimated from thermochemical data in the JANAF tables

Ion	A (cm^2)	k (eV^{-1})	α (eV)	T (eV)	JANAF T (eV)
BCl_3^+	1.6×10^{-16}	-2.4×10^{-3}	15	11.4	11.6
BCl_2^+	5.3×10^{-16}	-3.8×10^{-3}	21	12.5	12.4
BCl^+	1.0×10^{-16}	5.9×10^{-3}	24	19.4	19.5
Cl^+	2.4×10^{-16}	6.7×10^{-3}	80	22.3	26.7

The most abundant positive ion from threshold to 60 eV is BCl_2^+. By introducing a time delay between ion formation at 25 eV and ion cyclotron excitation and detection, we track the reactions of ion fragments with BCl_3 as shown in Fig. 2. The more extensively dissociated ions BCl^+ and Cl^+ react with BCl_3 to produce BCl_2^+ at rates of 5.3 ± 0.5 and $6.2 \pm 0.5 \times 10^{-10}\,cm^3 s^{-1}$, respectively. The Ar^+ ion also reacts rapidly:

$$Ar^+ + BCl_3 \rightarrow BCl_2^+ + (Ar, Cl)$$
$$k = 5.0 \pm 0.5 \times 10^{-10} cm^3 s^{-1}.$$

Based on the published value for the polarizability of BCl_3, $\alpha = 9.38 \times 10^{-24}\,cm^3$ [29], these reactions occur at about one-half of the Langevin limiting value. The reaction rates of BCl_x^+ with BCl_3 are the same whether the ions were formed by 25 eV or 50 eV electron impact. The depletion of Cl^+ is about 1.5 times faster at 50 eV, but our data cannot resolve whether this rate increase is attributable to spin-orbit, electronic, or translational excitation of the reactant Cl^+ ion at 50 eV.

Small quantities of HCl are observed, either from impurities in the BCl_3 cylinder, or as products of the reaction between BCl_3 and traces of water in the vacuum manifolds. We also observe the production of $BClOH^+$ that arises either from reaction of water vapor with BCl_3^+:

$$BCl_3^+ + H_2O \rightarrow BClOH^+ + (H, 2Cl)$$

or dissociative charge transfer to hydrolyzed BCl_3:

$$BCl_3 + H_2O \rightarrow BCl_2OH + HCl,$$
$$(Ar^+, BCl_3^+) + BCl_2OH \rightarrow BClOH^+ + Cl + (Ar, BCl_3).$$

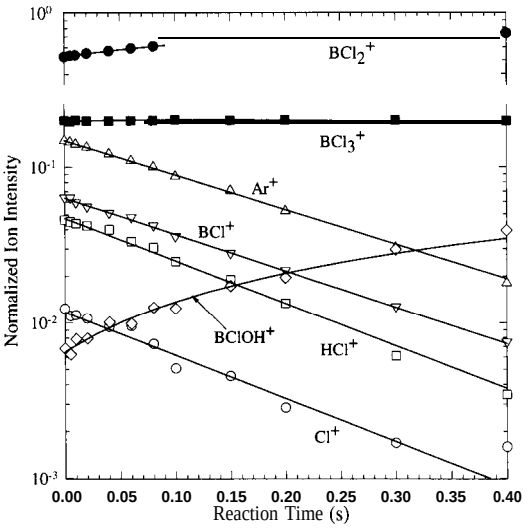

Fig. 2. Time evolution of positive ion species produced by 25 eV electron impact at a BCl_3 pressure of 3.2×10^{-7} Torr. Traces of HCl^+ are attributed to the reaction of BCl_3 with background water vapor. Points represent experimental data. Solid lines are fits of a kinetic model which gives the reaction rate coefficients presented in the text.

No $BClOH^+$ was observed in kinetic experiments during which all ions but BCl_2^+ were ejected.

Negative ions from electron attachment to BCl_3 were first examined between 10 and 60 eV. No anions attributable to direct dissociative attachment at these energies were observed. However, secondary electrons from positive ionization were trapped in the ICR cell, and these electrons produced substantial quantities of Cl^- and Cl_2^-. No boron-containing anions were observed by the secondary electron attachment.

In order to study dissociative attachment of electrons to BCl_3 at energies below 10 eV, we studied the negative ion intensities as a function of applied trapping potential. The results are shown in Fig. 3 at a primary electron energy of 50 eV. We note that the range of secondary electron energies in the trap is constrained both by their kinetic energy following ionization and by the applied trapping potential. As the trapping potential increases the mean energy of trapped secondary electrons rises, leading to increased dissociative attachment as shown in Fig. 3. We infer that the secondary electrons from positive ionization were trapped in the ICR cell, and dissociative attachment by these electrons produced substantial quantities of Cl-

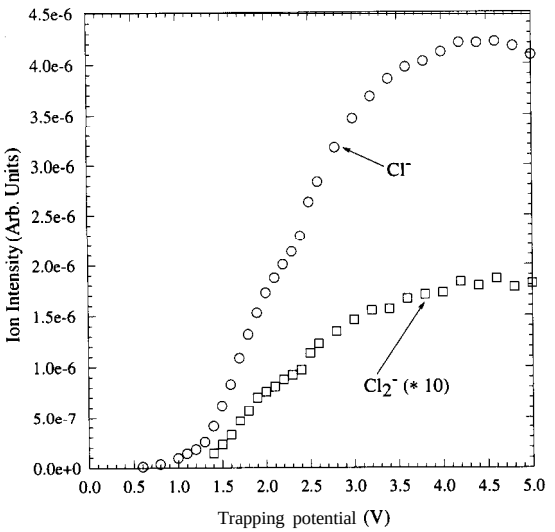

Fig. 3. Negative ion yields from trapped secondary electrons as a function of the applied trap bias. The primary electron energy is 50 eV.

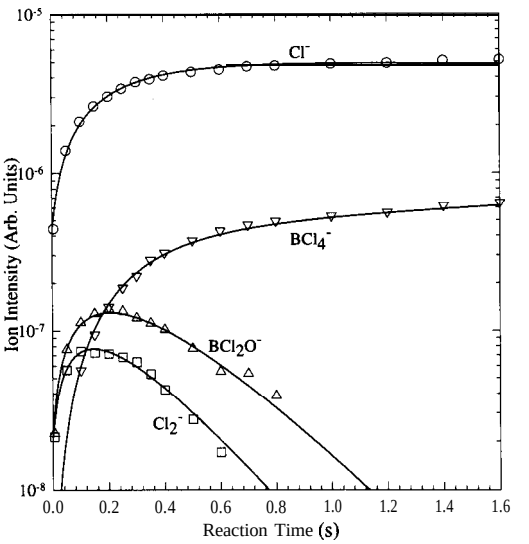

Fig. 4. Negative ion yields as a function of time delay between the generation of secondary electrons in the trap and the observation time. The increase in ion concentration over the first ≈ 400 ms is due to the attachment of trapped secondary electrons.

and Cl_2^-. The above conclusion is reinforced by the observation of negative ion production after cessation of the electron beam, as shown in Fig. 4. Although the energy resolution of our experiment is inferior to that of conventional crossed beam measurements for electron energies below 10 eV, we identify the low-energy attachment resonances and their product ions by FTMS.

Due to uncertainties in the number and in the energy distribution of trapped secondary electrons, the data summarized in Fig. 4 do not permit derivation of the rate coefficients for negative-ion molecule reactions. However, the data do reveal three features of anion chemistry in BCl_3. First, Cl_2^- reacts rapidly with BCl_3:

$$Cl, + BCl_3 \rightarrow BCl_4^- + Cl$$

but the rate for the Cl- reaction:

$$Cl- + BCl_3 \rightarrow BCl_4^-$$

is substantially slower. At present we cannot say whether the product BCl_4^- (from the latter reaction) is stabilized by emission of radiation or by a combination of a long vibrational lifetime and collisional quenching at $\approx 10^{-6}$ Torr. Second, the ion-molecule reaction:

$$Cl^- + BC13 \rightarrow Cl, + (B, 2Cl)$$

is not observed, indicating that Cl_2^- is produced only by the dissociative attachment of electrons to BCl_3. Both Cl- and Cl_2^- were reported in drift-dwell-drift electron swarm experiments [18] but later quadrupole mass spectrometry of BCl_3 plasmas reported only Cl- [9]. Finally, the data in Fig. 4 show that BCl_2O^- is formed by dissociative attachment to an impurity neutral such as BCl_2OH, rather than by a negative-ion molecule reaction. The formation of BCl_2OH is consistent with our observation of $BClOH^+$ in the cation kinetics experiments, and with a mechanism by which BCl_3 is proposed to scavenge oxygen in discharges [30].

4. Conclusions

Electron impact ionization of BCl_3 yields BCl_2^+, BCl_3^+, BCl^+, and Cl^+ with a total cross section of 1.0± 0.1 x 10^{-15} cm^2 between 30 and 60 eV. Ion-molecule reactions of BCl^+ and Cl^+ yield BCl_2^+ with rate constants of 5.3 ± 0.5 and 6.2 ± 0.5 x 10^{-10} cm^3 s-t, respectively. Dissociative attachment of low-energy electrons to BCl_3 yields primarily Cl- with smaller quantities of Cl_2^-. No boron-containing ions are found by dissociative attachment, but both Cl- and Cl_2^- re-

act with BCl_3 to produce BCl_4^-. No further clustering of BCl_4^- is observed. We infer that heavier anions observed by mass spectrometric sampling from BCl_3 plasmas are a result either of attachment to higher molecular weight species formed in the plasma or to reactions of anions with neutral radicals that are precluded at the pressures and charge densities used in the FTMS experiments.

Acknowledgements

The authors wish to thank Dr. Alan Garscadden for stimulating discussions and critical reviews, and the Air Force Office of Scientific Research for financial support.

References

[1] D.L. Flamm and V.M. Donnelly, Plasma Chem. Plasma Proc. I (1981) 317.
[2] J.W. Cobum, Plasma Chem. Plasma Proc. 2 (1982) 1.
[3] K.E. Greenberg, G.A. Hebner and J.T. Verdeyen, Appl. Phys. Lett. 44 (1984) 299.
[4] L.E. Kline, in: Nonequilibrium effects in ion and electron transport, eds. J.W. Gallagher, D.F. Hudson, E.E. Kunhardt and R.J. Van Brunt (Plenum, New York, 1990).
[5] A. Slaovi, F. Foulan, L. Fuchs, E. Foganassy and P. Siffert, Appl. Phys. A 50 (1990) 3 17.
[6] R.A. Gottscho, Phys. Rev. A 36 (1987) 2233.
[7] L.J. Overzet and L. Luo, Appl. Phys. Lett. 59 (1991) 161.
[8] J. Marriott and J.D. Craggs, J. Electron. Control 3 (1957) 194.
[9] Z.Lj. Petrovic, W.C. Wang, M. Suto, J.C. Han and L.C. Lee, J. Appl. Phys. 67 (1990) 675.
[IO] I.S. Buciel'nikova, Sov. Phys. JETP 35 (1959) 783.
[11] R. Nagpal and A. Garscadden, Appl. Phys. Lett. 64 (1994) 1626.
[12] G.R. Scheller, R.A. Gottscho, T. Intrator and D.B. Graves, J. Appl. Phys. 64 (1988) 4384.
[13] Z.J. Jabbour, K.E. Martus and K. Becker, Z. Phys. D 9 (1988) 263.
[14] M. Suto, C. Ye, J.C. Han and L.C. Lee, J. Chem. Phys. 89 (1988) 6653.
[15] L.C. Lee, J.C. Han and M. Suto, J. Chem. Phys. 91 (1989) 2036.
[16] PG. Gilbert, R.B. Siegel and K. Becker, Phys. Rev. A 41 (1990) 5594.
[17] F.W. Breitbarth, Plasma Chem. Plasma Proc. 12 (1992) 261.
[18] J.A. Stockdale, D.R. Nelson, F.J. Davis and R.N. Compton, J. Chem. Phys. 56 (1972) 3336.
[19] R.A. Gottshco and C.E. Gaebe, IEEE Trans. Plasma Sci. PS-14 (1986) 92.
[20] S. McGinnis, K. Rielh and PD. Haaland, Chem. Phys. Lett. 232 (1994) 99.
[21] J. Holtgrave, K. Riehl, D. Abner and PD. Haaland, Chem. Phys. Lett. 215 (1993) 548.
[22] PD. Haaland, J. Chem. Phys. 93 (1990) 4066.
[23] K. Riehl, Collisional detachment of negative ions using FTMS, Ph.D. Thesis, Air Force Institute of Technology (1992).
[24] A.G. Marshall, T.L. Wang and T.L. Ricca, J. Am. Chem. Soc. 107 (1985) 7893.
[25] S. Guan, J. Chem. Phys. 91 (1989) 775.
[26] PD. Haaland, Chem. Phys. Lett. 170 (1990) 146.
[27] R.C. Wetzel, EA. Baiocchi, T.R. Hays and R.C. Freund, Phys. Rev. A 35 (1987) 559.
[28] E. Krishnakumar and S.K. Srivastava, J. Phys. B: At. Mol. Opt. Phys. 21 (1988) 1055.
[29] R.C. Weast, ed., CRC Handbook of Chemistry and Physics, 66th Ed. (CRC Press, Boca Raton, 1985).
[30] K. Tokunaga, EC. Redeker, D.A. Danner and D.W. Hess, J. Electrochem. Soc. 128 (1981) 851.

Appendix E Ion Chemistry in hexafluoroethane, C_2F_6

Chem. Phys. Lett. ***310*, 52 (1999)**

27 August 1999

Chemical Physics Letters 310 (1999) 52-56

CHEMICAL PHYSICS LETTERS

www.elsevier.nl/locate/cplett

Partial ionization cross-sections of C_2F_6

C.Q. Jiao, A. Garscadden, P.D. Haaland *

Propulsion Directorate, Air Force Research Laboratory, Wright-Patterson AFB, OH 45433, USA

Received 26 April 1999

Abstract

The dissociative ionization of perfluoroethane, C_2F_6, by electron impact has been measured under single-collision conditions using Fourier transform mass spectrometry. The total ionization cross-section rises to a maximum value of $8.9 \pm 1.3 \times 10^{-16}$ cm^2 at 70 eV. CF_3^+ is the most prominent ion fragment at all energies, followed by $C_2F_5^+$, CF^+, and CF_2^+. $C_2F_6^+$ is not observed. The ratio of dissociative ionization to total dissociation increases from $27 \pm 5\%$ at 22 eV to $89 \pm 11\%$ at 70 eV. The total cross-section and the partitioning among the dissociative channels is examined in the context of the binary encounter Bethe (BEB) molecular orbital model. © 1999 Elsevier Science B.V. All rights reserved.

1. Introduction

Perfluoroethane, C_2F_6, is used as a precursor for reactive ion etching of semiconductors and as a gaseous dielectric for insulation. Earlier work on dissociative ionization of perfluoroethane includes magnetic sector measurements by Beran and Kevan [1] and quadrupole studies by Poll and Meischner [2]. A need for better quality C_2F_6 ionization cross-sections was recently noted in a review of its low-energy electron transport characteristics by Olthoff and Christophorou [3].

The partitioning of fragments among plausible dissociation channels is of both practical and fundamental significance. Fourteen of the 18 statistically possible fragment ions satisfy normal valence requirements:

$$C^+, F^+, F_2^+, CF^+, CF_2^+, CF_3^+, CF_4^+, C_2^+ ,$$

$$C_2F^+, C_2F_2^+, C_2F_3^+, C_2F_4^+, C_2F_5^+ \text{ and } C_2F_6^+ .$$

Only four of these ions are observed to form by low-energy electron impact: CF_3^+, $C_2F_5^+$, CF^+ and CF_2^+.

Others among this list of 14 are observed to form by dissociative ionization from different precursors. For example, $C_2F_3^+$ and $C_2F_4^+$, are formed by dissociative ionization of *c*-C_4F_8, and are therefore thermodynamically stable species (see, e.g., Ref. [4]). The selection among fragment channels is a result of dynamical constraints on either the electronic states to which C_2F_6 is excited, or on the trajectory followed by nuclei during the fragmentation of the excited ion state.

While theoretical estimates of ionization by electron impact using ab initio molecular orbital theory

* Corresponding author: Mobium Enterprises, 518 West Linden Street, Louisville, CO 80027-3124, USA. E-mail: phaaland@uswest.net

0009-2614/99/$ - see front matter © 1999 Elsevier Science B.V. All rights reserved.
PII: S0009-2614(99)00782-4

and the binary encounter Bethe (BEB) model have provided insight into the total ionization cross-sections for some molecular species [5], there is value in exploring whether these methods provide guidance on the number and relative importance of the partial ionization cross-sections as well. We will present a few observations and comments on this question for the case of C_2F_6 ionization below.

On a more practical note, the performance of plasma etch chemistries based on fluorocarbons generally – and C_2F_6 particularly – is constrained by ion kinetics. The partial ionization cross-sections can be integrated with the electron energy distribution of a gas discharge to evaluate the rates for production of each ion species. This initial ion species distribution may be modified by charge transfer collisions before the cations are extracted through a plasma sheath to the reactor boundaries. Combined with an understanding of the ion-molecule reaction rates for the plasma species, the partial ionization cross-sections permit estimates of the scaling of ion fluxes and composition with reactor pressure and gas mixture composition.

2. Experiment

Peffluoroethane C_2F_6 (Aldrich, 99%) is mixed with argon (99.999%, Matheson Research Grade) and admitted through a precision leak valve into a modified Fourier transform mass spectrometry (FTMS) system that has been described in detail elsewhere [6,7]. Ions are formed by electron impact in a cubic ion cyclotron resonance (ICR) trap cell at pressures in the 10^{-7} Torr range. An electron gun (Kimball Physics ELG-2, Wilton, NH) located 2 m from the trap irradiates the gas with a short (2-6 ms) pulse of a few hundred picocoulombs of low-energy electrons. The motions of ions produced by electron impact are constrained radially by a superconducting solenoidal magnetic field ($\approx$ 2 T) and axially by a nominal electrostatic trapping potential (l-2 V) applied to the trap faces that are perpendicular to the magnetic field. Ions of all mass-to-charge ratios are simultaneously and coherently excited into cyclotron orbits using a stored voltage waveform [8]. The image currents induced on the two remaining trap faces are then digitized and Fourier analyzed to yield a mass spectrum.

Calculation of the cross-section from the mass spectral intensities requires knowledge of the gas pressure, the electron beam current, and the number of ions produced. It is particularly important that the measurements are made during a time that is short enough to preclude perturbation of the species' distribution by charge transfer reactions. These calibration issues have been discussed elsewhere [6,7]. In the measurements reported here, we calibrate the cross-sections using ratios of the ion signals to those of argon, whose cross-section is known to $\pm$ 12% from the crossed-beam measurements of Wetzel and Freund [9].

The distribution of electron energies in the ion trap, based on the solution of Laplace's equation for the experimental geometry, is roughly Gaussian with a full-width-at-half-maximum (FWHM) of 0.5 eV due to the electrostatic trapping bias. The mean energy is accurate to f0.2 eV based on comparison of noble-gas ionization thresholds with spectroscopic data.

It is important to note that the ions are not actually collected in the FTMS experiment; only their electromagnetic influence on the antenna is recorded. As a result, the spectrometer sensitivity is neither mass nor species dependent for the results described here. We estimate the accuracy in the partitioning among ionic channels relative to argon to be $\pm$4%. Combined with the precision of the crossed-beam measurements on argon ($\pm$ 12% [9]), we estimate the magnitude of the of the cross-sections presented here to be accurate within $\pm$ 16%.

3. Results and discussion

The partial ionization cross-sections are displayed in Fig. 1. CF_3^+ is formed with the lowest threshold and in the highest yield at all energies out to 70 eV. The yields of CF_3^+ and $C_2F_5^+$ rise from threshold to 25 eV at similar rates, but the yield of carbon-carbon bond scission product increases more rapidly from 25 to 70 eV than that of carbon-fluorine cleavage. The present results are in plausible agreement with the early quadrupole measurements of Poll and

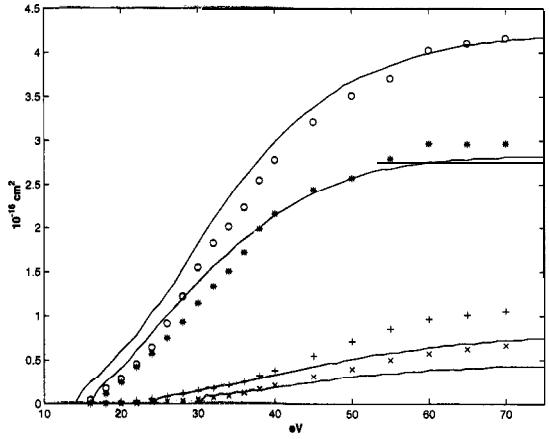

Fig. 1. Partial ionization cross-sections of C_2F_6: ∘, CF_3^+; ∗, $C_2F_5^+$; +, CF^+; X, CF_2^+. Solid lines are digitized quadrupole data from Ref. [2].

Meichsner as illustrated by the solid lines in Fig. 1 [2]. We find higher yields of CF' (20 eV) and CF_2^+ above 40 eV and a more gradual increase of cross-section with energy near threshold for CF_3^+ and $C_2F_5^+$.

The relatively high thresholds and small cross-sections for production of CF^+ (20 eV) and CF_2^+ (23 eV) imply that the rates of their formation from C_2F_6 in a plasma will be much less than those for CF_3^+ and $C_2F_5^+$ formation. One can also probe the evolution of ion composition due to charge transfer reactions by introducing a delay between ion formation and mass spectral evaluation in the FTMS experiment. In this way, we find that CF_3^+, $C_2F_5^+$ and CF^+ do not react with C_2F_6. However, CF_2^+ reacts with perfluoroethane to yield $C_2F_5^+$ with a rate coefficient of about 1.3 $\times 10^{-10}$ cm^3 s^{-1}. This coefficient is estimated by presuming charge transfer from argon [10]:

$$Ar^+ + C_2F_6 \rightarrow CF_3^+ + [Ar,CF_3]$$

$$Ar^+ + C_2F_6 \rightarrow C_2F_5^+ + [Ar,F]$$

occurs at the Langevin limiting value of 1.1 $\times 10^{-9}$ cm^3 s^{-1} for the measured polarizability of 6.2 $\times 10^{-24}$ cm^3 [11]. The product $C_2F_5^+$ is unreactive, so that the ion composition of a glow discharge that contains C_2F_6 should be be primarily CF_3^+, $C_2F_5^+$, and CF^+. The observation of other ion species in a plasma reactor can be thereby ascribed to alternate processes such as ionization of neutral radicals or the products of gas-phase neutral reactions.

The absence of the parent molecular ions, $C_2F_6^+$, implies that ionization of perfluoroethane by electrons is exclusively dissociative. The total dissociation cross-section has been reported by Winters and Inokuti to be 3.2 ± 0.6 $\times 10^{-16}$ cm^2 at 22 eV and 8.1 ± 1.6 $\times 10^{-16}$ cm^2 at 72 eV [12]. The total ionization cross-sections reported here are 0.9 ± 0.13 $\times 10^{-16}$ cm^2 and 8.9 ± 1.3 $\times 10^{-16}$ cm^2 at the same energies. At 22 eV, which is still well above the ionization thresholds, approximately 73 ± 5% of the total dissociation yields only neutral fragments. At 72 eV the dissociation is predominantly ionic within the combined uncertainties of the experimental measurements. (The upper bound for the neutral fraction is 22%.) Neutral species are also produced by dissociative ionization; for example F is a neutral product of the process that forms $C_2F_5^+$.

Fig. 2 displays the total experimental cross-sections recently reported by Nishimura [13] and the sum of the partial cross-sections presented here. These total ionization cross-sections are in quantitative agreement within the combined experimental uncertainties of the measurements.

Beran and Kevan [1] reported total cross-sections for a range of halocarbons at 20, 35, and 70 eV in

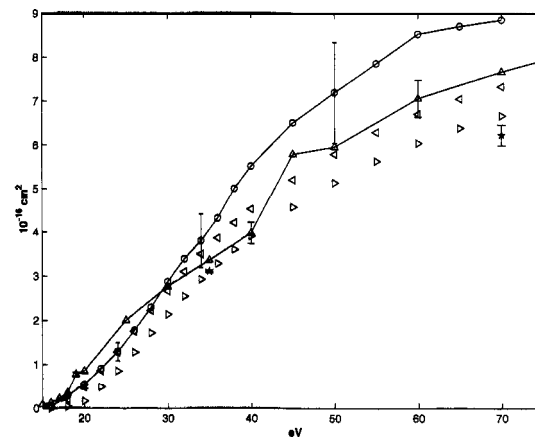

Fig. 2. Comparison of the present FTMS total ionization cross-section (∘), the ionization tube experimental values of Nishimura (▲) [13] and of Beran and Kevan (★) [1], and two BEB estimates using orbital energies of Kim (◁) [13] and energies of Winstead (▷) [17].

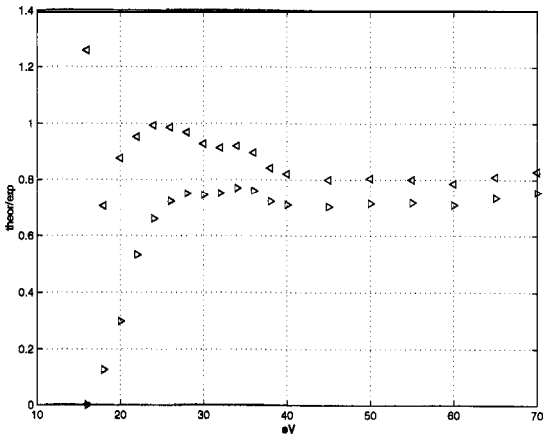

Fig. 3. Ratio of BEB cross-section estimates to the sum of the partial ionization cross-sections measured by FTMS. Calculations used RHF energies (D) and empirically adjusted CAS SCF energies (◁).

1969. All of the cross-sections presented in their paper were based on the magnitude of the argon ionization cross-section at 70 eV reported by Asundi and Kurepa in 1963 [14]. This value, 3.62 $x\ 10^{-16}$ cm^2, is substantially higher than that reported by Rapp and Englander-Golden 2.77 $x\ 10^{-16}$ cm^2 [15] in a total ionization tube, as well as more recent magnetic sector 2.80 $x\ 10^{-16}$ cm^2 [16] and crossed beam 2.91 $x\ 10^{-16}$ cm^2 [9] results. When the data of Beran and Kevan are scaled to the correct argon ionization cross-section [9] they are consistent with the present results at 20 eV but underestimate the total cross-section at 45 and 70 eV as depicted in Fig. 2.

The total ionization cross-section can be estimated using the BEB model [5]. Briefly, this model sums contributions to the total cross-section σ using ab initio estimates of the molecular orbital occupation numbers N, binding energies B, orbital U, and incident T kinetic energies according to the formula:

$$\sigma_{\mathrm{BEB}} = \frac{S}{t+u+1}\left[\frac{Q\ln t}{2}\left(1-\frac{1}{t^2}\right) + (2-Q)\left(1-\frac{1}{t}-\frac{\ln t}{t+1}\right)\right]$$

where

$$t=\frac{T}{B},\quad u=\frac{U}{B},\quad S = 4\pi a_o^2 N R^2/B^2,$$

a, is the Bohr radius, R is the Rydberg constant, and Q is a weighted integral of the target's continuum dipole oscillator strength that is routinely set equal to unity in the BEB method.

We also show in Fig. 2 two BEB estimates using different sets of molecular orbital energies. The first set are results of Hartree-Fock calculations at the RHF/6-311 + g * level of theory (◇) provided by Winstead and McKoy [17]. The second set (□) is derived from correlated wavefunctions with semi-empirical corrections to the binding energies as reported by Nishimura et al. [13] The BEB method with no empirical corrections to the HF wavefunctions is about 70% of the measured value above 25 eV. The BEB estimate is poor near threshold since its value drops to zero when the energy is less than the Koopman's theorem ionization potential. The BEB estimate accounts for over 80% of the measured cross-section using the correlated and empirically adjusted orbital energies. This behavior is illustrated in Fig. 3.

Motivated in part by this encouraging agreement we explored correlations between the orbital-by-orbital contributions and the measured partial ioniza-

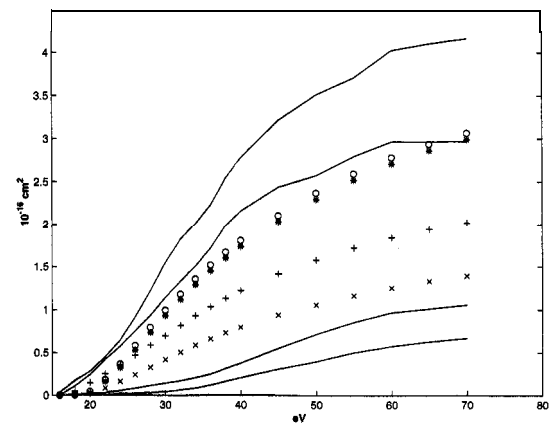

Fig. 4. Contributions to the BEB cross-section from orbitals of each symmetry scaled (by 1.4) to match the total cross-section at 70 eV. ∘, es; ∗, e,, +, a_{1g}, and X, a_{2u}. Solid lines are FTMS cross-sections.

tion cross-sections. The 33 filled molecular orbitals of C_2F_6 transform in four symmetry groups: $5e_g$, $5e_u$, $7a_{1g}$, and $6a_{2u}$. Twenty-five of these orbitals contribute to the BEB cross-sections below 70 eV. There are four pairs each of symmetry es and e_u, $5a_{1g}$, and $4a_{1u}$ filled orbitals. Summing the Hartree-Fock [17] contributions over each symmetry and scaling to match the measured total cross-sections yields the partial ionization estimates shown in Fig. 4. Although the numbers of symmetry groups and observed fragments are both four, the thresholds, shape, and relative magnitude of the cross-sections have only qualitative similarities. This hint of a correlation between orbital symmetry and partial ionization may be worthy of further investigation.

4. Conclusions

The partial ionization cross-sections of perfluoroethane C_2F_6 have been measured under single-collision conditions using FTMS. The results are consistent with the most recently published data for the total ionization cross-section, and the details of partitioning among the four charged products, CF_3^+, $C_2F_5^+$, CF^+, and CF_2^+ are quantified. Of these ions, only CF_2^+ reacts with the parent molecule at room temperature yielding $C_2F_5^+$, presumably by F^- transfer. The observation of ion species other than CF_3^+, $C_2F_5^+$, CF^+, and CF_2^+ in glow discharges can be ascribed to alternate processes such as ionization of neutral radicals or the products of gas-phase neutral reactions.

The ionization is also seen to be exclusively dissociative. Based on the published values of the total dissociation cross-section, the present results allow us to conclude that the the proportion of neutral dissociation decreases from 73% at 22 eV to less than 22% at 70 eV.

The BEB model provides reasonable estimates of the total ionization cross-section and, perhaps coincidentally, suggests qualitative features that correlate the symmetry of the molecular orbitals to the partial ionization cross-sections.

Acknowledgements

The authors would like to thank Charles DeJoseph for a thoughtful review of the manuscript. This work has been supported by the US Air Force Office of Scientific Research, The Air Force Research Laboratory at Wright-Patterson AFB, Ohio, and SEMATECH.

References

[1] J.A. Beran, L. Kevan, J. Phys. Chem. 78 (1969) 3866.
[2] H.U. Poll, J. Meichsner, Contrib. Plasma Phys. 27 (1987) 372.
[3] L.G. Christophorou, J.K. Olthoff, J. Phys. Chem. Ref. Data 27 (1998) 889. (1998).
[4] C.Q. Jiao, A. Garscadden, P.D. Haaland, Chem. Phys. Lett. 297 (1998) 121.
[5] Y.K. Kim, M.E. Rudd, Phys. Rev. A 50 (1994) 3594.
[6] K. Riehl, Collisional Detachment of Negative Ions using FTMS, Ph.D. Thesis, Air Force Institute of Technology, Wright-Patterson AFB, 1992.
[7] P.D. Haaland, Chem. Phys. Lett. 170 (1990) 146.
[8] S. Guan, J. Chem. Phys. 91 (1989) 775.
[9] R.C. Wetzel, F.A. Baioochi, T.R. Hayes, R.S. Freund, Phys. Rev. 35 (1987) 559.
[10] D.L. Smith, L. Kevan, J. Chem. Phys. 53 (1971) 2290.
[11] A.A. Maryott, F. Buckley, US Natl. Bur. Stand. Circular 537 (1957).
[12] H.F. Winters, M. Inokuti, Phys. Rev. A 25 (1982) 1420.
[13] H. Nishimura, W.M. Huo, M.A. Ah, Y.K. Kim, J. Chem. Phys. 110 (1999) 3811.
[14] R.K. Asundi, M.V. Kurepa, J. Electron. Control 15 (1963) 44.
[15] D. Rapp, P. Englander-Golden, J. Chem. Phys. 43 (1965) 1464.
[16] K. Stephan, H. Helm, T.D. Mark, J. Chem. Phys. 73 (1980) 3763.
[17] C. Winstead, B.V. McKoy, Orbital Potential and Kinetic Energies from the GAMESS Code at the HF/6-311 +g * Level of Theory, personal communication, 1998.

Appendix F Ionization of perfluoropropane, C_3F_8

Chem. Phys. Lett., ***325**, 203 (2000)*

ELSEVIER

Chemical Physics Letters 14204 (2000) xxx

CHEMICAL PHYSICS LETTERS

www.elsevier.nl/locate/cplett

Ionization of C_3F_8 by electron and ion impact

C.Q. Jiao, A. Garscadden, P.D. Haaland *

Propulsion Directorate, Air Force Research Laboratory, Wright-Patterson AFB, OH, 45433, USA

Received 27 March 2000; in final form 18 May 2000

Abstract

The dissociative ionization of perfluoropropane, C_3F_8, by electron impact has been measured under single collision conditions using Fourier Transform Mass Spectrometry. The total ionization cross-section rises to a maximum value of $1.24 \pm 0.20 \times 10^{-15}$ cm^2 at 140 eV. CF_3^+ is the most prominent ion fragment at all energies, followed by $C_3F_7^+$, CF^+, CF_2^+, $C_2F_4^+$ and $C_2F_5^+$; $C_3F_8^+$ is not observed. The ratio of dissociative ionization to total dissociation increases from $25 \pm 8\%$ at 22 eV to no less than 70% from 70 to 200 eV. Among the ion fragments only $C_3F_7^+$ reacts at room temperature to produce $C_2F_5^+$. © 2000 Elsevier Science B.V. All rights reserved.

1. Introduction

Perfluoropropane, C_3F_8, is used as a precursor for reactive ion etching of semiconductors, as a gaseous dielectric for insulation, and is a candidate for replacement of Halon fire suppressants. Earlier work on dissociative ionization of perfluoropropane includes magnetic sector measurements by Beran and Kevan [1] and quadrupole studies by Poll and Meischner [2]. A need for better quality C_3F_8 ionization cross-sections was recently noted in a review of its low energy electron transport characteristics by Christophorou and Olthoff [3].

The partitioning of fragments among plausible dissociation channels is of both practical and fundamental significance. Twenty-three of the 36 statistically possible fragment ions satisfy normal valence requirements:

C_3Fx^+ $(x = 0–8)$
$C_2F_x^+$ $(x = 0–6)$
CF_x^+ $(x = 0–4)$
F^+ and F_2^+.

Only six of these 23 ions are observed to form by low-energy electron impact:

CF_3^+
$C_3F_7^+$
CF^+
CF_2^+
$C_2F_4^+$
$C_2F_5^+$.

Others among this list of 23 are observed to form by dissociative ionization from different precursors. For example, $C_3F_5^+$ and $C_3F_2^+$ are formed by dissociative ionization of perfluorocyclobutane, and are therefore thermodynamically stable species [1]. The

* Corresponding author. Mobium Enterprises, 518 West Linden St., Louisville, CO 80027-3124. Fax: +1-303-665-9122; e-mail: phaaland@uswest.net

[1] See for example [4].

0009-2614/00/$ - see front matter © 2000 Elsevier Science B.V. All rights reserved.
PII: S0009-2614(00)00668-0

UNCORRECTED PROOF

selection among fragment channels is a result of dynamical constraints on either the electronic states to which C_3F_8 is excited, or on the trajectory followed by nuclei during the fragmentation of the excited ion state.

While theoretical estimates of ionization by electron impact using ab initio molecular orbital theory and the Binary Encounter Bethe (BEB) model have provided insight into the total ionization cross-sections for some molecular species [5], there may be value in exploring whether these methods provide guidance on the number and relative importance of the partial ionization cross-sections as well. We will present a few observations and comments on this question for the case of C_3F_8 ionization below.

On a more practical note, the performance of plasma etch chemistries based on fluorocarbons generally – and C_3F_8 particularly – is constrained by ion kinetics. The partial ionization cross-sections can be integrated with the electron energy distribution of a gas discharge to evaluate the rates for production of each ion species. This initial ion species distribution may be modified by charge transfer collisions before or while the cations are extracted through a plasma sheath to the reactor boundaries. Combined with an understanding of the ion–molecule reaction rates for the plasma species, the partial ionization cross-sections permit estimates of the scaling of ion fluxes and composition with reactor pressure and gas mixture composition.

2. Experiment

Perfluoropropane C_3F_8 (Aldrich, 99%) is mixed with argon (99.999%, Matheson Research Grade) and admitted through a precision leak valve into a modified Fourier Transform Mass Spectrometry (FTMS) system that has been described in detail elsewhere [6,7]. Ions are formed by electron impact in a cubic ion cyclotron resonance (ICR) trap cell at pressures in the 10^{-7} Torr range. An electron gun (Kimball Physics ELG-2, Wilton, NH) located 2 meters from the trap irradiates the gas with a short (2–6 ms) pulse of a few hundred picocoulombs of low-energy electrons. The motions of ions produced by electron impact are constrained radially by a superconducting solenoidal magnetic field (≈ 2 T) and axially by a nominal electrostatic trapping potential (1–2 V) applied to the trap faces that are perpendicular to the magnetic field. Ions of all mass to charge ratios are simultaneously and coherently excited into cyclotron orbits using a stored voltage waveform [8]. The image currents induced on the two remaining trap faces are then digitized and Fourier analyzed to yield a mass spectrum.

Calculation of the cross-section from the mass spectral intensities requires knowledge of the gas pressure, the electron beam current, and the number of ions produced. It is particularly important that the measurements are made during a time that is short enough to preclude perturbation of the species' distribution by charge transfer reactions. These calibration issues have been discussed elsewhere [6,7]. In the measurements reported here we calibrate the cross-sections using ratios of the ion signals to those of Argon, whose cross-section is known to $\pm 12\%$ from the crossed beam measurements of Wetzel and Freund [9].

The distribution of electron energies in the ion trap, based on the solution of Laplace's equation for the experimental geometry, is roughly Gaussian with a full-width-at-half-maximum of 0.5 eV due to the electrostatic trapping bias. The mean energy is accurate to ± 0.2 eV based on comparison of noble gas ionization thresholds with spectroscopic data.

It is important to note that the ions are not actually collected in the FTMS experiment; only their electromagnetic influence on the antenna is recorded. As a result, the spectrometer sensitivity *is neither mass nor species dependent* for the results described here. We estimate the accuracy in the partitioning among ionic channels relative to argon to be $\pm 4\%$. Combined with the precision of the crossed beam measurements on argon, $\pm 12\%$ [9], we estimate the magnitude of the cross-sections presented here to be accurate within $\pm 16\%$.

3. Results and discussion

The partial ionization cross-sections are displayed in Fig. 1a. Cleavage of a C–C bond to produce CF_3^+ has the lowest threshold and the highest yield at all

UNCORRECTED PROOF

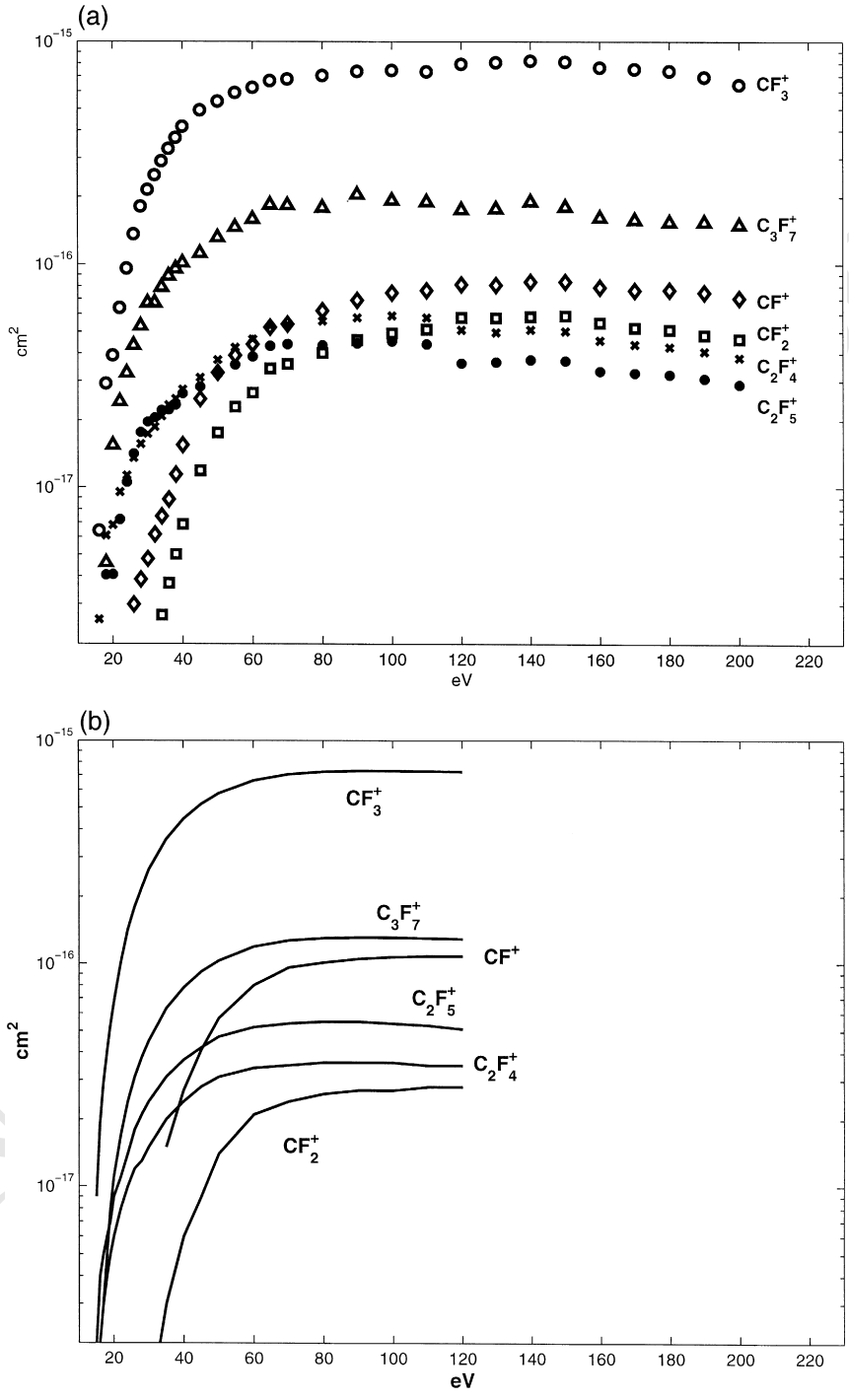

Fig. 1. Partial ionization cross-sections of perfluoropropane by (a) FTMS: ○, CF_3^+; △, $C_3F_7^+$; ◇, CF^+; □, CF_2^+; ×, $C_2F_4^+$; ●, $C_2F_5^+$; and (b) quadrupole mass spectrometry reported in Ref. [2].

Table 1
Comparison of cross-sections for electron impact dissociation (σ_d) and dissociative ionization (σ_i) of C_3F_8

Energy (eV)	σ_d (10^{-16} cm^2)	Error (10^{-16} cm^2)	σ_i (10^{-16} cm^2)	Error (10^{-16} cm^2)	σ_i/σ_d	min σ_i/σ_d	max σ_i/σ_d
22	4.39	±0.87	1.06	±0.17	0.25	0.17	0.35
72	11.0	±2.2	10.5	±1.7	0.95	0.67	1.38
100	11.6	±2.3	11.6	±1.9	1.00	0.70	1.45
125	11.8	±2.4	11.9	±1.9	1.00	0.70	1.47
200	10.0	±2.0	9.8	±1.6	0.98	0.68	1.42

The values in the min and max columns are computed presuming one sigma variation of the reported total and ionic dissociation cross-sections. The fact that all ionization is dissociative implies that values of $\sigma_i/\sigma_d > 1$ in the max σ_i/σ_d column are unphysical.

energies up to 200 eV. The next most abundant ion, $C_3F_7^+$, is the result of C–F bond scission and is formed in approximately 15% yield above 40 eV. This pattern is similar to that seen in dissociative ionization of perfluorethane, where CF_3^+ and $C_2F_5^+$ are the most abundant products [10]. $C_2F_4^+$ and $C_2F_5^+$ are formed with thresholds below 20 eV, while CF^+ and CF_2^+ have higher thresholds and larger cross-sections above 100 eV. The present results for CF_3^+ formation are in excellent agreement with the early quadrupole measurements of Poll and Meichsner as illustrated by the solid curves in Fig. 1b [2]. The total ionization cross-section reported by these authors is also in good agreement with the FTMS data. However, the partitioning among the remaining five dissociative pathways observed by FTMS differs from prior results, as can be seen in a detailed comparison of Fig. 1a and b. There are three

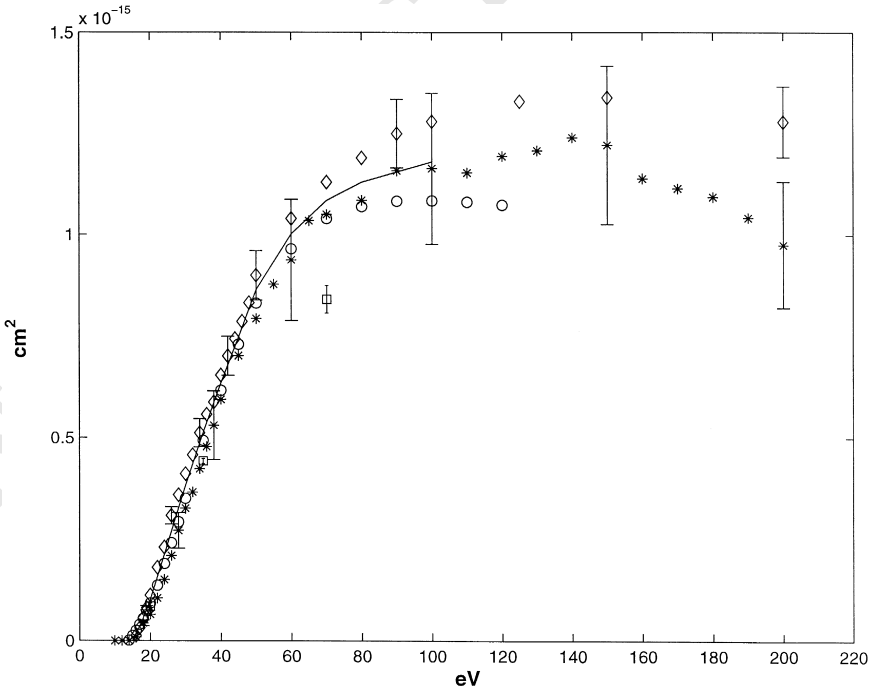

Fig. 2. Total ionization cross-sections for perfluoropropane. *, FTMS; ○, Poll [2]; ◇, Nishimura [12]; solid line, Christophorou and Olthoff [3]; □, Beran and Kevan [1].

arguments in favor of accepting the partitioning inferred by the FTMS measurements

- All ions are measured simultaneously, so that pressure or electron beam current fluctuations do not influence the relative ion yields.
- The ions are not collected as a current; only their electrostatic influence is recorded and this is independent of ion mass or chemical composition.
- The measurements are made at pressures and times that preclude charge transfer reactions from altering the measured species distribution.

The relatively high thresholds and small cross-sections for production of CF^+ (21 eV) and CF_2^+ (27 eV) imply that the rates of their formation from C_3F_8 in a plasma will be much less than those for CF_3^+ and $C_3F_7^+$ formation.

The absence of the parent molecular ions, $C_3F_8^+$, implies that ionization of perfluoropropane by electrons is exclusively dissociative. The total dissociation cross-section has been reported by Winters and Inokuti and is summarized in Table 1 [11]. At 22 eV, the lowest energy reported by Winters, the total dissociation cross-section is four times that for dissociative ionization. In other words, $25 \pm 8\%$ of the dissociation produces a positively charged fragment. The balance of dissociation is, by inference, into uncharged products. At energies between 72 and 200 eV, the total dissociation and dissociative ionization cross-sections are equal within the combined uncertainties of Winters' measurements and the present FTMS results. This dramatic increase in the ionic proportion of total dissociation with electron energy was also observed with perfluoroethane [10]. Note that neutral radicals are also produced even when $\sigma_i = \sigma_d$; for example F is a neutral product of the dissociative ionization process that forms $C_3F_7^+$.

Fig. 2 displays the total experimental cross-sections recently reported by Nishimura [12] and the sum of the partial cross-sections presented here. These total ionization cross-sections are in quantitative agreement within the combined experimental uncertainties of the measurements. Fig. 2 also shows

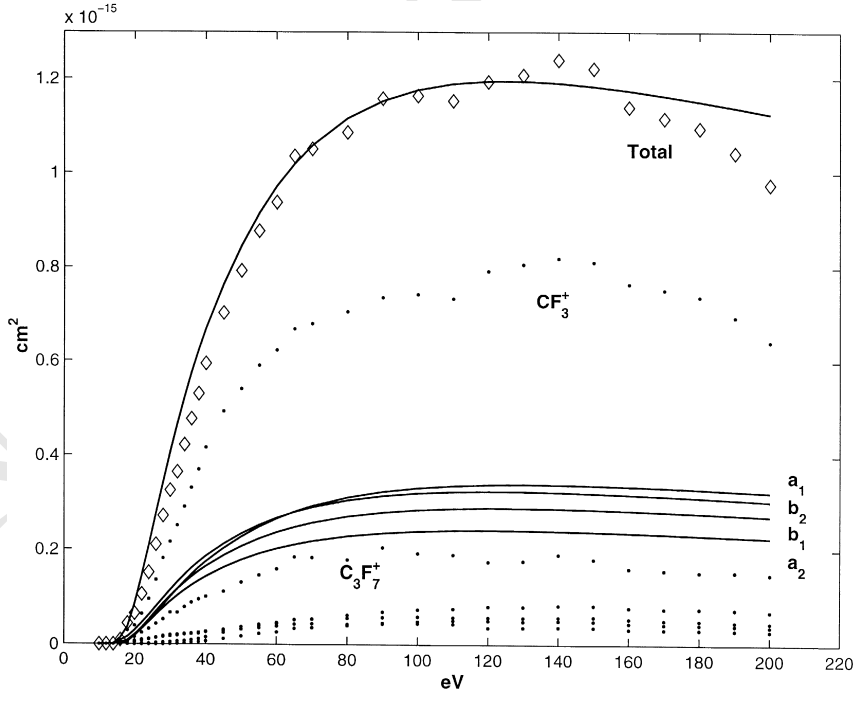

Fig. 3. BEB estimated cross-sections (solid lines) and FTMS results for total (◇) and partial (·) ionization. The measured values for CF_3^+ and $C_3F_7^+$ are labeled; other partial ionization cross-sections are more clearly discerned in Fig. 1. The contributions to the BEB cross-section for each of the four orbital symmetries are shown as solid lines.

the values recommended in the recent review by Christophorou [3].

Beran and Kevan [1] reported total cross-sections for a range of halocarbons at 20, 35 and 70 eV in 1969. All of the cross-sections presented in their paper were based on the magnitude of the argon ionization cross-section at 70 eV reported by Asundi and Kurepa in 1963 [13]. This value, 3.62×10^{-16} cm^2, is substantially higher than that reported by Rapp and Englander–Golden 2.77×10^{-16} cm^2 [14] in a total ionization tube, as well as more recent magnetic sector 2.80×10^{-16} cm^2 [15] and crossed beam 2.91×10^{-16} cm^2 [9] results. When the data of Beran and Kevan are scaled to the correct argon ionization cross-section [9] they are consistent with the present results at 20 and 35 eV but underestimate the total cross-section by about 20% at 70 eV.

The total ionization cross-section can be calculated using the Binary Encounter Bethe (BEB) model [5]. Briefly, this model sums contributions to the total cross-section σ using ab initio estimates of the molecular orbital occupation numbers N, binding energies B, orbital U, and incident T kinetic energies according to the formula:

$$\sigma_{\mathrm{BEB}} = \frac{S}{t+u+1}\left[\frac{Q\ln t}{2}\left(1-\frac{1}{t^2}\right) + (2-Q)\left(1-\frac{1}{t}-\frac{\ln t}{t+1}\right)\right]$$

where

$$t = \frac{T}{B},\ u = \frac{U}{B},\ S = 4\pi a_0^2 NR^2/B^2,$$

a_0 is the Bohr radius, R is the Rydberg constant, and Q is a weighted integral of the target's continuum dipole oscillator strength that is routinely set equal to unity in the BEB method.

Fig. 3 shows the results of BEB cross-sections estimates using CAS/SCF wavefunctions with semiempirical corrections to the binding energies as reported by Nishimura et al. [12]. The agreement between the FTMS total cross-sections (◇) and the calculated values is impressive. Motivated in part by

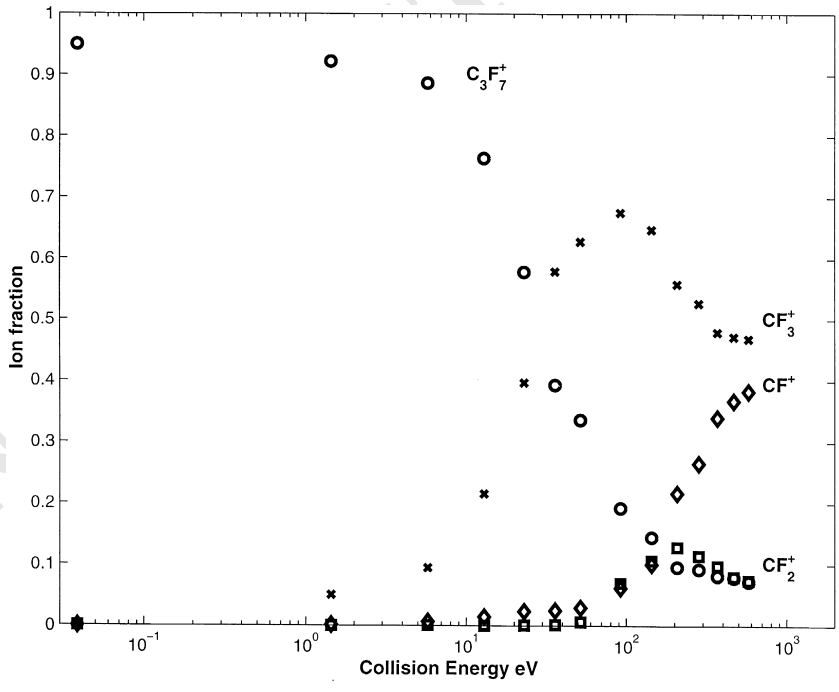

Fig. 4. Fate of translationally excited $C_3F_7^+$ (○) as a function of the center-of-mass kinetic energy to which the ion is excited. CF_3^+ (×) is formed at all energies above 1.5 eV, with CF^+ (◇) and CF_2^+ (□) being formed above 80 eV. Reactions occur at many collision energies as the ions' velocities cascade down following momentum transfer collisions.

UNCORRECTED PROOF

this agreement and similar results obtained for perfluoroethane [10] we explored correlations between the orbital-by-orbital contributions and the measured partial ionization cross-sections. The 45 filled molecular orbitals of C_3F_8 transform in four symmetry groups: $16a_1$, $7a_2$, $10b_1$ and $12b_2$. Thirty-four of these orbitals, $11a_1$, $6a_2$, $8b_1$ and $9b_2$, contribute to the BEB cross-sections below 200 eV. Summing the CAS Hartree–Fock contributions over each symmetry yields the partial ionization estimates also shown in Fig. 3. The contributions from each symmetry group shown as solid lines are approximately the same. However, the measured partial cross-sections shown as dotted lines on the linear *y*-scale of Fig. 3 bear no correlation to the symmetry-grouped BEB values. One might sum the a_1 and b_2 contributions to match the CF_3^+ cross-section and split the b_1 cross-section into four contributions to account for CF_2^+, $C_2F_4^+$, $C_2F_5^+$ and CF^+ while leaving the b_2 orbitals to account for $C_3F_7^+$, but these would be arbitrary assignments. None of the contributions grouped by symmetry have thresholds over 20 eV as observed for $C_2F_4^+$ and $C_2F_5^+$. We conclude that, although the BEB model provides a good estimate of the total ionization cross-section for C_3F_8, the partitioning among dissociative channels is not captured by grouping contributions of like orbital symmetry.

One can also probe the evolution of ion composition due to room-temperature charge transfer reactions by introducing a delay between ion formation and mass spectral evaluation in the FTMS experiment. In this way we find that the most abundant CF_3^+ ion does not react with C_3F_8. The next most abundant ion, $C_3F_7^+$, reacts with perfluoropropane to yield $C_2F_5^+$ and neutral products with a rate coefficient of approximately 2×10^{-10} cm^3 s^{-1}. $C_2F_5^+$, CF_2^+, CF^+ and $C_2F_4^+$ do not react at room temperature with perfluoropropane.

$C_3F_7^+$ was isolated in the trap by resonantly ejecting all of the other ions produced from 50 eV electron impact. 5% of these $C_3F_7^+$ ions yield CF_3^+ in the room-temperature trap within 300 ms. The remaining 95% of the $C_3F_7^+$ ions collide with perfluoropropane to produce $C_2F_5^+$. FTMS experiments do not resolve whether the excess energy in $C_3F_7^+$ that leads to CF_3^+ is electronic, vibrational, or rotational.

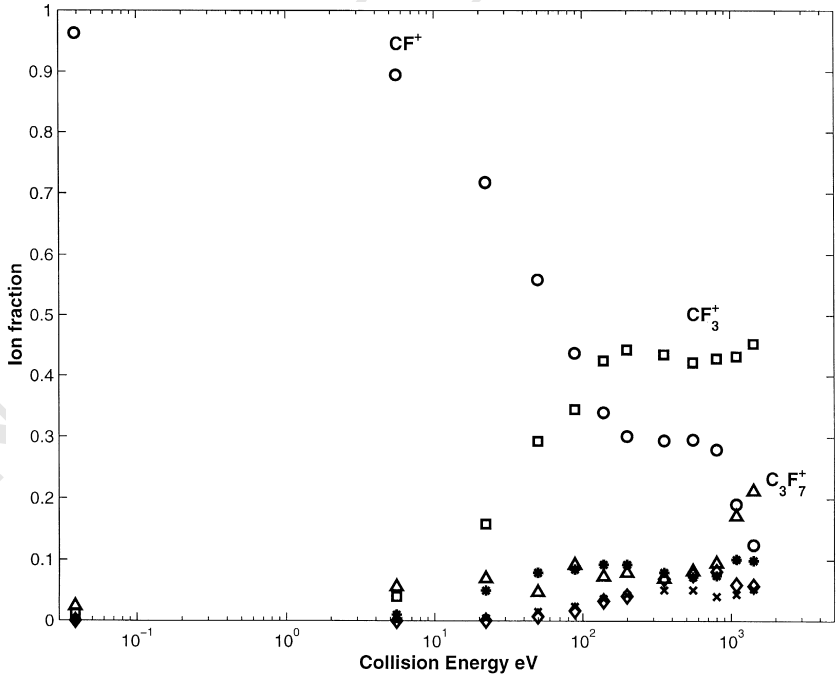

Fig. 5. Fate of translationally excited CF^+ (○) as a function of the center-of-mass kinetic energy to which the ion is excited. The most prominent products CF_3^+ (□) and $C_3F_7^+$ (△) are labeled. Low yields of CF_2^+ (◇), $C_2F_4^+$ (×) and $C_2F_5^+$ (*) are also shown.

UNCORRECTED PROOF

However, it is clear that internally excited $C_3F_7^+$ with enhanced reactivity is formed by 50 eV electron impact. This collisional decomposition of excited $C_3F_7^+$ may account in part for its smaller partial ionization cross-section reported by Poll and Meichsner [2].

Ionization of perfluoropropane by charge transfer was probed by selectively sweeping all but one ion species from the trap and exciting its cyclotron motion to larger orbits, then monitoring the fragmentation. We find that CF_3^+ is the predominant product of kinetically excited charge transfer whether the reactant ion is CF^+, CF_2^+, $C_2F_4^+$, $C_2F_5^+$, Ar^+ or $C_3F_7^+$. Typical results for the reactions of translationally excited $C_3F_7^+$ and CF^+ in Figs. 4 and 5. At room temperature 5% of the $C_3F_7^+$ ion is internally excited and has decomposed on the timescale of the measurements. The remaining, thermodynamically stable ion is converted to CF_3^+ starting at center-of-mass kinetic energies of 1.5 eV, with the dissociation or charge transfer half complete at 27 eV and maximized when the $C_3F_7^+$: C_3F_8 collision energy has been raised to 95 eV. As the energy increases above 90 eV new channels that produce CF^+ and CF_2^+ are opened at the expense of CF_3^+ production. Translationally hot CF^+ also produces CF_3^+ with a similar kinetic energy dependence as shown in Fig. 5. A $C_3F_7^+$ product channel opens at about 1 keV collision energy.

The low threshold and large cross-section for production of CF_3^+ and its failure to react further with perfluoropropane leads one to conclude that this species should dominate the reactive flux in a plasma that contains C_3F_8. This prediction is strengthened by the fact that conversion of the other five ion species to CF_3^+ occurs at kinetic energies comparable to those expected from the electrostatic sheath in typical plasma reactors. If the sheath is collisional, in other words if the collisional mean-free path is less than the sheath thickness, one expects further enhancement of the CF_3^+ flux by charge transfer.

4. Conclusions

The partial ionization cross-sections of perfluoropropane C_3F_8 have been measured under single collision conditions using Fourier Transform Mass Spectrometry. The results are consistent with the most recently published data for the total ionization cross-section, and the details of partitioning among the six charged products, CF_3^+, $C_3F_7^+$, CF^+, CF_2^+, $C_2F_4^+$ and $C_2F_5^+$ are quantified. Of these ions only $C_3F_7^+$ reacts with the parent molecule at room temperature, yielding $C_2F_5^+$. Translationally excited ion fragments do react with perfluoropropane yielding CF_3^+ as the principal product. The observation of ion species other than CF_3^+, $C_3F_7^+$, CF^+, CF_2^+, $C_2F_4^+$ and $C_2F_5^+$ in plasmas must therefore be ascribed to alternate processes such as ionization of neutral radicals, the products of gas-phase neutral reactions, or ion–radical reactions.

The ionization is also seen to be exclusively dissociative. Based on the published values of the total dissociation cross-section the present results allow us to conclude that the contribution of neutral dissociation to total dissociation decreases from 75% at 22 eV to less than 30% from 75 to 200 eV.

The Binary Encounter Bethe model provides a reasonable estimate of the total ionization cross-section, but partitioning the contributions among orbitals of like symmetry does not reproduce the observed fragmentation pattern.

Acknowledgements

This work has been supported by the U.S. Air Force Office of Scientific Research, The Air Force Research Laboratory at Wright-Patterson A.F.B., Ohio and SEMATECH.

References

[1] J.A. Beran, L. Kevan, J. Phys. Chem. 78 (1969) 3866.
[2] H.U. Poll, J. Meichsner, Contrib. Plasma Phys. 27 (1987) 359.
[3] L.G. Christophorou, J.K. Olthoff, J. Phys. Chem. Ref. Data 27 (1998) 889.
[4] C.Q. Jiao, A. Garscadden, P.D. Haaland, Chem. Phys. Lett. 297 (1998) 121.
[5] Y.K. Kim, M.E. Rudd, Phys. Rev. A 50 (1994) 3594.
[6] K. Riehl, Collisional Detachment of Negative Ions Using FTMS, Ph.D. Thesis, Air Force Institute of Technology, Wright-Patterson AFB, 1992.
[7] P.D. Haaland, Chem. Phys. Lett. 170 (1990) 146.
[8] S. Guan, J. Chem. Phys. 91 (1989) 775.

UNCORRECTED PROOF

[9] R.C. Wetzel, F.A. Baioochi, T.R. Hayes, R.S. Freund, Phys. Rev. 35 (1987) 559.
[10] C. Jiao, A. Garscadden, P. Haaland, Chem. Phys. Lett. 310 (1999) 52.
[11] H.F. Winters, M. Inokuti, Phys. Rev. A 25 (1982) 1420.
[12] H. Nishimura, W.M. Huo, M.A. Ali, Y.K. Kim, J. Chem. Phys. 110 (1999) 3811.
[13] R.K. Asundi, M.V. Kurepa, J. Electron. Control 15 (1963) 44.
[14] D. Rapp, P. Englander-Golden, J. Chem. Phys. 43 (1965) 1464.
[15] K. Stephan, H. Helm, T.D. Mark, J. Chem. Phys. 73 (1980) 3763.

UNCORRECTED PROOF

Appendix G Ionization of perfluorocyclobutane, c-C_4F_8

Chem. Phys. Lett., ***297*, 121 (1998).**

20 November 1998

CHEMICAL PHYSICS LETTERS

Chemical Physics Letters 297 (1998) 121-126

Ion chemistry in octafluorocyclobutane, c-C_4F_8

C.Q. Jiao [a], A. Garscadden [b,*], P.D. Haaland [a]

[a] *Mobium Enterprises, 5100 Springfield Pike, Dayton, OH 45431-1231, USA*
[b] *AFRL / PR, Bldg 18A, 1950 Fifth St., Wright-Patterson Air Force Base, OH 45433-7251, USA*

Received 13 July 1998; in final form 24 September 1998

Abstract

Cross-sections for electron impact ionization of octafluorocyclobutane (c-C_4F_8) have been measured from 10 to 200 eV by Fourier transform mass spectrometry. No parent ion is observed, and over half of the dissociative ionization yields $C_2F_4^+$ and $C_3F_5^+$. Eleven other fluorocarbon cations are produced with smaller cross-sections, giving a total ionization cross-section of (1.6 ± 0.2) X 10^{-15} cm^2 between 80 and 200 eV. Only CF_2^+ and $C_2F_3^+$ react further with the parent molecule to yield $C_3F_5^+$ as the primary product. No evidence of cationic polymerization was found. F^- and $C_4F_8^-$ are formed by electron attachment at energies below 10 eV, but neither reacts further with c-C_4F_8. © 1998 Elsevier Science B.V. All rights reserved.

1. Introduction

Octafluorocyclobutane (c-C_4F_8) is a good high-voltage insulator, and the electron attachment to this molecule has been extensively studied [1–18]. c-C_4F_8 is also used as a reagent for reactive ion etching of semiconductors [19], where recent studies have shown that positive ions are intimately involved in the surface deposition and etching processes [20]. Early data on the ionization cross-section of this fluorocarbon at 35 eV [4] and 70 eV [21] have recently been updated with quadrupole mass spectrometry measurements by Sugai and co-workers [22]. The sensitivity of quadrupole instruments is inherently nonlinear with mass, so here we present a complete characterization of the partial ionization of c-C_4F_8 using Fourier transform mass spectrometry (FTMS) technique.

Although positive ion formation by electron impact in plasmas is essential to maintain the conductivity that characterizes the plasma state, the stoichiometry of ion species can be modified by charge transfer reactions before ions diffuse to the boundary and are extracted by electrostatic sheath fields. We therefore also present an investigation of the evolution of positive and negative ion composition that results from reactions of the dissociatively ionized fragments with the parent c-C_4F_8.

2. Experimental

Octafluorocyclobutane (99 + %, TCI America) is mixed with argon (99.999% Matheson Research Grade) with a ratio (c-C_4F_8:Ar) of 1:2, and admitted through a precision leak valve into a modified Extrel FTMS system that has been described in detail else-

* Corresponding author. Fax: + 1 937 656 4657; E-mail: alan.garscadden@wl.wpafb.af.mil

0009-2614/98/$ - see front matter © 1998 Elsevier Science B.V. All rights reserved.
PII: S0009-2614(98)01107-5

where [23]. Ions are formed by electron impact in a cubic ion cyclotron resonance (ICR) trap cell at pressures in the 10^{-7} Torr range. An electron gun (Kimball Physics ELG2, Wilton, NH) irradiates that trap for 6 ms with a few hundred picocoulombs of low-energy electrons. The motions of the ions are constrained radially by a superconducting solenoidal magnetic field (~ 2 T) and axially by a nominal electrostatic potential (1 V) applied to the trap faces that are perpendicular to the magnetic field. Ions of all mass-to-charge ratios are simultaneously and coherently excited into cyclotron orbits using a stored waveform [24,25] applied to two opposing trap faces that are parallel to the magnetic field. Following cyclotron excitation, the image currents induced on the two remaining faces of the trap are amplified, digitized, and Fourier analyzed to yield a mass spectrum.

Calculation of cross-sections from the mass spectrum intensities requires knowledge of the gas densities, the electron beam current, and the number or ions produced. These calibration issues have been described previously [23,25,26]. The intensity ratios of the ions from c-C_4F_8 to Ar^+ give cross-sections relative to those for argon ionization [27] since the c-C_4F_8:Ar pressure ratio is quantified by capacitance manometry of the gas mixture. The absolute c-C_4F_8 pressure at the ICR trap that is needed for ion-molecule kinetic analysis is inferred from the rate coefficient of the known reaction of O_2^+ with c-C_4F_8 [28].

The distribution of electron energies in the trap, based on the solution of Laplace's equation for the experimental geometry, is roughly Gaussian with a full width at half maximum of 0.5 eV due to the electrostatic trapping bias [23]. The mean energy of the irradiating electrons is accurate to ± 0.2 eV based on comparison of noble gas ionization thresholds with spectroscopic data. We fit the cross-section data to an empirical functional form using a limited number of parameters:

$$\sigma = A \tanh \frac{\pi(\varepsilon - T)}{\alpha} e^{-k(\varepsilon - T)},$$

where σ is the cross-section, ϵ is the electron energy, T is the appearance potential, A scales the amplitude, α quantifies $d\sigma/d\epsilon$ near threshold, and k characterizes the higher-energy behavior.

3. Results and discussion

Electron impact ionization of c-C_4F_8 produces thirteen ion species, with $C_2F_4^+$ and $C_3F_5^+$ comprising over half of the yield from the threshold to 200 eV. Other fragment ions include CF_x^+ and $C_2F_x^+$ with x = 1-3, $C_3F_y^+$ with y = 1-4, and F^+. The molecular ion, $C_4F_8^+$, is not found by electron im-

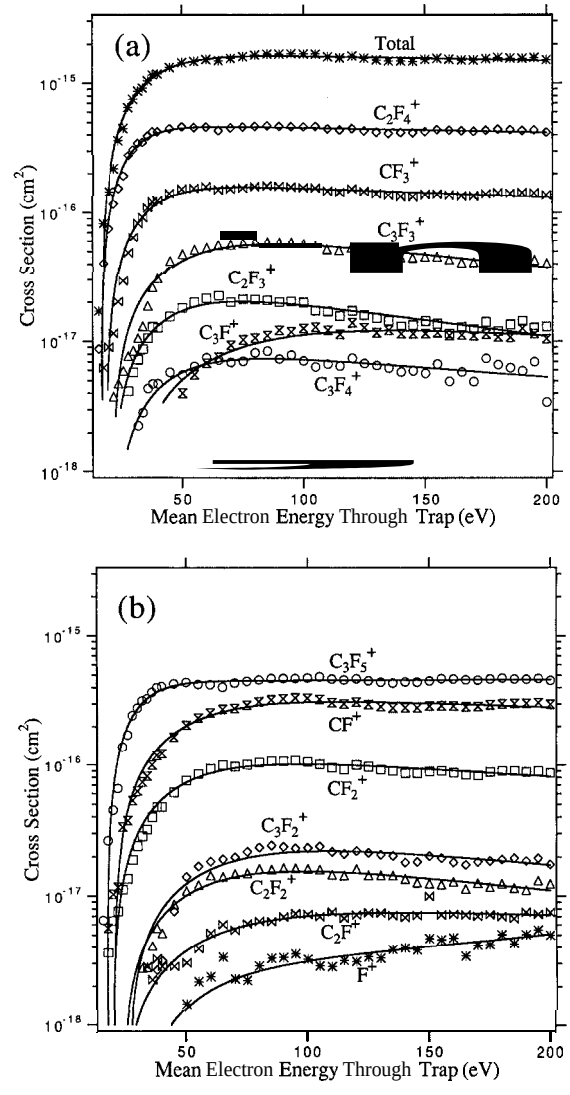

Fig. 1. (a) and (b): Cross-sections for ionization of c-C_4F_8 by electron impact. Points represent experimental data, and solid lines are fits of the equation described in the text.

pact. The total ionization cross-section reaches a maximum value of $(1.6 \pm 0.2) \times 10^{-15}$ cm^2 at 80 eV, and levels off thereafter. The cross-sections for each dissociative ionization process as a function of the electron energy are shown in Fig. 1 and the coefficients for our functional fit are summarized in Table 1. Data in Fig. 1 are compared to the previously reported findings, namely, the ionization cross-sections at 35 eV [4] and 70 eV [21] measured with magnetic mass spectrometers, and a recent quadrupole mass spectrometry measurement of the dissociative ionization [22]. There are significant differences in the dissociative ionization cross-sections among the data from these measurements including the present FTMS assessment. The quadrupole measurement by Sugai and co-workers [22] reports 6 ions while the FTMS measurement yields quantitative results for 13 species whose cross-sections exceed 10^{-18} cm^2. The FTMS technique is intrinsically independent of ion mass. The ions are not collected, rather their influence on the near-field antennae, which is a consequence only of their orbital motion and Maxwell's equations, is the measured quantity. Furthermore, the combination of low reagent pressures (10^{-7} Torr) and short observation times (ms) precludes modification of the ion ensemble by charge transfer collisions. Finally, the FTMS experiment setup lacks a proximal filament on which pyrolysis can produce new species that confound interpretation of the mass spectrum.

Table 1
Fitting parameters for dissociative ionization cross-sections. Ions are listed in the order of increasing mass. Also listed are the cross-sections at 70 eV, σ, in units of 10^{-16} cm^2

Ion	A (cm^2)	k (eV^{-1})	α (eV)	T (eV)	σ
F^+	2.4×10^{-18}	-4.2×10^{-3}	127	27.4	0.02
CF^+	3.7×10^{-16}	1.6×10^{-3}	146	20.4	2.8
C_2F^+	9.1×10^{-18}	1.4×10^{-3}	190	22.3	0.05
CF_2^+	1.3×10^{-16}	2.7×10^{-3}	138	19.8	0.97
C_3F^+	1.7×10^{-17}	2.7×10^{-3}	230	27.4	0.09
$C_2F_2^+$	2.4×10^{-17}	4.5×10^{-3}	166	23.4	0.15
CF_3^+	1.8×10^{-16}	$1.6 \sim 10^{-3}$	77	19.0	1.5
$C_3F_2^+$	3.4×10^{-17}	3.8×10^{-3}	177	25.7	0.20
$C_2F_3^+$	3.0×10^{-17}	5.6×10^{-3}	112	21.1	0.20
$C_3F_3^+$	8.5×10^{-17}	4.5×10^{-3}	140	21.4	0.56
$C_2F_4^+$	4.8×10^{-16}	8.0×10^{-4}	5	16.9	4.5
$C_3F_4^+$	9.6×10^{-18}	3.3×10^{-3}	111	21.9	0.07
$C_3F_5^+$	4.5×10^{-16}	-1.4×10^{-4}	5	6	17.5	4.3

Gas-phase reactions of the above positive ions with neutral c-C_4F_8 are studied by double resonance experiments. Each of the ions is isolated and the mass spectrum is recorded at programmed reaction times. Only CF_2^+ and $C_2F_3^+$ are found to react, yielding $C_3F_5^+$ as the major product ion, reactions (1)–(10).

$$CF_2^+ + c\text{-}C_4F_8 \rightarrow CF_3^+ + (C_4F_7)\ 14\% \quad (1)$$
$$\rightarrow C_2F_4^+ + (C_3F_6)\ 5\% \quad (2)$$
$$\rightarrow C_3F_3^+ + (C_2F_7)\ 2\% \quad (3)$$
$$\rightarrow C_3F_5^+ + (C_2F_5)\ 53\% \quad (4)$$
$$\rightarrow C_4F_6^+ + (CF_4)\ 6\% \quad (5)$$
$$\rightarrow C_4F_7^+ + (CF)\ 20\%, \quad (6)$$
$$C_2F_3^+ + c\text{-}C_4F_8 \rightarrow CF+ + (C_5F_{10})\ 3\% \quad (7)$$
$$\rightarrow C_2F_4^+ + (C_4F_7)\ 7\% \quad (8)$$
$$\rightarrow C_3F_5^+ + (C_3F_6)\ 81\% \quad (9)$$
$$\rightarrow C_4F_7^+ + (C_2F_4)\ 9\%. \quad (10)$$

Formulae in the parentheses of the equations do not necessarily imply the actual neutral product composition. These reactions do not significantly change the overall ion composition of a c-C_4F_8 plasma, since the relative concentrations of the reactant ions, CF_2^+ and $C_2F_3^+$, are very small. Therefore, one can expect that $C_2F_4^+$ and $C_3F_5^+$ are the major ionic species reaching the surface from the plasma. Reactions of several selected rare-gas ions with c-C_4F_8 are also studied, with major product ions shown in reactions (11)–(16).

$$Ar^+ + c\text{-}C_4F_8 \rightarrow C_2F_4^+ + (C_2F_4) + Ar\ 50\% \quad (11)$$
$$\rightarrow C_3F_5^+ + (CF_3) + Ar\ 46\%, \quad (12)$$
$$Kr^+ + c\text{-}C_4F_8 \rightarrow C_2F_4^+ + (C_2F_4) + Kr\ 81\% \quad (13)$$
$$\rightarrow C_3F_5^+ + (CF,) + Kr\ 16\%, \quad (14)$$
$$Xe^+ + c\text{-}C_4F_8 \rightarrow C_2F_4^+ + (C_2F_4) + Xe\ 46\% \quad (15)$$
$$\rightarrow C_3F_5^+ + (CF,) + Xe\ 52\%. \quad (16)$$

Minor product ions (with ~ 1% branching ratios) from Ar^+ reaction include F^+, CF^+, CF_3^+ and C_2F^+,

from Kr^+ reaction, F^+, CF_2^+ and C_2F^+, and from Xe^+ reaction, C_2F^+ and $C_4F_8^+$. Although no molecular ion is produced by electron impact, it is found as a minor product of charge transfer from Xe^+. The parent ion has an orbitally degenerate electronic structure and so is subject to the Jahn-Teller distortion. The energy liberated during distortion is too great for the molecular ion to remain bound, resulting in fragmentation forming mainly $C_2F_4^+$ and $C_3F_5^+$. The charge transfer reaction occurs over a much longer time scale, so that nuclear potential energy of the c-$C_4F_8^+$ can be shared with the departing Xe atom through the long-range Langevin potential. The result is stabilization of a distorted $C_4F_8^+$ ion that may or may not retain the cyclic structure.

Rate coefficients are obtained by fitting ordinary differential equations to the time varying ion distributions such as those shown in Fig. 2. Table 2 summarizes these coefficients for reactant ions formed by electron impact at 20, 35, and 50 eV. The rate coefficients are independent of the energy with which the reactant ion is formed within our experimental uncertainty. This implies that internal excitation of the reactant ion, if it occurs by energetic electron impact, does not change the charge transfer kinetics.

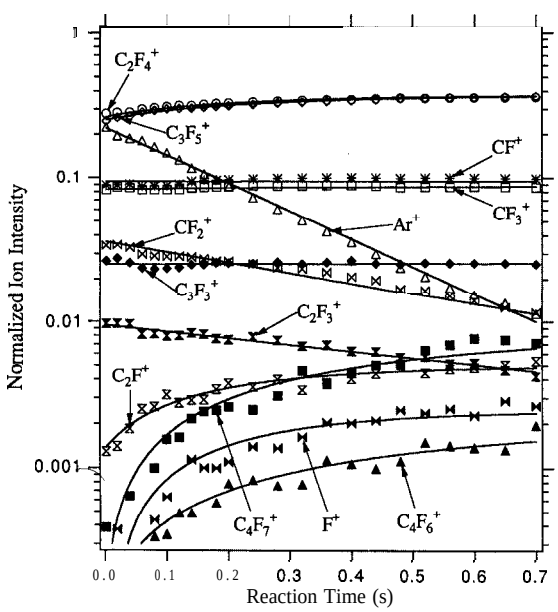

Fig. 2. Time evolution of positive ion species produced by 50 eV electron impact at a mixture of c-C_4F_8 and Ar (1:2) with a total pressure of 3.3 X 10^{-7} Torr. Data are shown only for the ions whose intensities change as the time. Points represent experimental data, and solid lines are fits of a kinetic model which gives the reaction rate coefficients presented in Table 2.

Table 2
Ion-molecule reaction rate coefficients in units of 10^{-9} cm^3 s^{-1}, measured in three separate experiments, l-3, in which the primary ions are formed by electron impact at 20, 35 and 50 eV, respectively

Reaction	Experiment 1	Experiment 2	Experiment 3
$CF_2^+ + C_4F_8$	–	0.47 ± 0.05	0.47 ± 0.05
$C_2F_3^+ + C_4F_8$	–	0.33 ± 0.05	0.30 ± 0.05
$Ar^+ + C_4F_8$	1.5 ± 0.2	1.3 ± 0.2	1.3 ± 0.2

Attachment is not probed by beam electrons in our FTMS instrument because space-charge limits propagation of low energy electron beams along the 1 m path from the electron gun to the ion trap. Instead, we use the secondary electrons that are produced by ionization of the reagent gases and are trapped in the ICR cell along with negative ions. In experiments, a 50 eV electron beam irradiates the ion trap for an extended period (80 ms). The secondary electrons produced at different locations along the trapping axis of the cell are born with different electrostatic potential energies. These electrons un-

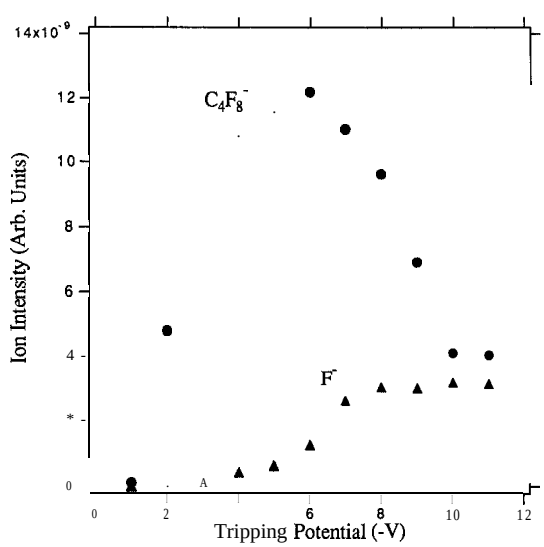

Fig. 3. Negative ion yields from trapped secondary electrons as a function of the applied trapping potential. The primary electron energy is 50 eV, and the electron beam period is 80 ms.

dergo damped harmonic motion in the trapping potential, where the damping arises from electron-neutral collisions with reagent gas. As the electrons cascade down in energy they have an opportunity to attach as well as be cooled by momentum transfer. Increasing the magnitude of the trapping potential increases the initial potential energy at which the secondary electrons are formed, so that processes with successively higher thresholds may be probed. Although this approach lacks the energy resolution of crossed beam measurements, it has the advantage that further reactions between anionic products of attachment and the parent gas may be conveniently probed. Fig. 3 shows the negative ion yield as a function of trapping potential for attachment to c-C_4F_8. Previous reports found a resonance for c-$C_4F_8^-$ peaking at 0.45 eV [8] and multiple resonance peaks for F^- at ~ 5 eV and higher energies [2,8]. Our data in Fig. 3 are qualitatively consistent with these findings. Production of F^- from c-C_4F_8 is a classic illustration of dissociative electron attachment, and has been extensively reported [2–4,9,14]. The observation of $C_4F_8^-$ at the low pressures ($<10^{-6}$ Torr) and long experiment times (up to 1 s) of FTMS is more unusual, since there are no departing fragments to satisfy energy conservation in the exit channel leading to a single anion. While emission of infrared photons may stabilize the association product, one of the ring bonds in c-$C_4F_8^-$ may be broken while retaining the stoichiometry of the parent molecule. No reaction is found between either $C_4F_8^-$ or F^- and neutral c-C_4F_8, which exclude the possibility that $C_4F_8^-$ is formed by the reaction of F^- with c-C_4F_8 during the extended electron beam period.

4. Conclusions

Thirteen positive ions are produced by electron impact on c-C_4F_8 with $C_2F_4^+$ and $C_3F_5^+$ to be the predominant fragment ions and a total ionization cross-section of $(1.6 \pm 0.2)\ x\,10^{-15}\ cm^2$ between 80 and 200 eV. No parent molecular ion $C_4F_8^+$ is observed. Relaxation of the ion composition by charge transfer reactions implies that ion fluxes will be comprised mainly of $C_2F_4^+$ and $C_3F_5^+$ under many plasma conditions. No evidence of cationic polymerization to form heavier ions was identified. Two negative ions are observed to form following impact of electrons with less than 10 eV of energy. F^- arises from standard dissociative attachment, while the formation of $C_4F_8^-$ involves either emission of a photon or stabilization by ring-opening. Neither F^- nor $C_4F_8^-$ reacts with c-C_4F_8.

Acknowledgements

The authors wish to acknowledge the Air Force Office of Scientific Research for supporting this research.

References

[1] A.A. Cbristodoulides, L.G. Christophorou, R.Y. Pai, CM. Tung, J. Chem. Phys. 70 (1979) 1156.
[2] I. Sauers, L.C. Christophorou, J.G. Carter, J. Chem. Phys. 71 (1979) 3016.
[3] R.M. Reese, V.H. Dibeler, F.L. Mohler, J. Res. Natl. Bur. Stand. 57 (1956) 367.
[4] M.M. Bibby, G. Carter, Trans. Faraday Soc. 59 (1963) 2455.
[5] M.V. Kurepa, 3rd Czech. Conf. on Electronics and Vacuum Physics Transactions 107 (1965).
[6] R. Grajower, C. Lifshitz, Isr. J. Chem. 6 (1968) 847.
[7] W.T. Naff, C.D. Cooper, J. Chem. Phys. 49 (1968) 2784.
[8] P.W. Harland, J.C.J. Thynne, Int. J. Mass Spectrom. Ion Phys. 10 (1972) 11.
[9] C. Lifshitz, R. Grajower, Int. J. Mass Spectrom. Ion Phys. 10 (1972) 25.
[10] K.M. Bansal, R.W. Fessenden, J. Chem. Phys. 59 (1973) 1760.
[11] F.J. Davis, R.N. Compton, D.R. Nelson, J. Chem. Phys. 59 (1973) 2324.
[12] L.G. Christophorou, D.L. McCorkle, D. Pittman, J. Chem. Phys. 60 (1974) 1183.
[13] P.W. Harland, J.L. Franklin, J. Chem. Phys. 61 (1974) 1621.
[14] R.L. Woodin, M.S. Foster, J.L. Beauchamp, J. Chem. Phys. 72 (1980) 4223.
[15] L.G. Christophorou, R.A. Mathis, D.R. James, D.L. McCorkle, J. Phys. D: Appl. Phys. 14 (1981) 1889.
[16] S.M. Spyrou, S.R. Hunter, L.G. Christophorou, J. Chem. Phys. 83 (1985) 641.
[17] A.A. Christodoulides, L.G. Christophorou, D.L. McCorkle, Chem. Phys. Lett. 139 (1987) 350.
[18] T.M. Miller, R.A. Morris, A.E.S. Miller, A.A. Viggiano, J.F. Paulson, Int. J. Mass Spectrom. Ion Process. 135 (1994) 195.
[19] H. Kazumi, K. Tago, Jpn. J. Appl. Phys. 34 (1995) 2125.
[20] Y. Gotoh, T. Kure, Jpn. J. Appl. Phys. 34 (1995) 2132.
[21] J.A. Beran, L. Kevan, J. Phys. Chem. 73 (1969) 3866.
[22] H. Toyoda, M. Iio, H. Sugai, Jpn. J. Appl. Phys. 36 (1997) 3730.

[23] K. Riehl, Collisional detachment of negative ions using FTMS, Ph.D. Thesis, Air Force Inst. Technol., Wright-Patterson AFB, OH, 1992.
[24] A.G. Marshall, T.L. Wang, T.L. Ricca, J. Am. Chem. Soc. 107 (1985) 7893.
[25] S. Guan, J. Chem. Phys. 91 (1989) 775.
[26] P.D. Haaland, Chem. Phys. Lett. 170 (1990) 146.
[27] R.C. Wetzel, F.A. Baioochi, T.R. Hayes, R.S. Freund, Phys. Rev. 35 (1987) 559.
[28] R.A. Morris, T.M. Miller, A.A. Viggiano, J.F. Paulson, J. Geophys. Res. 100 (1995) 1287.

Appendix H Ionization of nitrogen trifluoride, NF_3

Submitted to Chemical Physics Letters, February, 2001

Ionization of NF_3 by electron impact

P.D. Haaland, C.Q. Jiao, and A. Garscadden

Propulsion Directorate, Air Force Research Laboratory, Wright-Patterson AFB, Ohio, 45433

Abstract

The dissociative ionization of NF_3 by electron impact has been measured by Fourier Transform Mass Spectrometry (FTMS). The total ionization cross section rises to a maxiumum value of $2.4 \pm 0.4 \times 10^{-16} cm^2$ at 140 eV. Estimates of the total cross section using *Ab initio* energies with the Binary Encounter Bethe [1] or Deutsch Mark [2] models are roughly twice the measured values. The partial cross sections creating NF_x^+ $(x = 0, 1, 2, 3)$, F^+, and NF_x^{2+} $(x = 1, 2, 3)$ are reported. Differences between the FTMS results and quadrupole data and fast atom beam results of Tarnovsky *et al.* [3] are discussed.

1 Introduction

Nitrogen trifluoride (NF_3) provides efficient *in situ* plasma etching and thermal cleaning of semiconductors and liquid crystal display panels. Its advantages over fluorocarbon based compositions include higher etch rates for equivalent plasma power densities, better etch selectivity, minimal residual contamination, and negligible global warming potential. [4] This etch precursor is produced in large quantities; demand for NF_3 in Japan increased to 150 tons in 1999 and was expected to double in 2000 [5]; BOC Edwards has launched construction of a facility to produce 250,000 kg/year in Pelindaba, South Africa. [6] NF_3 is also used as an oxidizer in high power HF and DF chemical lasers, [7] and as a reagent for chemically reactive interface mass spectrometry [8]. Naturally occuring NF_3 has recently been identified in fluorites and metamorphic rocks. [9]

The dissociative ionization of this small molecule is also interesting as support for tests of quantum mechanical constraints on the partitioning among fragments in ionization processes. [10] Electron impact ionization of NF_3 has been studied with magnetic sector, quadrupole, and fast atomic beam techniques by Tarnovsky *et al.*[3] The cross section for production of the parent NF_3^+

ion was quantified, as were values for generation of NF^+, and NF_2^+. Upper bounds were placed on the yields of N^+, and F^+.

In this letter we extend the dynamic range of prior work on partial ionization of NF_3 to quantify the partitioning among fragments and to identify dication formation processes. We also compare the total ionization cross sections to estimates based on *ab initio* electronic structure and the Binary Encounter Bethe model of Kim and Rudd. [1]

2 Experiment

Nitrogen trifluoride NF_3 (Scott Specialty Gases, 99%) was mixed with argon (99.999%, Matheson Research Grade) and admitted through a precision leak valve into a modified Fourier Transform Mass Spectrometry (FTMS) system that has been described in detail elsewhere. [11,12] No impurities other than very small traces of water vapor were identified in the mass spectrum. Ions are formed by electron impact in a cubic ion cyclotron resonance (ICR) trap cell at pressqures in the 10^{-7} Torr range. An electron gun (Kimball Physics ELG-2, Wilton, NH) located 2 meters from the trap irradiates the gas with a short (2-6 ms) pulse having a few hundred picocoulombs of low-energy electrons. The motions of ions produced by electron impact are constrained radially by a superconducting solenoidal magnetic field ($\approx$ 2 T) and axially by a nominal electrostatic trapping potential (1-2 V) applied to the trap faces that are perpendicular to the magnetic field. Ions of all mass to charge ratios are simultaneously and coherently excited into cyclotron orbits using a stored voltage waveform. [13] The image currents induced on the two remaining trap faces are then digitized and Fourier analyzed to yield a mass spectrum.

Calculation of the cross section from the mass spectral intensities requires knowledge of the gas pressure, the electron beam current, and the number of ions produced. It is particularly important that the measurements are made during a time that is short enough to preclude perturbation of the species' distribution by charge transfer reactions. These calibration issues have been discussed elsewhere. [11,12] In the measurements reported here we calibrate the cross sections using ratios of the ion signals to those of Argon, whose cross section is known to $+/-12\%$ from the crossed beam measurements of Wetzel and Freund. [14]

The distribution of electron energies in the ion trap, based on the solution of Laplace's equation for the experimental geometry, is roughly Gaussian with a full-width-at-half-maximum of 0.5 eV due to the electrostatic trapping bias. The mean energy is accurate to $\pm 0.2eV$ based on comparison of noble gas ionization thresholds with spectroscopic data.

It is important to note that the ions are not actually collected in the FTMS experiment; only their electromagnetic influence on the antenna is recorded. As a result, the spectrometer sensitivity *is neither mass nor species dependent* for the results described here. We estimate the accuracy in the partitioning among ionic channels relative to argon to be $\pm 4\%$. Combined with the precision of the crossed beam measurements on argon,$\pm 12\%$[14], we estimate the magnitude of the of the cross sections presented here to be accurate within $\pm 16\%$.

3 Results and Discussion

Five singly charged ions, $N^+, F^+, NF_x^+ (x = 1, 2, 3)$ as well as three dications, $NF_x^{2+}, (x = 1, 2, 3)$ were observed to form with cross sections exceeding $10^{-20} cm^2$ below 200 eV. The high mass resolution of FTMS was particularly useful in distinguishing the contributions of F^+ and H_3O^+ at a nominal mass of 19 amu, as illustrated in figure 1. Experimental results for each of the eight ionized products are shown in figure 2.

Ionization of NF_3 has been reported using fast atom beam, magnetic sector, and quadrupole instruments by Tarnovsky *et al.* [3]. These measurements were calibrated, as were the present results, with reference to the crossed beam determinations of argon ionization by Wetzel and Freund.[14] The cross sections for production of the parent NF_3^+ ion and the total ionization cross section are in excellent agreement among the various methods. There are differences, however, in the partitioning among dissociatively ionized fragment channels as can be seen in table 1 for 70 eV electron impact and more generally in figure 3. One way to rationalize these differences is to consider the internal energy of molecules that comprise the fast atom beam. NF_3 is ionized in a Colutron ion source and the NF_3^+ ions are accelerated to several keV, then neutralized by charge transfer from Xe. Internal vibrational [15] or electronic [16] excitation in the collisionally neutralized molecule may play a role in the enhanced fragmentation observed in the beam experiments.

The dynamic range of the FTMS experiments reveal cross sections for N^+ and F^+ shown in figure 2, and are consistent with the upper bounds of 0.1 and $0.3x10^{-16} cm^2$ reported by Tarnovsky *et al.* The yield for the doubly charged ions is small, with the ordering among NF_x^{2+} yields different than that for the corresponding monocations.

The total ionization cross section can be calculated using the Binary Encounter Bethe (BEB) model.[1] Briefly, this model sums contributions to the total cross section σ using *ab initio* estimates of the molecular orbital occupation numbers N, binding energies B,orbital U, and incident T kinetic energies according to

the formula:

$$\sigma_{BEB} = \frac{S}{t+u+1}\left[\frac{Q\ln t}{2}\left(1-\frac{1}{t^2}\right)+(2-Q)\left(1-\frac{1}{t}-\frac{\ln t}{t+1}\right)\right]$$

where

$$t = \frac{T}{B}, u = \frac{U}{B}, S = 4\pi a_o^2 NR^2/B^2,$$

a_o is the Bohr radius, R is the Rydberg constant, and Q is a weighted integral of the target's continuum dipole oscillator strength that is routinely set equal to unity in the BEB method.

Figure 4 shows the results of BEB cross section estimates using orbital binding and kinetic energies computed by Winstead from *ab initio* theory at the RHF/6-311+G(2d) level of theory. [17] This overstimation is retained when the experimental ionization potential is used with uncorrelated wavefunctions at a similar level of theory. [18] Theoretical estimates using the Deutsch-Mark formalism also overestimate the magnitude of the total ionization cross-section by a factor of ≈ 2, where similar discrepancies between theoretical and experimental values were found for NF_x and CF_x ionization. [2] Huo has recently reported cross sections based on the Binary Encounter Dipole method [1] using correlated wavefunctions for the first four ionization potentials. [19] The results of these calculations are in much better agreement with the present experimental results than those of either the BEB or DM approach.

NF_3 displays the intriguing characteristic that, with the exception of F_2^+, all possible ion fragments are observed. Similar results have been reported for isovalent NH_3.[20] The parent NH_3^+ ion is formed with a low threshold, but yields of more extensively dissociated NH^+ and NH_2^+ are higher above 80 eV. The proportion of atomic H^+ and N^+ are lower than that of the parent ion, and one doubly charged ion is reported. Quantitative comparison of the thresholds and cross sections for ammonia and nitrogen trifluoride displays different ordering, but the only qualitative differences in the spectra are the formation of diatomic H_2^+ and the absence of $NH_x^{2+}(x=1,2)$ from the ammonia spectra. The electronic structures of NF_x and NF_x^+ have been extensively studied, primarily with a view to establishing the thermodynamic properties of various ion and neutral species. [21,22] The ground electronic state is orbitally non-degenerate, so that no Jahn-Teller distortion from C_{3v} symmetry is predicted, although the lowest energy conformation is predicted to have a larger dihedral angle than that of neutral NF_3 . [17] Closer examination of the potential energy of the NF_3^+ ion potential energy surfaces may, on comparison with those for NH_3^+, provide insight into quantum constraints on the fragmentation patterns of these small molecular ions.

4 Conclusions

The cross sections for ionization of nitrogen trifluoride by electron impact have been measured from threshold to 200 eV by Fourier Transform Mass Spectrometry. The cross section for production of $NF_3^+(0.38 \pm 0.06x10^{-16}cm^2)$ and the total cross section $(2.4 \pm 0.4x10^{-16}cm^2)$ are in excellent agreement with earlier measurements. The yield of less extensively dissociated NF_2^+ is found to be higher than previously reported, and full cross sections for N^+ and F^+ are reported. Three dications, $NF_x^{2+}(x = 1, 2, 3)$, are also observed to form with cross sections of $(2.7, 34,$ and $8.4x10^{-20}cm^2)$, respectively, at 100 eV. The Binary Encounter Bethe and Deutsch-Mark models overestimate the total ionization cross section by a factor of about 2. It is suggested that comparison of the fragmentation patterns for ammonia and nitrogen trifluoride may provide insight into quantum constraints on dissociative ionization.

Table 1
Comparison of partial ionization cross sections from FTMS, fast atom beam, quadrupole, and magnetic sector techniques ([3]) following 70 eV electron impact.

species	FTMS	error	Beam	error	Quadrupole	error	Sector
NF_3^+	0.38	±0.06	0.347	± 0.03	0.35	±0.03	0.348
NF_2^+	1.58	±0.25	1.05	±0.20	1.03	±0.05	
NF^+	0.44	±0.07	0.70	± 0.15	0.49	±0.04	
N^+	0.024	±0.004	<0.3		0.33	±0.05	
F^+	0.004	±0.0006	<0.1		0.09	±0.01	

Fig. 1. Fourier Transform mass spectrum of NF_3 at 45 eV allows discernment of ion signals between dissociative ionization product F^+ from H_3O^+ that is produced from the very fast protonation of background water vapor.

Fig. 2. Partial ionization cross sections for electron impact on NF_3 from threshold to 200 eV. Legend: $(+)NF_2^+$, $(\circ)NF^+$, $(*)NF_3^+$, $(x)F^+$, $(\square)N^+$, $(\diamond)NF_2^{2+}$, $(\bigtriangledown)NF_3^{2+}$, and $(\bigtriangleup)NF^{2+}$.

Fig. 3. Comparison of partial ionization cross sections for production of singly charged fragments from the fast atom beam method of ref [3] ($\circ$) and FTMS (solid lines).

Fig. 4. BEB estimated cross sections using RHF/6-311+G(2d) wavefunctions × [17], correlated wavefunctions and the BED model according to Huo [18](solid line), FTMS data including contributions from dications ($\circ$), and expermental results of Tarnovsky *et al.* ($\diamond$).

Acknowledgements

This work has been supported by the U.S. Air Force Office of Scientific Research and SEMATECH.

References

[1] Y.K. Kim and M.E. Rudd, *Phys. Rev.*, **A50** (1994) 3594.

[2] H. Deutsch, K. Becker, S. Matt, and T.D. Mark, *Int. J. Mass Spec.*, *197*, 37 (2000).

[3] V. Tarnovsky, A. Levin, K. Becker, R. Masner, and M. Schmidt, *International Journal of Mass Spectrometry and Ion Processes*, **133**, (1994), 175.

[4] Air Products web-site http://www.airproducts.com/gases/elecspgas.html

[5] Japan Chemical Week, August 24, 2000. Available at (http://www.chemnews-japan.com)

[6] H.U. Poll and J. Meichsner, *Contrib. Plasma Phys.*, **27** (1987) 359.

[7] E.A. Dorko and J.L. Moller, eds., Gas and Chemical Lasers and Intense Beam Applications, SPIE Proceedings Vol. 3268, pp. 342.

[8] Hengchang Song and Fred J. Abramson, *J. Am. Soc. Mass Spectrom.*,**6**,(1995), 421.

[9] J. Harnisch, M. Frische, R. Borchers, A. Eisenhauer, and A. Jordan, *Geophys. Res. Lett.*,**27**,(2000),1883.

[10] C. Jiao, A. Garscadden, and P. Haaland,*Chem. Phys. Lett.*, **310**, 52 (1999).

[11] K. Riehl, Collisional detachment of negative ions using FTMS, Ph.D. Thesis, Air Force Institute of Technology, Wright-Patterson AFB, 1992.

[12] P.D. Haaland, *Chem. Phys. Lett.*, **170** (1990) 146.

[13] S. Guan, *J. Chem. Phys.*, **91‘**, (1989) 775.

[14] R.C. Wetzel, F.A. Baioochi, T.R. Hayes, and R.S. Freund, *Phys. Rev.*, **35** (1987) 559.

[15] R.J. Shul, T.R. Hayes, R.C. Wetzel, F.A. Baiocchi, and R.S. Freund, *J. Chem. Phys.*, **89**, 4042 (1988).

[16] T.R. Hayes, R.C. Wetzel, F.A. Baiocchi, and R.S. Freund, *J. Chem. Phys.*, **88**, 823 (1988).

[17] C. Winstead and B.V. McKoy, personal communication, October, 2000.

[18] W. Huo, http://www.ipt.arc.nasa.gov/database1.html), January 2001.

[19] W. Huo, NASA, personal communication (February 2001).

[20] T.D. Mark, F. Egger, and M. Cheret, *J. Chem. Phys.*, **67**, (1977), 3795.

[21] M. Aschi and F. Grandinetti, *J. Mol. Struct. (Theochem)*, **497**, (2000), 205.

[22] A. Ricca, *Chem. Phys. Lett.*, **300**, 80 (1999) and **294**, 454 (1998).

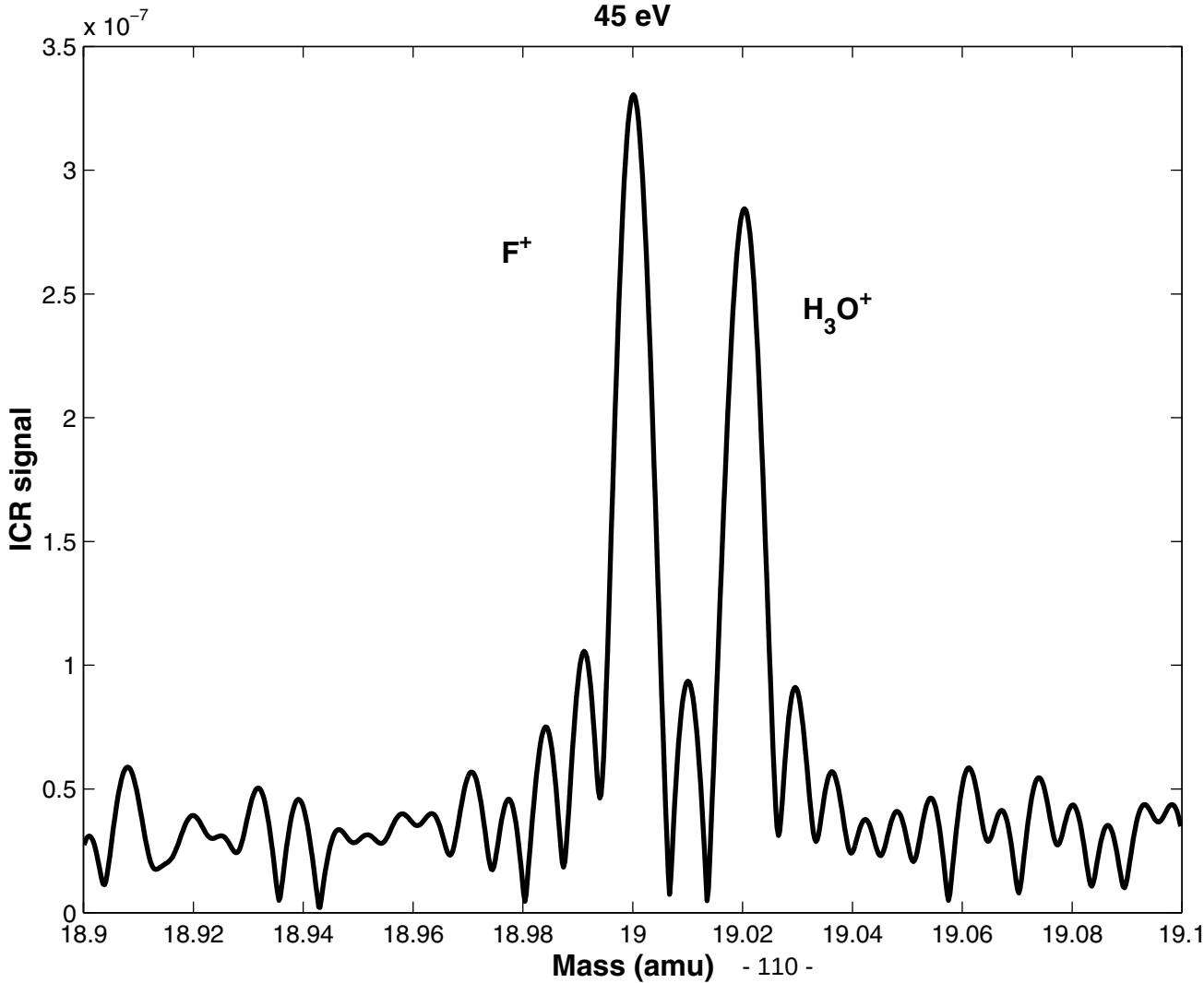
45 eV
x 10^-7
3.5
3
2.5
2
1.5
1
0.5
0
ICR signal
F+
H3O+
18.9
18.92
18.94
18.96
18.98
19
19.02
19.04
19.06
19.08
19.1
Mass (amu)

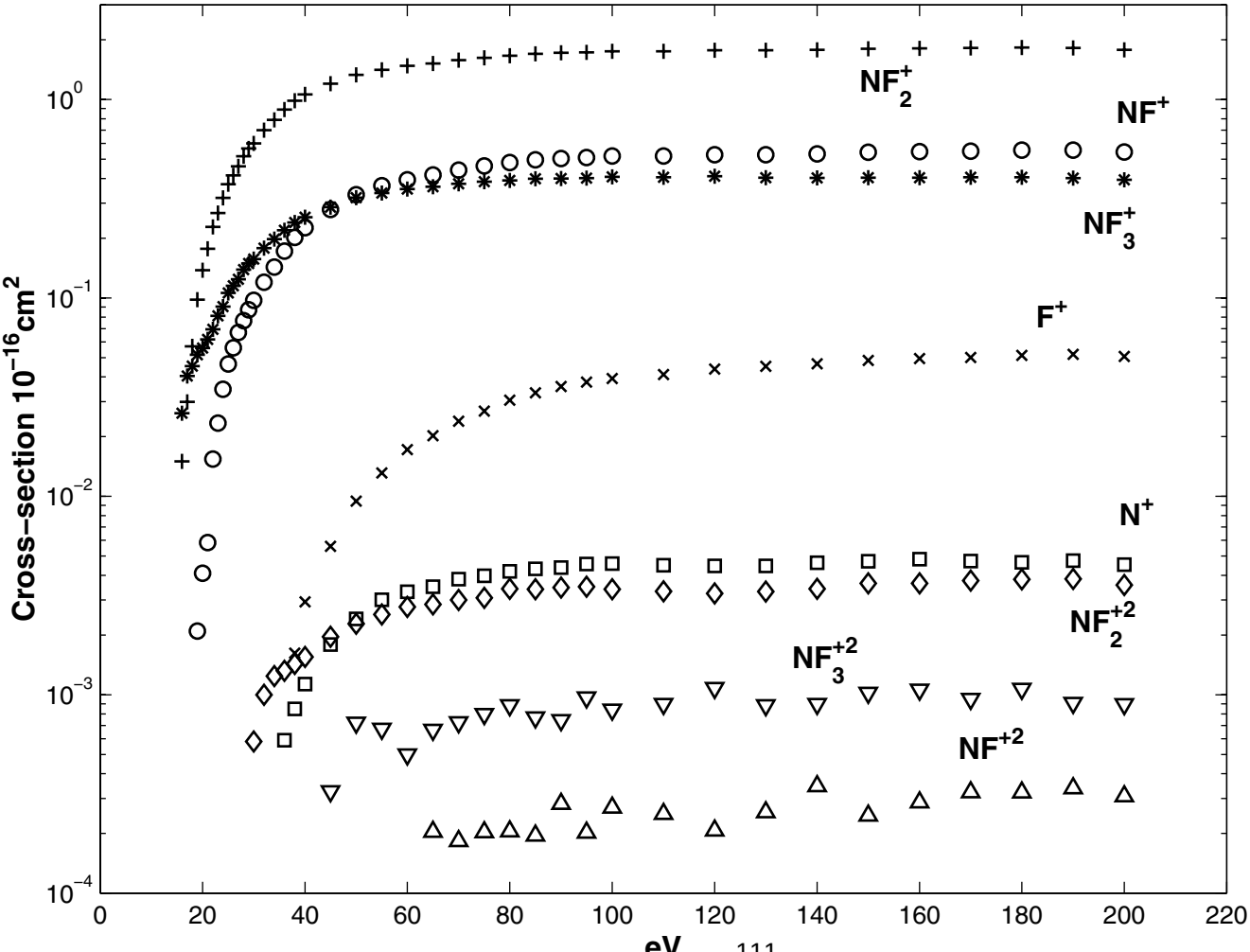
Cross−section 10^{-16}cm^2
eV
NF_2^+
NF^+
NF_3^+
F^+
N^+
NF_2^{+2}
NF_3^{+2}
NF^{+2}
10^0
10^{-1}
10^{-2}
10^{-3}
10^{-4}
0
20
40
60
80
100
120
140
160
180
200
220

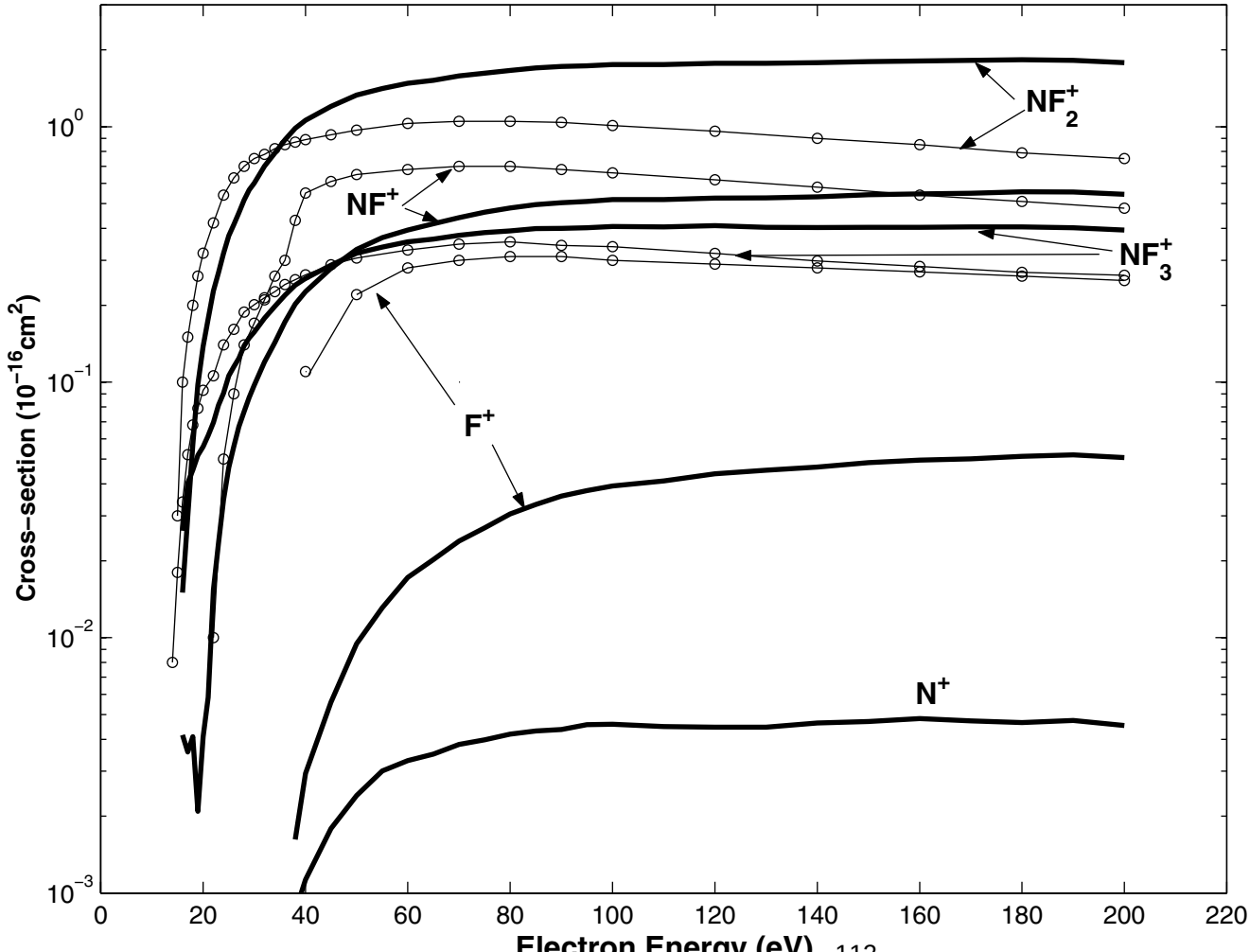
NF_2^+
NF^+
NF_3^+
F^+
N^+
Cross-section (10^{-16}cm^2)
10^0
10^{-1}
10^{-2}
10^{-3}
0
20
40
60
80
100
120
140
160
180
200
220
Electron Energy (eV)

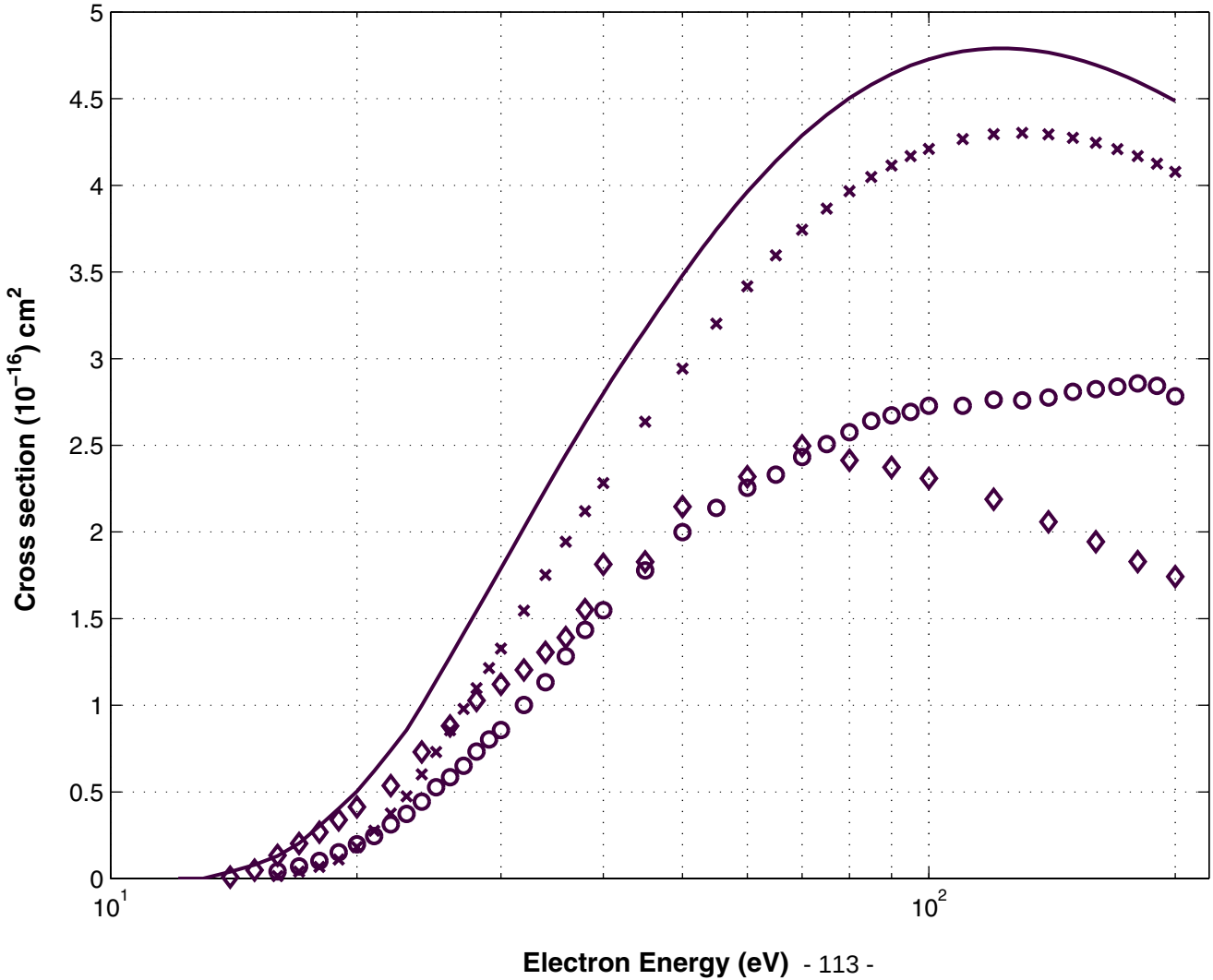
Cross section (10^{-16}) cm^2
Electron Energy (eV)
0
0.5
1
1.5
2
2.5
3
3.5
4
4.5
5
10^1
10^2

Appendix I Ionization of tetraethyl germane, $Ge(C_2H_5)_4$

J. Phys. B.:At. Mol. Opt. Phys.,*32, 1639 (1999).*

J. Phys. B: At. Mol. Opt. Phys. 32 (1999) 1639-1646. Printed in the UK PII: S0953-4075(99)96311-3

Ionization of tetraethylgermanium, $GeEt_4$

C Q Jiao†, A Garscadden‡, C DeJoseph Jr‡§ and P D Haaland†

† Mobium Enterprises, Inc., 5100 Springfield Pike, Dayton, OH 45431-1231, USA
‡ Air Force Research Laboratory, Wright-Patterson AFB, OH 45433-7919, USA

Received 28 July 1998

Abstract. The ion chemistry in tetraethylgermanium ($GeEt_4$) has been examined by Fourier-transform mass spectrometry under single-collision conditions in the 10^{-7} torr pressure range. The cross sections for electron impact ionization of $GeEt_4$ are measured from threshold to 70 eV. The molecular ion and 15 fragment ions from the electron-molecule collision are observed with a total cross section of 3.5 ± 0.4 x 10^{-15} cm^2 at 70 eV. All fragment ions, except $GeC_6H_{15}^+$, are found to react readily with $GeEt_4$ to yield $GeC_6H_{15}^+$, with rate coefficients in the range of 2-5 x 10^{-10} cm^3 s^{-1} Small yields of digermanium cluster ions are observed at higher reactant pressures.

1. Introduction

Amorphous materials can be divided into two categories based on their electronic structures and properties: amorphous semiconductors and amorphous dielectrics. The transition between the dielectric and semiconducting properties occurs as the preparation conditions for these materials change [1–5]. One such transition is described in recent studies of germanium:carbon films prepared by plasma deposition from alklylated germanes [6–15]. Gazicki and his co-workers [10–15] correlated the stoichiometry and bulk electrical properties of films deposited from tetraethylgermanium plasma with radio-frequency power levels. They link the transition from dielectric to semiconducting films to changes in the composition of the plasma. In spite of the previous research activities, and the fact that these germanium:carbon films are important elements of coatings and semiconductors, only limited information about the electron impact ionization of tetraethylgermanium has been reported, namely, the cracking patterns at 50 eV [16] and 70 eV [17]. In this paper we present measurements of the ionization cross sections of tetraethylgermanium ($GeEt_4$) for electron energies from threshold to 70 eV. Rate coefficients for the reactions of fragment ions and Ar^+ with neutral $GeEt_4$ are also reported.

2. Experimental

Tetraethylgermanium (99%, Aldrich) gas is mixed with argon (99.999% Matheson Research Grade) in a $GeEt_4$:Ar of 1: 1.3, as determined by capacitance manometry. The mixture is admitted through a precision leak valve into a modified Extrel Fourier-transform mass spectrometry (FTMS) system which has been described in detail elsewhere [18]. Ions are formed by electron impact in a cubic ion cyclotron resonance (ICR) trap cell at pressures in the 10^{-7} torr range. An electron gun (Kimball Physics ELG2, Wilton, NH) irradiates the trap with

§ Present address: AFRL/PRPS, Bldg 450, 2645 Fifth Street Ste 13, Wright-Patterson AFB, OH 45433-7919, USA.

a few hundred picocoulombs of low-energy electrons. The motions of the ions are constrained radially by a superconducting solenoidal magnetic field (~ 2 T) and axially by an electrostatic potential (1 V) applied to the trap faces that are perpendicular to the magnetic field. Ions of all mass-to-charge ratios are simultaneously and coherently excited into cyclotron orbits using a stored waveform [19,201 applied to two opposing trap faces which are parallel to the magnetic field. Following cyclotron excitation, the image currents induced on the two remaining faces of the trap are amplified, digitized and Fourier analysed to yield a mass spectrum.

The calculation of cross sections from the mass spectrum intensities requires a knowledge of the gas densities, the electron beam current and the number of ions produced. These calibration issues have been described previously [18,211. The intensity ratios of the ions from $GeEt_4$ to Ar^+ give cross sections relative to those for argon ionization [22] since the $GeEt_4$:Ar pressure ratio is fixed.

The distribution of electron energies in the trap, based on the solution of Laplace's equation for the experimental geometry, is roughly Gaussian with a full width at half maximum of 0.5 eV due to the electrostatic trapping bias [18]. The mean energy of the irradiating electrons is accurate to f0.2 eV based on comparison of noble gas ionization thresholds with spectroscopic data. We fit the cross section data to an empirical functional form:

$$\sigma = \mathrm{A}\tanh \frac{\pi(\varepsilon - T)}{\alpha} \mathrm{e}^{-k(\varepsilon - T)}$$

where σ is the cross section, ε is the electron energy, $\boldsymbol{T}$ is the appearance potential, ***A scales*** the amplitude, α quantifies $\mathrm{d}\sigma/\mathrm{d}\varepsilon$ near threshold and $\boldsymbol{k}$ characterizes behaviour at energies $\gg T$.

3. Results and discussion

Tetraethylgermanium ionization was first reported 30 years ago with cracking patterns at 50 and 70 eV [16, 17]. At these energies the most abundant ion is $GeC_4H_{11}^+$, with minimal but detectable concentrations of $Ge(C_2H_5)_4^+$. The present measurements confirm the cracking patterns at 50 and 70 eV and provide new data on dissociative ionization at other electron energies that are important for plasma processing. The calibration with Ar and the lack of mass dependence in the detection sensitivity of our FTMS instrument quantify the partial ionization cross sections for this molecule.

Of the 378 ion stoichiometries which might be formed on statistical grounds by ionization of $Ge(C_2H_5)_4$, only 15 are formed with cross sections greater than 2 x 10^{-18} cm^2. The most abundant ion fragments that contain Ge are illustrated in scheme 1 with relative yields at 70 eV shown in parentheses. The neutral fragments in the scheme are only our suggestions and no bonding arrangements are shown since these are not measured in our experiments. Ions containing no Ge atoms have lower intensities and include $C_3H_7^+$ (0.9%), $C_3H_5^+$ (0.1%), $C_2H_5^+$ (1.9%), $C_2H_4^+$ (0.2%), $C_2H_3^+$ (1.6%) and $C_2H_2^+$ (0.2%). These ion stoichiometries are based on exact mass measurements. The total ionization cross section at 70 eV is 13 times that of Ar, 3.5 $\pm$ 0.4 x 10^{-15} cm^2. More than 95% of the ions produced by electron impact contain the Ge atom. The cross sections for each dissociative ionization process are shown from threshold to 70 eV in figure 1, and the coefficients for our functional fit are summarized in table 1. The first three to emerge are the molecular ion $GeC_8H_{20}^+$ and the two largest fragment ions $GeC_6H_{15}^+$ and $GeC_4H_{11}^+$, $GeC_6H_{15}^+$ is the most abundant ion from threshold to 25 eV. Above 25 eV, $GeC_4H_{11}^+$ has the largest partial ionization cross section. Over 95% of the ionization is dissociative, so that the present data provide lower bounds for the total dissociation cross section of this molecule by electron impact. Note also that neutral fragments whose composition is not measured in these experiments are also produced by dissociative ionization.

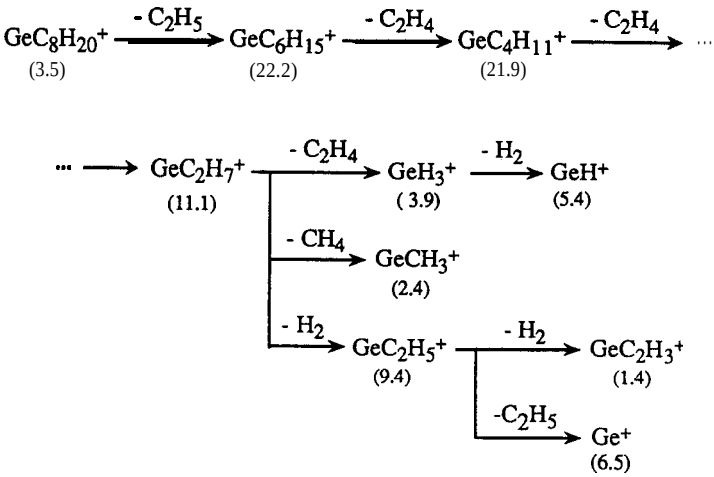

Scheme 1.

Table 1. Fitting parameters for dissociative ionization cross sections of $GeEt_4$. Ions are listed in the order of decreasing mass. Also listed are the cross sections, σ, at 70 eV.

Ion	A (cm*)	k (eV^{-1})	α (eV)	T (eV)	σ at 70 eV (10^{-16} cm^2)
$GeC_8H_{20}^+$	8.9×10^{-17}	-5.8×10^{-3}	15	10.4	1.2
$GeC_6H_{15}^+$	6.1×10^{-16}	-4.6×10^{-3}	22	10.7	7.8
$GeC_4H_{11}^+$	9.2×10^{-16}	-1.2×10^{-3}	49	11.9	9.8
$GeC_2H_7^+$	4.6×10^{-16}	3.1×10^{-3}	74	16.8	3.9
$GeC_2H_5^+$	4.7×10^{-16}	5.2×10^{-3}	88	22.2	3.3
$GeC_2H_3^+$	4.2×10^{-17}	-6.1×10^{-3}	50	37.7	0.50
$GeCH_3^+$	6.0×10^{-17}	-7.1×10^{-3}	33	26.7	0.83
GeH_3^+	1.4×10^{-16}	-2.7×10^{-3}	91	22.5	1.4
GeH^+	1.8×10^{-16}	-2.9×10^{-3}	95	22.2	1.9
Ge^+	1.7×10^{-16}	-9.1×10^{-3}	96	23.1	2.3
$C_3H_7^+$	2.5×10^{-17}	-4.5×10^{-3}	35	15.6	0.31
$C_3H_5^+$	1.2×10^{-17}	2.0×10^{-2}	110	31.7	0.04
$C_2H_5^+$	6.8×10^{-17}	-4.0×10^{-3}	93	24.8	0.68
$C_2H_4^+$	1.4×10^{-17}	1.7×10^{-2}	108	33.2	0.09
$C_2H_3^+$	4.9×10^{-17}	-1.7×10^{-2}	101	26.3	0.90
$C_2H_2^+$	3.8×10^{-17}	1.9×10^{-2}	267	38.9	0.08

We track the reactions of ion fragments with $GeEt_4$ by introducing a delay between the ion formation at 50 eV and ion cyclotron excitation and detection, as shown in figure 2. Using double-resonance techniques? we have found that Ar^+ reacts with $GeEt_4$ to form $GeC_6H_{15}^+$ (70%), $GeC_2H_7^+$ (22%) and $C_3H_7^+$ (8%) with branching ratios shown in parentheses. $GeC_6H_{15}^+$ is unreactive for products of $Ge(C_2H_5)_4$ pressure and times of less than 10^{-7} torr s. All other fragment ions react rapidly with $GeEt_4$ to form $GeC_6H_{15}^+$ on this collisional time scale. Table 2 summarizes our measured bimolecular reaction rate coefficients. The reaction rates

† For a review of the double-resonance technique in FTMS, see [23].

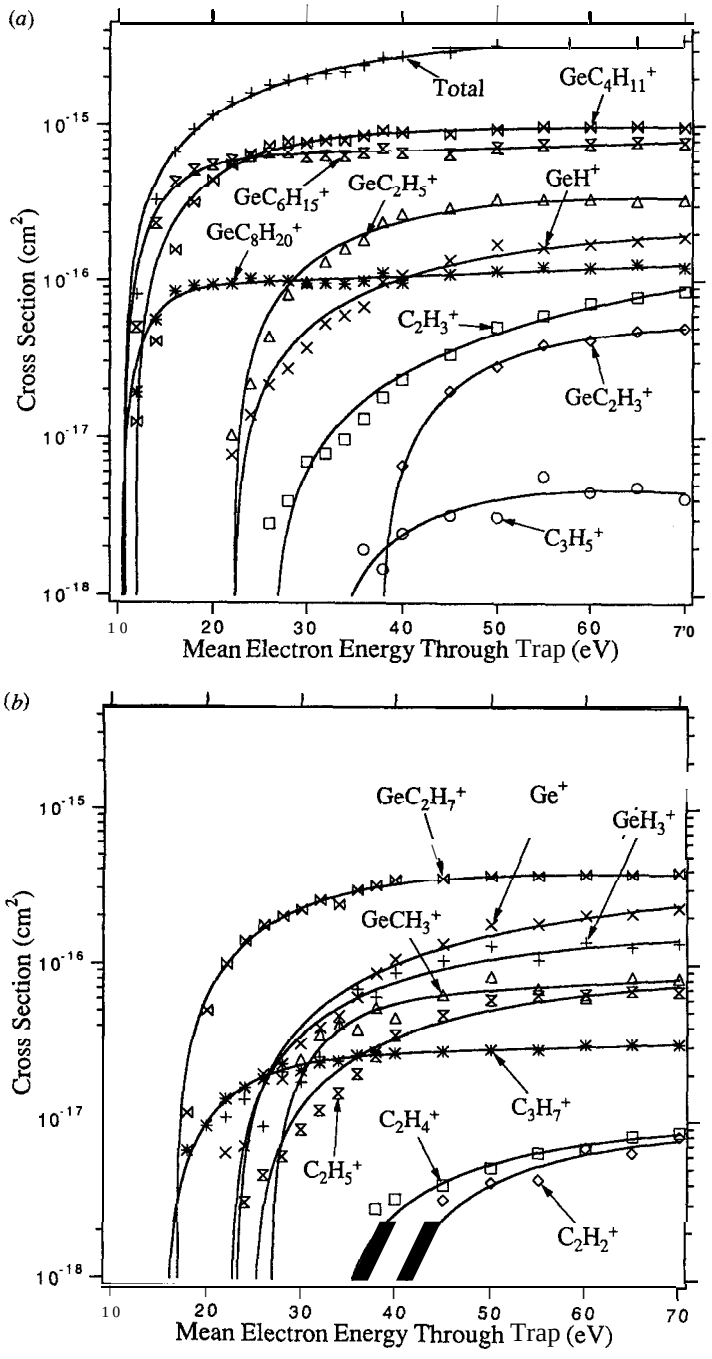

Figure 1. Cross sections (cm^2) for ionization of $GeEt_4$ by electron impact. Points represent experimental data, and full curves are fits of the equation described in the text.

are identical to within 10% experimental uncertainty when the electron energy with which the reactant ions are formed is 20, 35 or 50 eV. If products of dissociative ionization are produced

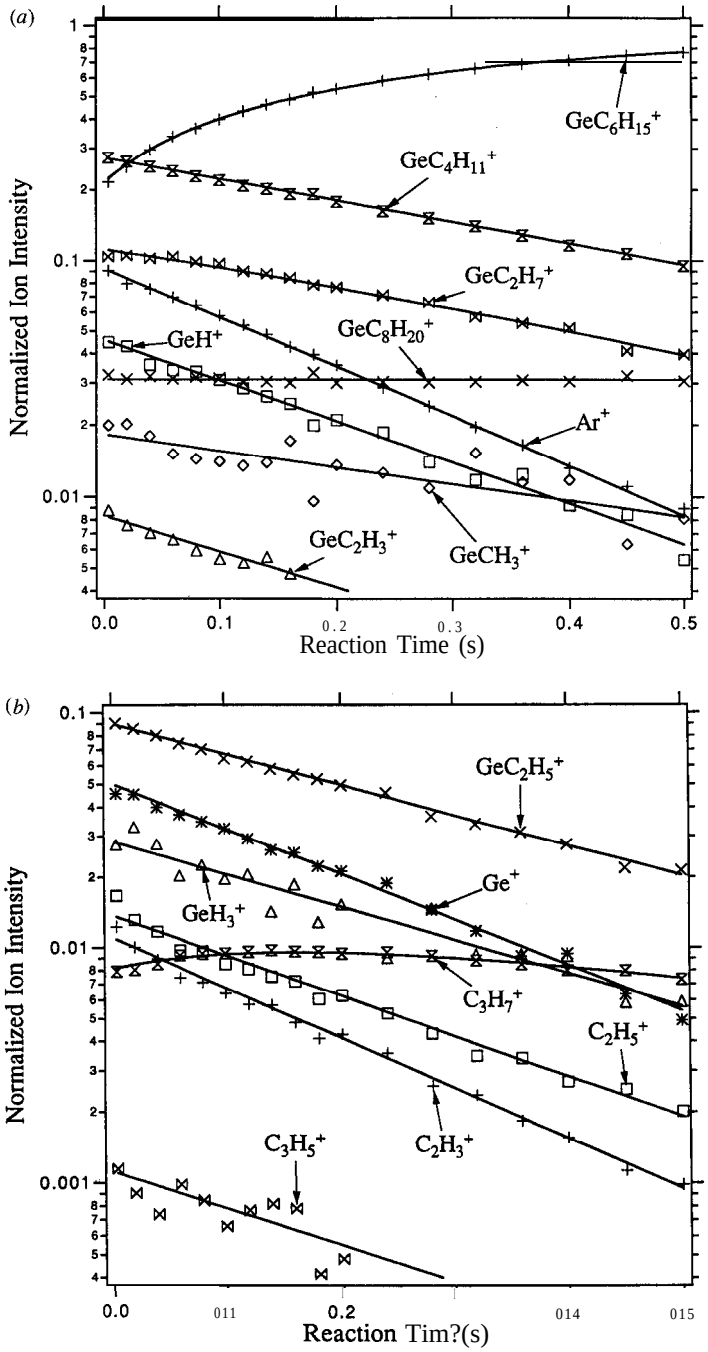

Figure 2. Time evolution of positive ion species produced by 50 eV electron impact at a mixture of GeEt$_4$ and Ar (1: 1.3) with a total pressure of 6.8×10^{-7} torr. Points represent experimental data, and full curves are fits of a kinetic model which gives the reaction rate coefficients presented in table 2.

Table 2. Ion-molecule reaction rate coefficients in units of 10^{-10} cm^3 s^{-1}, measured in three separate experiments, l-3, in which the primary ions are formed by electron impact at 20, 35 and 50 eV, respectively.

	Reaction rate coefficients		
Reactant ion	Experiment 1	Experiment 2	Experiment 3
$GeC_4H_{11}^+$	2.3 ± 0.2	2.4 ± 0.2	2.2 ± 0.2
$GeC_2H_7^+$	2.7 ± 0.3	2.6 ± 0.3	2.7 ± 0.3
$GeC_2H_5^+$		3.0 ± 0.3	3.1 f0.3
$GeC_2H_3^+$	—		3.6 ± 0.4
$GeCH_3^+$	—	1.7 ± 0.2	1.7 ± 0.2
GeH_3^+	—	3.5 ± 0.4	3.3 ± 0.4
GeH^+		4.1 ± 0.4	4.2 ± 0.4
Ge^+	—	4.6 ± 0.5	4.6 ± 0.5
$C_3H_7^+$	1.8 ± 0.2	1.8 ± 0.2	1.7 ± 0.2
$C_3H_5^+$	—		3.7 ± 0.4
$C_2H_5^+$	—	4.2 ± 0.4	4.1 f0.4
$C_2H_4^+$ [a]			
$C_2H_3^+$	—	5.2 ± 0.5	5.1 f0.5
$C_2H_2^+$ [a]			
Ar^+	5.2 ± 0.5	5.1 ± 0.5	5.0 ± 0.5

[a] Values for these ions are not available because of their intensities being too low to permit reliable measurements.

with extra internal energy as the electron energy is increased they do not have enhanced or reduced reactivity with the parent gas. Division of the reaction rates by the square root of the reduced mass reveals that the probability of reaction per Langevin collision is constant to within 25% for all ions except $GeCH_3^+$ and $C_3H_7^+$.

Although the ion ensemble produced by electron impact in a plasma depends on the distribution of electron energies in the discharge, $GeC_4H_{11}^+$ and $GeC_6H_{15}^+$ generally dominate the ion distribution because of their low thresholds and large cross sections. However, relaxation of the ion ensemble by charge transfer collisions occurs at pressure-time products in the 10^{-7} torr s range, increasing the proportion of $GeC_6H_{15}^+$ at the expense of all of the more extensively dissociated fragment ions. This chemistry is strikingly similar to our earlier observations on the isoelectronic $Si(CH_3)_4$ molecule, where charge transfer from lighter ions and Ar^+ leads to $Si(CH_3)_3^+$.

Gazicki and co-workers [15] have examined the effluent of a 70 mtorr radio-frequency plasma containing 1.5% $GeEt_4$ in argon using quadrupole mass spectrometry. Their mass spectra at 70 eV show no parent ion in the *m/e* 183-193 range and a ratio of $GeC_6H_{15}^+$ to $GeC_4H_{11}^+$ of over 20 at the lowest (7 W) plasma power. The absence of the parent ion may be due to a mislabelling of the mass scale in their figure 4. If we assume that all of the $GeC_4H_{11}^+$ comes from dissociative ionization of $GeEt_4$ then the precursor is at least 95% dissociated by their 7 W plasma.

Gazicki and his co-workers have also observed powder products in a separate study on $GeEt_4$ plasmas [24]. They rationalize the observed binary-particle size distribution by suggesting two different growth mechanisms. Inspired by clustering studies of silicon hydride cations in silane plasmas [25, 26] we probed the reactions of $GeC_6H_{15}^+$ and $GeC_8H_{20}^+$ with neutral $GeEt_4$ at pressure-time products of up to 5 x 10^{-6} torr s. Two Ge dimer ions, $Ge_2C_6H_{17}^+$ and $Ge_2C_8H_{21}^+$, were slowly formed (reaction rates $< 10^{-12}$ cm^3 s^{-1}). This result implies that

cationic polymerization of neutral $GeEt_4$ is not responsible for dust production. Ion-radical, radical-radical, anion-radical and anion-molecule collisions remain candidates for cluster formation. We do not observe negative ions from dissociative attachment to GeC_8H_{20}, but anions may be formed by electron attachment to neutral radicals that are produced in the plasmas.

4. Summary

Electron impact ionization of $GeEt_4$ produces the molecular ion $GeC_8H_{20}^+$ and 15 ionic fragments with a total cross section of $3.5 \pm 0.4 \times 10^{-15}$ cm^2 at 70 eV. Most of the fragment ions contain Ge, with less than 5% yield of hydrocarbon ions. Below 25 eV, $GeC_6H_{15}^+$ is the most abundant ion, while above 25 eV $GeC_4H_{11}^+$ has the largest partial ionization cross section. Smaller fragment ions undergo rapid reactions with $GeEt_4$ to form $GeC_6H_{15}^+$, with rate coefficients in the range of 2-5 x 10^{-10} cm^3 s^{-1}. $GeC_6H_{15}^+$ reacts with $GeEt_4$ to produce $Ge_2C_6H_{17}^+$ and $Ge_2C_8H_{21}^+$ at rates of less than 10^{-12} cm^3 s^{-1}. The reaction rates are independent of the electron energy with which the reactant ions are formed. Ar^+ reacts with $GeEt_4$ with a rate coefficient of 5.1 x 10^{-10} cm^3 s^{-1}, producing $GeC_6H_{15}^+$ with smaller yields of $GeC_2H_7^+$ and $C_3H_7^+$. Taken together, the cross sections and rate data imply that $GeC_6H_{15}^+$ dominates the ion flux to surfaces under many plasma conditions.

Acknowledgment

The authors wish to thank the Air Force Office of Scientific Research for financial support.

References

[1] Mott N F 1967 ***Adv. Phys.* 16 49**
[2] Cohen M H, Fritzsche H and Ovshinsky S R 1969 *Phys.* ***Rev. Left. 22*** 1065
[3] Tyczkowski J 1989 ***Thin Solid Films* 168 175**
[4] Tyczkowski J and Sielski J 1990 ***Thin Solid Films* 187** 1
[5] Tyczkowski J, Odrobina E, Kazimierski P, Bassler H, Kisiel A and Zema ***N*** 1992 ***Thin Solid Films 209 250***
[6] Sadhir R K, James W J and Auerbach R A 1984 ***J. Appl. Polym.*** *Sci.:* ***Appl. Polym. Symp. 38 99***
[7] Tyczkowski J, Kazimierski P and Odrobina E 1993 *Surf.* ***Coat. Technol. 60 609***
[8] Tyczkowski J, Kazimierski P and Szymanowski H 1993 ***Thin Solid Films* 241291**
[9] Tyczkowski J and Kazimierski P 1994 ***J. Phys. D: Appl. Phys. 27*** 179
[10] Gazicki M, Pirker K, Schallauer R and Fallmann W 1990 ***Thin Solid Films* 187 5** 1
[11] Tyczkowski J, Oderobina E, Gazicki M and Olcaytug F 1991 *J. Non-Cryst.* ***Solids* 137-138 875**
[12] Gazicki M, Szymanowski H and Schalko J 1993 ***Thin Solid Films 230 81***
[13] Gazicki M, Szymanowski H, Tyczkowski J, Malinovsdy L, Schalko J and Fallmann W 1995 ***Thin Solid Films*** 256 31
[14] Gazicki M, Potrzebowski M J, Tyczkowski J and Schalko J 1995 ***Thin Solid Films 258*** 10
[15] Gazicki M, Szymanowski H, Tyczkowski J, Schalko J and Olcaytug F 1996 ***J.*** *Vac. Sci.* ***Technol.*** A 14 2835
[16] de Ridder J J and Dijkstra G 1967 ***Rec.*** *Trav.* ***Chim. Pays-Bus 86 737***
[17] Glockling F and Light J R C 1968 ***J. Chem.*** *Soc.* A 717
[18] Riehl K 1992 Collisional detachment of negative ions using FTMS *PhD* ***Thesis*** Air Force Institute of Technology
[19] Marshall A G, Wang T L and Ricca T L 1985 ***J. Am.*** *Chem. Soc.* **107 7893**
[20] Guan S 1989 ***J.*** *Chem.* ***Phys.* 91775**
[21] Haaland P D 1990 *Chem.* ***Phys. Left.* 170 146**
[22] Wetzel R C, Baioochi F A, Hayes T R and Freund R S 1987 ***Phys. Rev. 35 559***

[23] Freiser B S 1988 ***Techniques for the Study of Ion Molecule Reactions*** vol 20, ed J M Farrar and W H Saunder (New York: Wiley) ch 2
[24] Gazicki M, Tycskowski J, Szymanowski H, Potrzebowski M J, Blasinska A and Fallmann W 1994 ***J. Chem. Vapor Depos. 2 269***
[25] Mandich M L, Reents W D Jr and Kolenbrander K D 1990 *J. Chem. Phys.* ***92 437***
[26] Kushner M J 1988 *J. Appl.* ***Phys. 63 2532***

Appendix J Ion Chemistry of trimethylsilane, $SiH(CH_3)_3$

Int. J. Mass Spec., ***184, 83 (1999).***

ELSEVIER

International Journal of Mass Spectrometry 184 (1999) 83-88

International Journal of Mass Spectrometry

Ionization of trimethylsilane, $(CH_3)_3SiH$

C.Q. Jiao[a], A. Garscadden[b,*], P.D. Haaland[a]

[a] *Mobium Enterprises, Inc., 5100 Springfield Pike, Dayton, OH 45431-1231, USA*
[b] *Air Force Research Laboratory, Wright-Patterson AFB, OH 45433-7251, USA*

Received 15 July 1998; accepted 4 November 1998

Abstract

Cross sections for electron impact ionization of trimethylsilane from threshold to 70 eV have been measured using Fourier transform mass spectrometry. High resolution mass spectra show that the parent ion $Si(CH_3)_3H^+$ is not formed by electron impact. Only one of the 15 ions produced by dissociative ionization lacks a silicon atom. The total ionization cross section is 1.5 X 10^{-15} cm^2 at 70 eV. $(CH_3)_2SiH^+$ and $(CH_3)_3Si^+$ comprise over half of the ions produced by electron impact, but charge transfer reactions of $(CH_3)_2SiH^+$ and lighter ions yield $(CH_3)_3Si^+$ at pressure-time products in the 10^{-7} Torr s range. The implication of this ion chemistry is that ion fluxes to the walls of trimethylsilane plasmas are predominantly $(CH_3)_3Si^+$. (Int J Mass Spectrom 184 (1999) 83-88) © 1999 Elsevier Science B.V.

Keywords: Electron; Ion; Ionization; Reaction; ***Cross*** section

1. Introduction

The use of volatile silicon compounds for plasma enhanced chemical vapor deposition of semiconducting and insulative films requires their ionization by electron impact in plasmas. Although both silane (SiH_4) and tetramethylsilane $(CH_3)_4Si$ are tetracoordinate molecules, their ion chemistries are quite different. Electron impact on SiH_4 produces a $^2T_2$ ion that is Jahn-Teller unstable and dissociates to SiH_3^+ and SiH_2^+; no parent SiH_4^+ is observed [1]. By contrast, a small yield of $(CH_3)_4Si^+$ is produced from tetramethylsilane [2]. Silane ion fragments polymerize with silane to give stable clusters with up to four silicon centers [3], but reactions of the ion fragments produced by dissociative ionization of tetramethylsilane with the parent gas do not lead to the ionic silicon polymerization [2].

Here we report measurements of the ionization cross sections and charge transfer reactions in trimethylsilane, a molecule that has both Si-H and Si–CH, bonding. This gas is a precursor for plasma enhanced chemical vapor deposition of amorphous silicon carbide films [4,5] and has applications for abrasion and chemically resistant coatings as well as semiconductor device elements.

2. Experimental

Trimethylsilane (99.99%, United Chemical Technologies, Inc.) gas is mixed with argon (99.999% Matheson Research Grade) with a ratio of 1:1 as determined by capacitance manometry. The mixture

* Corresponding author. E-mail: Alan.Garscadden@wl.wpafb.af.mil

1387-3806/99/$20.00 © 1999 Elsevier Science B.V. All rights reserved
PII S1387-3806(98)14270-7

is admitted through a precision leak valve into a modified Extrel Fourier transform mass spectrometry (FTMS) system that has been described in detail elsewhere [6]. Ions are formed by electron impact in a cubic ion cyclotron resonance (ICR) trap cell (5 cm on a side) at pressures in the 10^{-7} Torr range. An electron gun (Kimball Physics ELG2, Wilton, NH) irradiates the trap for 6 ms with a few hundred picocoulombs of low-energy electrons. The motions of the ions are constrained radially by a superconducting solenoidal magnetic field (-2 T) and axially by an electrostatic potential (1 V) applied to the trap faces that are perpendicular to the magnetic field. Ions of all mass-to-charge ratios are simultaneously and coherently excited into cyclotron orbits using a stored waveform [7,8] applied to two opposing trap faces that are parallel to the magnetic field. The excitation period is -2 ms and the radius of ion cyclotron orbits after the excitation is -0.5 cm. Following cyclotron excitation, the image currents induced on the two remaining faces of the trap are amplified, digitized, and Fourier analyzed to yield a mass spectrum. The data acquisition time is typically 2 ms.

Calculation of cross sections from the mass spectrum intensities requires knowledge of the gas densities, the electron beam current, and the number of ions produced. These calibration issues have been described previously [6]. The intensity ratios of the ions from $(CH_3)_3SiH$ to Ar^+ give cross sections relative to those for argon ionization since the $(CH_3)_3SiH$:Ar pressure ratio is fixed.

The distribution of electron energies in the trap, based on the solution of Laplace's equation for the experimental geometry, is roughly Gaussian with a full width at half maximum of 0.5 eV due to the electrostatic trapping bias [6]. The mean energy of the irradiating electrons is accurate to ±0.2 eV based on comparison of noble gas ionization thresholds with spectroscopic data. We fit the cross section data to an empirical functional form:

$$\sigma = A \tanh \frac{\pi(\epsilon - T)}{\alpha} e^{-k(\epsilon - T)}$$

where σ is the cross section, ϵ is the electron energy, T is the appearance potential, A scales the amplitude, α quantifies d $\sigma/d\epsilon$ near threshold, and k characterizes behavior at energies $\gg T$.

The monoisotopic mass spectral patterns were calculated using the isotope abundances for silicon: ^{28}Si (92.28%), ^{29}Si (4.67%), and ^{30}Si (3.05%), and for carbon: ^{12}C (98.9%) and ^{13}C (1.1%).

3. Results and discussion

Of the 15 ions produced by electron impact on trimetbylsilane the $(CH_3)_2SiH^+$ and $(CH_3)_3Si^+$ together account for more than half of the total yield. Other fragments include $SiC_2H_x^+$ with x = {1,3,5,6}, $SiCH_y^+$ withy = {1–5}, and SiH_z^+ with z = {0,1,3}. Except for traces of CH_3^+ formed above 40 eV all of the ion fragments contain silicon. The cross sections are displayed in Fig. l(a) and (b), with parameters for the fitted curves summarized in Table 1. The total ionization cross section at 70 eV is 5.1 ± 0.5 X 10^{-15} cm^2. Although cracking patterns of trimethylsilane at selected energies have been reported [9–11], this account is the first complete presentation of the energy-dependent partial ionization cross sections.

Fig. 2 shows high resolution spectra at masses where evidence of an undissociated molecular ion should be seen. The peaks near m/e = 74 and 75 are shown to arise from the naturally abundant isotopes of silicon and carbon, proving that the $Si(CH_3)_3H^+$ is not formed by electron impact. Based on our detection sensitivity, the cross section for producing the parent ion must be less than 2 X 10^{-18} cm^2. The observation of $Si(CH_3)_3H^+$ (50%) following Penning ionization by Ar* ($^3P_2$) [12] of trimethylsilane shows that this ion is thermodynamically stable; it is not formed by electron impact because of the short interaction time and unfavorable momentum considerations compared with Penning ionization.

Figs. 3(a)-(c) illustrates the fate of all ions produced by 50 eV electron impact as they are allowed to collide with neutral trimethylsilane. The trimethylsilyl cation, $Si(CH_3)_3^+$, is produced by hydride transfer reactions of all lighter ion fragments with $(CH_3)_4Si$. $Si(CH_3)_3^+$ reacts slowly (k = 6 x 10^{-12} cm^3 s^{-1})

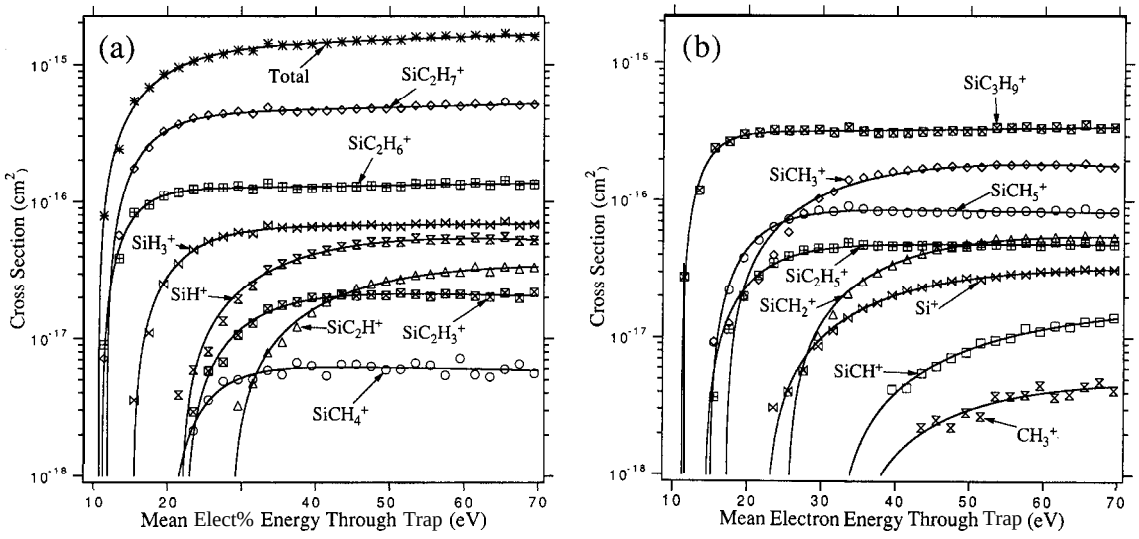

Fig. 1. (a) and (b) Cross sections (cm^2) for ionization of $(CH_3)_3SiH$ by electron impact. Points represent experimental data, and solid lines are fits of the form described in the text.

with trimethylsilane to yield a cluster ion $Si_2C_6H_{19}^+$. This association reaction requires either emission of a photon or a vibrationally excited intermediate that survives at least for milliseconds to be collisionally stabilized at our experimental pressures.

Most of the remaining ion kinetics can be summarized by the overall methide and hydride transfer reactions:

$$R^+ + (CH_3)_3SiH \rightarrow SiC_2H_7^+ + (RCH,) \quad (1)$$

$$R^+ + (CH_3)_3SiH \rightarrow SiC_3H_9^+ + (RH) \quad (2)$$

with branching ratios summarized for each applicable R in Table 2. The SiH^+ ion also produces $SiCH_3^+$ with a 15% branching ratio, and the yield of CH_3^+ from dissociative ionization was too small to quantify its reactions.

Table 1
Fitting parameters for dissociative ionization cross sections; ions are listed in the order of the decreasing intensities at 70 eV that are shown in the last column

Ion	A (cm^2)	k (eV^{-1})	α (eV)	T (eV)	σ at 70 eV (10^{-16} cm^2)
$SiC_2H_7^+$	4.3×10^{-18}	-3.2×10^{-3}	26	11.9	5.1
$SiC_3H_9^+$	3.1×10^{-18}	-1.9×10^{-3}	15	11.2	3.5
$SiCH_3^+$	2.8×10^{-16}	6.9×10^{-3}	87	17.2	1.8
$SiC_2H_6^+$	1.2×10^{-18}	-1.8×10^{-3}	19	11.2	1.3
$SiCH_5^+$	8.9×10^{-17}	1.4×10^{-3}	29	15.0	0.83
SiH_3^+	6.5×10^{-17}	-9.9×10^{-4}	32	15.4	0.68
$SiCH_2^+$	8.5×10^{-17}	7.6×10^{-3}	91	25.4	0.54
SiH^+	8.1×10^{-17}	7.6×10^{-3}	83	21.8	0.53
$SiC_2H_5^+$	4.9×10^{-18}	2.0×10^{-4}	33	14.3	0.48
SiC_2H^+	4.4×10^{-17}	4.2×10^{-3}	86	28.5	0.34
Si+	3.8×10^{-17}	2.2×10^{-3}	86	22.4	0.32
$SiC_2H_3^+$	2.4×10^{-18}	3.1×10^{-3}	43	22.4	0.22
$SiCH^+$	1.5×10^{-17}	-3.1×10^{-3}	96	31.8	0.14
$SiCH_4^+$	6.6×10^{-17}	2.3×10^{-3}	28	20.2	0.06
CH_3^+	8.0×10^{-18}	8.8×10^{-3}	114	33.4	0.04

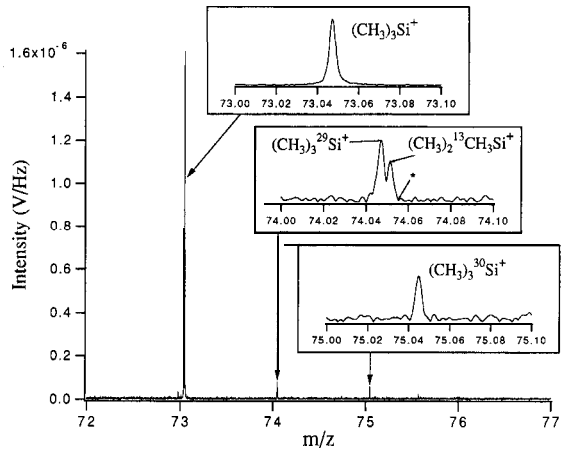

Fig. 2. High resolution mass spectrum of $(CH_3)_3SiH$ acquired at 30 eV. It shows the absence of the molecular ion, $(CH_3)_3SiH^+$, which has the mass-to-charge ratio position marked by asterisks in the inset.

Double resonance experiments allowed the isolation of channels for the production in small yield of disilicon cations $Si_2C_4H_{11}^+$, $Si_2C_3H_9^+$, $Si_2C_3H_{11}^+$, and $Si_2C_6H_{19}^+$ with branching ratios shown below in parentheses. These following reactions are in addition to reaction (1) and (2)

$$Si^+ + Si(CH_3)_3H \rightarrow Si_2C_3H_9^+ + H \ (27\%) \quad (3)$$

$$SiCH_3^+ + Si(CH_3)_3H \rightarrow Si_2C_4H_{11}^+ + (H_2) \ (7\%) \quad (4)$$

$$SiC_2H_3^+ + Si(CH_3)_3H \rightarrow Si_2C_3H_9^+ + (C_2H_4) \ (72\%) \quad (5)$$

$$SiC_2H_5^+ + Si(CH_3)_3H \rightarrow Si_2C_3H_{11}^+ + (C_2H_4) \ (46\%) \quad (6)$$

$$SiC_3H_9^+ + Si(CH_3)_3H \rightarrow Si_2C_6H_{19}^+ \ (100\%) \quad (7)$$

and are quantified in Table 2. Among the products of these dimerization reactions only $Si_2C_3H_{11}^+$ undergoes further reaction with trimethylsilane:

$$Si_2C_3H_{11}^+ + Si(CH_3)_3H \rightarrow Si_2C_4H_{13}^+ + (SiC_2H_8) \quad (8)$$

The other disilicon alkylcations react only with background moisture to produce oxygen-containing disilicon cations. This behavior lies between the clustering of silane, which proceed to tetra-silicon ions before slowing, and tetramethylsilane, which exhibits no cationic polymerization.

Since argon is commonly used as a diluent in plasma processing we have also measured the reaction of Ar^+ with trimethylsilane with products and branching ratios shown in

$$Ar^+ + Si(CH_3)_3H \rightarrow SiH_3^+ + (C_3H_7 + Ar) \ (29\%)$$
$$\rightarrow SiCH_3^+ + (C_2H_5 + H_2 + Ar) \ (11\%)$$
$$\rightarrow SiCH_5^+ + (C_2H_5 + Ar) \ (8\%)$$
$$\rightarrow SiC_2H_3^+ + (CH, + 2H_2 + Ar) \ (5\%)$$
$$\rightarrow SiC_2H_5^+ + (CH_3 + H_2 + Ar) \ (14\%)$$
$$\rightarrow SiC_2H_6^+ + (CH, + Ar) \ (4\%)$$
$$\rightarrow SiC_2H_7^+ + (CH_3 + Ar) \ (19\%)$$
$$\rightarrow SiC_3H_9^+ + (H + Ar) \ (10\%) \quad (9)$$

We have repeated the ion kinetic studies for ions produced by electron impact at 20, 35, and 70 eV to probe for chemistry driven by ions with vibrational, electronic, or rotational excitation. As summarized in Table 2, all reaction rates reported here are independent of the electron energy with which the reactant ions are formed. If internally excited ions are produced at elevated electron energies they are neither more nor less reactive than their counterparts formed at lower electron energies.

On first inspection the Ar^+ reaction would complicate the composition of ion fluxes in trimethylsilane plasmas. However, each of the ion products in reaction (9) reacts rapidly according to reactions (1) and (2) so that the ion composition is largely $Si(CH_3)_3^+$ at pressures and residence times used in plasma processing. We have previously found identical film stoichiometries, SiC_3, using Auger electron spectroscopy of films produced in trimethylsilane and tetramethylsilane plasmas [13], as would be expected for ionic deposits from these two gases since each delivers $Si(CH_3)_3^+$ ions to the surface [14]. The ionic mechanism was further supported, in the earlier study, with film thickness modification by a magnetic field. In sum, the power and pressures of trimethylsilane and

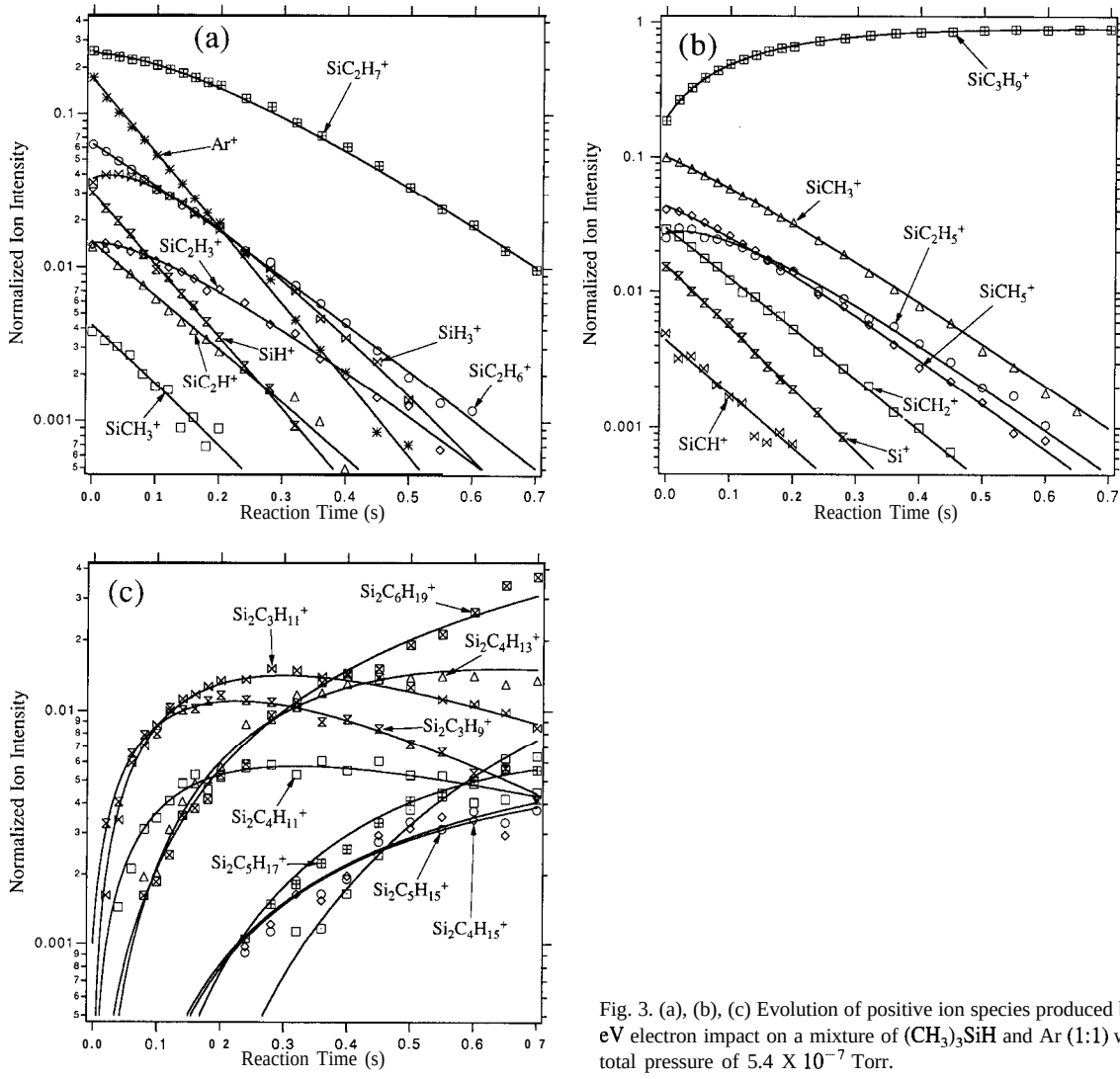

Fig. 3. (a), (b), (c) Evolution of positive ion species produced by 50 eV electron impact on a mixture of $(CH_3)_3SiH$ and Ar (1:1) with a total pressure of 5.4 X 10^{-7} Torr.

tetramethylsilane plasmas can be tuned to deliver ion fluxes with the same composition to a substrate. This has practical value since liquid tetramethylsilane is less expensive and easier to handle than trimethylsilane gas.

4. Conclusion

Electron impact ionization of trimethylsilane produces no $Si(CH_3)_3H^+$. Dissociative ionization produces 15 ionic fragments, only one of which lacks a silicon atom, with a total cross section of $1.5 \pm 0.5 \times 10^{-15}$ cm^2 at 70 eV. Over half of the ion yield is comprised of $Si(CH_3)_3^+$ and $SiH(CH_3)_2^+$. Although produced in higher yield by electron impact, $SiH(CH_3)_2^+$ reacts rapidly with trimethylsilane to produce $Si(CH_3)_3^+$. Lighter ions react rapidly to form $Si(CH_3)_3^+$ and $SiH(CH_3)_2^+$, so that trimethylsilane plasmas produce $Si(CH_3)_3^+$ at the expense of other ion species. Cationic polymerization yields ions with only two silicon atoms; no trisilicon cations were formed. The stability of the parent molecular ion and the

Table 2
Branching ratios of reactions (1) and (2) for selected reactant ions (see the text); also listed are the rate coefficients measured with reactant ions formed by dissociative ionization at different electron energies

		Branching ratios [a]		Reaction rate coefficients			
m/z	Ion	rxn.1	rxn.2	20 eV [b]	35 eV [b]	50 eV [b]	70 eV [b]
28	Si^{+} [c]	35	38		10.7	10.7	10.5
29	SiH^{+} [d]	41	44		10.9	10.9	10.6
31	SiH_3^+	72	28	10.6	10.6	10.6	10.3
41	$SiCH^+$	53	47		9.3	9.3	9.4
42	$SiCH_2^+$	44	56		8.8	8.8	8.6
43	$SiCH_3^+$ [c]	23	70	7.5	7.5	7.4	7.3
44	$SiCH_4^+$	52	48		10.1	10.1	9.9
45	$SiCH_5^+$	67	33	8.1	8.1	8.1	8.0
53	SiC_2H^+	17	83	...	8.1	8.1	8.5
55	$SiC_2H_3^+$ [c]	15	13	. .	7.3	7.1	7.1
57	$SiC_2H_5^+$ [c]	25	29	7.9	7.9	7.8	7.8
58	$SiC_2H_6^+$	17	83	7.3	7.3	7.3	7.1
59	$SiC_2H_7^+$		100	6.9	6.9	6.9	6.2
73	$SiC_3H_9^+$ [e]			0.06	0.06	0.06	0.06
103	$Si_2C_3H_{11}^+$ [e]			2.1	2.1	1.9	1.9

[a] Branching ratios of reactions (1) and (2), respectively, for the selected ions. See the text.
[b] Electron energies at which the reactant ions are formed.
[c] Si^+, $SiCH_3^+$, $SiCH_3^+$, and $SiC_2H_5^+$ also undergo clustering reactions (3)–(6), respectively.
[d] SiH^+ also produces $SiCH_3^+$ with a 15% branching ratio.
[e] $SiC_3H_9^+$ and $Si_2C_3H_{11}^+$ undergo reactions (7) and (8), respectively

extent of cationic polymerization of trimethylsilane lie between those for silane and tetramethylsilane.

Acknowledgements

We wish to acknowledge the Air Force Office of Scientific Research for financial support.

References

[1] P.D. Haaland, Chem. Phys. Lett. 170 (1990) 146.
[2] S. McGinnis, K. Riehl, P.D. Haaland, Chem. Phys. Lett. 232 (1995) 99.
[3] M.L. Mandich, W.D. Reents Jr., K.D. Kolenbrander, J. Chem. Phys. 92 (1990) 437.
[4] M. Lelogeais, M. Ducarroir, Thin Solid Films 197 (1991) 257.
[5] W. Zhang, M. Lelogeais, M. Ducarroir, Jpn. J. Appl. Phys., Part 1 31 (1992) 4053.
[6] K. Riehl, *Collisional Detachment of Negative Ions Using FTMS*, Ph.D. thesis, Air Force Institute of Technology, Dayton, OH, 1992.
[7] A.G. Marshall, T.L. Wang, T.L. Ricca, J. Am. Chem. Soc. 107 (1985) 7893.
[8] S. Guan, J. Chem. Phys. 91 (1989) 775.
[9] R.W. Crawford, P.C. Crawford, C.H. Otto, US Atomic Energy Commission, 1969, UCRL—50808, 26 pp.
[10] B.G. Hovrock, R.W. Kiser, J. Phys. Chem. 66 (1962) 155.
[11] G.P. Van Der Kelen, 0. Volders, H. Van Onckelen, Z. Eeckhaut, Z. Anorg. Allgem. Chem. 338 (1965) 106.
[12] D.R. Anderson, V.M. Bierbaum, C.H. Depuy, J.J. Grabowski, Int. J. Mass Spectrom. Ion Phys. 52 (1983) 65.
[13] Unpublished experimental results.
[14] See [2] for the ion chemistries in tetramethylsilane.